REQ. NO.3-9019

CONTRACT REPORT NO. OSU 83-00050

PILOT PLANT STUDIES OF FLUIDIZED COAL COMBUSTION

H.A. Becker, R.K. Code, R. McCleave, and J.R. Stephenson
Department of Chemical Engineering
Queen's University at Kingston
Kingston, Canada

Technical Report QFBC.TR.85.1
Queen's Fluidized Bed Combustion Laboratory

Prepared for
Energy Mines and Resources Canada
Energy Research Laboratories, CANMET
Ottawa, Canada

301 pp

MICROMEDIA

PILOT PLANT STUDIES OF FLUIDIZED COAL COMBUSTION

Final Report by
H.A. Becker, R.K. Code, R.W. McCleave
and J.R. Stephenson
Department of Chemical Engineering
Queen's University at Kington
Kingston, Canada

Technical Report QFBC.TR.85.1
Queen's Fluidized Bed Combustion Laboratory

Work on this project was conducted under the auspices of the Canada Centre for Mineral and Energy Technology, Energy, Mines and Resources Canada

DSS File Number: 24SU.23440-3-9019

DSS Contract Serial Number: OSU83-00050

CANMET Scientific Authority: Dr. E.J. Anthony

ABSTRACT

Combustion of high-sulphur Eastern Canadian coals (Evans and Devco) with the addition of Eastern Canadian limestones (Havelock, Sysco and Calpo) for sulphur capture has been studied in a pilot-scale atmospheric fluidized combustion (AFBC) system. In addition, an Appalachian coal (Kentucky No. 9) with an Appalachian limestone (Reed) was investigated. The coals, with the exception of the Evans, behaved very much like Minto (Eastern Canadian) and Devco coals as described in a previous report. The Evans coal, however, gave evidence of higher reactivity, showing greater sensitivity to recycle of cyclone catch and generally higher combustion efficiencies. The Sysco, Calpo and Reed limestones were similar in performance and not as good as the Havelock; Havelock generally requires one unit less of Ca/S ratio to achieve equal sulphur capture, other conditions being equal. One other important high-sulphur Canadian fuel, of a very different nature, namely Syncrude coke (residue of tar sands processing) was tested, using a Western (Athabasca) limestone for sulphur capture. Fitting of these results to correlations of combustion efficiency developed for the coals suggested a remarkable similarity of magnitudes. However, closer examination suggests that the effects of bed temperature and recycle are considerably greater than for the coals. Sulphur capture in the Syncrude coke runs remained surprizingly high (over 80 %) up to just over 1000 °C but then fell rapidly, becoming negligible around 1100 °C. The finding of good sulphur capture at quite high temperatures agrees with results reported by Friedrich, Lee, Desai and Kuivalainen on tests of burning Syncrude coke in an atmospheric recirculating fluidized bed (ARFBC) system at the Hans Ahlstrom Laboratory. Syncrude coke is quite high in vanadium; it was determined that the vanadium effectively remains fixed in the ash of the coke and does not become concentrated in any of the leaving solids streams except to the degree that the ash does so.

RESUME

On a étudié la combustion des charbons de l'Est du Canada à haute teneur en soufre (l'Evans et le Devco) avec l'addition de pierres à chaux de l'Est du Canada (la Havelock, la Sysco et la Calpo) pour l'interception du soufre dans un système pilote à combustion atmosphérique fluidifiée (AFBC). On a étudié en outre un charbon des Appalaches (Kentucky no.9) avec une pierre à chaux appalachienne. Les charbons, à l'exception de l'Evans, se sont comportés tout à fait comme les charbons Minto (de l'Est du Canada) et Devco, comme on l'a indiqué dans un rapport antérieur. Cependant, les essais utilisant le charbon Evans ont mis en evidence une réactivité plus élevée, plus de susceptibilité aux procédés de recupération par cyclone dans les pots à poussière, des rendements de combustion plus élevés. Les pierres à chaux Sysco, Calpo et Reed se sont comportées presque de la même façon, mais étaient inférieures à la Havelock; la Havelock permet de diminuer le rapport Ca/S d'une unité pour obtenir une interception égale du soufre, les autres conditions étant les mêmes. Par ailleurs, on a fait des essais avec le coke Syncrude (sous-produit du traitement des sables bitumineux), d'une haute teneur en soufre et d'une nature très différente, utilisant une pierre à chaux de l'Ouest (Athabaska) pour l'interception du soufre. La corrélation des résultats obtenus avec ceux concernant les rendements de combustion établis pour les charbons a mis en évidence une similarité remarquable dans les ordres de grandeur. Cependant, un examen plus rigoureux suggère que les effets de la température de la couche de combustion et de la récupération sont nettement plus importants que pour les charbons. Le taux d'interception du soufre dans les coulées à coke Syncrude a été remarquablement élevé (plus de 80%) jusqu'à un peu plus de 1000° C. pour baisser rapidement ensuite cependant, devenant négligeable aux alentours de 1100° C. Nos observations concernant la bonne interception de soufre à des températures relativement élevées correspondent avec les résultats donnés par Friedrich, Lee, Desai et Kuivalainen de tests faits sur la combustion du coke Syncrude dans un système avec lit à fusion fluidifié recirculant à l'air libre (ARFBC) au laboratoire Hans Ahlstrom. Le coke Syncrude contient beaucoup de vanadium; on a établi que le vanadium demeure fixé dans les cendres du coke et ne devient concentré dans aucun des courants de matières solides évacuées sauf où les cendres le sont elles-mêmes.

PREFACE

This is the Final Report on work performed under a contract with Supply and Services Canada (DSS) under the auspices of the Canada Centre for Mineral and Energy Technology (CANMET), Energy, Mines and Resources Canada:

Title: Pilot plant studies of fluidized coal combustion

DSS File No.: 24SU.23440-3-9019

DSS Contract Serial No.: 0SU83-00050

Principal Investigators: Dr. H.A. Becker and Dr. R.K. Code (Department of Chemical Engineering) and Dr. J.T.N. Atkinson (Department of Metallurgical Engineering), Queen's University at Kingston, Kingston,
Ontario K7L 3N6
Telephone (613) 547-3045

Scientific Authority: Dr. E.J. Anthony, Building 1, Energy Research Laboratories, CANMET, Haanel Drive, Bells Corners, Ontario

Postal address: Energy Research Laboratories, CANMET, c/o 555 Booth Street, Ottawa, Ontario K1A 0G1
Telephone (613) 996-4570, ext. 185

Science Procurement Manager:
Mrs. J.P.S. Sztramko, Science and Professional Services Directorate, Supply and Services Canada, 11C1 Place du Portage--Phase III, 11 Laurier Street, Hull, Quebec K1A 0S5
Telephone: (819) 997-7398

Commencement date: 13 June 1983

Delivery date: 31 March 1985

Consignee: Energy, Mines and Resources Canada, Energy Research Laboratories, CANMET, c/o 555 Booth Street, Ottawa, Ontario
K1A 0G1

Three professionals were employed on the contract: Mr. Robert W. McCleave (Research Associate), Mr. John R. Stephenson (Research Associate), and Mr. Ross McLean (Technician). Another professional, Miss Marie Yorke (Technician) was employed with funding provided by an NSERC Strategic Grant. Undergraduate students were employed as Summer Research Assistants, one each year on contract funds and the others on NSERC grant and Ontario Ministry of Energy (Experience '83 and Experience '84) funds: Miss Marilyn McInerney and Mr. Peter Tuovi in 1983, and Mr. Duncan Boswell, Mr. Francesco Castagna and Mr. Donald McGuire in 1984.

Three Ph.D. students conducting thesis research on fluidized bed combustion particpated: Mr. Michel Couturier, Mr. Fernando Preto, and Mr. Jia Qu Zhang. One M.Sc. student, Mr. David Poirier, was also so engaged.

A number of bench-scale and theoretical studies were carried on complementing the pilot plant investigations. A part of the cost of these was met through a Strategic Grant (Energy) from the Natural Sciences and Engineering Research Council.

The cooperation of the Tennessee Valley Authority, who provided for our use quantities of the coal and limestone used in trials on their 20 MW demonstration plant, as well as data on their operating conditions, is gratefully acknowledged.

Last but not least, it is a pleasure to acknowledge the dedication, patience, good humour, and unfailing helpfulness of our Scientific Authority, Dr. E.J. Anthony.

CONTENTS

NOTATION 9

N.1 General remarks 9
N.2 Intensive variables 9
N.3 Extensive variables 9
N.4 Fluxes 10
N.5 Stream labelling 10
N.6 Flux ratios 11
N.7 Summary of notation 11

1. INTRODUCTION 22

1.1 Background 22
1.2 The work undertaken and done under the subject contract 23
    1.2.1 Specifications of the pilot plant 23
    1.2.2 Instrumentation and analysis capabilities 25
    1.2.3 Experimental design 29
    1.2.4 Specifications of the pilot plant trials 30
    1.2.5 Supporting studies specified by the contract 34
1.3 Scope of the report 35
1.4 Significance 37

2. THE QUEEN'S AFBC PILOT PLANT FACILITY 40

2.1 Introduction 40
2.2 The combustor 40
2.3 The exhaust gas train 51
2.4 The coal and limestone feed systems 52
2.5 The cyclone dust recycle system 52

2.6 Air supply and flows 53
2.7 Instrumentation and analytical systems 54

3. OPERATING PROCEDURES 57

3.1 Cold startup 57
3.2 Hot start of a run 59
3.3 Procedure during runs, after startup 61
3.4 Criteria for the approach of steady state conditions 63
3.5 Post-shutdown measurements 66
3.6 Manpower and scheduling considerations 66

4. MATERIALS 68

4.1 Introduction 68
4.2 Fuels 69
  4.2.1 Sources and preparation of the fuels . . . 69
  4.2.2 Proximate/Ultimate analyses 70
  4.2.3 Ash analyses 70
  4.2.4 Higher heating values 71
  4.2.5 Ash fusion temperatures and free swelling indexes 71
  4.2.6 Particle size distributions 71
4.3 Limestone sorbents 83
  4.3.1 Sources and preparation of sorbents . . . 83
  4.3.2 Chemical analyses 88
  4.3.3 Particle size distributions 88
4.4 Product solids 97
  4.4.1 Chemical analyses and particle size distribution 97

5. EVANS TRIALS 104

5.1 Introduction 104

5.2 The carbon balance 104
5.2.1 Carbon content of the product solids . . . 104
5.2.2 Distribution of carbon loss 109
5.2.3 Distribution of fuel carbon among products 111
5.2.4 Division of carbon between cyclone and baghouse solids 122
5.2.5 Correlation of overhead carbon loss . . . 122
5.2.6 Carbon burn-up efficiency 127
5.2.7 Carbon balance check 128
5.3 The sulphur balance 131
5.3.1 The sulphur content of the product solids 131
5.3.2 Distribution of sulphur among the product solids 131
5.3.3 Sulphur capture efficiency 133
5.3.4 Sulphur balance check 138
5.4 The fuel nitrogen balance 145
5.4.1 Emission levels of nitrogen oxides 145
5.4.2 The N/C ratio in the product solids . . . 145
5.4.3 Effect of operating conditions on the conversion of fuel N to NO_x 150
5.5 The hydrogen balance 154
5.5.1 The H/C ratio in the product solids . . . 154
5.5.2 Effect of operating conditions on the H/C ratio in the solids 156

6. SYNCRUDE COKE TRIALS 159

6.1 Introduction 159
6.2 The carbon balance 163
6.2.1 Carbon content of solids 163
6.2.2 Flux distribution 163
6.2.3 Total carbon balance 167
6.2.4 Combustion inefficiency 167
6.3 The sulphur balance 171

6.3.1 Sulphur content of solids 171
6.3.2 Flux distribution 174
6.3.3 Sulphur capture 174
6.3.4 Total sulphur balance 177
6.4 The nitrogen balance and NO_x 177
6.5 Carbon monoxide 181
6.6 Vanadium 181
6.7 Fuel-ash flux distribution 185

7. DEVCO AND KENTUCKY NO. 9 TRIALS 190

7.1 Introduction 190
7.2 The carbon balance 190
7.2.1 Carbon content of the product solids . . . 190
7.2.2 Distribution of carbon loss 195
7.2.3 Distribution of fuel carbon among products 197
7.2.4 Division of carbon between cyclone and baghouse solids 204
7.2.5 Correlation of overhead carbon loss 208
7.2.6 Carbon burnup efficiency 211
7.2.7 Carbon balance check 215
7.3 The sulphur balance 215
7.3.1 The sulphur content of the product solids 215
7.3.2 Distribution of sulphur among the product solids 218
7.3.3 Sulphur capture efficiency 220
7.3.4 Sulphur balance check 223
7.4 The fuel nitrogen balance 229
7.4.1 Emission levels of nitrogen oxides 229
7.4.2 The N/C ratio in the product solids . . . 229
7.4.3 Effect of operating conditions on the conversion of fuel N to NO_x 235
7.5 The hydrogen balance 235

7.5.1 The H/C ratio in the product solids . . . 235
7.5.2 Effect of operating conditions on the H/C ratio in the solids 238

8. DISCUSSION OF RESULTS ON CARBON LOSS AND SULPHUR CAPTURE 245

8.1 Introduction 245
8.2 Overhead carbon loss 245
8.3 Bed product carbon loss 252
8.4 Comparison of carbon loss with the Ahlstrom trials on Syncrude coke 257
8.5 Sulphur capture 263

9. HEAT TRANSFER 268

9.1 Introduction 268
9.2 Configuration of the arrays of in-bed tubes 268
9.3 Evaluation of heat transfer coefficients 270
9.4 Results and discussion 275
9.4.1 Results 275
9.4.2 Effect of operating conditions on h_o 281

10. CONCLUSION 290

10.1 Summary of findings 290
10.2 Unfinished comparisons 292
10.3 Recommendations 292
10.4 Results on supporting studies 294

REFERENCES 296

NOTATION

N.1 General remarks

The AFBC pilot plant operation is complex enough so that, as in the treatment of large plants generally, a systematic approach to notation is desirable and even necessary. In the following summary, the system adopted in this report is first explained. The list of symbols and definitions is then presented.

N.2 Intensive variables

The symbols employed for the major intensive variables are ones quite commonly used in the related theory of transport phenomena, thermodynamics, and chemical reactor analysis: T for temperature, P for pressure, ρ for density, c_p for specific heat capacity at constant pressure, w_i for the mass fraction of component i (element or compound) in a material, and x_i for the mole fraction of species i in a molecular mixture. In the specification of material composition, the concepts of mass ratio W_i and mole ratio X_i are also used but (unless otherwise noted) only in the following sense: W_i is the mass of component i per unit mass of water-free (moisture-free) material, and X_i similarly is the molar mass of i per unit molar mass of water-free molecular mixture. Thus

$$W_i \equiv w_i/(1 - w_{H_2O}),$$

$$X_i \equiv x_i/(1 - x_{H_2O}).$$

These concepts are useful for discussing solids compositions on the dry basis, and gas compositions on a water-free ("dry gas") basis. Our gas analysis instruments, for example, were perforce set up to give dry-gas analyses.

N.3 Extensive variables

Standard symbols are employed herein for these too: m for inertial (ordinary) mass of material, n for molar mass of material (moles), V for volume of material, Q for heat, etc.

N.4 Fluxes

Instead of introducing wholly new symbols for fluxes (mass material flux, molar material flux, heat flux, etc.), we follow the convenient and economical convention of using the symbol for the extensive variable with a dot placed over it. Thus $\dot{m}$ is mass material flux, $\dot{n}$ is molar material flux, $\dot{V}$ is volumetric material flux, $\dot{Q}$ is heat flux, etc. This fluxional dot notation should not be confused with the now generally disused Newton dot notation for the time derivative; e.g., $\dot{m}$ is not dm/dt, the time-rate of change of mass of a system, but simply mass flux (the mass flowrate of a material stream).

N.5 Stream labelling

For a simple system, single-letter subscripts may be adequate to identify all material streams, and possibly none may be needed. Here, however, a more complex but systematic approach is warranted which can easily handle any present or future problems. In general, a subscript m denotes the m'th stream in a set. Streams are placed in three categories: feed streams (entering the plant), product streams (leaving the plant), and transfer streams (between units in the plant). We then label specific feed streams as F1, F2, F3, ... ; specific product streams as P1, P2, P3, ... ; and specific transfer streams as T1, T2, T3, ...

Figure N.1 shows the basic streams in the present pilot plant and their assigned labels. Table N.1 explains the labels. Some special notational questions are dealt with as follows:

- the pilot plant has numbers of two-phase streams, generally composed of co- or counter-flowing solids and gas. Suppose it is wished to consider only the solids component of stream T6; we then append a symbol S (for solids), making it T6S.

If we were considering only the gas, it would be T6G.

- it is necessary in some contexts to consider a combination or set of streams, e.g., all the solid products leaving the system, or all the air supplied to the combustor. In the general case, such sets might be labelled like individual streams; e.g., F13 might identify a certain set of feed streams, and F13S the solids component of that set. However, because the number of such cases actually considered herein is small, we have opted for distinctive alphabetical labels for the important ones, Table N.1.

- for certain basic feedstreams and product streams which are common to all FBC processes and which are involved in many arguments herein, we have defined alternative single-letter labels, Tables N.1 and N.2, which are used almost everywhere in the text.

N.6 Flux ratios

The symbol ϕ_{mn} is used to denote the mass flux ratio $\dot{m}_m/\dot{m}_n$, where m denotes the m'th material stream and n the n'th material stream. Both m and n can represent combinations of, as well as single, streams. This concept is particularly useful in showing how fluxes are partitioned; e.g.:

- $\phi_{mp} = \dot{m}_m/\dot{m}_p$, m = b, c or h, gives the partitioning of solid products between bed product, cyclone product, and baghouse product

- $\phi_{C,mf} = \dot{m}_{C,m}/\dot{m}_{C,f}$, m = b, c or h, gives the carbon loss in the bed product, cyclone product, and baghouse product as a fraction of the fuel carbon fed.

N.7 Summary of notation

Table N.2 lists all the symbols used and their definitions.

Table N.1. Notation for identifying material streams. Read in conjunction with Fig. N.1.

General Code	Special short code	Stream
Feed streams:		
F1	f	fuel (here coal)
F2	s	sorbent (here limestone)
F3	--	fluidizing air
F4	--	recycle transport air
F5	--	air-lock purge air
Product streams:		
P1	--	bed product (here bed material removed as overflow)
P2	--	cyclone product (cycloned dust removed as product)
P3	--	baghouse product (dust filtered out by baghouse)
P4	--	stack product, two-phase, consisting of gaseous products and particulate emissions; the "fluegas"
P5	--	leak of air-lock purge air to atmosphere, from the air-lock valve
Transfer streams:		
T1	--	solids feed system to air-lock valve, two-phase, coal and limestone going forward and leaking air-lock purge air going backward (the only counterflow two-phase stream)
T2	--	air-lock valve to combustor, two-phase, consisting of coal, limestone, and air-lock purge air

Table N.1 cont'd

T3	--	combustor freeboard to cyclone, two-phase, consisting of gaseous products and elutriated solids
T4	--	cyclone to recycle system, two-phase, consisting of cycloned dust and leaking exhaust gas
T5	--	recycle system to combustor, two-phase, consisting of recycling dust, recycle transport air, and recycling leaked exhaust gas
T6	--	cyclone to baghouse, two-phase, consisting of gaseous products and of dust escaping the cyclone
Components of two-phase streams:		
P4G	--	gaseous portion of the "fluegas"
P4S	--	solid portion of the "fluegas", the particulate emissions
T1S, T2S	--	solid portion of streams T1 and T2, the coal and limestone going to the combustor
T1G	--	purge air leaking from air lock valve, feeding product stream P5
T3S	e	elutriated solids leaving combustor, going to the cyclone
T3G	x	gas leaving combustor, going to cyclone (code x refers specifically to values at combustor exit)
T4S	d	cycloned solids (dust) leaving cyclone
T4G	--	gas leak from cyclone, due to induction by dust recycle system
T5S	--	recycling solids, cyclone to combustor
T5G	--	gas carrying the recycling solids; recycle transport air plus gas leak T4G
T6S	--	solids escaping cyclone, to baghouse
T6G	--	gas leaving cyclone for baghouse

Table N.1 cont'd

Combinations of separate streams:

FA	a	= F3 + F4 + T2G = F3 + F4 + F5 - P5, the combustion air
PO	o	= P2 + P3, the overhead product solids
PS	p	= P1 + P2 + P3 + P4S, the product solids (or product particles)

Table N.2. Summary of notation

Subscripts--special codes for material streams (see Table N.1 for a general listing):

a	combustion air, in aggregate
b	bed product (material removed directly from the bed, here by gravity overflow)
c	cyclone product (cycloned solids not recycled)
d	cycloned solids (dust)
e	elutriated solids (flyash)
f	fuel (here coal)
g	stack gas
h	baghouse product (solids)
m	the m'th material stream or combination of streams
n	the n'th material stream or combination of streams
o	overhead product solids (cyclone c and baghouse b combined)
p	product solids (particles), in aggregate
r	recycled cycloned solids
s	sorbent (here limestone)

Variables:

A_b	cross-sectional area of bed, m^2
B'	heat transfer conductance per unit length of in-bed tube, tube-side fluid to bed, $W/m \cdot K$

Table N.2 cont'd

c_p	specific heat capacity at constant pressure, J/kg K
COT	continuous-mode operating time, s (see Sect. 3.4)
D_i	inside tube diameter, m
D_o	outside tube diameter, m
D_p	particle diameter, m. Here determined by sieve analysis
$\hat{D}_p$	characteristic diameter for particles of mixed size, m: defined by $D_p = \hat{D}_p$ at $F_D = 1/2$
F_D	distribution function, $F_D = F_D(D_p)$, of particle size in a population: the mass fraction of particles smaller than the argument value of D_p; the "mass fraction undersize". Here determined by sieve analysis
g	acceleration due to gravity, m/s^2
h_i	tube-side (inside) heat transfer coefficient for in-bed tubes, W/m^2K
h_o	bed-side (outside) heat transfer coefficient for in-bed tubes, W/m^2K
$\Delta h_{c,f}$	specific enthalpy of combustion of fuel, J/kg
H_s	settled bed height, m: the bed height observed after gradually reducing the gas flow until fluidization ceases and the bed comes to rest (becomes "fixed")
k	thermal conductivity, W/m·K
k_w	thermal conductivity of tube wall, W/m·K
K_b	ratio of pressure drop across bed to weight of bed per unit area

Table N.2 cont'd

L	total in-bed length of the tubes in a series-connected cooling circuit, m
m	mass of material (inertial), kg
m_b	bed mass (holdup), kg
$\dot{m}$	mass flux, kg/s
$\dot{m}_m$	mass flux of the m'th material stream, kg/s. See list of subscripts at head of this table for specific codes
$\dot{m}_{D;m}$	size-resolved mass flux of the m'th material stream, kg/m·hr, so $\dot{m}_{D,m}\, dD_p$ is the mass flux of particles and is the size range D_p, $D_p + dD_p$
$\dot{m}_{i,m}$	mass flux of component i (compound or element) carried by the m'th material stream, kg/s. Some specific components: $CaCO_3$, CaO, CO_2, SO_2, C, H, N, S
n	molar mass of material, mol
$\dot{n}$	molar flux of material, mol/s
$\dot{n}_m$	molar flux of the m'th material stream, mol/s
$\dot{n}_{i,m}$	molar flux of molecular species i carried by the m'th material stream, mol/s
n_t	number of in-bed tubes
Nu	$= h_i D_i/k$ Nusselt number for tube-side heat transfer
P	pressure, Pa
P°	standard pressure, 101.325 kPa
P_{fb}	freeboard gas pressure, Pa

Table N.2 cont'd

$(\Delta P)_b$	pressure drop across bed, Pa
Pr	ν/α, Prandtl number (here for coolant in in-bed tubes)
Q	heat, J
$\dot{Q}$	heat flux out of system, W
$\dot{Q}_b$	heat flux out of bed, W
$\dot{Q}'$	heat flux per unit length of in-bed tube, W/m
r	$= \dot{m}_r/\dot{m}_d$, recycle fraction: fraction of cycloned dust that is returned to combustor
R	$= \dot{m}_r/\dot{m}_c$, recycle ratio: ratio of recycled cycloned dust to that not recycled
R	multiple correlation coefficient (in multiple linear regression analysis)
Re	$= 4\dot{m}/\pi\mu D_i$, Reynolds number for coolant flow through in-bed tube
Re_{mf}	$= D_p v_{mf}/\nu$, particle Reynolds number in bed at minimum fluidization
S	surface, m^2
S_p	particle surface, m^2
S'''	surface area of particles in unit volume of space (in bed or in a bulk sample), m^{-1}
t	time, s
T	temperature, K
T°	standard temperature, 273.15 K
T_b	bed temperature, K

Table N.2 cont'd

T_i	inside surface temperature of in-bed tube, K
T_o	outside surface temperature of in-bed tube, K
T_w	wall temperature of in-bed tube (recognizing that $T_o \simeq T_i$), K
$T_{w,0}$	value of T_w at start of an in-bed cooling circuit, K
$T_{w,L}$	value of T_w at end of an in-bed cooling circuit, K
v	superficial gas velocity up combustor, m/s. Also called the fluidizing velocity. Here computed as $\dot{n}_x \tilde{V}^\circ (T_b/T^\circ)(P^\circ/P_{fb})$, where $\dot{n}_x$ is the molar gas flux at combustor exit.
v_{mf}	minimum fluidizing velocity, m/s: the value of v at the point of incipient fluidization as indicated by the graph of $(-\Delta P)_b$ vs. v, following the standard procedure
v_{ms}	minimum slugging velocity, m/s: value of v at the onset of slugging
$\tilde{V}^\circ$	standard molar volume, 22.413 m^3/kmol
V_p	particle volume, m^3
w_i	mass fraction of component i (compound or element) in a material
$w_{i,m}$	value of w_i in the m'th material stream
W_i	mass ratio of component i (element or compound) in a material. Here defined only as $W_i = w_i/(1 - w_{H_2O})$, thus as the mass fraction d.b. (dry basis)
$W_{i,m}$	value of W_i in the m'th material stream
x	distance along an in-bed cooling circuit, m

Table N.2 cont'd

x_i	mole fraction of molecular species i in a molecular mixture
$x_{i,m}$	value of x_i in the m'th material stream
X_i	mole ratio of molecular species i in a molecular mixture. Here defined only as $X_i = x_i/(1 - x_{H_2O})$, thus as the mole fraction d.b. (dry basis)
$X_{i,m}$	value of X_i in the m'th material stream
α	$= k/\rho c_p$, thermal diffusivity
ε	void fraction in a bed (fraction of space not occupied by particles)
ε_a	excess air level: $\dot{n}_a/\dot{n}_{a,st} - 1$, where $\dot{n}_{a,st}$ is the stoichiometric (theoretical) air requirement for complete combustion. Also expressed as a percentage
η_C	carbon burnup efficiency, %: $100(1 - \dot{m}_{C,p}/\dot{m}_{C,f})$
η_Q	bed cooling coefficient: $\dot{Q}_b/\dot{m}_f\,(-\Delta h_{c,f})$
η_{SO_2}	SO_2 capture efficiency, %: $100(1 - \dot{n}_{SO_2,x}/\dot{n}_{S,f})$
μ	viscosity, kg/m·s
μ_w	value of coolant viscosity at temperature T_w, kg/m·s
ν	$= \mu/\rho$, kinematic viscosity, m^2/s
ρ	density, kg/m^3
ρ_p	particle density, kg/m^3
ρ_g	gas density, kg/m^3

Table N.2 cont'd

τ_b	$= m_b/\dot{m}_b$, estimate of residence time of bed product in combustor, s
τ_p	$= m_b/\dot{m}_p$, mean residence time of solid products (in aggregate) in combustor, s
ϕ_a	mixture strength: $\dot{m}_a/\dot{m}_{a,st} = 1 + \varepsilon_a$, ratio of air supplied to air theoretically (stoichiometrically) required for perfect combustion
ϕ_{mn}	$= \dot{m}_m/\dot{m}_n$, mass flux ratio of the m'th and n'th material streams
$\phi_{i,mn}$	$= \dot{m}_{i,m}/\dot{m}_{i,n}$, mass flux ratio of component i (compound or element) in the m'th and n'th material streams

1. INTRODUCTION

1.1 Background

A pilot plant for studying atmospheric fluidized bed combustion (AFBC) was built and commissioned under the initial contract of this series in the period 1979--81 and is described in the final report on that activity (Becker and Code 1982). The second contract, for the period 1981--83, inaugurated the work the pilot plant was made for: to investigate the burning of Canadian candidate fuels by AFBC, particularly high-sulphur fuels, using Canadian limestones as sorbents for SO_2 removal. The coals used were Minto from New Brunswick and Devco from Cape Breton, with a Havelock Nova Scotia limestone. The results of these trials are described in the final report (Becker and Code 1983). The present subject contract, the third, for 1983--85, continued the work on Maritime coals and limestones, adding one new coal and two new limestones. To expedite comparison with results elsewhere, work was also done with the Appalachian coal and limestone used by the Tennessee Valley Authority in their program with a 20 MW plant. Trials were also carried but with an important and very different high-sulphur Canadian fuel, namely Syncrude coke, the solid residue from tar sands extraction at the Syncrude plant in Alberta. A new contract, the fourth, has been awarded for 1985--87 which involves a considerable proportion of fundamental work besides trials on interesting Canadian coals and sulphur sorbents not yet tested; the title is, "A Program of Pilot Scale R&D on Bubbling Bed Atmospheric Fluidized Bed Combustion".

1.2 The work undertaken and done under the subject contract

1.2.1 Specifications of the pilot plant

The contract work statement specified as necessary the following features of the pilot plant:

1. The pilot scale fluidized bed combustor (hereafter described as the rig) will have the following features:

    a) A square or rectangular cross-section with a bed area of at least 0.1 m^2.

    b) A freeboard of uniform cross-section and a height of at least 4.8 m.

    c) Inbed cooling tubes capable of controlling bed temperature in the range of 750 °C - 950 °C with a precision of at least ± 20 °C.

    d) Capability for underbed and overbed feed by a screw feed or equivalent system and pneumatic injection of both fuel and limestone.

e) A recycle capacity which permits a recycle rate of up to 2:1 and allows the recycle rate to be both controlled and measured over this range. In order to ensure a good quality of fluidization, no more than 10 % of the fluidizing air may be used for the recycle and ancillary purposes, the rest of the air must go through the distributor plate, for underbed and overbed feed and no more than 20 % may be used for recycle and other purpose, for pneumatic feeding of fuel and limestone. Measurements and calculations to demonstrate that these criteria have been met, will be expected.

f) The rig will have both a cyclone and a baghouse filter and a capability of collecting and measuring the solid flows to these systems during the combustion trials.

g) The rig will be run at fluidizing velocities from 1 to 4 m/s, bed temperatures of 750 - 1000 °C and excess air level of up to 25 % and will be capable of continuous operation for periods of up to 60 hours.

h) The unit will have both an underbed and overflow system capable of removing bed solids to maintain bed levels constant and it will be possible to collect all the bed solids at the end of a run to permit "bed hold-up" to be measured and allow residence times to be estimated.

The system indeed had all the features mentioned. In the event, however, because of the many variables to be studied, certain limitations on the experimental design were accepted for the subject work. In particular:

[] solids feeding was all done by underbed screw feeders

[] bed level was controlled by an overflow port

Some of the other specifications, though, were exceeded. Bed temperatures in the Syncrude trials, for example, ranged up to 1150 °C, which was there found to be necessary.

1.2.2 Instrumentation and analysis capabilities

The contract specified the following capabilities:

2. The rig will have the following instrumentation and analysis capabilities:

   a) Pressure distribution across the distributor plate and the bed must be measured both manometrically and with a pressure transducer, so that the pressures may be logged electronically.

   b) The temperatures in the bed must be measured at a minimum of 3 different heights above the distributor plate. The temperature in the freeboard must also be continuously monitored by a reliable means with due recognition of radiation effects (i.e. by aspirating temperature probes); calibration and experimental validation of freeboard temperature measurements must be presented in justification. At least every 0.5 m above the splash zone should be covered.

c) Spoon probes and aspirating probes must also be employed in the freeboard for measuring particulate fluxes. These probes must be calibrated in a 3-dimensional cold model with an I.D. of at least 100 mm.

d) Solid sampling during combustion trials from the bed must be carried out with a probe designed to quench the sample collected in-situ in order to allow a representative sample of the bed material to be collected to determine the carbon loading of the bed.

e) The bed hold-up is to be determined for every run by collecting and weighing all the bed material at the end of each run to permit residence times to be estimated.

f) The flowrates of all solid streams must be accurately determined (i.e. coal, limestone, bed product (both underflow and overflow), cyclone product, baghouse product and cyclone recycle). A complete mass-balance will be carried out for each run and a sieve analysis of all feed and product streams shall be performed.

g) Flowrates and input and output temperatures of all coolant streams including those for bed and the freeboard must be measured.

h) The usual "continuous" instrumental monitoring of CO_2, CO, O_2, NO_x, SO_2 and hydrocarbons will be carried out. Output of these instruments will be logged electronically so that the data may be processed by an electronic data processing device, so that the processed data be quickly available to CANMET. In addition, the H_2O concentration in the flue gas stream must be monitored.

i) The gas shall be sampled both in the bed and freeboard using cooled probes designed to "immediately" quench the gases such that the probes will see within 5 to 10 % of the CO and NO_x present at that particular location. Calculations using the most recent kinetic data available in the literature must be produced to validate these measurements.

j) The contractor is to perform ultimate and proximate analysis on each fuel and measure the total sulphur and carbon content of each solid stream. Atomic absorption and X-ray fluorescence is to be used in analyzing ash on at least one sample of each solid stream for each run.

k) When using large sizes of coal (> 10 mm) and limestone (> 1 mm) attention shall be paid to possible segregation effects in the bed and quantitative measurements made to ascertain the accumulation of any size fraction in the bed.

Practical difficulties were encountered in two of the areas mentioned:

[] an aspirating temperature probe was built but the degree of miniaturization required was at the limits of feasibility. The probe needs further development by a researcher (a graduate student will serve) whose time is not largely committed to a busy operating role in the teamwork (particularly manning shifts) of the pilot plant trials. This work will be completed and the probe applied in our new contract.

[] problems were also encountered in using dust sampling probes in the pilot plant. The spoon probe, developed by the AFBC research team at the Massachusetts Institute of Technology, has been found to be of questionable value as a quantitative device. In the difficult environment of the splash zone of a fluidized bed, and up to the transport disengagement height, aspirating probes of conventional dust-sampling design are also of very questionable performance. Development work on better probes is going on in the research group of Dr. Maurice Bergougnou at the University of Western Ontario, and we hope to apply some of the results in our new contract.

1.2.3 Experimental design

The contract particularly specified certain features of the experimental designs to be employed in the trials:

3. For each fuel at least 20 tests shall be performed representing at least 300 hour of testing for that fuel. Typical tests are to last from 15 to 40 hours and "steady-state" conditions may be not be assumed to occur until at least 3 turnovers of bed material have occurred. For the rig at CANMET this would normally occur at around 12 hours of operation. Calculations and measurements will be expected to confirm that 3 bed turnovers have been achieved.

   In any case of a coal with a low softening temperature, specifically Evans and possibly the TVA Coal (this decision will be taken by the Scientific Authority (SA)) some very long runs will be carried out to ascertain whether there is any tendency for clinkering to occur and if so to determine the conditions under which the clinkering occurs.

This will mean at least one run of at least 50 hours at a temperature of 900 °C and further long runs at lower temperatures (850 °C and 800 °C) if clinkering does not occur at these temperatures.

Throughout these trials good experimental design shall be used to plan the trials both at the beginning and for subsequent corrections. The designs shall be approved by the Scientific Authority; acceptable designs may include 2 level fractional or hybrid of these, e.g. multilevel fractional designs.

Here the requirement of twenty runs with each fuel could not be carried out in full, owing to practical limitations of time, budget and luck. The worst case was that of the TVA trials for which insufficient coal was received, due to a misjudgment by the hauler, and circumstances conspired as well in other ways, so in the end only a small number of runs was completed. However, adequately long run times were obtained in all the successful trials and long total operating times were logged in most sets of trials. There should thus be little question about the validity of the runs for representing steady-state performance.

1.2.4 Specifications of the pilot plant trials

The contract gave the following specifications of the essential features of the trials that were to be carried out:

4. Trials shall be carried out on Evans coal and Havelock limestone to determine the effect of bed conditions on combustion efficiency and limestone performance. The main parameters to be varied are bed temperature (between 750 - 950 °C); fluidizing velocity (between 1 and 4 m/s); recycle rate (0 - 5 times the feed rate) and Ca/S ratio (between 1 - 4). Runs should be carried out in the overbed and underbed feed mode although the bulk of the trials may be carried out in the "best" mode by agreement with the SA. The exact conditions for these trials are left to the contractor, subject to the constraints laid down in the requirement and work statement, but in any case these must be approved by the SA.

5. Combustion trials will be carried out on Devco coal and two of the "best" limestones that would be commercially available for the CFB Summerside FBC boiler.

   a) At least 5 limestones available commercially in the maritime region will be tested via TGA. The "best" two will be selected dependent on these results and any obtained by the bench-scale apparatus at EMR in consultation with, and with the agreement of, the SA.

   b) The same criteria given for testing with Evans coal will be applied to the tests with Devco.

6. Combustion trials will be carried out on Syncrude coke and Fort McMurray limestone.

   a) The effect of fluidizing velocity (up to 4 m/s), recycle rate (up to at least 5 times the feed rate) and bed temperatures (up to at least 1000 °C) will be examined.

   b) All tests may be restricted to the inbed feed mode unless results indicate that satisfactory combustion efficiencies (> 95 %) and sulphur capture (> 90 % with Ca/S ratio $\leq$ 4:1) can be obtained with overbed feed mode. Both screw feed and pneumatic feed systems may be used, however, at least one trial will be carried out with pneumatic injection of the fuel.

   c) Samples will be taken from the bed, cyclone and baghouse to be analyzed for Ni and V and inventories of these two elements and the effect of bed conditions on the fate of these two species will be examined. Particular care will be given to determine whether bed conditions cause these metals to be concentrated in any solid stream or any size fraction of any solid stream, excluding the baghouse samples whose size range will be assumed to be uniform.

   d) The same general criteria specified for the combustion trials with Evans coal will be followed except where an exception has been made in Section 5.

7. Combustion trials will be carried out with the coal and limestone used for the TVA 20 MW pilot plant for CANMET.

   a) The purpose of these trials is to provide scaling criteria to determine the effect of bed size on the combustion performance of coal and limestone in an FBC. This will allow predictions about the behaviour of large industrial beds to be made from data obtained by pilot scale or bench scale rigs. In consequence, the conditions of these trials will be decided in consultation with the SA as results become available from the TVA 20 MW unit and the "6 by 6 foot" unit at Alliance, Ohio. The criteria laid down by the work statement are to apply and any deviations from these criteria must be approved by the SA.

1.2.5 Supporting studies specified by the contract

The contract specified a number of supporting studies complementing the pilot plant trials:

8. Three-dimensional cold modelling studies must be performed using bed ash to study heat transfer, hydrodynamics of the bed and the elutriation.

a) The cold model shall have tubes of the same cross-section as those used in the rig and it must be possible to duplicate the geometry of the tube arrangement used in the bed. At least one of the tubes will be designed to permit heat transfer coefficients at its surface to be measured.

b) The model will be at least half-scale and should operate at velocities up to 4 m/s. It must be transparent or permit easy visual inspection for photographic recording and it must permit testing of solids loading aspirating and spoon probes. The freeboard must in any case extend to at least 3 m.

c) Elutriation studies must be performed in a 3-dimensional cold model which will permit all the solids elutriated at any given height up to 4.8 m above the bed and at similar superficial fluidizing velocities (up to 4 m/s) as experienced by the rig to be collected. Should the contractor feel it desirable to build another unit for these purposes, the half scale criteria need not apply to unit but it must have a diameter or characteristic length of at least 100 mm.

d) The contractor is to be fully familiar with the mathematical models and correlations available to predict heat transfer, hydrodynamics and elutriation, e.g. the model due to Beer et al. at M.I.T. and he is to test these against both cold modelling and results from the pilot scale rig to determine which are best and if possible to develop a new and better model to describe these phenomena.

9. TGA work on each of the calcined limestone used in this work in synthetic atmospheres containing SO_2 and SO_3 will be expected to generate the kinetic data suitable for use in the Westinghouse and Argonne models for sulphur sorption. The porosity of the calcined limestone must be measured.

These studies were carried on by graduate students supported by an NSERC Strategic Grant: Mr. Michel Couturier, Mr. Fernando Preto, and Mr. Jia Qu Zhang, all Ph.D. candidates, and Mr. David Poirier, M.Sc. candidate.

1.3 Scope of the report

The report is confined to presenting the results of the pilot plant trials. Results on the supporting studies will be presented in other reports, theses and papers to follow. In particular:

[] Mr. Michel Couturier has completed his research on calcination and SO_2 sorption of limestone by TGA and his Ph.D. thesis is nearly ready. The thesis will be available as a QFBC Technical Report.

[] Mr. Fernando Preto has completed his research on mathematical modelling and on heat and mass transfer and his Ph.D. thesis is in the last stages of typing. This thesis also will be issued as a QFBC Technical Report. A separate report has been prepared on the model and its computer code and will soon be available.

[] Mr. Jia Qu Zhang is well advanced in his study of the burning of single large coal particles using a bench scale reactor. His Ph.D. thesis is expected to be ready in about a year from now.

[] Mr. David Poirier is far advanced in his study of carbon transport from the combustor and will be submitting his M.Sc. thesis within six months.

[] Mr. Robert W. McCleave, one of our Research Associates and a co-author of this report, is continuing work on bench scale studies of elutriation, using a cold model, and is using this for an M.Sc. degree toward which he has been working part-time.

The presentation of the pilot plant results in this report is complete in respect to the experimental results. The interpretation, however, is a subject of continuing work and our most definitive and complete version of that will appear in scientific journal and symposium papers to follow. Because of the pressure and time constraints surrounding the preparation of this report, a thorough analysis with full use of mathematical models and mechanistic arguments had to be deferred.

1.4 Significance

As noted in the final report (Becker and Code 1983) on the preceding contract, the Queen's pilot plant project is part of an effort, originating in the Energy Research Laboratories, CANMET, Energy, Mines and Resources Canada (EMR) to promote and support the development and application of fluidized bed combustion in Canada. The effort is spurred by the fact that Canada has great resources of candidate fuels for FBC, and at the same time a need to strictly limit the emissions of sulphur dioxide from combustion processes. Other projects in the EMR program include:

- a pilot plant like the present one, located at the Energy Research Laboratories of EMR, described in a report by Hector, Desai, Friedrich and Anthony (1981)

- a pilot plant for investigating corrosion in in-bed tubes, located at Point Tupper, N.S., operated by Nova Scotia Power Corp.

- the first Canadian demonstration plant, consisting of two FBC boilers, located at Canadian Forces Base, Summerside, P.E.I.

Two reports on this project are available (Taylor and Friedrich 1982; Razbin and Friedrich 1983).

Canada, through EMR, is a participant in the International Energy Agency (IEA) Agreement for Cooperation in the Field of Atmospheric Fluidized Combustion in Industrial or District Heating Boilers. The present project thus contributes, as well, to this international cooperative effort. Descriptions of all the projects in progress in the countries taking part in the IEA agreement may be found in the annual reports of the Executive Committee for the agreement.

The present endeavour also has significance beyond carrying out research required by EMR. In the engineers, technicians and graduate students involved, professionals are being trained for work in the technology. A Canadian centre of expertise and investigative resources complementing those at EMR has been established. Finally, for its part in supporting graduate students, bench scale studies, and theoretical work through a Strategic Energy Grant, and providing instruments such as the TGA apparatus and a C/H/N analyzer through equipment grants, useful work is being done in an area of research, namely energy, that has been designated as being of strategic national importance by the Natural Sciences and Engineering Research Council of Canada. In respect of the first point, it may be noted that the two coming Ph.D. graduates of the program, Mr. Michel Couturier and Mr. Fernando Preto, have obtained appropriate employment and are already working, the former as an Assistant Professor of Chemical Engineering at the University of New Brunswick with research in fluidized bed combustion and SO_2 emission abatement and the latter as a combustion research scientist in laboratories of our sponsor--the Energy Research Laboratories of CANMET. Our first Research Associate and project engineer, Mr. David Liang, has also joined CANMET, to work in research on corrosion in fluidized bed combustion. An M.Sc. candidate who still has to finish writing his thesis, Mr. Kian McCaldon, is working as a combustion engineer with Pratte and Whitney Canada.

Interest in our program by graduate students has been very strong; we have been taking as many as we can handle, and the training is clearly filling a need.

2. THE QUEEN'S AFBC PILOT PLANT FACILITY

2.1 Introduction

The AFBC pilot plant at Queen's University is described in an earlier technical report (Becker & Code 1982) hereinafter referred to as QFBC.TR.82.1. Thus, the presentation here is limited to a brief review of salient features of the system. Several minor modifications and new components introduced after the issuance of QFBC.TR.82.1 are also described. The pilot plant in its present configuration is shown schematically in Fig. 2.1.

2.2 The combustor

The main unit in the system is the fluidized bed combustor, Fig. 2,2, which consists of ten modules. The chamber cross-section is nearly square, 381 mm by 406 mm, 0.155 m^2 cross-sectional area, in all modules except the top module which is transitional. From bottom to top, the modules are:

1. The windbox, a new redesigned unit installed after QFBC.TR.82.1 was issued. It is light in weight and is attached to module 3 by just four bolts, facilitating rapid removal and reattachment. The windbox is regularly dropped after each run or series of connected runs, for a number of purposes: to dump the bed for weighing (determination of holdup), to remove accumulated unfluidizable stone particles, and to allow examination of the

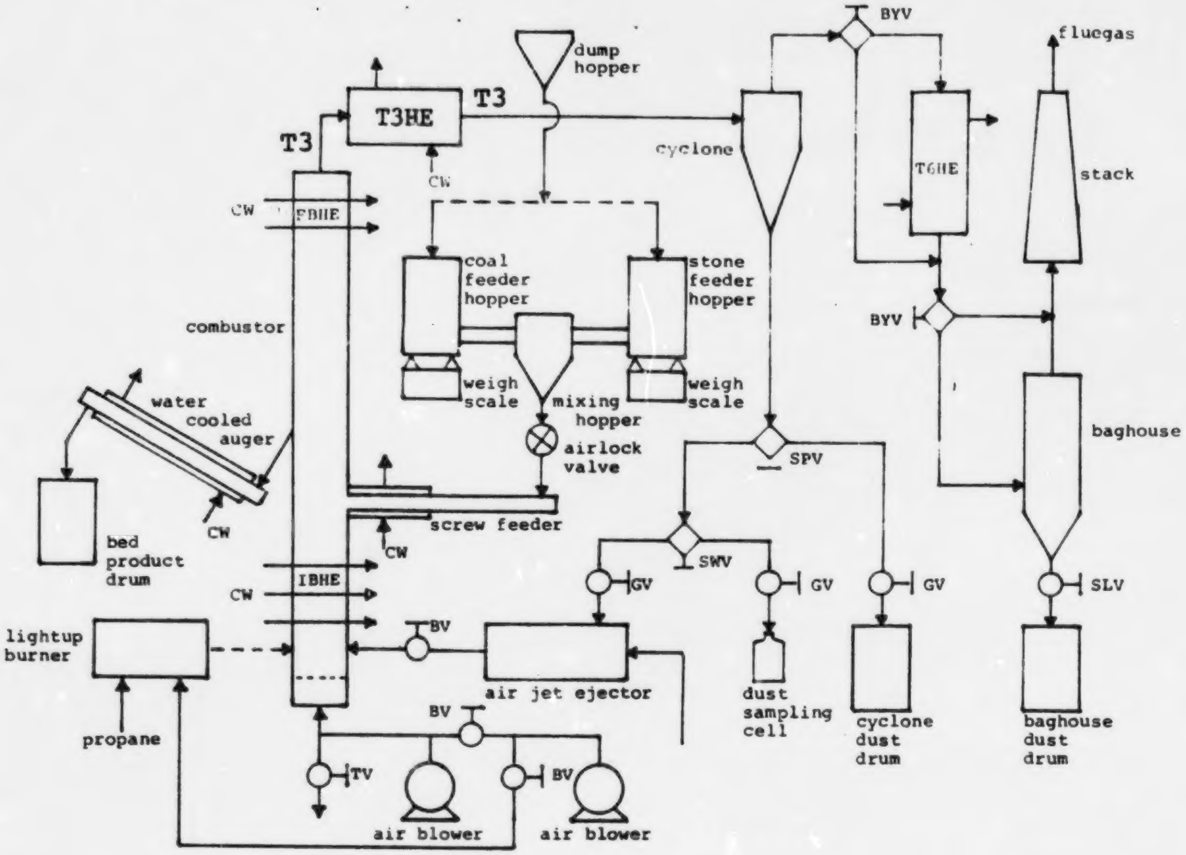
BYV
fluegas
dump hopper
T3HE
T3
T3
cyclone
CW
T6HE
stack
CW
FBHE
coal feeder hopper
stone feeder hopper
combustor
BYV
water cooled auger
weigh scale
mixing hopper
weigh scale
baghouse
airlock valve
SPV
screw feeder
CW
CW
bed product drum
SWV
IBHE
CW
GV
GV
GV
SLV
BV
lightup burner
air jet ejector
dust sampling cell
cyclone dust drum
baghouse dust drum
BV
propane
TV
BV
air blower
air blower

Fig. 2.1. Flowsheet of the AFBC pilot plant. Acronyms:

BV	ball valve
BYV	by-pass valve
CW	cooling water
FBHE	freeboard heat exchanger
GV	gate valve
HP	high pressure
IBHE	in-bed heat exchanger
SLV	slide lock valve
SPV	splitter valve
SWV	switch valve
TV	throttling valve
T3HE	heat exchanger cooling transfer stream T3
T6HE	heat exchanger cooling transfer stream T6

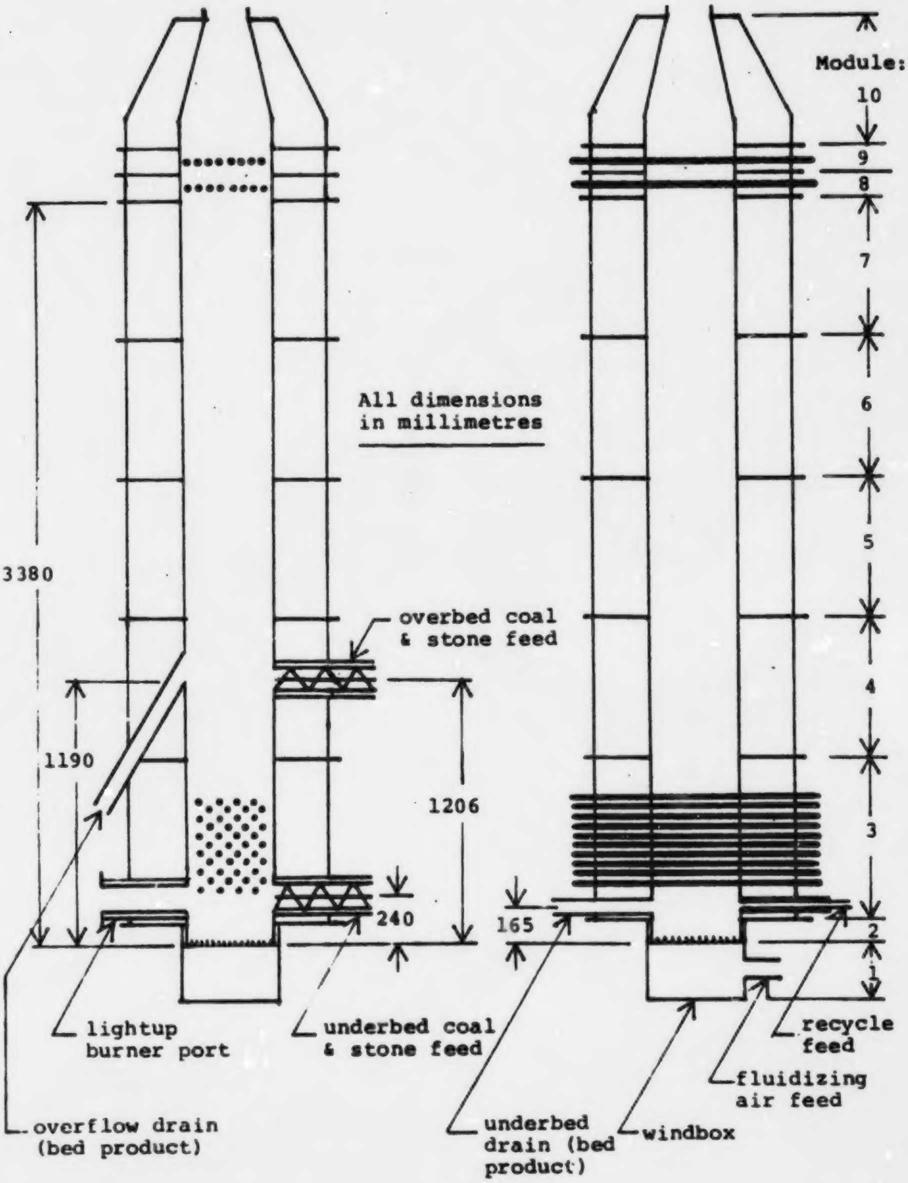
Module:
10
9
8
7
6
5
4
3
2
1
All dimensions in millimetres
3380
1190
1206
240
165
overbed coal & stone feed
lightup burner port
underbed coal & stone feed
overflow drain (bed product)
underbed drain (bed product)
windbox
fluidizing air feed
recycle feed

Fig. 2.2. Principal dimensions and features of the combustor

in-bed heat-exchange tubes and refractory walls and linings. Air is fed to one side of the windbox through a 75-mm diameter port and a short diverging duct which expands to the full width of the chamber below the distributor plate. The chamber height is 100 mm and the volume, including the short diverging duct section, is 0.019 m^3.

The distributor plate, which forms the top of the windbox, was fabricated from 0.5-in (12.7 mm) thick steel plate, 15.75 in by 14.75 in (400 mm by 375 mm). The 105 dispersion caps are arranged in 11 alternating rows of 10 and 9 caps in a triangular pitch. The centre-to-centre distances between caps are 1.548 in (39.32 mm) within rows and 1.341 in (34.06 mm) between rows. The arrangement of the dispersion caps on the distributor plate is illustrated in Fig. 2.3. The caps were assembled from 1.5-in (38.1 mm) long sections of 0.5-in (S-80; 21.3 mm OD; 13.9 mm ID) and 7.35-in (186.7 mm) long sections of 0.25-in (S-80; 13.7 mm OD; 7.67 mm ID) heavy wall, 304 stainless steel pipe. The 0.25-in sections were inserted into the 0.5-in sections and the tops of the caps were sealed by welded 304 stainless steel rivets to form hemispherical heads. The bottom ends of the sections of 0.25-in pipe were threaded with 0.25-in NPT. Six, 1.4-mm diameter injection nozzles were drilled at 60° intervals through the walls of the concentric pipe sections, 7.6 mm below the base of the hemispherical heads. The location of the injection nozzles 30.5 mm above the plate provides an insulating layer of undisturbed solids

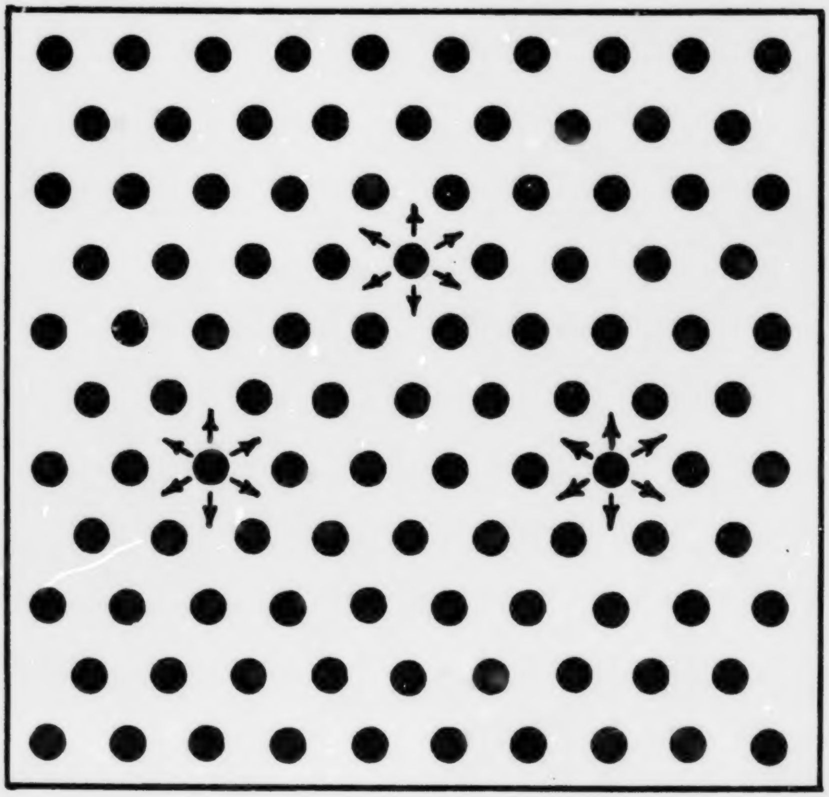

Fig. 2.3. Arrangement of dispersion caps on distributor plate

for protection of the plate from the high temperatures in the bed. In addition, two 3/16-in (4.76 mm) diameter holes, located 2 in (5.1 mm) below the bottom of the 0.5-in pipe sections, were drilled on opposite sides of the 0.25-in pipe sections to allow passage of air from the air chest to the injection nozzles. In the final assembly, the 0.5-in pipe sections of the caps rest on gasket washers on the surface of the plate and the longer 0.25-in pipe sections pass through holes drilled in the distributor plate and in the steel plate which forms the bottom of the air chamber. The threaded ends of the 0.25-in pipe sections which project through the bottom of the air chamber were tightened and sealed by 'CAJON' brass pipe caps. In the attachment of the dispersion caps, care was taken to position the nozzles so that the issuing jets are directed towards the spaces between adjacent caps (Fig. 2.3).

The air-dispersion system described above was used for the trials on Evans coal and Syncrude coke. Deterioration of the hemispherical heads on the dispersion caps required the replacement of this unit, for the remainder of the work, with an earlier version described by Becker and Code (1983). In the older unit, air is fed through a 75-mm diameter port, in the middle of one side, to an internal chamber with a height of 254 mm and a volume of 0.039 m^3. The 9.5-mm thick distributor plate is fitted with 100 dispersion heads uniformly spaced on a rectangular pitch 37.5 mm by 37.8 mm (Fig. 2.4). The dispersion heads are 12.7-mm diameter stainless steel cap

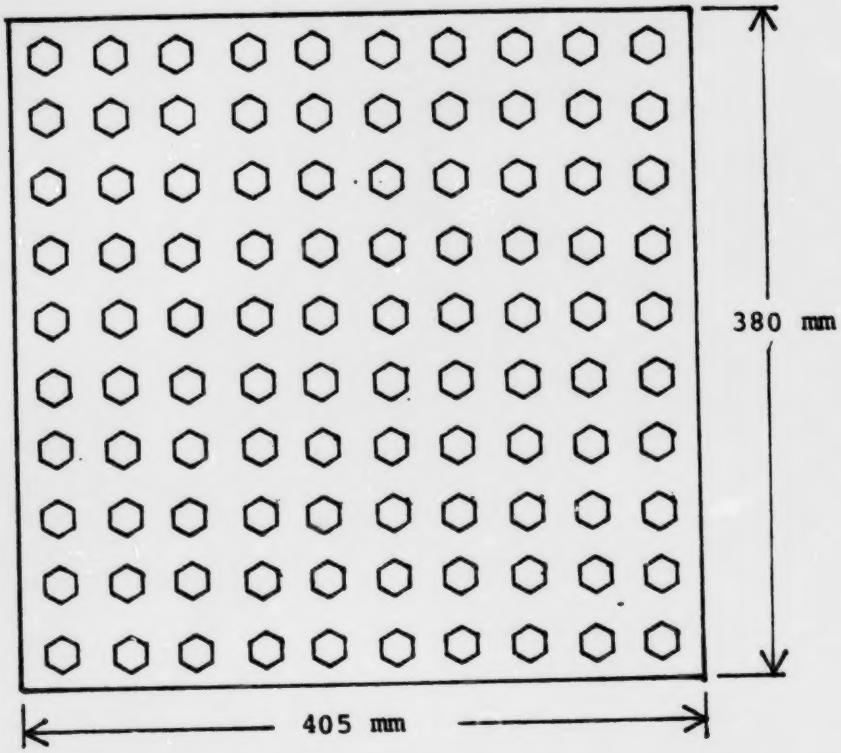
380 mm
405 mm

Fig. 2.4. Arrangement of the dispersion heads on the distributor plate

screws drilled at 90° intervals with four horizontal discharge holes just under the cap which intersect the air feed hole drilled from the threaded end axially along the centerline.

2. A waterwall downward extension, 102 mm high, added after QFBC.TR.82.1. It is clamped between modules 1 and 3. Its function is to reasonably increase the distance between the distributor plate and the underbed solids (coal and limestone) feedport, in order to improve the quality of fluidization and mixing at the solids feedpoint and to provide greater capacity for the accumulation of rocks (if any) before these interfere with the dispersion of the entering solids.

3. The in-bed heat exchanger module, 737 mm high. Rectangular openings in two opposite walls of this unit are fitted with panels containing a matrix of ports for the insertion of cooling tubes spanning the bed when in operation. The panels are refractory-lined on the inside and water-jacketed on the outside. The tubes are of 21.3 mm OD (1/2-inch standard) steel pipe. Figure 2.5 shows the port geometry. Ports not occupied by tubes are either capped or used for other purposes such as sampling, temperature probing, and feeding solids. This module also contains the ports, Fig. 2.2, for underbed feeding of coal and limestone, connection of the lightup burner, pneumatic injection of recycled cyclone dust, and underbed discharge of bed solids.

4--7. Four internally identical modules, each 635 mm high.

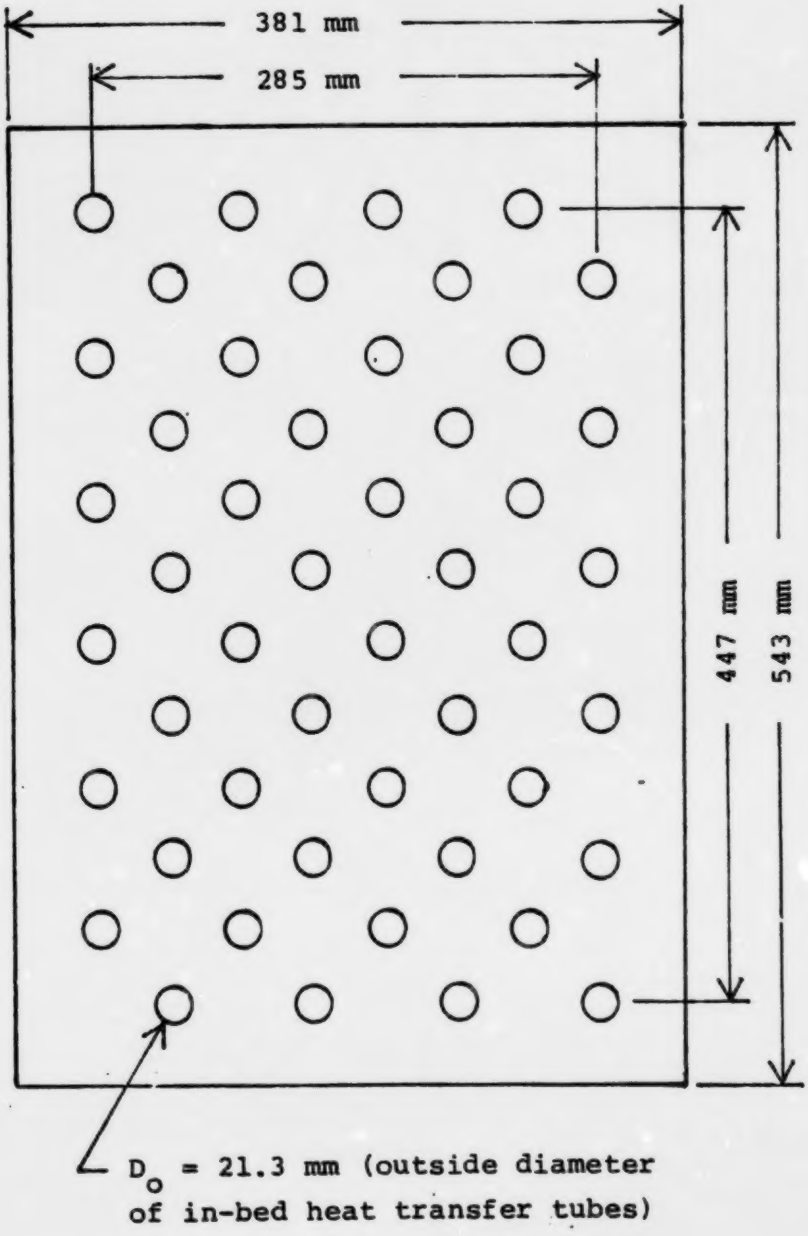
381 mm
285 mm
447 mm
543 mm
D_o = 21.3 mm (outside diameter of in-bed heat transfer tubes)

Fig. 2.5. Distribution of ports for in-bed heat exchange tubes

The lowest has, Fig. 2.2, on opposite sides, two solids transport ports: a bed overflow port allowing overflow of bed solids into a 77.9 mm ID (3 inch std.) drain pipe set at 30° to the vertical, and an overbed feed port for coal and limestone. These modules, and module 3 as well, are all fitted with numerous ports for insertion of sampling probes, thermocouples, and pressure taps. Details are given by Becker and Code (1982).

8. & 9. Two crossflow freeboard heat exchanger modules, each 120 mm high and each containing a horizontal row of eight tubes carrying cooling water. The vertical distance from the distributor plate to the lower bank of cooling tubes is 3.34 m. The cooling tubes were removed from both modules after trial 840501 and a second shell-and-tube heat exchanger was installed before the cyclone separator.

10. A transition module, 610 mm high, with a contraction at the end, leading into the exhaust ducting carrying the exhaust gases to the external heat exchangers, cyclone and baghouse. This module is fitted with ports for exhaust-gas sampling.

Modules 3--10 are made up of 231 mm thick refractory brick wall contained in a steel shell 6.3 mm thick.

In summary:

o the combustor has provision for overbed and underbed feeding.

- bed solids may be removed by overflow or by underbed extraction. These are the means of controlling the solids holdup, or the bed height.

- heat is extracted from the bed via the in-bed heat exchanger tubes (in module 3), the waterwall extension (module 2), and the water-jacketed panels accommodating the in-bed tubes in module 3.

- recycled cyclone dust may be injected into the bed through the port in module 3 indicated in Fig. 2.2 or through any of the unused ports for in-bed heat exchanger tubes.

- heat is extracted from the gases at the end of the freeboard by the freeboard heat exchanger (removed after trial 840501).

- the height of the combustion chamber from the distributor plate at its bottom to the first row of freeboard heat exchanger tubes at the top with the waterwall extension (module 2) in place, is 3.34 m.

- the bottom rim of the bed overflow port, with the waterwall extension in place, is 1.19 m above the distributor plate. This, then, is the nominal bed height when holdup is controlled by overflow.

2.3 The exhaust gas train

The exhaust gases pass through the following units on their way to the stack:

1. A short duct fitted with a spring-loaded explosion vent.

2. Two shell-and-tube heat exchangers with the gases on the tube-side and cooling water on the shell-side, labelled T3HE (heat exchanger cooling transfer stream T3, Fig. 2.1). This drops the temperature below levels for appreciable chemical reaction and to a level suitable for the cyclone separator, below 425 °C.

3. The cyclone dust separator.

4. A cross-flow heat exchanger with the gases in the shell, water in the tubes, labelled T6HE (heat exchanger cooling transfer stream T6, Fig. 2.1). This provides control of the gas temperature entering the baghouse and going to the stack.

5. The baghouse.

The explosion vent and the gas quenching heat exchangers were installed after QFBC.TR.82.1 was issued. The first heat exchanger incorporates a single pass tube bundle assembled from 19, 1.52-m lengths of 1.5-in standard steel pipe (48.3 mm OD; 40.9 ID) and enclosed in a 282-mm ID cylindrical shell formed from 1/8-in (3.2 mm)-steel plate. The second exchanger, installed after the removal of the tube banks from the freeboard heat exchanger modules (after trial 840501), is identical to the first exchanger with the exception that the tube bundle is one-half as long (0.76 m).

A bypass valve permits partial bypassing of heat exchanger T6HE in order to prevent overcooling and condensation in the stack gas. Another bypass valve permits bypassing of the baghouse until the gas temperature for entering the baghouse has been suitably adjusted. Details are given in QFBC.TR.82.1.

2.4 The coal and limestone feed systems

The coal and limestone are charged through a dump hopper, located at floor level in the laboratory above the pilot plant, to the two feed hoppers mounted on the platforms of electronic weigh scales on the mezzanine level of the pilot plant. The metered feed streams from the coal and limestone hoppers enter a mixing hopper and are fed through a rotary air-lock valve ('star feeder') to an auger which discharges into the bed. The feed system may be operated in either overbed or underbed feed modes. More detailed descriptions of the equipment are given in the report by Becker and Code (1982).

2.5 The cyclone dust recycle system

The dust stream leaving the cyclone is split in two by an adjustable splitter valve. One part, of mass flux $\dot{m}_r$, is recycled. The other, of mass flux $\dot{m}_c$, is drawn off as product.

The recycle fraction $r = \dot{m}_r \backslash \dot{m}_d$ is continuously variable, by means of the valve, from zero to unity, where $\dot{m}_d = \dot{m}_r + \dot{m}_c$ is the total mass flux of dust leaving the cyclone. This adjustable splitter valve was added after the issuance of QFBC.TR.82.1. The previous valving was "on-off"; either none or all of the dust was recycled.

The recycle dust stream flows, by gravity and suction, into an air-jet ejector which acts as the pump for pneumatic reinjection into the bed. A switch valve just before the ejector allows diversion of the recycle stream to a sampling cup, for material sampling and for determination of flow rate by collecting the stream over a measured time interval.

The terminal parts of the recycle line are of 1/2-inch standard (15.8 mm OD) stainless steel pipe. These parts are short and straight. The long curved section connecting them is of 19.0 mm ID rubber sand-blasting hose.

2.6 Air supply and flows

Fluidizing air, fed to the windbox and dispersed into the bed of solids through the distributor plate, is supplied by a Roots rotary lobe blower. Combustion air for the lightup burner is supplied by a second Roots blower. This second unit is also used to supply additional air for operation of the bed at high fluidization velocities. Dust recycle air is supplied from the laboratory high-pressure air line, as is a small flow of air injected into the coal/limestone feed line to offset gas leakage through the rotary air lock valve and to block escape of bed gases through the valve. The recycle air flux in the work described herein was normally about 18 kg/hr. The spillage of purge air into the combustor from under the air-lock valve was 2 kg/hr. The fluidizing air flux was 250--450 kg/hr and made up 90--95 % of the air supplied.

2.7 Instrumentation and analytical systems

The gas and solids sampling probes, the gas and solids analysis systems, the temperature and pressure measurement systems, and the data acquisition and processing system are described in the report by Becker and Code (1982). In summary, infrared analyzers are used for on-line measurement of CO, CO_2 and SO_2 concentrations, a paramagnetic analyzer for O_2, a chemiluminescence analyzer for NO and NO_x, and a gas chromatograph for unburnt hydrocarbons. Specifics on the analytical instruments used for gas analysis are summarized in Table 2.1. Similar details on the solids analysis systems are given in Table 2.2. The instrumentation is interfaced with a microcomputer (Hewlett-Packard 9836A) and a printer-plotter (Hewlett-Packard 7470) for data acquisition and processing. Pressure taps are interfaced with the computer through a scanning valve and pressure transducer with backup measurements by a bank of manometers. Thermocouples, used for temperature measurement, are also interfaced with the computer with backup at critical points in the gas and water circuits by dial thermometers.

Table 2.1 Instrumentation for Gas Analysis

INSTRUMENT	DETECTOR TYPE	GAS SPECIES
Beckman Model 864	Infrared	CO_2
Beckman Model 864	Infrared	CO
Horiba PIR 2000	Infrared	SO_2
Beckman Oxygen Analyzer	Paramagnetic	O_2
Thermo Electron NO-NO_x Analyzer Model 10	Luminescence	NO-NO_x
Hewlett Packard G.C.	Thermal Conductivity	CH_4
Model 5880 A	Flame Ionization	H.C.

Table 2.2 Instrumentation for Solids Analysis

Instrument	Analysis	Sample type
Fisher Coal Analyzer Model 490	moisture	all
	volatiles	fuel
	fixed carbon	fuel
	ash = (100%-LOI)	all
Fisher Sulfur Analyzer Model 475	sulfur	* all
Leco CHN Determinator Model 600	CHN	all
Fisher Accumet pH Meter Model 825 MP	calcium	** all
Parr Bomb Calorimeter Model 13031	calorific value	*** fuel
Ro-Tap Sieve Shaker Model B and Tyler Sieve Series	particle size	all

* includes composite fuel ash samples

** analysis of fuel performed on above composite

*** analyses performed on three median samples, with respect to ash content

3. OPERATING PROCEDURES

3.1 Cold startup

The normal procedure for startup from cold conditions was as follows:

1. Attach the lightup burner to the combustor.

2. Charge the combustor with bed material from a previous run (or, lacking that, with limestone), in quantity 80--100 % of the expected steady-state holdup. To minimize the time required to reach steady state, the material should be as similar as possible to that expected from the current run.

3. Fully close the pre-baghouse heat exchanger (T6HE) bypass valve, Fig. 2.1, directing the whole exhaust gas flow through this exchanger.

4. Fully open the baghouse bypass valve, Fig. 2.1, directing the whole exhaust gas flow around the baghouse.

5. Establish cooling water flows to all heat exchangers and cooling jackets.

6. Establish a fluidizing airflow sufficient to give good agitation, typically a fluidizing velocity under cold conditions around 0.4 m/s (corresponding to 1.5 m/s at 850 °C).

7. Establish normal operating flows of recycle air and solids feedline (air-lock valve) purge air.

8. Start the lightup burner at low fire. Increase the firing rate at 150 °C and 300 °C bed temperature.

9. Commence feeding coal and limestone at 600 °C bed temperature.

10. When it reaches 850 °C, slump the bed (turn off the fluidizing and recycle air flows and coal and limestone feeds), quickly disconnect the lightup burner, and cover its port in the combustor with a blind flange.

11. Restart the airflows, with the fluidizing air at the expected operating level. Recommence feeding coal and limestone.

12. Attach the bed product cooler (water-cooled auger) and, at its discharge, a product collection barrel.

13. Adjust the air, coal and limestone feedrates to produce the desired steady-state operating conditions. Most commonly, in the present work, the operating bed temperature, excess air level, and Ca/S ratio were fixed and the flows were adjusted to meet these.

14. When the bed depth reaches its expected (or planned) steady-state value, as indicated by the bed pressure drop, open the valve at the bed-solids discharge port and commence removing bed material to maintain constant bed depth. In the present work, bed depth was regulated by overflow, using the overflow port located 1.2 m above the distributor. Note that limestone feeding in steps 7--12 did not always follow the indicated normal pattern; the limestone feedrate was generally manipulated

as necessary to produce the expected steady-state bed depth before being adjusted to give the desired Ca/S ratio.

15. Adjust the bypass valve on the pre-baghouse heat exchanger (partly bypassing some of the exhaust gas flow around the heat exchanger) so that the temperature of the recombined streams after the exchanger is appropriate for the baghouse (normal operating temperature 150 °C, maximum 200 °C). Then close the baghouse bypass valve, directing the full exhaust gas flow through the baghouse.

16. In startup and in subsequent operation, adjust all cooling water flows so exit temperatures are no higher than 60 °C. This rule ensured avoidance of boiling. Finally, adjust the cooling water flowrates through the bed-cooling heat exchange devices (in-bed tubes, combustor tube-wall cooling jackets) so as to allow reasonably accurate readings of both water flowrates and temperature rises.

Figure 3.1 shows a representative record of bed temperature. The time required to reach operating temperature was typically 2-1/2 to 3 hr. Higher rates of temperature rise are attainable but dangerous to the refractory walls of the combustor.

3.2 Hot start of a run

Whenever possible, several runs were conducted in series without stoppage between runs. This saved the time otherwise

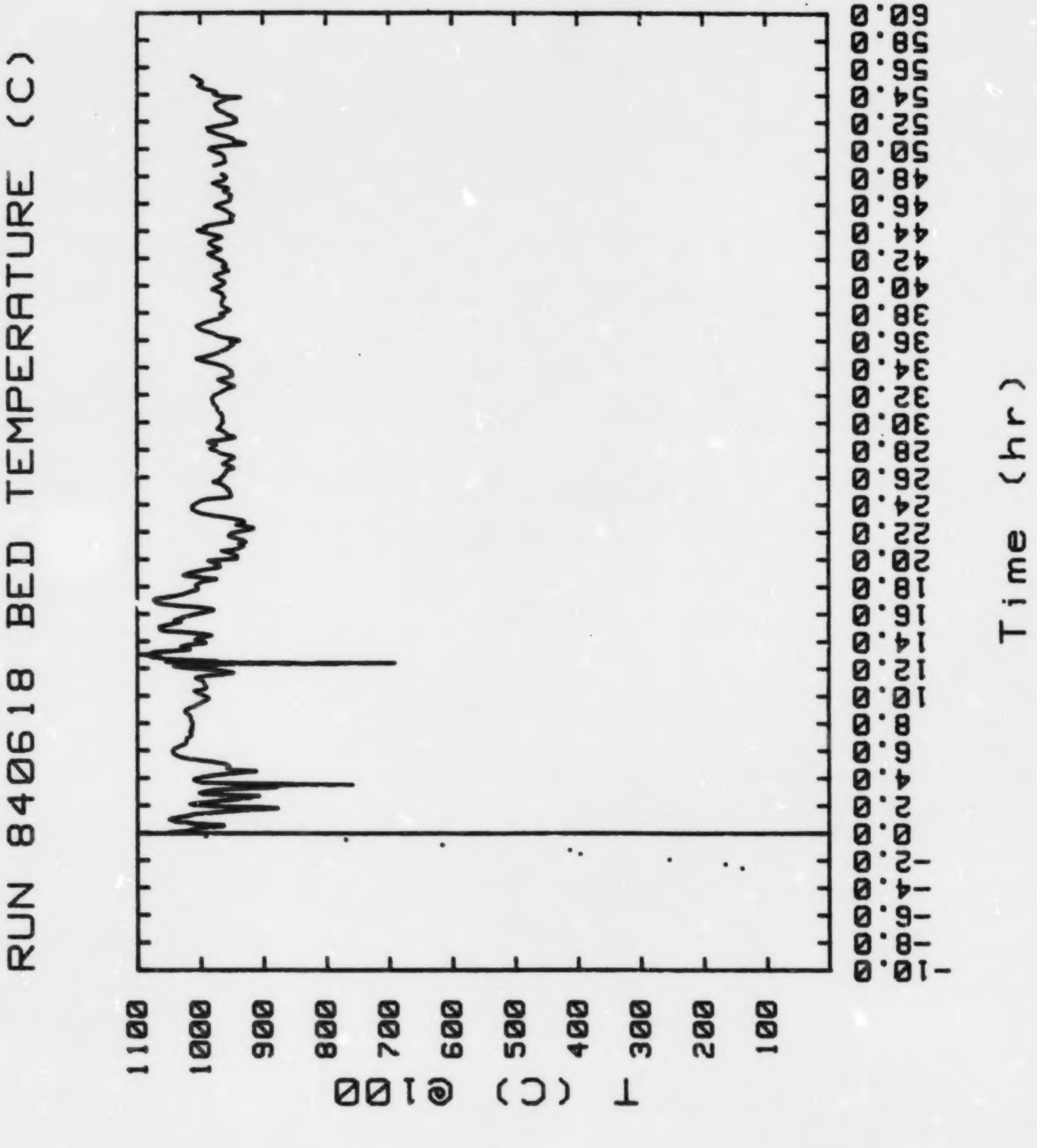

Fig. 3.1. Representative record of bed temperature.

required for startup from cold conditions and increased production (runs completed per week). The input variables which may be changed from one run to the next are limestone particle size, Ca/S ratio (through limestone feedrate), coal particle size, bed temperature, and/or cyclone solids recycle ratio. The simplest adjustment to make and the one usually made in the current work was to change the cyclone solids recycle ratio. The coal burning rate could not be changed significantly, the bed cooling surface (primarily the in-bed heat exchange tubes) being fixed.

3.3 Procedure during runs, after startup

Full data collection generally began with the start of bed-solids removal. Thereafter the following variables were recorded at suitably close intervals:

- weights of the coal and limestone feeder hoppers, to determine the feedrates of coal and stone
- cooling water temperatures and flowrates
- air temperatures and data for determining air flowrates (manometer readings indicating pressure drop across orifices, etc.)
- solid effluent production (bed solids, cyclone dust, baghouse dust). Bed solids were collected in a barrel for a period of 1-1/2 to 6 hr (depending on the production rate and the planned duration of the run). The barrel

was then replaced and the mass of bed material collected was determined by weighing. The same procedure was followed with the cyclone product. The baghouse product, however, accumulated in the baghouse hopper over the entire duration of a run and was dumped and weighed only at the end. The production rate of baghouse dust was usually low (1--3 kg/hr) and the baghouse dust collection hopper was thus too crude a device to allow meaningful determination of that rate by dumping at relatively short intervals.

- the mass recycle rate of cyclone dust. Determined by diverting the recycle flow into a sampling cell for a short time. Sampling times ranged from 15 s to 180 s.
- gas composition at combustor exit (O_2, CO, CO_2, SO_2, NO, NO_x, unburnt hydrocarbons). The only unburnt hydrocarbon in detectable quantities in the current work was CH_4.
- temperatures in bed and freeboard and at other critical points in the system as indicated by fixed thermocouple probes
- static pressures in the windbox, at several levels in the bed, and at other significant points in the system.

3.4 Criteria for the approach of steady state conditions

To ensure that runs were carried on sufficiently long so that the steady state was approached closely enough to yield results representing that state with negligible error, emphasis was placed on the length of operating time relative to the residence time of solids in the bed. An obvious estimate of such a residence time is

$$\tau_p = m_b/\dot{m}_p \tag{3.1}$$

$$\dot{m}_p = \dot{m}_b + \dot{m}_c + \dot{m}_h$$

where m_b is the mass of solids in the bed (the mass holdup) and $\dot{m}_p$ is the total mass efflux of product solids, the sum of the bed product flux $\dot{m}_b$ (bed material withdrawn by overflow or mechanical extraction), the cyclone product flux $\dot{m}_c$, and the baghouse product flux $\dot{m}_h$. This estimate is, however, rather naive. A worst-case estimate would have it that bed product, cyclone product, and filter product all have different residence times, but those of the latter two are very small and their contributions to the holdup are correspondingly small. Hence emphasis should be placed on the residence time of bed product,

$$\tau_b \simeq m_b/\dot{m}_b \tag{3.2}$$

One of the useful features of gas-fluidized beds is the vigorous agitation and mixing of the bed produced by fluidization.

For the present argument, it is reasonable to suppose that the mixing is virtually perfect. The residence time distribution of bed product is then

$$F(\tau) \simeq \exp\left(-\tau/\tau_b\right), \qquad (3.3)$$

where $F(\tau)$ is the probability that a particle will stay in the bed for a time τ after entering it (or, for a collection of particles leaving the bed, $F(\tau)$ is the fraction that were in the bed for a time less than τ). The consequence of this is that if we consider the particles that are in the bed at a given time t, a mass fraction $1/e = 0.368$ of these will still be there at time $t + \tau_b$. After two residence times τ_b, the fraction remaining is $1/e^2 = 0.135$, and after three it is $1/e^3 = 0.050$. One may thus conclude that if t is the operating time from the instant when the approach to steady state is begun, then at $t + 2\tau_b$ the system must be very close to steady state, and at $t + 3\tau_b$ it should be fully arrived by any reasonable definition. This is a valid conclusion for our system because the establishment of a full population of particles with steady-state characteristics, which effectively happens when the initial population has been flushed out, is the slowest step in the approach to steady state. Other processes, the slowest of which is the heating of the refractory combustor walls to the point where they take negligible heat from the bed, are all considerably faster. In this argument, the starting time for operation towards the steady state may be practically regarded as the time at which removal of bed material is begun and bed turnover thus initiated. At this time the bed temperature in our work was generally near the desired level, and the coal and limestone feedrates were at or near their final set points. The act of starting continuous removal of material from the bed to maintain a constant holdup marked the initiation of fully continuous operation. We shall hereinafter call the operating time measured from this instant the COT time (Continuous-mode Operating Time).

Our earlier work (see Section 5, Becker and Code, 1983) shows that the above criterion for attainment of steady state conditions was always sufficient, and often more than enough. For example, when a run was begun hot, with no significant interruption between it and the preceding run, and the change of operating conditions was a comparatively mild one such as a change of coal particle size, then the system effectively equilibrated after a COT time lapse as short as one residence time τ_b. However, it was also clear that the rule of "steady state at $2\tau_b$--$3\tau_b$" should normally be adhered to. In-run indications of steady state from temperatures and gas analyses can be seriously misleading. As indicated above, it is the particle characteristics that take longest to equilibrate, and since the solids chemical analyses could not be done during a run, only after, the final and decisive judgment on the effective arrival of steady state could only be made retrospectively.

The question of reaching the steady state is of great importance. Practically, it is steady-state data that are most wanted and needed. Transient-state data are also desired, of course, in regard to questions of control, stability, load-following, fuel-changing, etc., but then the experiments should be designed to answer questions about the particular types of transients that are of interest.

3.5 Post-shutdown measurements

When the system had been shut down and cooled, the windbox was dropped and the bed material was collected, passed through a 1/4-inch screen and both fractions were weighed. The screening of the bed material, which was normal procedure in the preparation of the initial charge of solids to the combustor, also allowed the determination of the mass fraction of large particles. The mass fraction of large particles was used as a measure of the significance of stratification during operation with the accumulation of unfluidizable or poorly fluidized particles at the bottom of the bed.

3.6 Manpower and scheduling considerations

The frequent need for long runs to ensure close approach to steady state, and the efficient practice of conducting several runs in series without stoppages between, meant that manpower had to be deployed in shifts. The minimum shift size was two workers. Because the normally available manpower was sufficient only for two shifts, a twelve-hour shift length was usually used.

During the hot summer months when additional manpower became available through the employment of students, the shift length was reduced to eight hours. The operating time per week was then between 24 and 72 hours, depending on the nature of the runs involved. When feeding coal of large particle diameter, for example, accumulation of "rocks" (unfluidizable large stone particles) in the bed usually forced relatively early shut-down to allow removal of this material.

4. MATERIALS: FUELS, LIMESTONE SORBENTS AND PRODUCT SOLIDS

4.1 Introduction

The feed materials used in this project cover a variety of solid fuels and limestone sorbents. If the various size fractions are considered separately, eight fuels and eight sorbents were used. The fuels and limestones, with the exception of the Kentucky No. 9 coal and Reed limestone and the Syncrude coke and Athabasca limestone, are from the maritime provinces of Nova Scotia and New Brunswick. The Kentucky No. 9 coal and Reed limestone are used as feed materials at the Tennessee Valley Authority's (TVA's) 20 MW, pilot, fluidized-bed, power plant at Paducah, Kentucky. Syncrude coke, a potential energy source which is currently being stockpiled, is a byproduct of Esso's synthetic crude oil process at Ft. McMurray, Alberta. Athabasca limestone is quarried locally in the Ft. McMurray area.

Evans coal (Inverness County, Nova Scotia) is ranked as high-volatile B bituminous with a free swelling index (FSI) of 1 to 2 (ASTM classification) while Devco coal (Cape Breton, Nova Scotia) is ranked as high-volatile A bituminous with a FSI in the range of 5 to 8 (Tibbetts and Montgomery, 1976). Adibhatla and Jones (1984) give a FSI of 6.5 for Western Kentucky No. 9 coal. The sulphur content of the fuels used range from 4--5% for Devco and Kentucky No. 9 coals to 6--7% for Evans coal and Syncrude coke. With this high a sulphur content treatment of the combustion products is required for the removal of SO_2.

Some representative chemical analyses and particle size distributions of the three streams of product solids are also included in this section of the report.

4.2 Fuels

4.2.1 Sources and preparation of the fuels

The Evans coal was purchased from the Evans Coal Mines Ltd., Inverness County, Nova Scotia. The coal was supplied in three sizes: -1 1/4 inch (fuel used at Summerside, P.E.I., fluidized-bed, thermal plant); -3/4 +1/4 inch (stocker pea); and -1/4 inch (fines).

The Syncrude coke was supplied by Syncrude Canada Ltd., Ft. McMurray, Alberta. The coke feed was prepared by passing the material through a 1/4-inch screen to remove oversize agglomerates.

The Western Kentucky No. 9 coal was purchased from the Tennessee Valley Authority, Paducah, Kentucky. The -2-inch coal was crushed in a roll mill and screened through a 1/4-inch screen by a local Kingston quarry operator. The -1/4-inch fraction was used as feed material. The larger size fraction was barrelled and placed in storage.

The Devco coal was supplied by the Cape Breton Development

Corporation (CBDC), Sydney, Nova Scotia. The -2-inch material was crushed and screened as described above for the Kentucky No. 9 coal. Two size fractions were used as feed: -1/4 inch and -3/4 +1/4 inch.

4.2.2 Proximate/Ultimate analyses

Proximate analyses, sulphur analyses and carbon, hydrogen, nitrogen (CHN) analyses were performed on samples of the various fuels in the QAFBC Laboratory. The results are summarized and compared with analyses obtained by other workers in Table 4.1 through Table 4.8. Minto coal (Becker and Code, 1983) which was used as a fuel in one run (840501) has been included in the summary. The analyses are on a dry basis and published values have been converted to this basis for comparison. Note that allowance was made for the sulphur content of the ash in estimating the oxygen content by difference. Analyses, obtained by commercial analysts, for the various forms of sulphur present in Syncrude coke and Kentucky No. 9, Minto and Devco coals are included in the summaries.

4.2.3 Ash analyses

For convenient reference the ash analyses have been included along with the proximate/ultimate analyses in Table 4.1 through Table 4.8. Our analyses were restricted to calcium and sulphur. More complete analyses reported by other workers have been included in the summaries.

4.2.4 Higher heating values

Higher heating values (HHV) on an ash-free and moisture-free basis (calorific value of combustible matter) of the fuels are given in Table 4.1 through Table 4.8. The values reported were determined in the QAFBC Laboratory using a Parr combustion calorimeter. The results reported by other workers have been converted to an ash-free moisture-free basis for comparison.

4.2.5 Ash fusion temperatures and free swelling indexes

Published values of the ash fusion temperatures and free swelling indexes for the fuels are summarized in Table 4.9 and Table 4.10. Fusion temperatures for Syncrude coke and Devco coal are listed for both reducing conditions and oxidizing conditions. Reducing conditions apply to the values listed for the other fuels. Since corresponding temperatures are higher under oxidizing conditions than under reducing conditions, agglomeration and subsequent clinker formation should not be a problem under normal operation (oxidizing conditions, absence of hot spots) in the optimum temperature range for sulphur capture.

4.2.6 Particle size distributions

Particle size distributions determined by sieve analysis are summarized in Table 4.11. The particle diameter $\hat{D}_p$ which we have used to characterize a size fraction is listed in the column $F_D = 0.5$, i.e., the particle diameter corresponding to a mass fraction undersize of 0.5. The particle size distributions for the 8 fuels are also illustrated graphically on log-probability

Table 4.1 Chemical analyses of Evans coal, nominal size -1/4 inch.

Proximate/Ultimate Analysis
(weight %, dry basis)

Reporter	QAFBC[a]	TM[b]	
MOIS	2.3	5.5	
ASH	17.0	15.7	
VCM	34.1	37.7	
FCM	48.9	46.7	
C	67.6	65.0	
H	4.3	4.2	
N	1.1	1.3	
S	6.4	6.2	
O	4.5	7.6	
HHV (MJ/kg)	32.8	31.8	(ash-free and moisture-free basis)

Ash Analysis
(weight %, ignited basis)

Reporter	QAFBC[a]	TM[b]
SiO_2		24.5
Al_2O_3		13.8
Fe_2O_3		23.0
TiO_2		0.4
CaO	7.4	15.3
MgO		1.3
Na_2O		1.8
K_2O		1.5
SO_3	12.8	19.2
P_2O_5		0.7

---

[a] Present lot of coal, average of eleven samples. Oxygen, O, estimated by difference with allowance for the sulphur, S, content of the ash.

[b] Tibbetts and Montgomery (1976), average of three samples (ERL No. 2092-76, 2095-75 and 4006-74).

Table 4.2 Chemical analyses of Evans coal, nominal size -3/4 +1/4 inch.

Proximate/Ultimate Anaysis
(weight %, dry basis)

Reporter	QAFBC[a]	TM[b]	
MOIS	1.9	5.7	
ASH	11.7	12.5	
VCM	35.0	37.2	
FCM	53.4	50.3	
C	70.2	67.6	
H	4.5	4.5	
N	1.2	1.4	
S	6.8	6.7	
O	5.9	7.3	
HHV(MJ/kg)	32.1	32.2	(ash-free and moisture-free basis)

Ash Analysis
(weight %, ignited basis)

Reporter	QAFBC[a]	TM[b]
SiO_2		29.1
Al_2O_3		15.5
Fe_2O_3		37.0
TiO_2		0.5
CaO	4.8	5.7
MgO		0.8
Na_2O		1.9
K_2O		1.5
SO_3	7.1	6.6
P_2O_5		0.9

---

[a] Present lot of coal, average of nine samples. Oxygen, O, estimated by difference with allowance for the sulphur, S, content of the ash.

[b] Tibbetts and Montgomery (1976), average of three samples (ERL No. 2090-76, 2904-75 and 4005-74).

Table 4.3 Chemical Analysis of Evans coal, nominal size -5/4 inch, $\hat{D}_p$ 16.7 mm.

Proximate/Ultimate Analysis
(weight %, dry basis)

Reporter	QAFBC[a]	
MOIS	2.0	
ASH	12.3	
VCM	35.4	
FCM	52.4	
C	71.1	
H	4.5	
N	1.2	
S	6.7	
O	4.7	
HHV(MJ/kg)	33.3	(ash-free and moisture-free basis)

Ash Analysis
(weight %, ignited basis)

Reporter	QAFBC[a]
CaO	6.2
SO_3	9.9

---

[a] Present lot of coal, average of eighteen samples. Oxygen, O, estimated by difference with allowance for the sulphur, S, content of the ash.

Table 4.4 Chemical analyses of Syncrude coke.

Proximate/Ultimate Analysis
(weight %, dry basis)

Reporter	QAFBC[a]	ERL[b]	SC[c]
MOIS	1.4	1.6	1.6
ASH	6.9	6.7	7.1
VCM	6.4	6.8	-
FCM	86.7	86.5	-
C	83.7	82.0	79.9
H	1.6	1.4	1.9
N	1.9	2.1	1.7
S	6.8	7.0	6.8
O	0	0.8	2.6
HHV(MJ/kg)	32.1	32.2	32.3 (ash-free and moisture-free basis)

Sulphur Forms[d]
(weight %, dry basis)

pyritic	0.007
sulphatic	0.016
organic	6.39
total	6.4

Ash Analysis
(weight %, ignited basis)

Reporter	QAFBC[a]	ERL[b]	SC[c]
SiO_2		44.6	41.3
Al_2O_3		25.2	25.1
Fe_2O_3		10.5	10.9
TiO_2		3.0	3.6
CaO	5.6	5.2	3.9
MgO		1.4	
Na_2O		1.3	
K_2O		1.9	
V_2O_5		3.8	3.7
NiO		1.5	1.3
SO_3	15.6		

---

[a] Present lot of coke, average of the analyses of 16 samples.

[b] Anthony (1984), analysis performed on sample from same shipment as present lot (ERL No. 2651-84).

[c] Heaton (1984), based on composite sample collected from production during two months in 1984.

[d] Analysis of single sample by commercial analyst.

Table 4.5 Chemical analyses of Minto coal.

Proximate/Ultimate Analysis
(weight %, dry basis)

Reporter	QAFBC[a]	TM[b]
MOIS	0.8	3.0
ASH	17.4	18.8
VCM	33.7	32.5
FCM	49.3	48.8
C	68.3	66.3
H	4.1	4.3
N	0.8	0.9
S	7.4	8.0
O	2.4	1.7
HHV(MJ/kg)	34.6	34.9 (ash-free and moisture-free basis)

Sulphur Forms[c]
(weight %, dry basis)

pyritic	3.4
sulphatic	0.8
organic	2.2
total	6.4

Ash Analysis
(weight %, ignited basis)

Reporter	QAFBC[a]	TM[b]
SiO_2		28.3
Al_2O_3		11.1
Fe_2O_3		43.2
TiO_2		0.7
CaO	4.8	3.8
MgO		0.8
Na_2O		2.8
K_2O		0.9
SO_3	7.1	3.5
P_2O_5		2.3

---

[a] Becker and Code (1983), present lot of coal, average of the analyses of nine samples (three samples each from three particle size fractions). Oxygen, O, by difference with allowance for the sulphur, S, content of the ash.

[b] Tibbetts and Montgomery (1976), representative run of mine sample (ERL No. 2073-76).

[c] Analysis of single sample by commercial analyst.

Table 4.6 Chemical analyses of Western Kentucky No. 9 coal.

Proximate/Ultimate Analysis
(weight %, dry basis)

Reporter	QAFBC[a]	IMMR[b]
MOIS	7.1	2.1
ASH	18.0	14.1
VCM	35.0	35.7
FCM	46.9	50.3
C	64.8	71.4
H	4.6	4.8
N	1.3	1.3
S	4.3	4.1
O	7.9	4.3
HHV(MJ/kg)	31.6	32.9 (ash-free and moisture-free basis)

Sulphur Forms[c]
(weight %, dry basis)

pyritic	1.3
sulphatic	1.4
organic	1.9
total	4.6

Ash Analysis
(weight %, ignited basis)

Reporter	QAFBC[a]	IMMR[b]
SiO_2		42.9
Al_2O_3		16.1
Fe_2O_3		25.6
TiO_2		0.9
CaO	9.3	4.4
MgO		1.3
K_2O		2.4
SO_3	11.8	4.4
P_2O_5		0.1

---

[a] Present lot of coal, average of the analyses of fourteen samples. Oxygen, O, by difference with allowance for the sulphur, S, content of the ash.

[b] Adibhatla and Jones (1984), composite sample collected during AFBC trials (No. 40, 41 and 42).

[c] Analysis of one sample by commercial analyst.

Table 4.7 Chemical analyses of Devco coal, nominal size -3/4 +1/4 inch.

Proximate/Ultimate Analysis
(weight %, dry basis)

Reporter	QAFBC[a]	TM[b]	CBDC[c]
MOIS	1.2	4.8	-
ASH	19.7	4.9	16.0
VCM	32.4	38.2	34.7
FCM	47.9	56.8	49.3
C	65.3	80.5	67.8
H	4.2	5.6	5.1
N	1.1	1.6	1.3
S	4.7	3.2	4.8
O	5.7	4.2	5.0
HHV(MJ/kg)	33.3	35.9	33.6 (ash-free and moisture-free basis)

Ash Analysis
(weight %, ignited basis)

Reporter	QAFBC[a]	TM[c]	CBDC[c]
SiO_2		13.8	39.1
Al_2O_3		18.0	22.3
Fe_2O_3		64.9	31.2
TiO_2		0.5	0.3
CaO	7.3	1.2	1.4
MgO		0.3	1.1
Na_2O		0.4	0.5
K_2O		0.5	1.8
SO_3	8.8	1.1	1.4
P_2O_5		0.7	0.3

---

[a] Present lot of coal, average of the analyses of 18 samples.

[b] Tibbetts and Montgomery (1976), one sample (ERL No. 3999-74).

[c] Campbell (1981), composite sample from one week's output (CBDC File No. A81-330).

Table 4.8 Chemical analysis of Devco coal, nominal size -1/4 inch.

Proximate/Ultimate Analysis
(weight %, dry basis)

Reporter	QAFBC[a]	QAFBC[b]	CBDC[c]	TM[d]	
MOIS	3.7	2.4	-	3.1	
ASH	20.0	20.0	16.0	19.6	
VCM	31.9	33.6	34.7	33.2	
FCM	48.1	46.5	49.3	47.2	
C	64.7	64.7	67.8	67.3	
H	4.4	4.1	5.1	4.8	
N	1.2	1.1	1.3	1.4	
S	4.3	5.4	4.8	2.8	
O	5.5	4.7	5.0	4.1	
HHV(MJ/kg)	32.9	31.5	33.6	35.3	(ash-free and moisture-free basis)

Sulphur Forms[e]
(weight %, dry basis)

pyritic	2.1
sulphatic	0.5
organic	1.6
total	4.2

Ash Analysis
(weight %, ignited basis)

Reporter	QAFBC[a]	QAFBC[b]	CBDC[c]	TM[d]
SiO_2		41.6	39.1	50.6
Al_2O_3		23.8	22.3	28.5
Fe_2O_3		23.7	31.2	12.9
TiO_2			0.3	0.5
CaO	7.3	1.0	1.4	0.6
MgO		0.1	1.1	1.0
Na_2O		0.2	0.5	0.7
K_2O		0.1	1.8	3.6
SO_3	1.8		1.4	0.4
P_2O_5			0.3	0.0

---

[a] Present lot of coal, average of the analyses of thirteen samples.

[b] Becker and Code (1983), analysis by commercial analyst on previous lot of coal.

[c] Campbell (1981), composite sample from one week's output (CBDC File No. A81-330).

[d] Tibbetts and Montgomery (1976), one sample (ERL No. 4001-74).

[e] Analysis of one sample by commercial analyst.

Table 4.9 Ash fusion temperatures and free swelling indexes of fuels.

Fuel	Evans	Minto	Syncrude	Syncrude
Reporter	TM[a]	TM[b]	ERL[c]	ERL[c]
Conditions	Reducing	Reducing	Reducing	Oxidizing
IT, °C	1075	1066	1276	1182
ST, °C	1114	1099	1315	1362
HT, °C	1203	1138	1360	1382
FT, °C	1271	1216	1443	1482
FSI	1.5	5.0		

IT, initial deformation temperature

ST, spherical softening temperature

HT, hemispherical softening temperature

FT, fluid temperature

FSI, free swelling index

[a] Tibbetts and Montgomery (1976), average values for three samples, -3/4 +1/4 inch (ERL No. 2090-76, 2904-75, and 4005-74).

[b] Tibbetts and Montgomery (1976), representative run of mine sample (ERL No. 2073-76).

[c] Friedrich et al (1982).

Table 4.10 Ash fusion temperatures and free swelling indexes of fuels.

Fuel	KY No.9	Devco	Devco	Devco
Reporter	IMMR[a]	TM[b]	CBDC[c]	CBDC[c]
Conditions	Reducing	Reducing	Reducing	Oxidizing
IT, °C	1087	1121	1091	1259
ST, °C	1101	1177	1141	1319
HT, °C	1117	1193	1186	1368
FT, °C	1212	1321	1310	1406
FSI	6.5	5.5		

IT, initial deformation temperature

ST, spherical softening temperature

HT, hemispherical softening temperature

FT, fluid temperature

FSI, free swelling index

[a] Adibhatla and Jones (1984), composite sample collected during AFBC trials (No. 40, 41 and 42).

[b] Tibbetts and Montgomery (1976), single sample, -3/4 +1/4 inch, (ERL No. 3999-74).

[c] Campbell (1981), composite sample from one week's output (CBDC File No. A81-330).

Table 4.11 Particle size distributions of fuels

		Fraction by mass undersize, F_D					
		0.02	0.10	0.20	0.50	0.80	0.95
Fuel	Nominal size (inches)	Particle diameter determined by sieve analysis, mm					
Evans	-1/4	0.07	0.52	1.17	3.34	6.77	10.25
Evans	-3/4 +1/4	0.27	2.41	5.13	8.82	11.57	14.60
Evans	-5/4	3.54	8.62	11.68	16.72	21.81	25.80
Syncrude		0.084	0.14	0.17	0.26	0.32	0.55
Minto	-7/8	0.21	2.15	4.45	10.06	16.19	19.28
Kentucky No. 9	-1/4	0.16	0.45	0.80	2.28	4.42	6.29
Devco	-3/4 +1/4	1.50	6.35	7.79	11.20	16.84	22.39
Devco	-1/4	0.058	0.26	0.61	2.09	4.22	6.40

plots in Fig. 4.1 through Fig. 4.4.

4.3 Limestone sorbents

4.3.1 Sources and preparation of sorbents

The Havelock limestone sorbents were supplied in three size fractions by Havelock Lime Works, Havelock, New Brunswick. The -6 +20 mesh fraction and the -10 mesh fraction were shipped in bags. The -16 +100 mesh fraction was shipped in bulk, barrelled and placed in storage for later use.

The Athabasca limestone, quarried in the Ft. McMurray area of Alberta, was shipped in barrels and screened to -14 mesh at the QAFBC Laboratory. The oversize fraction was crushed and screened to -12 mesh by a local Kingston quarry operator.

The Reed limestone was shipped in bulk as -3-inch material by the Tennessee Valley Authority from their pilot, fluidized-bed, power plant at Paducah, Kentucky. The stone was then crushed and screened to -8 mesh by a local Kingston quarry operator.

The Sysco limestone, quarried at Irish Cove, Cape Breton, was supplied by the Sydney Steel Co., Sydney, Nova Scotia. The material was shipped in bulk as -3/16 inch, 'fines' rejects from steel mill operations and screened to -8 mesh at the QAFBC Laboratory. The oversize fraction was crushed and screened to -8 mesh at the Ontario Research Foundation, Mississauga.

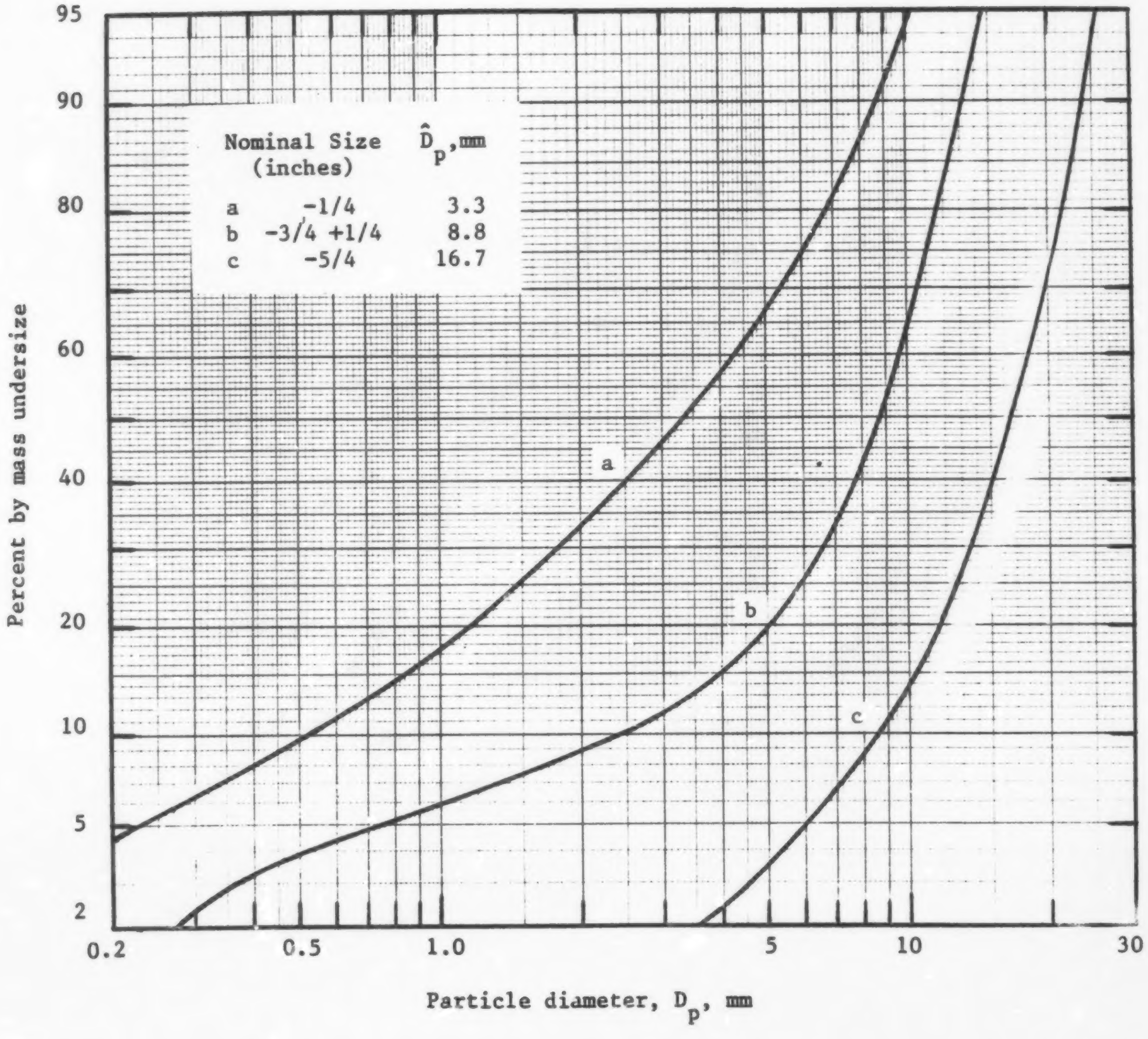

Fig. 4.1 Particle size distributions of the three fractions of Evans coal.

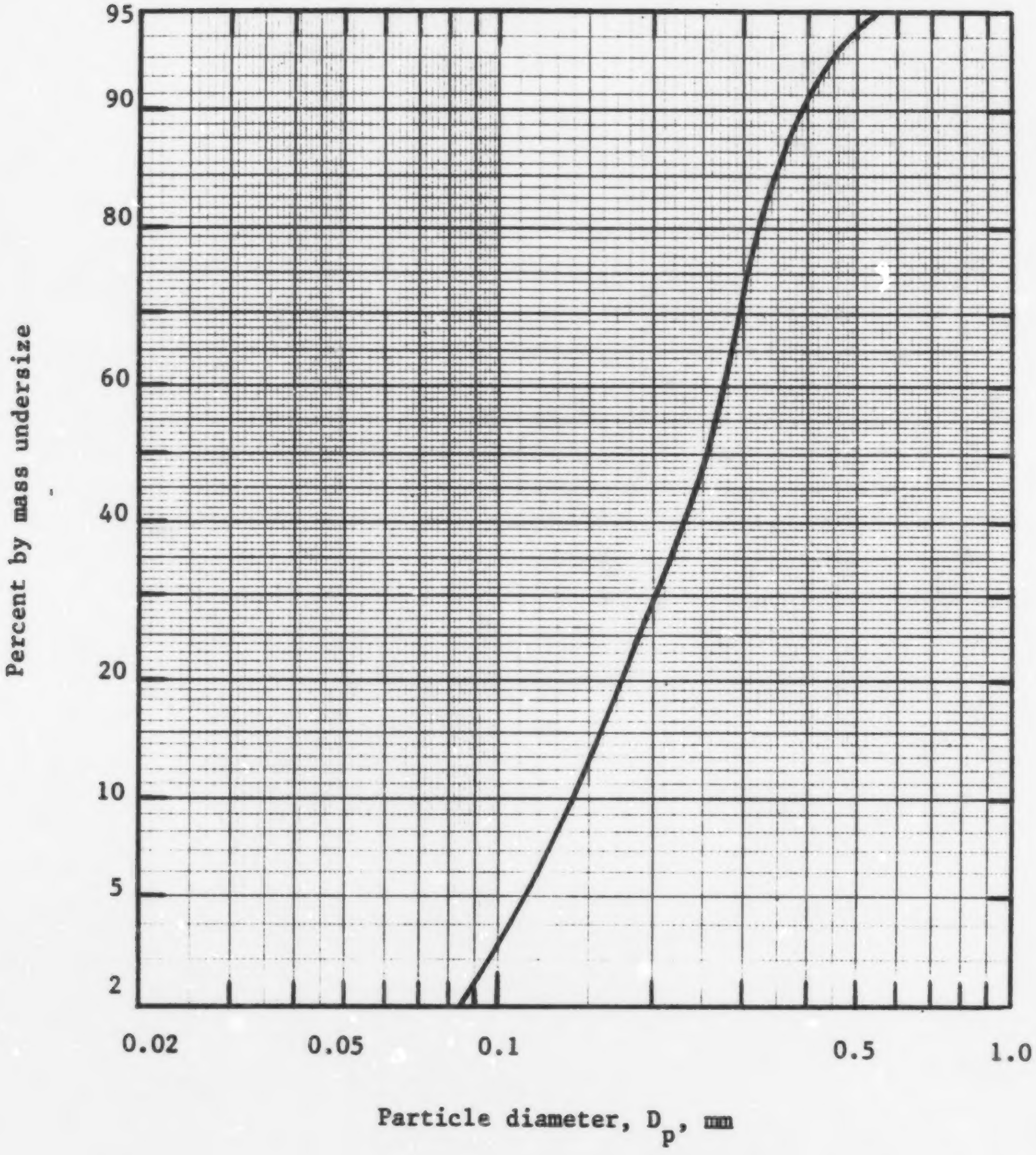

Fig. 4.2 Particle size distribution of Syncrude coke.

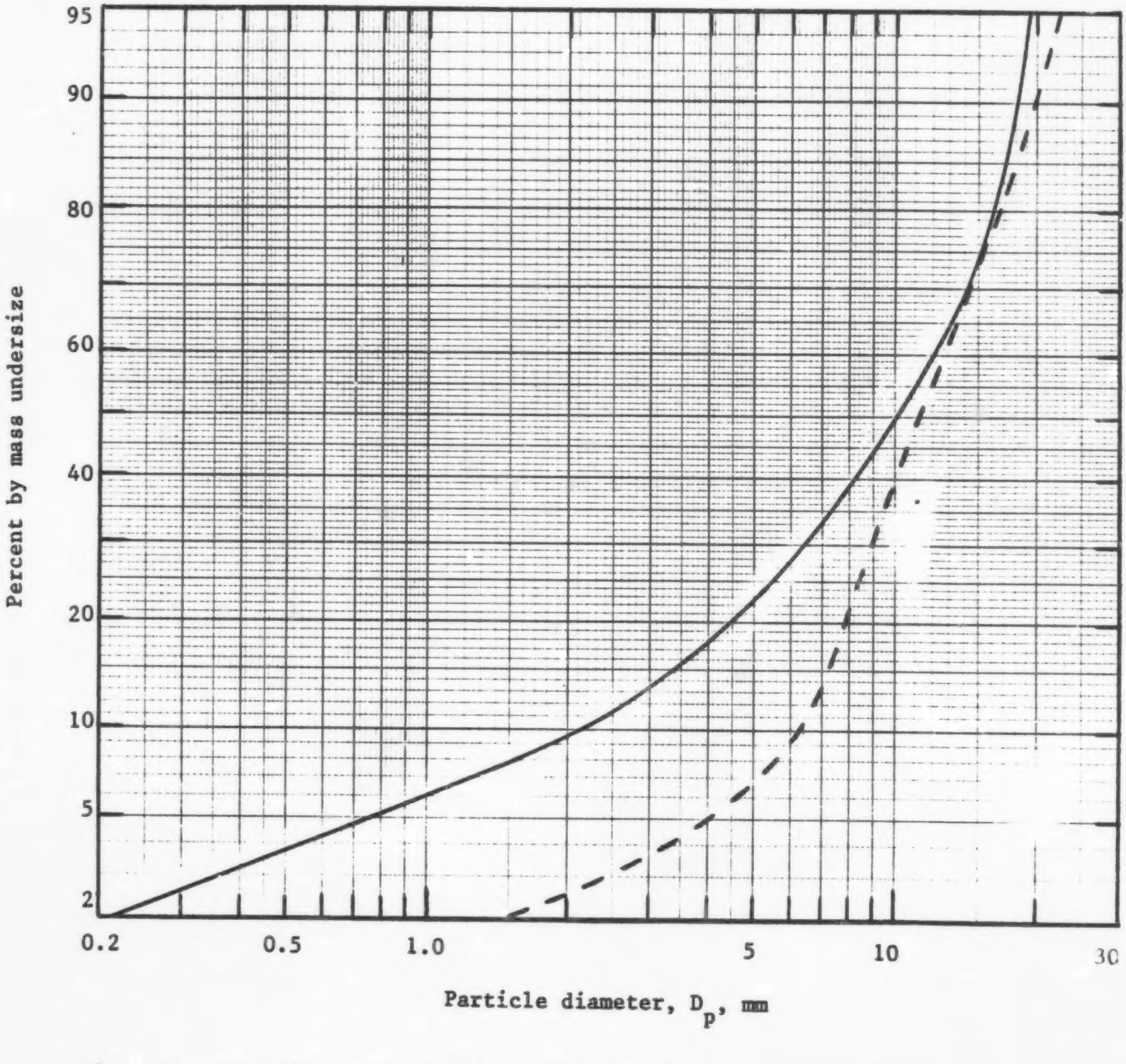

Fig. 4.3 Particle size distributions of Minto and Devco coals.

Key:		Coal	Nominal size (inches)	$\hat{D}_p$, mm
	———	Minto	- 7/8	10.06
	— — —	Devco	- 3/4 + 1/4	11.20

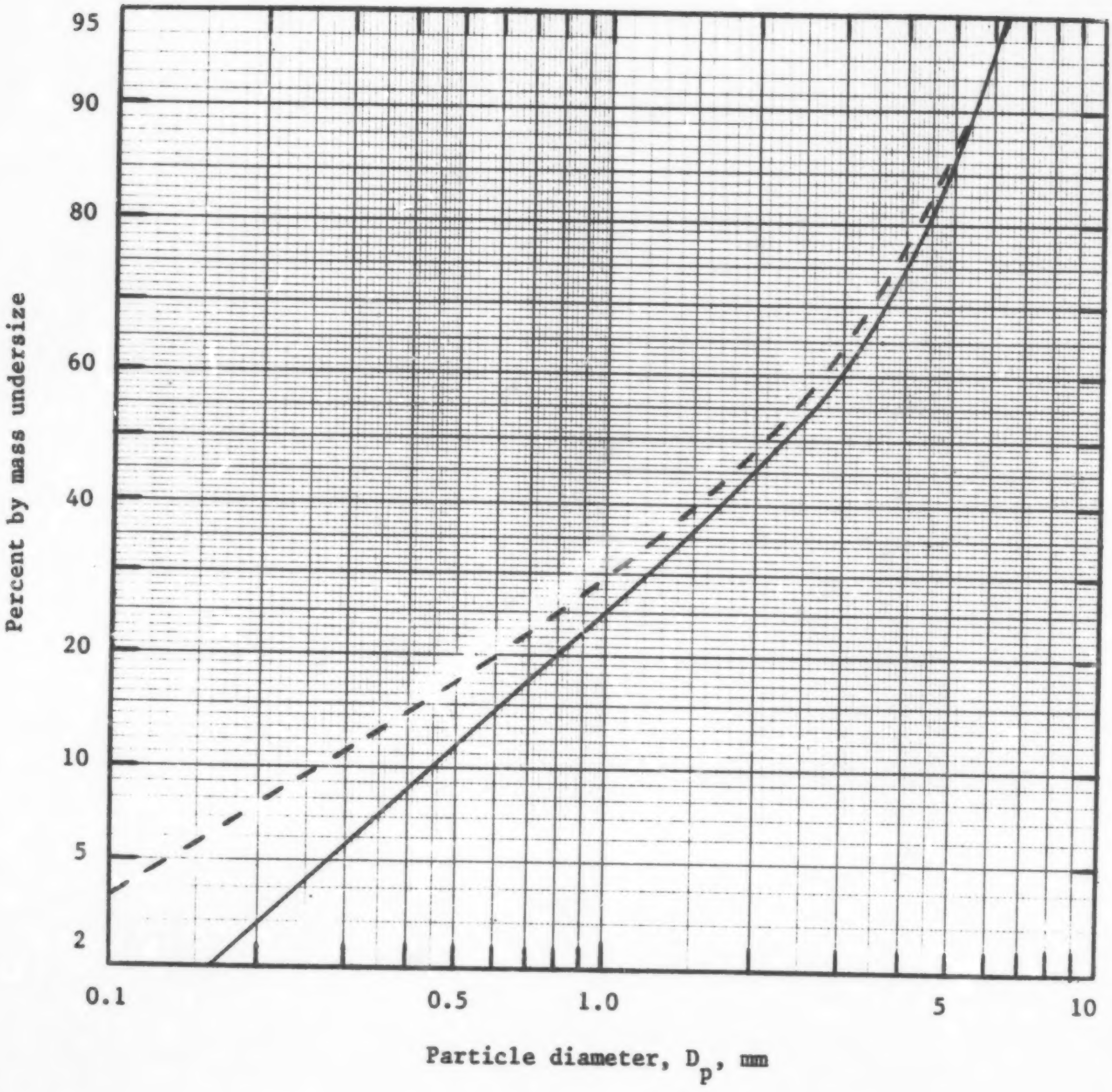

Fig. 4.4 Particle size distributions of Devco and Kentucky No. 9 coals.

Key:	Coal	Nominal size (inches)	$\hat{D}_p$, mm
— — —	Devco	- 1/4	2.09
———	Kentucky No. 9	- 1/4	2.28

The Calpo limestone, quarried at Antigonish, Nova Scotia, was supplied by Havelock Lime Works, Havelock, New Brunswick. The material was shipped in bulk as -1/4 inch and screened to -8 mesh at the QAFBC Laboratory. The oversize fraction was crushed and screened to -8 mesh at the Ontario Research Foundation, Mississauga.

4.3.2 Chemical analyses

Chemical analyses obtained in the QAFBC Laboratory on samples of the five limestones used as SO_2 sorbents are given in Table 4.12 through Table 4.16. The results of other analysts on limestones from the same sources are included in the tables for comparison.

4.3.3 Particle size distributions

Particle size distributions determined by sieve analysis on samples from the 8 size fractions used as SO_2 sorbents are summarized in Table 4.17. The size distributions are also illustrated graphically on log-probability plots in Fig. 4.5 through Fig. 4.7.

Table 4.12 Composition of Havelock limestone, nominal size -16 +100 mesh, $\hat{D}_p$ 0.49 mm.

Reporter	Composition, wt % QAFBC[a]	QAFBC[b]	MSL[c]
MOIS	0.2		
LOI	42.1	42.6	42.2
ASH	57.9	57.4	57.8
CO_2	43.3		
CaO	55.0	54.3	54.1
MgO		0.4	0.4
SiO_2		0.9	2.5
Fe_2O_3		0.5	0.3

[a] Present lot of stone, average of five samples.

[b] Becker and Code (1983), previous lot of stone.

[c] Hamer (1983), average of eight samples (all samples excluding NB-1-4).

Table 4.13 Composition of Reed limestone, nominal size -8 mesh, $\hat{D}_p$ 1.1 mm.

Reporter	Composition, wt % QAFBC[a]
MOIS	0.1
LOI	39.7
ASH	60.3
CO_2	40.3
CaO	48.5

[a] Present lot of stone, average of five samples.

Table 4.14 Composition of Calpo limestone, nominal size - 8 mesh, $\hat{D}_p$ 1.1 mm.

	Composition, wt %	
Reporter	QAFBC[a]	MSL[b]
MOIS	0.8	
LOI	40.4	
ASH	59.6	
CO_2	42.0	
CaO	49.9	53.8
MgO		0.4
SiO_2		1.5
Al_2O_3		0.1
Fe_2O_3		0.3
Na_2O		0.02
K_2O		0.02
SO_3		0.3

[a] Present lot of stone, average of analyses of five samples.

[b] Hamer (1983), sample no. NS-10.

Table 4.15 Composition of Sysco limestone, nominal size - 8 mesh, $\hat{D}_p$ 1.4 mm.

	Composition, wt %		
Reporter	QAFBC[a]	MSL[b]	MSL[b]
MOIS	0.4		
LOI	40.4		
ASH	59.6		
CO_2	42.0		
CaO	50.5	52.9	52.9
MgO		0.5	0.7
SiO_2		1.2	2.4
Al_2O_3		0.3	0.4
Fe_2O_3		0.3	0.6
Na_2O		0.03	0.03
K_2O		0.04	0.04
SO_3		0.05	0.30

[a] Present lot of stone, average of analyses of five samples.

[b] Hamer (1983), sample no. NS-1 and sample no. NS-9.

Table 4.16 Composition of Athabasca limestone.

	Composition, wt %				
Reporter	QAFBC[a]	ERL[b]	COMM[c]	MSL[d]	MSL[d]
MOIS	0.6				
LOI	36.5	35.2			
ASH	63.5	65.8			
CO_2	37.1	33.8			
CaO	44.7	41.2	37.6	51.2	42.4
SiO_2		13.6	20.7	6.0	14.4
Al_2O_3		3.3	4.5	1.3	3.9
Fe_2O_3		1.4	2.0	1.0	1.6
TiO_2		0.3			
P_2O_5		0.1			
MgO		0.0	1.1	1.2	1.2
SO_3		1.4		0.3	
Na_2O		0.0		0.03	0.04
K_2O		1.0		0.2	0.9
BaO		0.1			
SrO		0.02			

[a] Present lot of stone, average of the analyses of ten samples.

[b] Anthony (1984), sample no. FMLS-1.

[c] Analysis of single sample by commercial analyst.

[d] Hamer (1983), sample no. SY-1 and sample no. SY-2.

Table 4.17 Particle size distributions of limestone sorbents

		Fraction by mass undersize, F_D					
		0.02	0.10	0.20	0.50	0.80	0.95
Stone	Nominal size (mesh)	Particle diameter, D_p, determined by sieve analysis, mm					
Havelock	- 6 + 20	0.79	1.14	1.31	1.72	2.27	2.80
Havelock	-16 +100	0.082	0.20	0.29	0.49	0.81	1.80
Havelock	-10	0.024	0.044	0.061	0.16	0.64	1.16
Athabasca	-14	0.06	0.10	0.14	0.34	0.77	1.06
Athabasca	-12	0.07	0.13	0.33	0.94	1.32	1.51
Calpo	- 8	0.17	0.40	0.57	1.07	1.72	2.20
Reed	- 8	0.08	0.20	0.41	1.08	1.82	2.22
Sysco	- 8	0.18	0.36	0.62	1.36	2.17	2.68

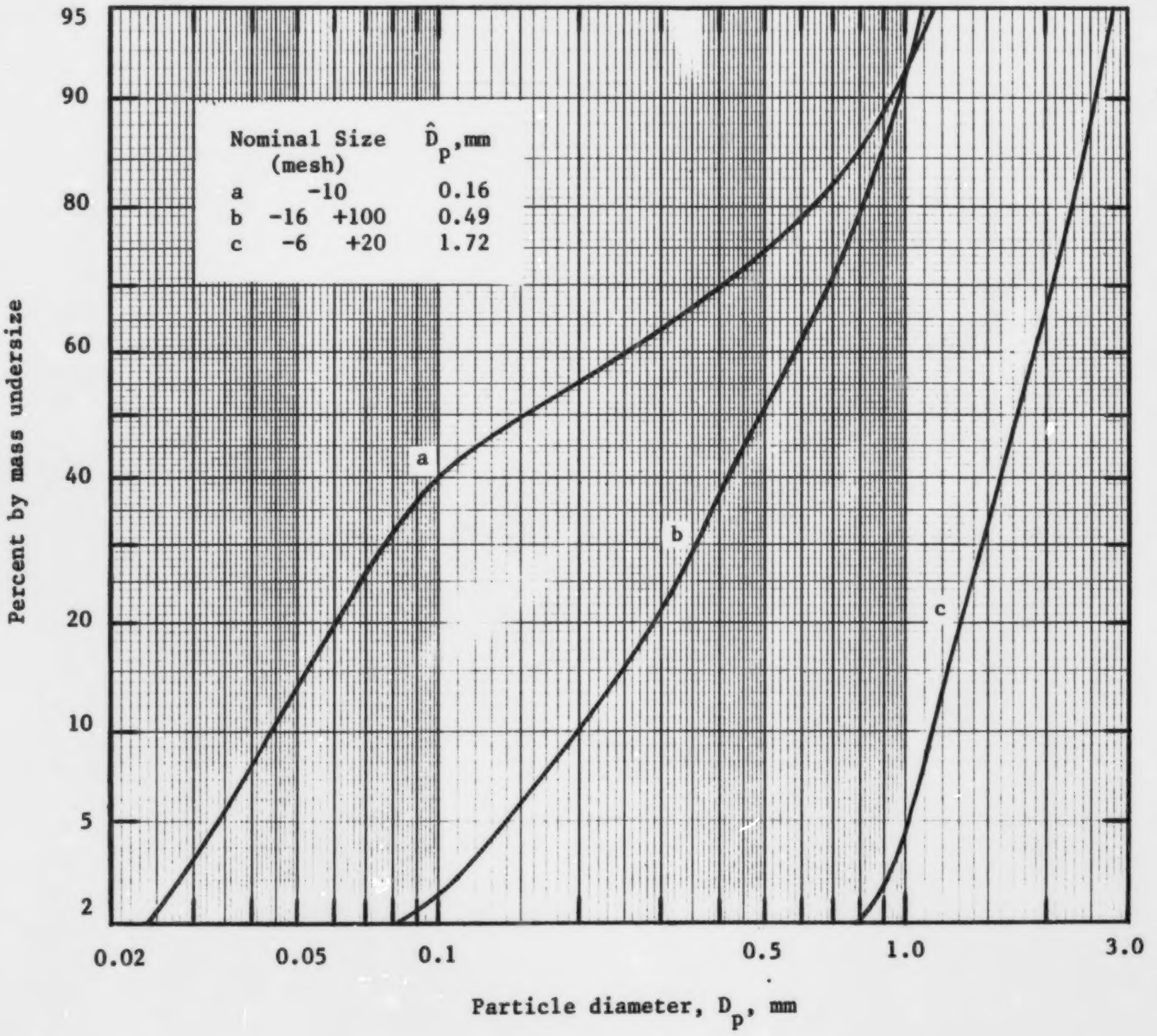

Fig. 4.5 Particle size distributions of Havelock limestone sorbents.

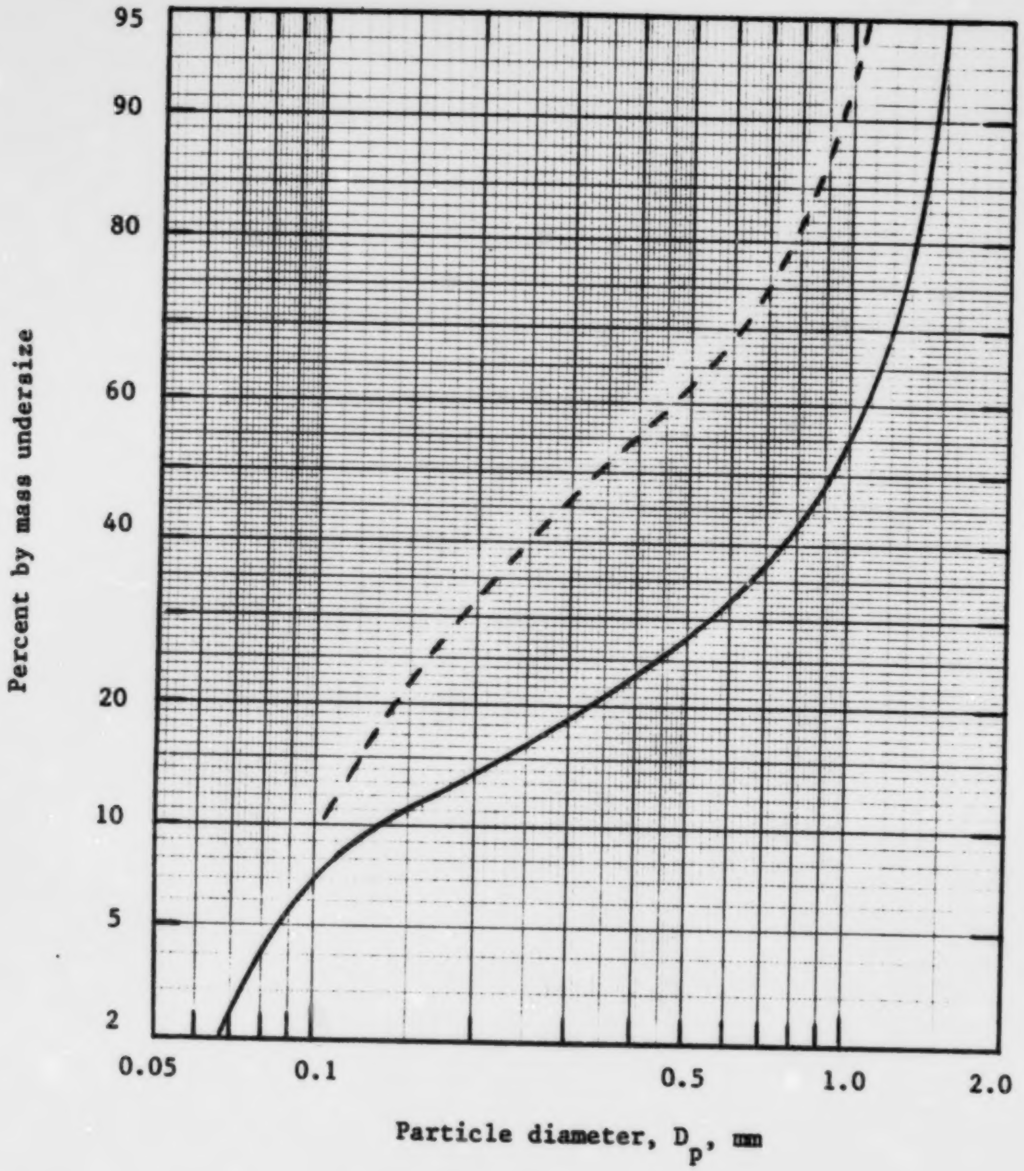

Fig. 4.6 Particle size distributions of Athabasca limestone sorbents.

Key:

	Nominal size (mesh)	$\hat{D}_p$, mm
— — —	- 14	0.34
———	- 12	0.94

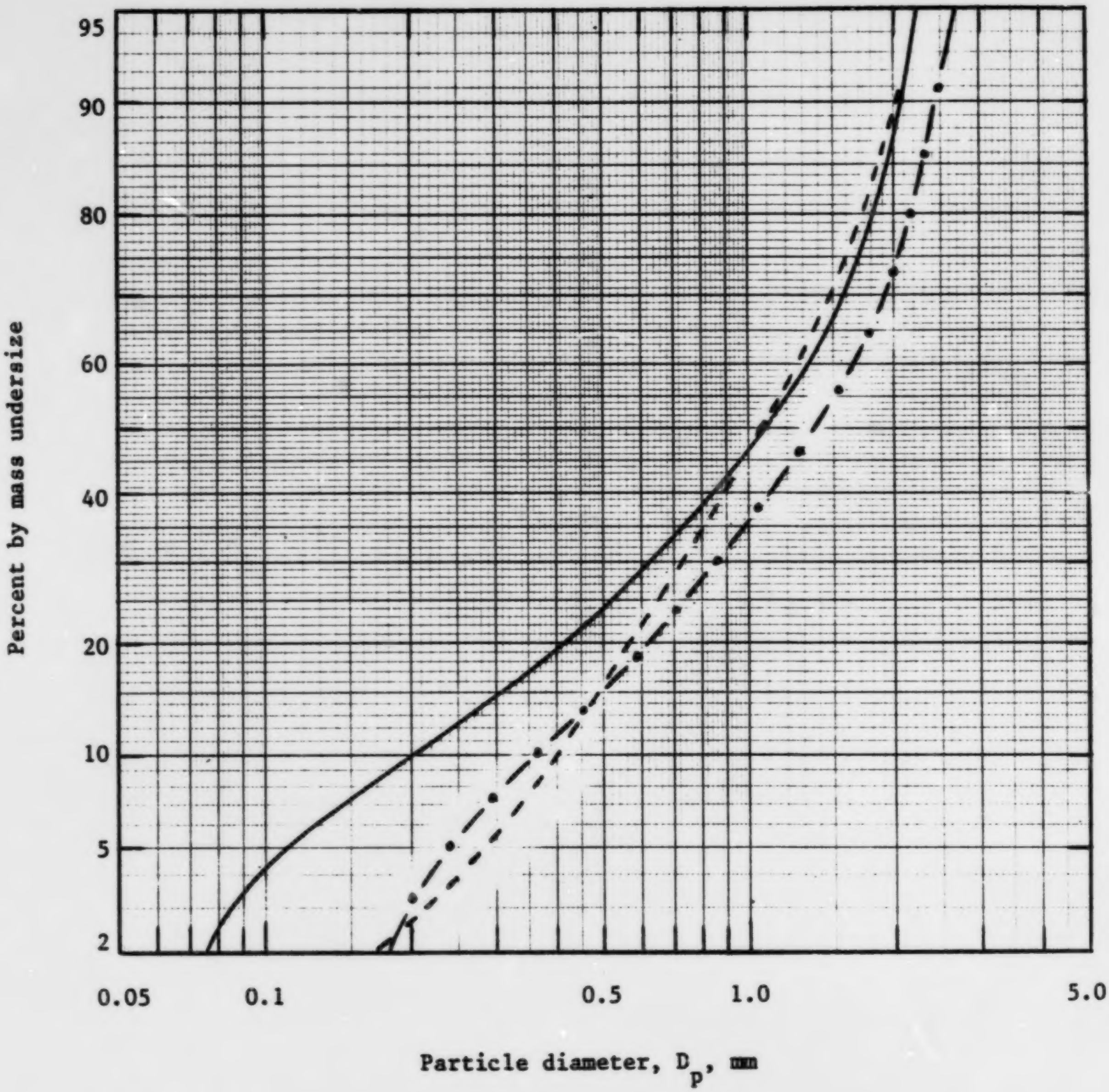

Fig. 4.7 Particle size distributions of Calpo, Reed and Sysco limestone sorbents.

Key:	Stone	Nominal size (mesh)	$\hat{D}_p$, mm
— — —	Calpo	- 8	1.07
———	Reed	- 8	1.08
— • —	Sysco	- 8	1.36

4.4 Product Solids

4.4.1 Chemical analyses and particle size distribution

Chemical analyses of selected samples of the cyclone solids, overflow bed solids and baghouse solids are summarized in Table 4.18 through Table 4.20. Representative particle size distributions of the three streams of product solids are given in Table 4.21 through Table 4.23. This information is included in this section of the report to illustrate the range of chemical concentrations and particle sizes in the product solids. A more complete tabulation is available in the recent report by Becker et al. (1985).

Table 4.18 Chemical analyses of selected samples of cyclone solids.

		Fuel	Sorbent			Weight %, dry basis					
Run No.	Sample No.	$\hat{D}_p$, mm	$\hat{D}_p$, mm	MOIS	LOI	ASH	C	H	N	S	Ca
		Evans	Havelock								
831124	0715-0945	16.7	0.49	0.14	11.96	88.04	10.98	0.43	0.23	6.9	33.7
840105	1015-1315	3.3	1.72	0.03	4.29	95.71	3.83	0.40	0.07	6.9	26.7
840215	0515-0815	8.8	0.49	0.12	11.49	88.51	10.80	0.31	0.17	6.0	26.7
		Syncrude	Athabasca								
840612	0345-0615	0.26	0.34	0.15	16.76	83.24	16.29	0.19	0.27	5.7	28.2
840703	2300-0301	0.26	0.34	0.81	5.66	94.34	6.45	0.00	0.12	5.0	27.5
840814	1455-1845	0.26	0.94	0.31	10.15	89.85	11.15	0.00	0.12	3.7	30.2
		KY No. 9	Reed								
841112	0615-0715	2.3	1.1	0.20	17.47	82.53	14.63	0.10	0.18	2.1	35.3
841119	0350-0423	2.3	1.1	0.24	13.14	86.86	11.89	0.07	0.19	5.2	31.3
		Devco	Sysco								
841127	2145-2320	2.1	1.4	0.21	11.99	88.01	11.96	0.07	0.31	4.0	29.1
850121	0200-0445	11.2	1.4	0.24	19.84	80.16	19.25	0.15	0.41	4.0	--
		Devco	Calpo								
841218	1515-1650	2.1	1.1	0.31	12.75	87.25	12.76	0.08	0.14	4.0	25.3
850115	1035-1300	11.2	1.1	0.00	20.61	79.39	19.45	0.17	0.37	3.6	--

Table 4.19 Chemical analyses of selected samples of overflow bed solids.

Run No.	Sample No.	Fuel $\hat{D}_p$, mm	Sorbent $\hat{D}_p$, mm	Weight %, dry basis							
				MOIS	LOI	ASH	C	H	N	S	Ca
		Evans	Havelock								
831124	0900-1330	16.7	0.49	0.21	1.79	98.21	1.46	0.37	0.03	12.6	37.5
840105	1200-1440	3.3	1.72	0.03	2.97	97.03	1.06	1.00	0.03	8.2	41.0
840215	1500-1635	8.8	0.49	0.00	1.52	98.48	1.41	0.17	0.03	7.8	44.1
		Syncrude	Athabasca								
840612	0430-0630	0.26	0.34	0.07	1.13	98.87	0.96	0.01	0.02	7.7	28.2
840703	0316-0715	0.26	0.34	0.03	1.19	98.81	1.05	0.00	0.00	8.8	30.7
840814	1105-1505	0.26	0.94	0.04	1.75	98.25	1.57	0.02	0.05	6.0	40.3
		KY No. 9	Reed								
841112	0620-0815	2.3	1.1	0.05	3.78	96.22	1.32	0.03	0.02	8.0	36.9
841119	0355-0423	2.3	1.1	0.02	2.19	97.81	0.87	0.04	0.01	9.6	30.9
		Devco	Sysco								
841127	2025-2225	2.1	1.4	0.26	0.65	99.35	0.43	0.00	0.04	8.1	35.5
850121	2100-0100	11.2	1.4	0.01	1.08	98.92	1.02	0.02	0.00	14.7	--
		Devco	Calpo								
841218	1530-1730	2.1	1.1	0.00	0.59	99.41	0.33	0.01	0.04	7.8	39.0
850115	1100-1300	11.2	1.1	0.00	1.56	98.44	1.51	0.00	0.00	11.8	--

Table 4.20 Chemical analyses of selected samples of baghouse solids.

	Fuel	Sorbent			Weight %, dry basis					
Run No.	$\hat{D}_p$, mm	$\hat{D}_p$, mm	MOIS	LOI	ASH	C	H	N	S	Ca
	Evans	Havelock								
831124	16.7	0.49	0.14	10.18	89.82	9.52	0.22	0.28	4.6	11.8
840105	3.3	1.72	0.41	19.67	80.33	17.89	0.40	0.43	4.6	11.8
840215	8.8	0.49	0.62	12.32	87.68	11.34	0.19	0.30	5.0	11.4
	Syncrude	Athabasca								
840612	0.26	0.34	1.16	8.56	91.44	3.54	0.35	0.28	6.1	24.1
840703	0.26	0.34	0.43	4.74	95.26	2.02	0.15	0.15	6.0	22.6
840814	0.26	0.94	1.43	1.70	98.30	0.75	0.05	0.15	7.1	26.4
	KY No. 9	Reed								
841112	2.3	1.1	1.67	13.95	86.05	8.10	0.53	0.07	8.4	13.6
841119	2.3	1.1	0.57	12.92	87.08	11.89	0.16	0.26	5.2	12.2
	Devco	Sysco								
841127	2.1	1.4	1.16	16.04	83.96	12.23	0.16	0.34	4.6	14.4
850121	11.2	1.4	23.06	18.16	81.84	10.18	0.27	0.29	5.1	--
	Devco	Calpo								
841218	2.1	1.1	2.03	15.59	84.41	12.84	0.18	0.36	4.0	9.6
850115	11.2	1.1	32.76	23.09	76.91	10.04	0.33	0.17	5.0	--

Table 4.21 Particle size distributions of cyclone solids.

Fraction by mass undersize, F_D:					0.02	0.10	0.20	0.50	0.80	0.95
Run No.	Fuel	$\hat{D}_p$, mm	Sorbent	$\hat{D}_p$, mm	Particle diameter, D_p, by sieve analysis, mm					
840501	Minto	10.1	Havelock	0.16	0.02	0.03	0.04	0.08	0.26	0.48
840605	Syncrude	0.26	Havelock	0.16	0.02	0.03	0.03	0.07	0.13	0.17
840612	Syncrude	0.26	Athabasca	0.34	0.02	0.04	0.07	0.13	0.18	0.27
840814	Syncrude	0.26	Athabasca	0.94	0.02	0.03	0.04	0.07	0.14	0.23
840820	Syncrude	0.26	Athabasca	0.94	0.02	0.03	0.05	0.10	0.15	0.22
841112	KY No. 9	2.3	Reed	1.1	0.02	0.03	0.05	0.13	0.31	0.52
841119	KY No. 9	2.3	Reed	1.1	0.02	0.03	0.04	0.08	0.19	0.44
841127	Devco	2.1	Sysco	1.4	0.02	0.03	0.04	0.11	0.29	0.46
841204	Devco	2.1	Sysco	1.4	0.02	0.03	0.04	0.08	0.22	0.45
850121	Devco	11.2	Sysco	1.4	0.02	0.03	0.04	0.10	0.22	0.35
850304	Devco	11.2	Sysco	1.4	0.02	0.03	0.04	0.12	0.26	0.41
841218	Devco	2.1	Calpo	1.1	0.02	0.03	0.04	0.09	0.28	0.47
850107	Devco	2.1	Calpo	1.1	0.02	0.03	0.04	0.09	0.21	0.36
850115	Devco	11.2	Calpo	1.1	0.02	0.03	0.04	0.10	0.22	0.34

Table 4.22 Particle size distributions of overflow bed solids.

Fraction by mass undersize, F_D:					0.02	0.10	0.20	0.50	0.80	0.95
Run No.	Fuel	$\hat{D}_p$, mm	Sorbent	$\hat{D}_p$, mm	Particle diameter, D_p, by sieve analysis, mm					
840501	Minto	10.1	Havelock	0.16	0.06	0.13	0.22	0.44	0.61	0.77
840605	Syncrude	0.26	Havelock	0.16	0.03	0.08	0.10	0.16	0.20	0.38
840612	Syncrude	0.26	Athabasca	0.34	0.04	0.11	0.26	0.42	0.61	0.86
840814	Syncrude	0.26	Athabasca	0.94	0.03	0.14	0.31	0.57	0.88	1.21
840820	Syncrude	0.26	Athabasca	0.94	0.03	0.10	0.20	0.40	0.75	1.15
841112	KY No. 9	2.3	Reed	1.1	0.12	0.33	0.49	0.72	1.02	1.54
841119	KY No. 9	2.3	Reed	1.1	0.06	0.27	0.36	0.60	0.87	1.51
841127	Devco	2.1	Sysco	1.4	0.14	0.43	0.59	0.91	1.52	2.27
841204	Devco	2.1	Sysco	1.4	0.08	0.20	0.36	0.67	1.00	1.64
850121	Devco	11.2	Sysco	1.4	0.09	0.25	0.33	0.51	0.91	2.19
850304	Devco	11.2	Sysco	1.4	0.08	0.20	0.30	0.46	0.82	1.55
841218	Devco	2.1	Calpo	1.1	0.09	0.34	0.52	0.84	1.35	2.17
850107	Devco	2.1	Calpo	1.1	0.08	0.31	0.45	0.87	1.47	2.22
850115	Devco	11.2	Calpo	1.1	0.07	0.16	0.29	0.59	1.39	2.28

Table 4.23 Particle size distributions of baghouse solids.

Fraction by mass undersize, F_D:					0.02	0.10	0.20	0.50	0.80	0.95
Run No.	Fuel	$\hat{D}_p$, mm	Sorbent	$\hat{D}_p$, mm	Particle diameter, D_p, by sieve analysis					
840501	Minto	10.1	Havelock	0.16	0.02	0.02	0.02	0.03	0.04	0.05
840612	Syncrude	0.26	Athabasca	0.34	0.02	0.02	0.02	0.03	0.05	0.06
840820	Syncrude	0.26	Athabasca	0.94	0.02	0.02	0.02	0.03	0.04	0.05
841112	KY No. 9	2.3	Reed	1.1	0.02	0.04	0.05	0.07	0.12	0.14
841127	Devco	2.1	Sysco	1.4	0.02	0.03	0.04	0.05	0.08	0.09
841218	Devco	2.1	Calpo	1.1	0.02	0.03	0.04	0.06	0.07	0.09

5. EVANS TRIALS

5.1 Introduction

The work on Evans coal consisted of 17 runs - 16 runs using Havelock limestone as a SO_2 sorbent and a final run in which the limestone was replaced by a local Kingston sand. Three particle size distributions of the coal with mean particle diameters, $\hat{D}_p$, of 16.7 mm, 8.8 mm, and 3.3 mm were used as feed. The mean particle diameters of the two particle size distributions of the limestone were 1.72 mm and 0.49 mm. The operating conditions for the 17 runs are summarized for convenient reference in Table 5.1.

5.2 The carbon balance

5.2.1 Carbon content of the product solids

The carbon content of the three product streams of solids as functions of bed temperature, excess air level, and recycle fraction is illustrated in Fig. 5.1 to Fig. 5.3. The ranges of carbon content are: 0.2--1.8 % for the bed solids, 3--15 % for the cyclone solids, and 5--18 % for the baghouse solids. As expected, the elutriated solids have a much higher carbon content than the bed material. There is an indication of a drop in carbon content with increasing bed temperature and increasing excess air under the constraint of other factors being constant. There is some tendency for the carbon content of the bed and baghouse

Table 5.1. Operating conditions for the runs with Evans coal.

Run	n_t	Coal		Stone		Ca/S	Air		r	T_b, °C	v, m/s	τ_p, hr	τ_b, hr	COT, hr
		$\hat{D}_p$, mm	$\dot{m}_f$, kg/hr	$\hat{D}_p$, mm	$\dot{m}_s$, kg/hr		$\dot{m}_a$, kg/hr	ε_a, %						
		Evans		Havelock										
831115	12	16.7	46.4	0.49	39.0	4.14	354	-21.9	0.000	869	2.1	2.1	5.5	19.1
831122	12	16.7	43.9	0.49	15.3	1.72	368	-14.2	0.000	877	2.1	4.4	10.9	34.7
831124	12	16.7	48.3	0.49	17.7	1.80	377	-20.1	0.555	865	2.2	4.6	10.8	18.7
831213	14	16.7	45.5	1.72	29.2	3.16	435	-2.1	0.000	877	2.5	3.1	5.5	19.1
831214	14	16.7	45.6	1.72	28.2	3.04	442	-0.8	0.607	879	2.6	3.3	5.4	12.3
840105	8	3.3	48.7	1.72	23.3	2.47	460	2.0	0.965	835	2.6	3.9	5.3	11.4
840111	6	3.3	41.9	1.72	20.7	2.55	360	-7.3	0.924	835	2.0	4.5	6.8	19.3
840117	4	3.3	19.6	1.72	4.6	1.22	263	45.2	0.945	873	1.5	13.3	18.8	44.6
840124	4	3.3	26.6	0.49	14.6	2.83	263	6.6	0.963	831	1.5	5.4	8.4	23.5
840126	4	3.3	26.8	0.49	13.8	2.67	269	8.6	0.000	874	1.6	5.2	10.0	15.8
840207	8	8.8	32.7	0.49	9.7	1.43	359	14.2	0.000	897	2.1	6.8	15.9	37.2
840215	12	8.8	41.7	0.49	20.3	2.35	383	-4.5	0.555	908	2.3	3.9	6.9	16.0
840216	12	8.8	35.7	0.49	20.0	2.70	386	12.3	0.000	837	2.2	3.5	8.1	11.0
840313	4	16.7	24.2	0.49	13.6	2.77	260	9.7	1.000	858	1.5	7.9	9.1	23.0
840314	4	16.7	22.5	0.49	13.2	2.89	263	19.3	0.000	915	1.6	6.3	11.5	11.0
840320	4	16.7	20.7	0.49	7.4	1.75	249	23.2	0.000	879	1.5	9.2	12.8	36.5
		Evans		Sand										
840404	4	16.7	24.2	0.95	20.9	0.00	253	7.2	0.000	882	1.5	4.1	5.4	5.8

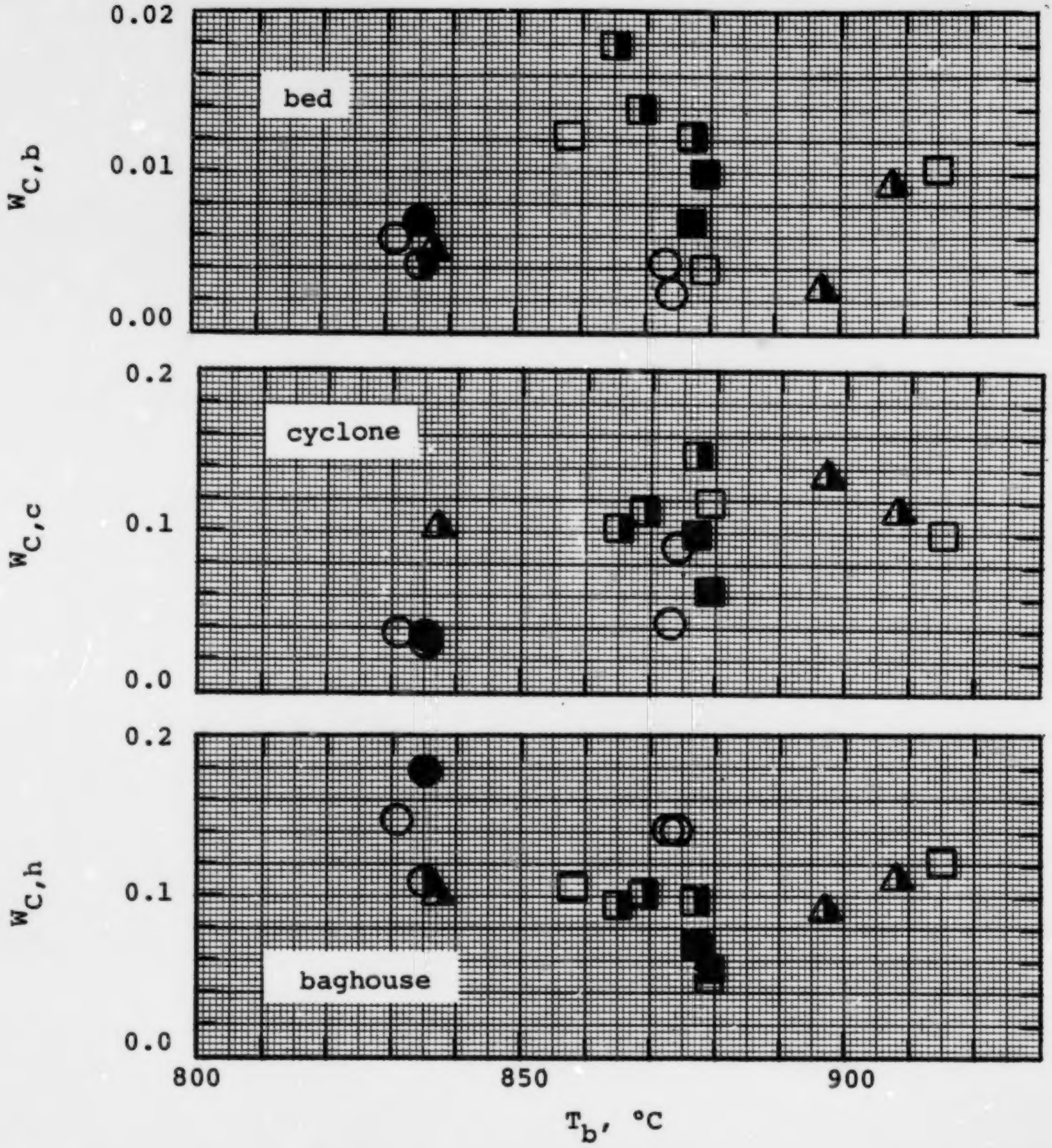

Fig. 5.1. Mass fraction carbon in solids vs. bed temperature T_b.

Key to symbols:

			v, m/s				coal $\hat{D}_p$, mm
○	△	□	1.5-1.6	○	◑	●	3.3
◑	◮	◨	2.0-2.3	△	◮	▲	8.8
●	▲	■	2.5-2.6	□	◨	■	16.7

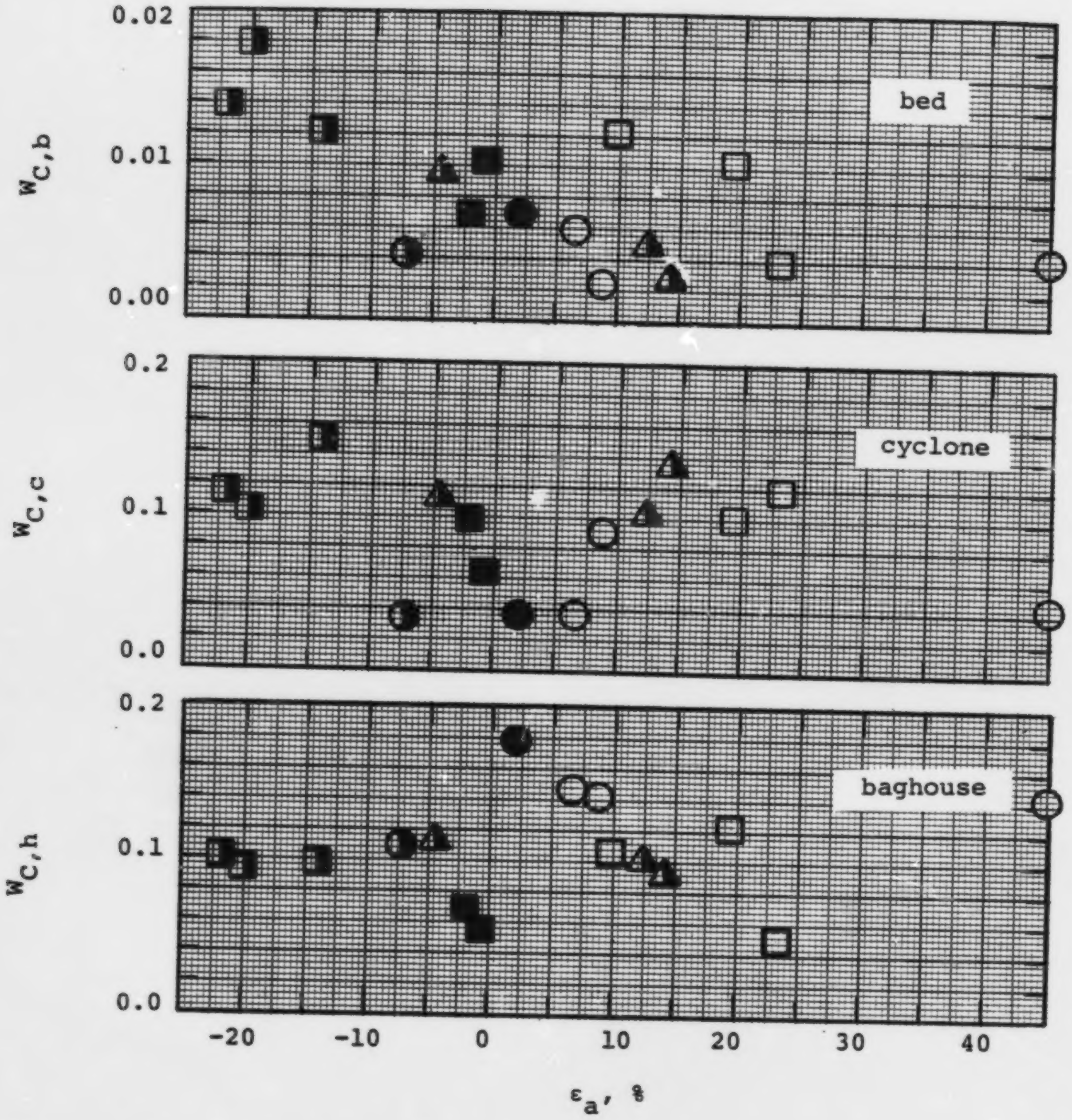

Figure 5.2. Mass fraction carbon in solids vs. excess air level ε_a.

Key to symbols:

	v, m/s		coal $\hat{D}_p$, mm
○ △ □	1.5-1.6	○ ◐ ●	3.3
◐ ◭ ◧	2.0-2.3	△ ◭ ▲	8.8
● ▲ ■	2.5-2.6	□ ◧ ■	16.7

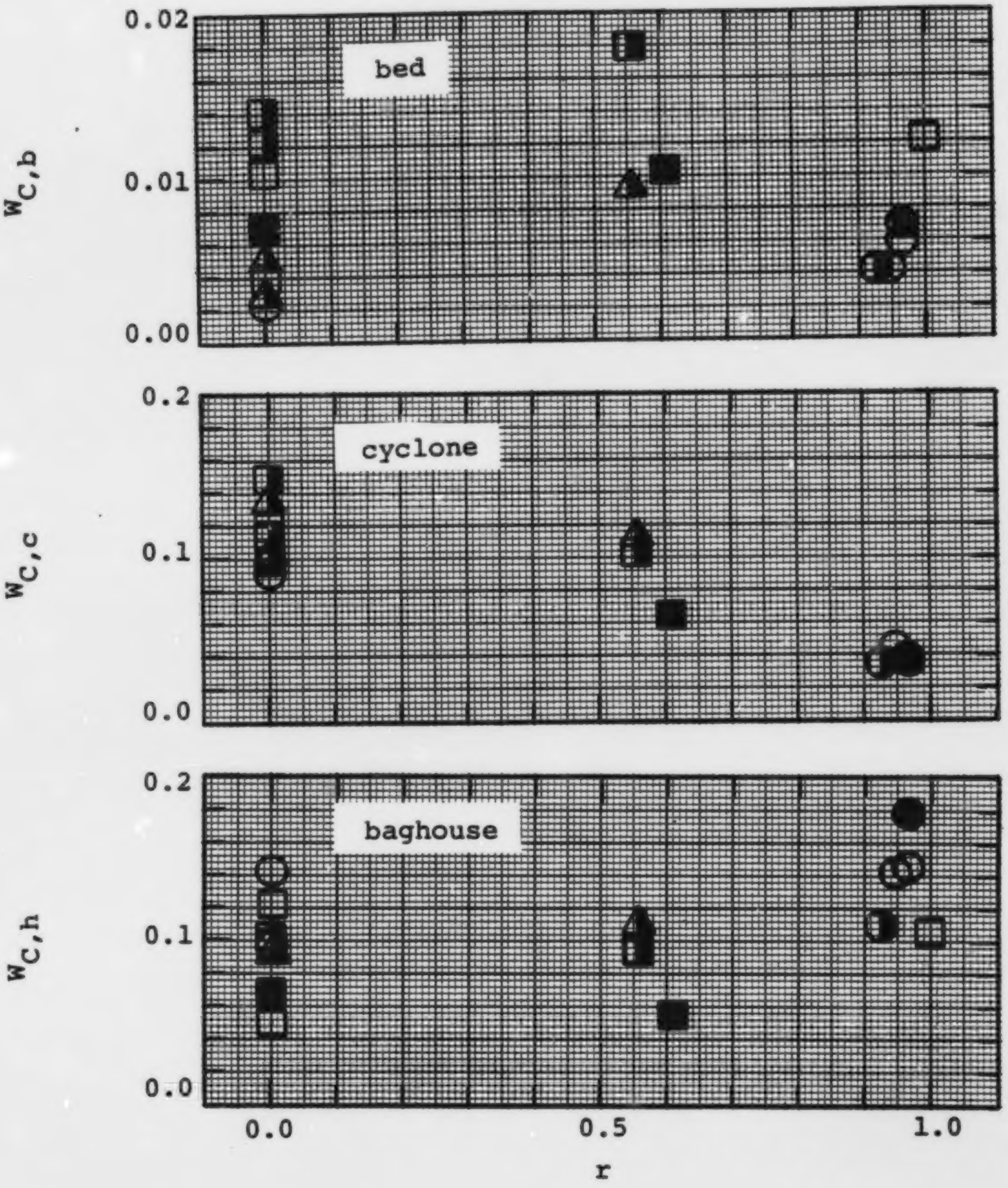

Fig. 5.3. Mass fraction carbon in solids vs. recycle fraction r.

Key to symbols:

	v, m/s		coal $\hat{D}_p$, mm
○ △ □	1.5-1.6	○ ◐ ●	3.3
◐ ◭ ◨	2.0-2.3	△ ◭ ▲	8.8
● ▲ ■	2.5-2.6	□ ◨ ■	16.7

products to increase with increasing recycle fraction but the carbon content of the cyclone solids shows a marked decrease with an increase in r. The plots should not be viewed in isolation but in consultation with the operating conditions summarized in Table 5.1.

5.2.2 Distribution of carbon loss

The distribution of carbon loss among the streams of solids from the bed, cyclone and baghouse is shown in Fig. 5.4. The distribution is presented in terms of a flux ratio of carbon loss in an individual stream to the total carbon loss in the solids. The recycle fraction, r, was selected as the abscissa variable in Fig. 5.4 and its effect is obvious, i.e., as r increases a greater portion of the carbon loss must be carried by the bed overflow and baghouse streams. This effect is not significant, however, until r exceeds a value of approximately 0.6. At zero recycle the major portion, 80 to 95 %, of the carbon loss is carried by the cyclone solids. The corresponding ranges for the bed overflow and baghouse streams are 1 to 11 % and 2 to 14 %, respectively. The effect of r is not significant in the range $0 < r < 0.5$. At a recycle fraction of 0.5, the value of the flux ratio for the cyclone solids is still approximately 0.8 while the corresponding values for the bed overflow and baghouse streams are 0.12 and 0.08, respectively. The results in the region of total recycle, $0.9 < r < 1.0$, are more scattered due to the much sharper effect of r. In this region the portion of the carbon loss carried by the cyclone solids drops rapidly from 40 % at $r = 0.9$ to 0 %

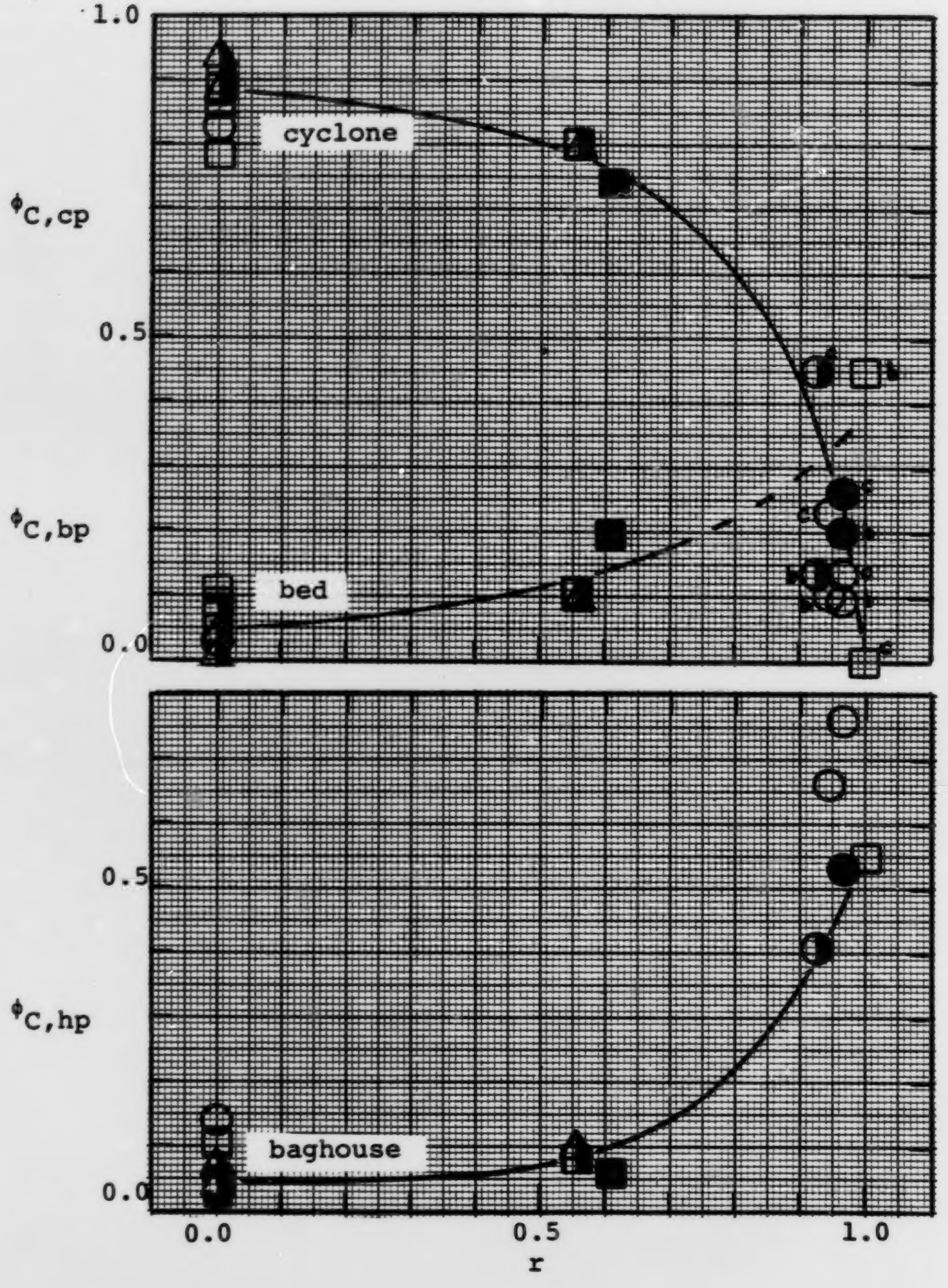

Fig. 5.4 . Distribution of carbon loss among solids from bed, cyclone and baghouse - flux ratio of carbon loss in an individual stream to total carbon loss in the solids.

Key to symbols:

			v, m/s				coal $\hat{D}_p$, mm
○	△	□	1.5-1.6	○	◐	●	3.3
◐	◭	◧	2.0-2.3	△	◭	▲	8.8
●	▲	■	2.5-2.6	□	◧	■	16.7

at $r = 1.0$. At total recycle of cyclone solids, the one experimental run gave 45 % for the bed overflow and 55 % for the baghouse stream.

5.2.3 Distribution of fuel carbon among products

The ratio of the carbon flux in individual product streams to the carbon flux in the feed may be used to examine the fate of the carbon in the fuel. Such flux ratios for the three streams of product solids are plotted in Fig. 5.5 through Fig. 5.9 as functions of bed temperature, excess air level, recycle fraction, total solids efflux per unit bed area, and bed solids efflux per unit bed area. Only the flux ratios for the three streams of product solids are included in the figures since it is obvious that the difference between the sum of the flux ratios and unity is the fraction of the fuel carbon which is converted to gaseous products. Since the bed mass per unit area, m_b/A_b, is approximately constant from run to run, the abscissa variables in Fig. 5.8 and Fig. 5.9, $\dot{m}_p/A_b$ and $\dot{m}_b/A_b$, may be taken as inverse measures of the characteristic solids residence times $\tau_p = m_b/\dot{m}_p$ and $\tau_b = m_b/\dot{m}_b$ in any qualitative interpretation of the behavior of the flux ratios.

As recommended earlier, the figures should be examined in conjunction with the operating conditions in Table 5.1. In order to assist in the interpretation various symbols are used in the figures to indicate ranges for certain operating conditions. Only a qualitative interpretation is possible at this stage of

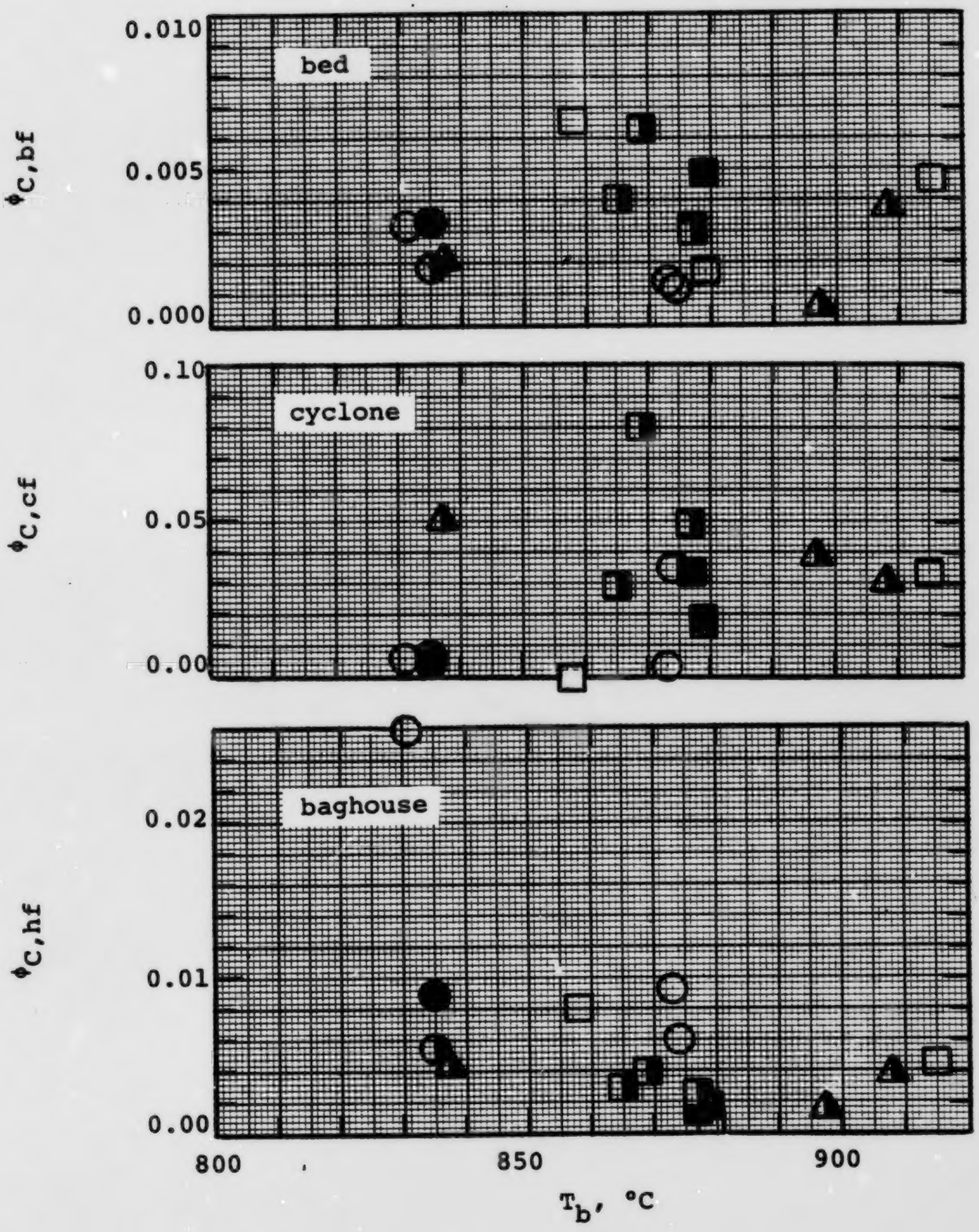

Fig. 5.5. Flux ratios of carbon loss in individual streams of solids from bed, cyclone and baghouse to carbon fed in fuel, vs. bed temperature, T_b.

Key to symbols:

	v, m/s		coal $\hat{D}_p$, mm
○ △ □	1.5-1.6	○ ◐ ●	3.3
◐ ◭ ◧	2.0-2.3	△ ◭ ▲	8.8
● ▲ ■	2.5-2.6	□ ◧ ■	16.7

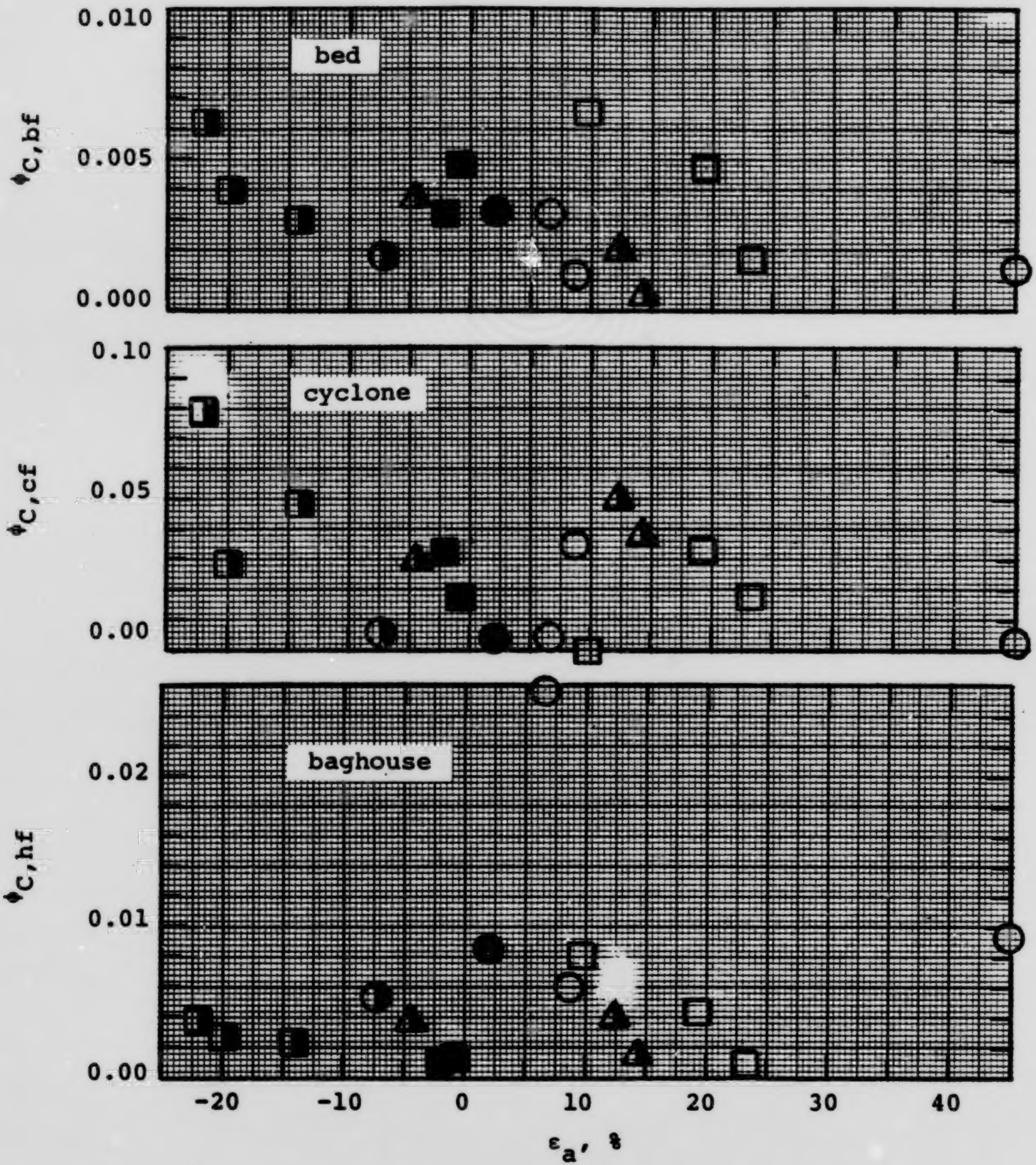

Fig. 5.6. Flux ratios of carbon loss in individual streams of solids from bed, cyclone and baghouse to carbon fed in fuel, vs. excess air level, ε_a.

Key to symbols:	v, m/s		coal $\hat{D}_p$, mm
○ △ □	1.5-1.6	○ ◐ ●	3.3
◐ ▲ ◨	2.0-2.3	△ ▲ ▲	8.8
● ▲ ■	2.5-2.6	□ ◨ ■	16.7

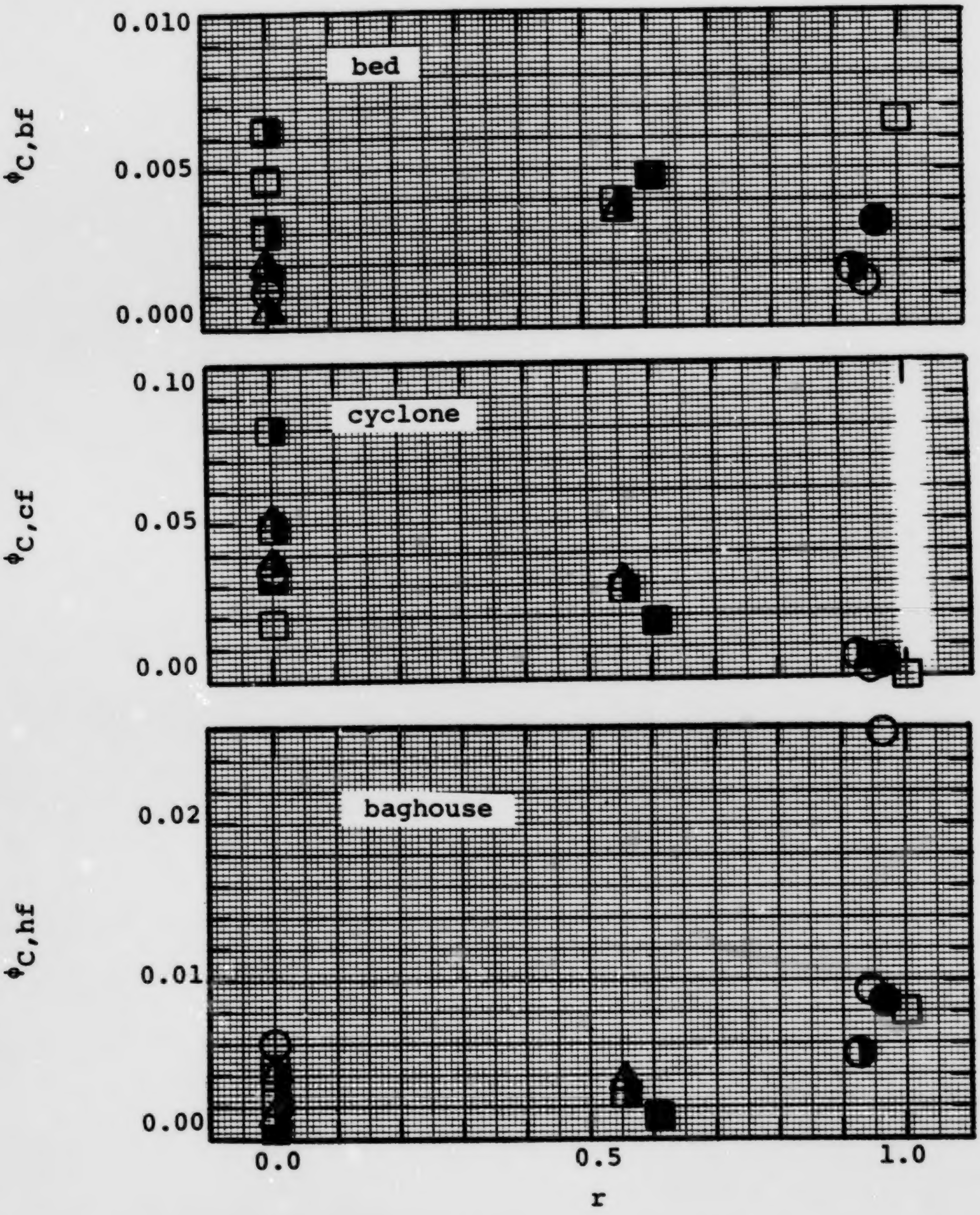

Fig. 5.7. Flux ratios of carbon loss in individual streams of solids from bed, cyclone and baghouse to carbon fed in fuel, vs. recycle fraction, r.

Key to symbols:

			v, m/s				coal $\hat{D}_p$, mm
○	△	□	1.5-1.6	○	◑	●	3.3
◑	◭	◨	2.0-2.3	△	◭	▲	8.8
●	▲	■	2.5-2.6	□	◨	■	16.7

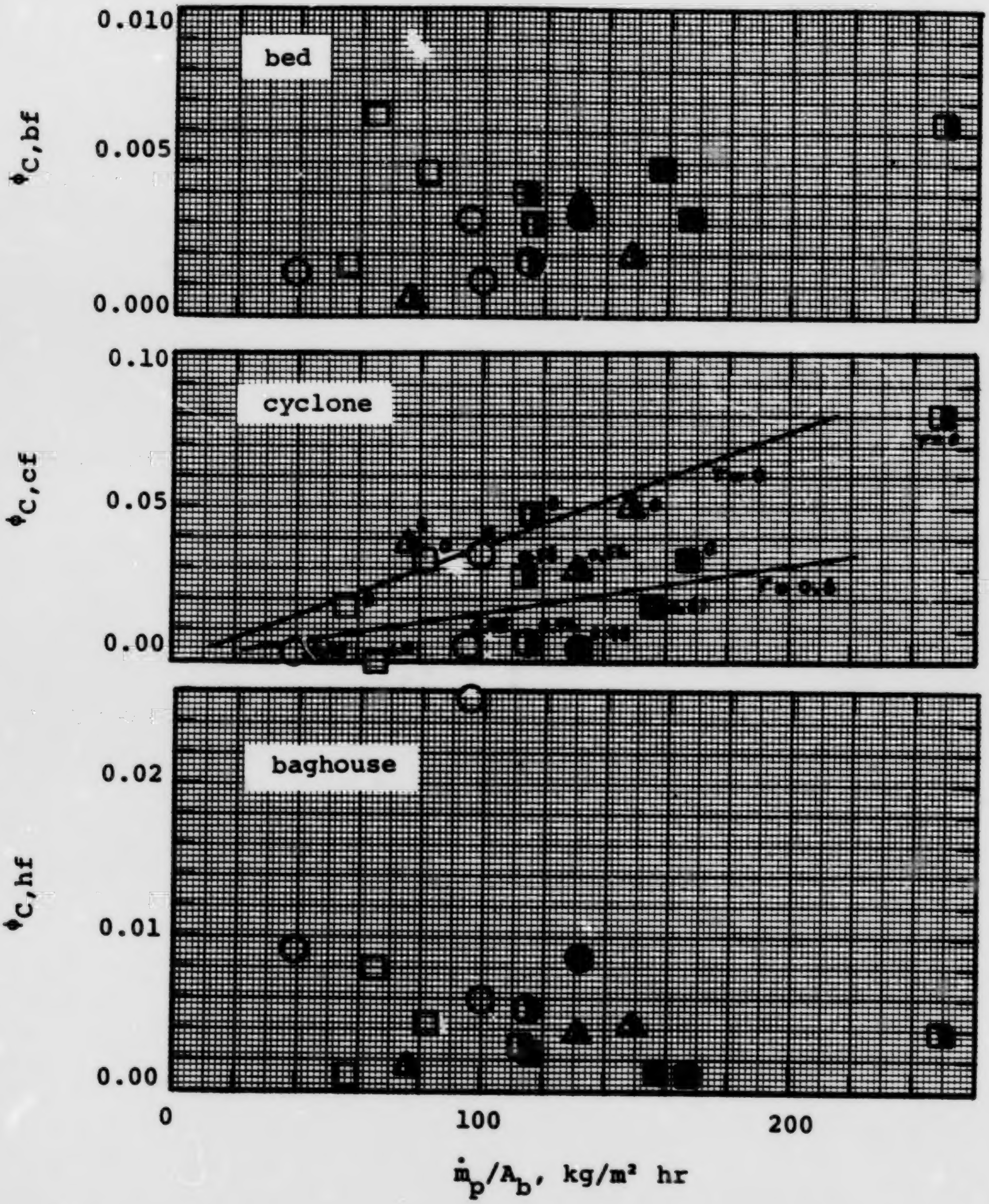

Fig. 5.8. Flux ratios of carbon loss in individual streams of solids from bed, cyclone and baghouse to carbon fed in fuel, vs. total solids efflux per unit bed area, $\dot{m}_p/A_b$.

Key to symbols:

	v, m/s		coal $\hat{D}_p$, mm
○ △ □	1.5-1.6	○ ◐ ●	3.3
◐ ◭ ◧	2.0-2.3	△ ◭ ▲	8.8
● ▲ ■	2.5-2.6	□ ◧ ■	16.7

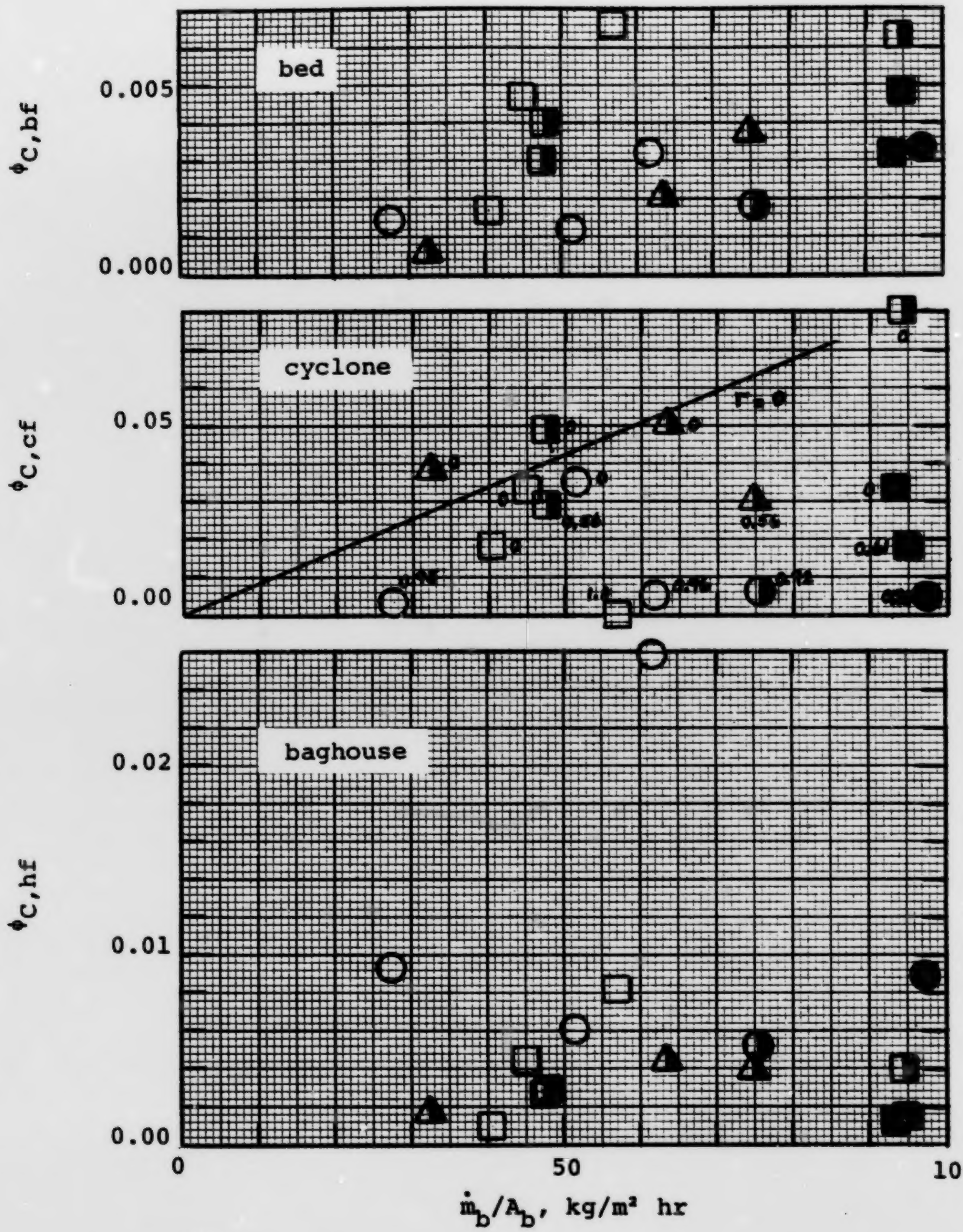

Fig. 5.9. Flux ratios of carbon loss in individual streams of solids from bed, cyclone and baghouse to carbon fed in fuel, vs. bed solids efflux per unit bed area, $\dot{m}_b/A_b$. See Fig. 5.8 for a key to the symbols.

the work because of the large number of factors which may have an effect on the performance of the process. In addition to the factors selected as abscissa variables in the figures, coal particle size, limestone particle size and fluidizing velocity should also be considered.

For a fixed coal particle size and fixed range of fluidizing velocity, examination of Fig. 5.5 indicates a reduction in carbon loss in the three streams of product solids with increasing bed temperature over the range 830 °C to 900 °C. This behavior is in qualitative agreement with our earlier work on Minto coal (Becker and Code, 1983). There is also an indication that this effect may be more pronounced for the low range of fluidizing velocity. Such indications should only be interpreted as trends since the apparent magnitude of an effect in a given figure may be due in part to an enhancing effect by a change in another process variable. For example, the apparent pronounced effect of a temperature increase may be due in part to a concurrent increase in the excess air level. Similarly, what may appear to be a contradiction to the generalization on the effect of temperature may be due to the counteracting effect of a decrease in the excess air level.

The effect of excess air level (Fig. 5.6) parallels the effect of temperature. The effect is greatest for the cyclone product at low levels of excess air. This statement requires qualification and affords an opportunity of illustrating the argument given in the preceding paragraph. Consider the three points on the extreme left of the chart for the cyclone solids in Fig. 5.6 (half-shaded squares; coal $\hat{D}_p$ 16.7 mm; v 2.0-2.3 m/s). In examining the sharp decrease in the value of the flux ratio from 0.08 to 0.03 as the excess air level is changed from -22 % to -20 % consideration needs to be given to the effect of the change in recycle fraction from 0 to 0.56 (Fig. 5.7). The effect of temperature is small and negative since the corresponding change in temperature is from 869 °C to 865 °C. The two runs at -22 % and -14 % excess air were for zero recycle and the corresponding change in the flux ratio from 0.08 to 0.05 is a more realistic measure of the effect of change in excess air level. But again the enhancing effect of temperature from 869 °C to 877 °C needs to be considered in interpreting this value.

The effect of recycle on the flux ratios for the three streams of solids is illustrated in Fig. 5.7. The marked decrease in the flux ratio for the cyclone solids with increase in recycle fraction results from an increase in carbon burn-off and the withdrawal of less solids as cyclone product. The withdrawal of less solids from the cyclone places an increased solids burden on the bed overflow and baghouse streams and even with an increase in carbon burn-off the increase in solids burden results in an increase in the flux ratio. The net result of an increase in recycle fraction is a reduction in the total carbon loss.

The flux ratios for the three streams of solids are plotted vs. the total solids efflux per unit bed area, $\dot{m}_p/A_b$, in Fig. 5.8 and vs. the bed solids efflux per unit bed area, $\dot{m}_b/A_b$, in Fig. 5.9. It was pointed out earlier that the abscissa variables may be interpreted as inverse measures of the characteristic solids residence times $\tau_p = m_b/\dot{m}_p$ and $\tau_b = m_b/\dot{m}_b$, and as expected, an increase in residence time (decrease in $\dot{m}_p/A_b$ or $\dot{m}_b/A_b$) results in a decrease in the flux ratio. At a fixed recycle fraction, this is particularly evident on the chart for the cyclone solids. In order to clarify the plot the symbols have been identified with the recycle fraction for the run.

In addition to the factors discussed above, the possible effect of coal particle size, limestone particle size, and fluidizing velocity should also be considered. There is no clear evidence of a significant effect of feed particle size. In the case of fluidizing velocity, one would expect a significant increase in carbon loss with an increase in fluidizing velocity due to increased elutriation. This topic is treated later in the development of a correlation for overhead carbon loss.

The total carbon loss expressed as a flux ratio with respect to the fuel carbon, or simply the fraction of the fuel carbon which is lost in the product solids, is shown in Fig. 5.10 and Fig. 5.11 as a function of the bed temperature, excess air level, recycle fraction, total solids efflux per unit bed area, and bed solids efflux per unit bed area. The total carbon loss

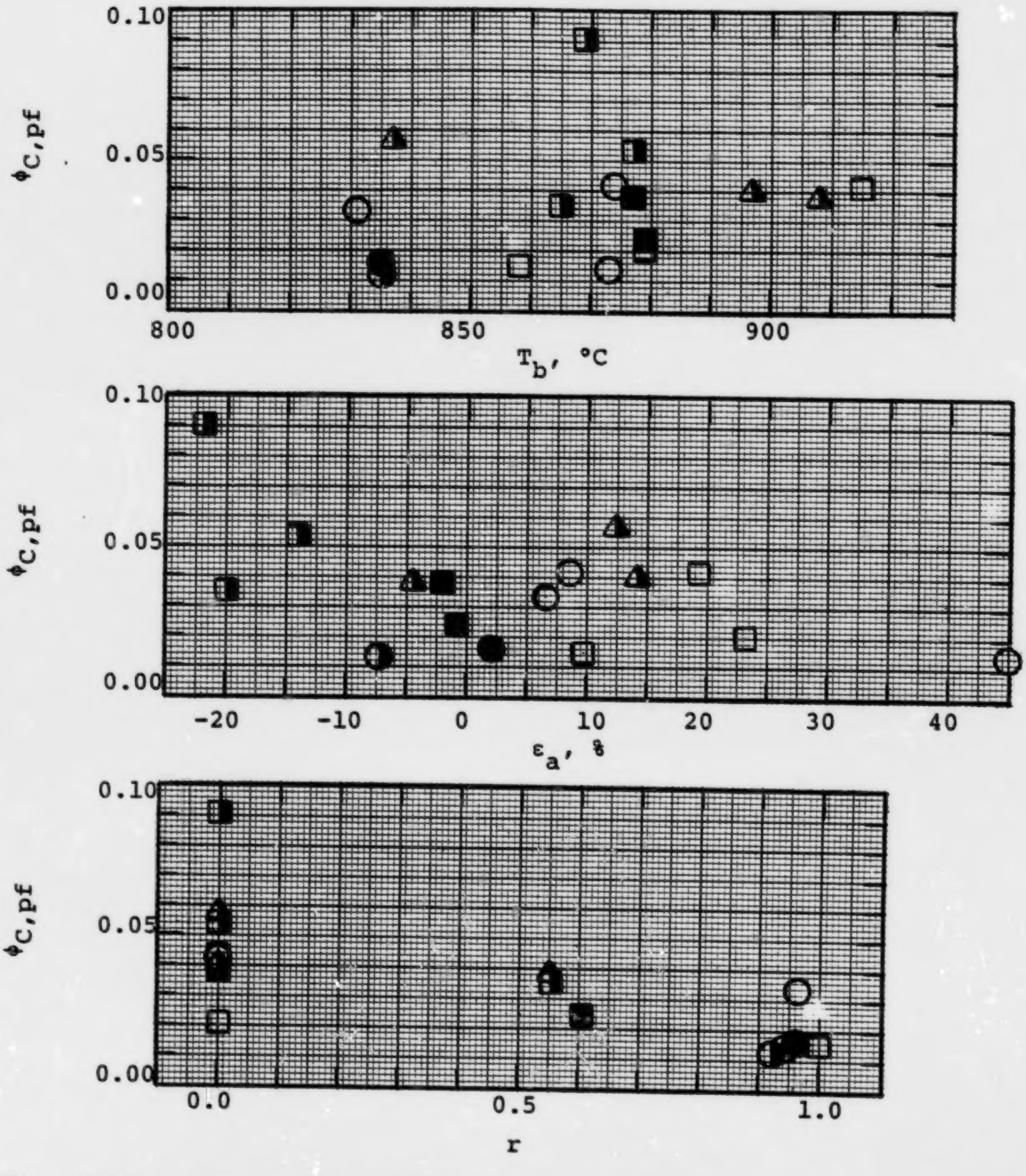

Fig. 5.10. Flux ratio of carbon loss in solids to carbon fed in fuel, vs. bed temperature, T_b, excess air level, ε_a, and recycle fraction, r.

Key to symbols:

	v, m/s		coal $\hat{D}_p$, mm
○ △ □	1.5-1.6	○ ◐ ●	3.3
◐ ◮ ◨	2.0-2.3	△ ◮ ▲	8.8
● ▲ ■	2.5-2.6	□ ◨ ■	16.7

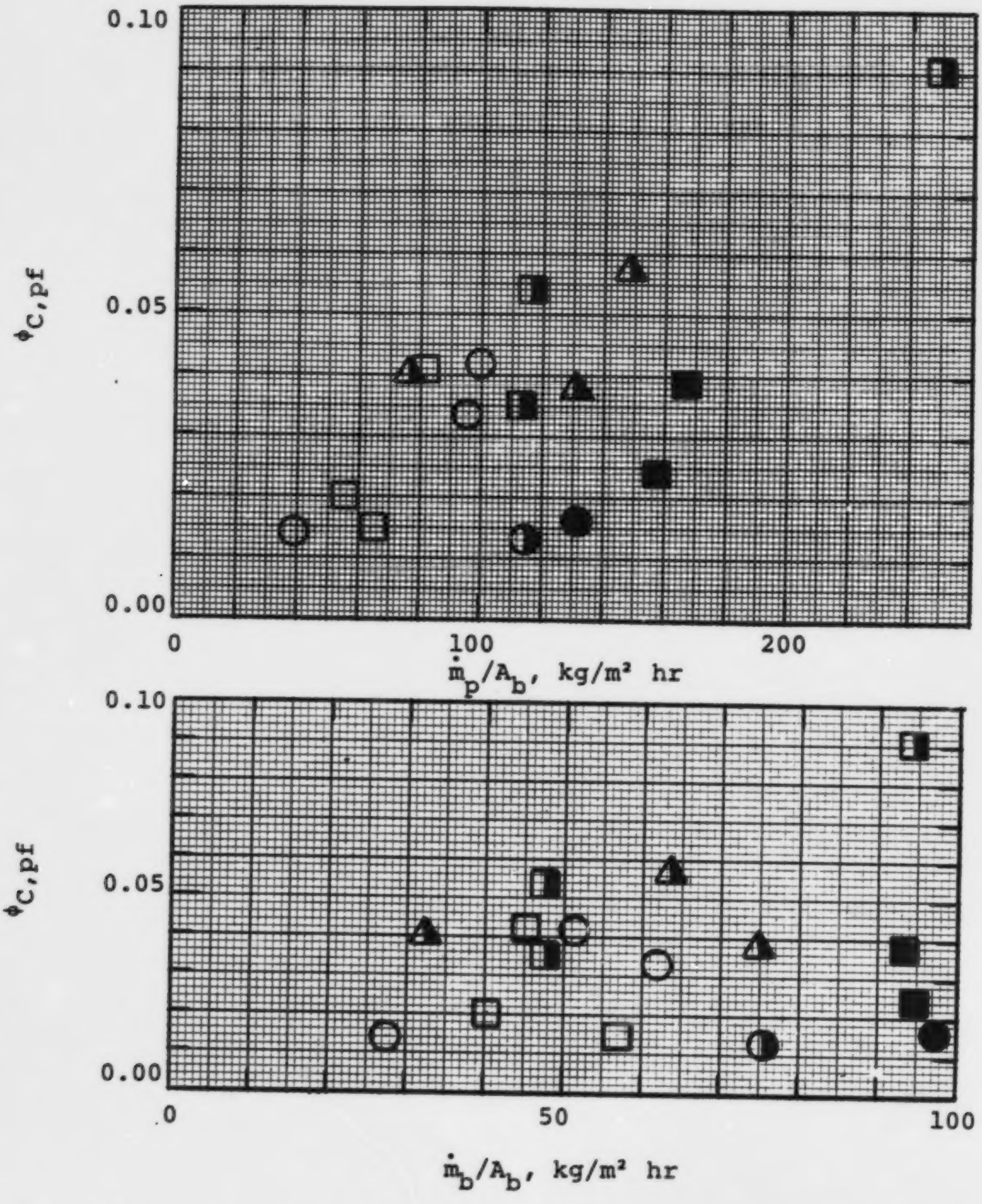

Fig. 5.11. Flux ratio of carbon loss in solids to carbon fed in fuel, vs. total solids efflux per unit bed area, $\dot{m}_p/A_b$, and bed solids efflux per unit bed area, $\dot{m}_b/A_b$.

Key to symbols:

			v, m/s				coal $\hat{D}_p$, mm
○	△	□	1.5-1.6	○	◑	●	3.3
◑	◮	◨	2.0-2.3	△	◮	▲	8.8
●	▲	■	2.5-2.6	□	◨	■	16.7

in the solids ranged from 1.5 % to 9 % of the fuel carbon. This range is similar to the 2.5 % to 11.5 % observed in the earlier work on Minto coal (Becker and Code, 1983). The trends with respect to T_b, ε_a, $\dot{m}_p/A_b$, and $\dot{m}_b/A_b$, although not as distinct, are similar to those observed for the carbon loss in the individual streams of solids. Of particular interest here is the effect of r on the total carbon loss. The net effect of a decrease in the total carbon loss with an increase in recycle fraction is clearly shown in Fig. 5.10. Typically, the total carbon loss is reduced from 4--6 % of the fuel carbon at $r = 0$ to 1--2 % in the region $0.9 < r < 1.0$.

5.2.4 Division of carbon between cyclone and baghouse solids

The pronounced effect of recycle fraction on the flux ratios has been noted already. The dependency of the flux ratio of the carbon loss in the cyclone solids to the carbon loss in the baghouse solids on the non-recycle fraction is examined in Fig. 5.12. Although the same trend is observed, the log-log plot is not as linear as the result for Minto coal (Becker and Code, 1983).

5.2.5 Correlation of overhead carbon loss

Overhead carbon loss refers to that portion of the elutriated carbon going overhead which is not returned as recycle, i.e., it is the sum of carbon losses in the cyclone solids and baghouse solids. Background material on the development of an empirical model for overhead carbon loss is given by Becker and Code (1983). In power-law form the proposed correlating equation may be expressed as

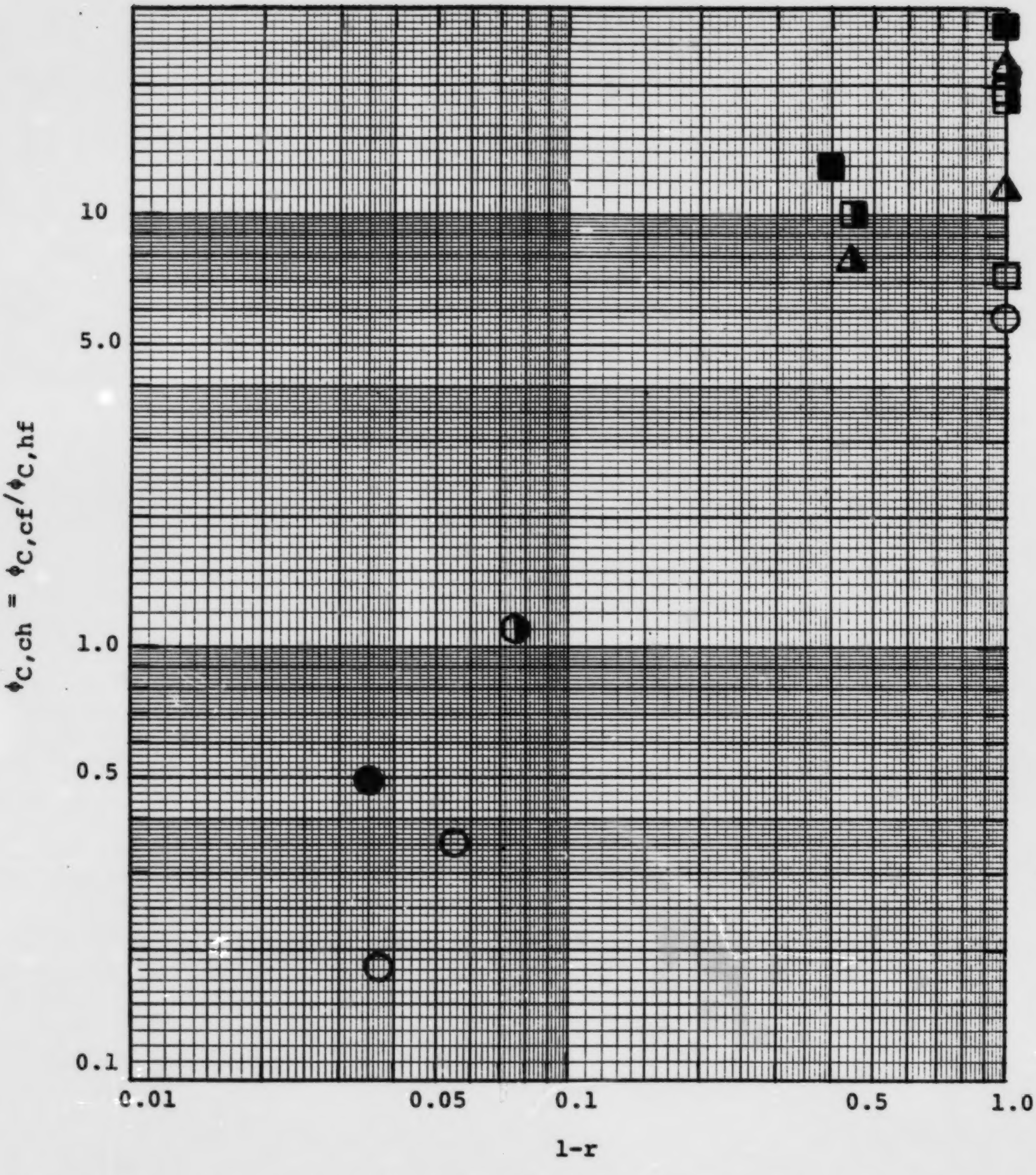

Fig. 5.12. Flux ratio of carbon loss in cyclone solids to carbon loss in baghouse solids, vs. the non-recycle fraction 1-r. A key to the symbols accompanies Fig. 5.13.

$$(\dot{m}_{C,o}/\dot{m}_{C,f}) = C_o\, v^{a_1}\, \hat{D}_p^{\,a_2}\, \phi_a^{\,a_3}$$
$$\exp(a_4 r)\, \exp(a_5/T_b) \qquad (5.2.1)$$

Multiple linear regression on the 16 data points for Evans coal with Havelock limestone as the SO_2 sorbent gave the following result:

$$(\dot{m}_{C,o}/\dot{m}_{C,f}) = 0.00206\, v^{0.584}\, \hat{D}_p^{\,-0.354}\, \phi_a^{\,-0.712}$$
$$\exp(-0.940 r)\, \exp(2833/T_b) \qquad (5.2.2)$$

The mean limestone particle diameter in millimetres was taken as the characteristic particle diameter $\hat{D}_p$. The fluidizing velocity, v, is in m/s and T_b is the bed temperature in K. The factor $\phi_a = \dot{m}_a/\dot{m}_{a,st} = 1 + \varepsilon_a$, where $\dot{m}_{a,st}$ is the stoichiometric air requirement, is the 'mixture strength' of Stover et al (1981).

The observed overhead carbon loss is compared with the carbon loss predicted by Eq. 5.2.2 in Fig. 5.13. Values of the coefficient C_o calculated using values of the carbon loss for individual runs are compared with the statistically fitted value in Fig. 5.14. Following our earlier work on Minto coal, coal particle diameter was not included in the model equation. This does not appear to have introduced any significant bias into the empirical result, i.e., the calculated values for C_o for the three coal particle diameters scatter on both sides of the statistically fitted value for C_o in Fig. 5.14. Also, solids residence time does not appear in the correlation. This is fortunate since the more appropriate residence time of the elutriated carbon-containing

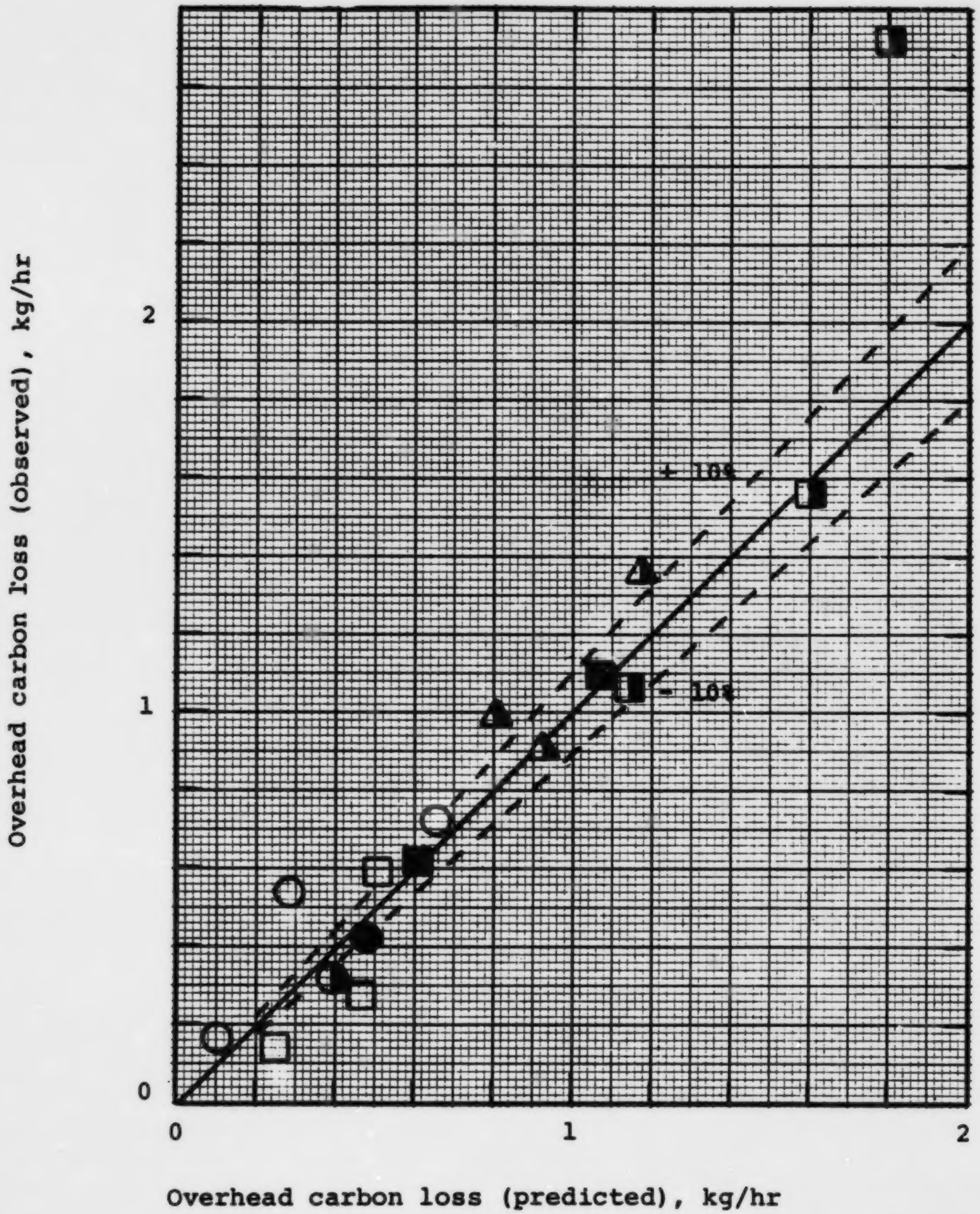

Fig. 5.13. A comparison of overhead carbon losses with values predicted by Eq. 5.2.2.

Key to symbols:			v, m/s				coal $\hat{D}_p$, mm
○	△	□	1.5-1.6	○	◐	●	3.3
◐	◭	◧	2.0-2.3	△	◭	▲	8.8
●	▲	■	2.5-2.6	□	◧	■	16.7

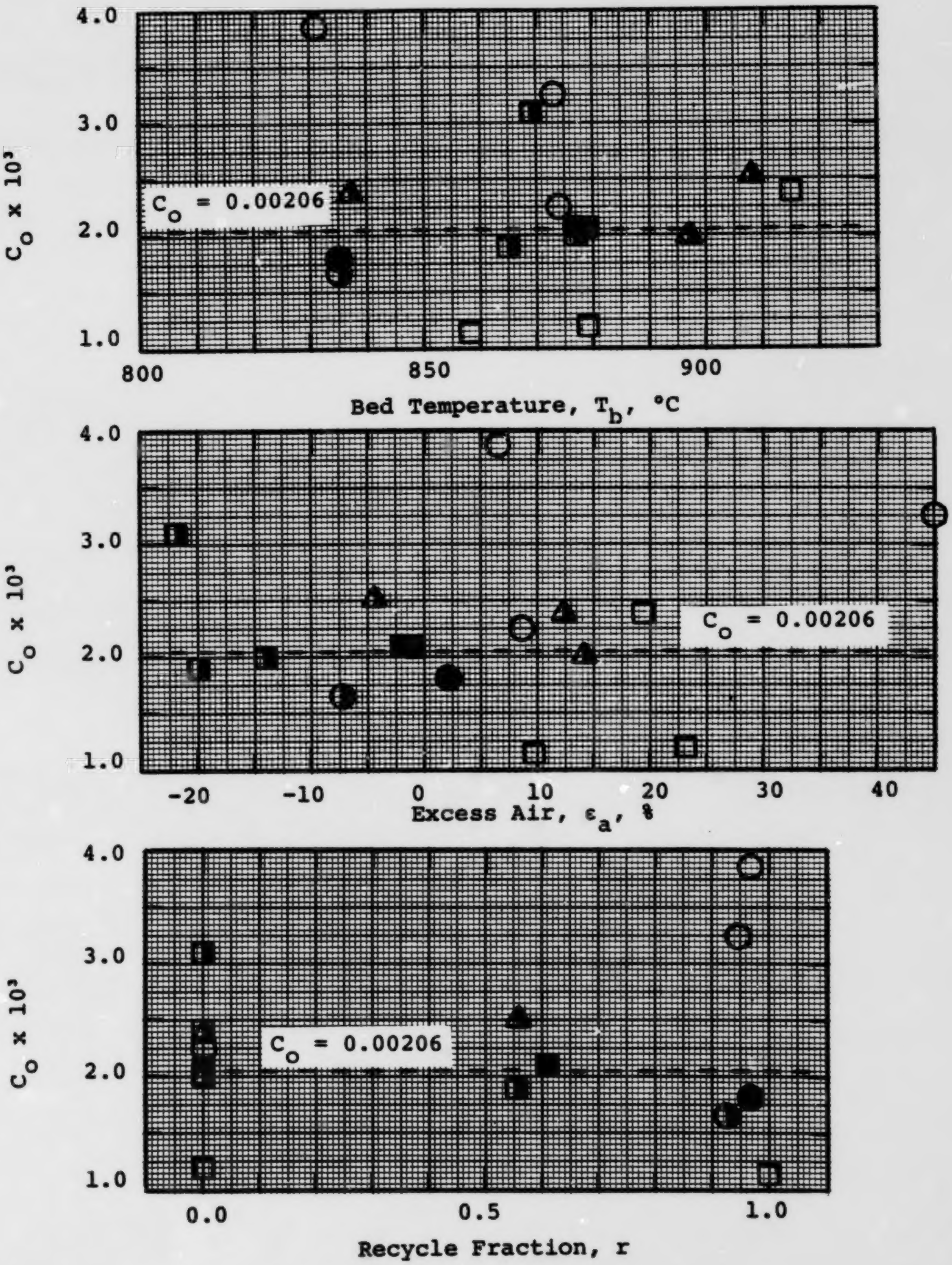

Fig. 5.14. The coefficient, C_o, in the correlation for overhead carbon loss, calculated using values of carbon loss for individual runs. $C_o = 0.00206$ is the statistically fitted value. A key to the symbols accompanies Fig. 5.13.

particles is unknown. The lack of a need to include residence time is probably due to the correlation of residence time and fluidizing velocity by operating constraints, i.e., an increase in fluidizing velocity requires an increase in both coal and limestone feedrates at a given Ca/S ratio.

The empirical values of the coefficient C_o and the five a's are considerably different from corresponding values in our earlier work on Minto and Devco coals (Becker and Code, 1983). However, the accompanying signs are the same indicating the same qualitative behavior. Although the value of the exponent $a_2 = -0.35$ vs. -0.74 for the earlier work indicates a smaller effect of particle diameter, both values predict a decrease in overhead carbon loss with an increase in $\hat{D}_p$. In the case of recycle fraction, the current value of -0.94 for a_4 predicts a 60 % reduction in carbon loss while the value of -0.36 for a_4 in the earlier work indicates only a 30% reduction as r changes from 0 (no recycle of cyclone solids) to 1 (complete recycle). Although the temperature dependency is smaller for the current work ($a_5 = 2800$ vs. $a_5 = 5200$ for the earlier work) both results indicate the correct direction, i.e., a decrease in overhead carbon loss with an increase in bed temperature.

5.2.6 Carbon burn-up efficiency

The effect of bed temperature, excess air level, and recycle fraction on the carbon burn-up efficiency, defined as

$$\eta_C = 100(1 - \dot{m}_{C,p}/\dot{m}_{C,f}) \tag{5.2.3}$$

is examined in Fig. 5.15. With the exception of the first run (831115; T_b = 869 °C; ϵ_a = -22 %; r = 0) with an efficiency of 90.9 %, the efficiencies ranged from 94.3 % to 98.7 %. A second measure of the completeness of burning, the combustion efficiency, may be defined in terms of heat effects, i.e., the ratio of the actual heat release by chemical reaction to the heat release if the fuel were completely oxidized. Provided sufficient oxygen is present to produce predominantly CO_2 in the product gases, there should be little difference in these two efficiencies. In this particular system there are two additional minor heat effects: the endothermic calcination of the limestone and the exothermic sulphation of the calcium oxide. Per unit calcium the exothermic effect is approximately 3 times the endothermic effect so that at normal levels of sorbent utilization the sulphation reaction more than compensates for the endothermic calcination of the limestone.

5.2.7 Carbon balance check

In this final topic in the subsection on the carbon balance, the total carbon flux per unit bed area accounted for in the product streams is compared in Fig. 5.16 with the total carbon flux per unit bed area in the feed streams. Only two runs (831122 and 831124) gave unsatisfactory carbon balance checks. The checks for the remaining runs in Fig. 5.16 fall close to or

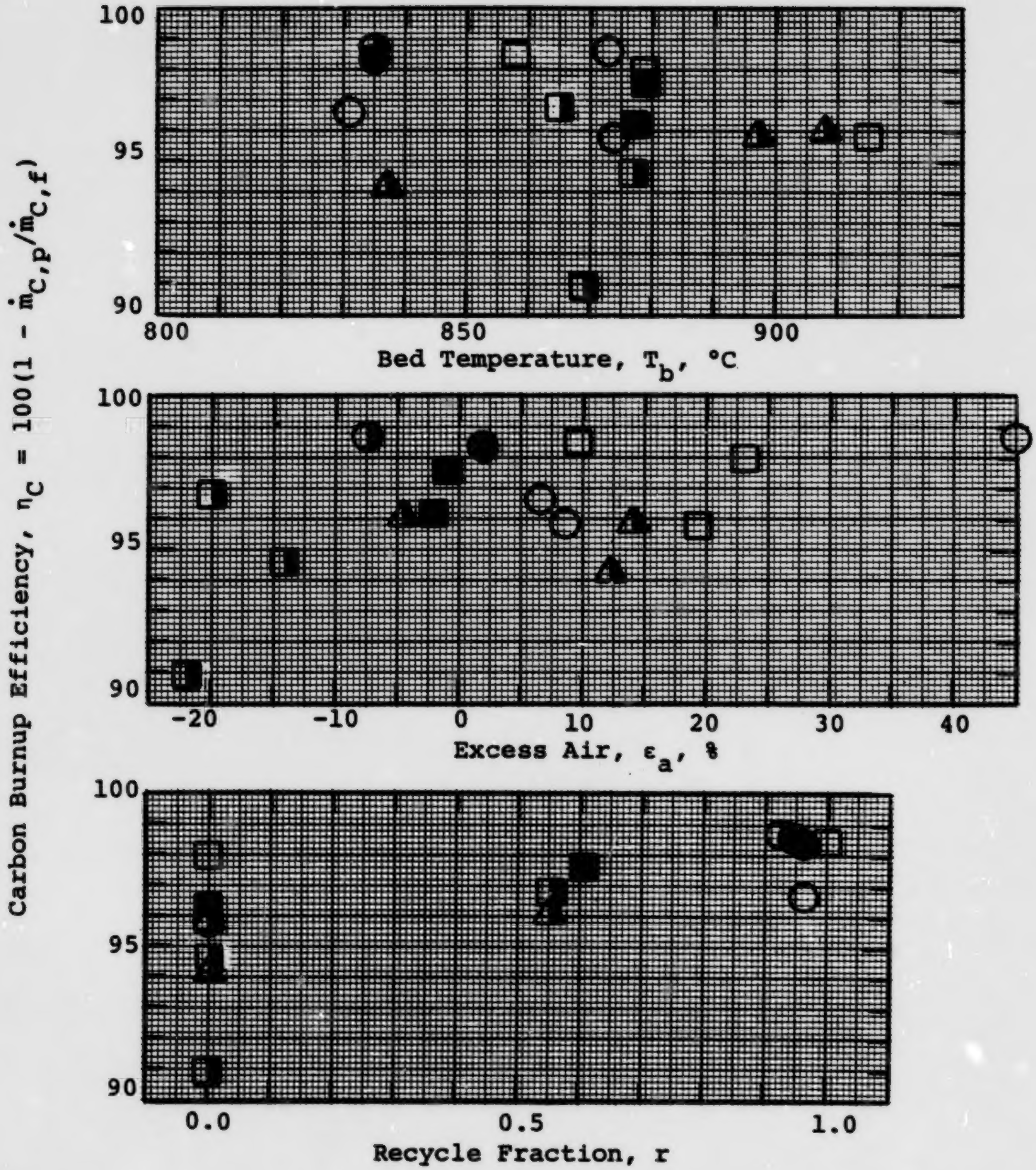

Fig. 5.15. Carbon burnup efficiencies for the fluidized-bed combustion of Evans coal.

Key to symbols:	v, m/s		coal $\hat{D}_p$, mm
○ △ □	1.5-1.6	○ ◐ ●	3.3
◐ ◭ ◧	2.0-2.3	△ ◭ ▲	8.8
● ▲ ■	2.5-2.6	□ ◧ ■	16.7

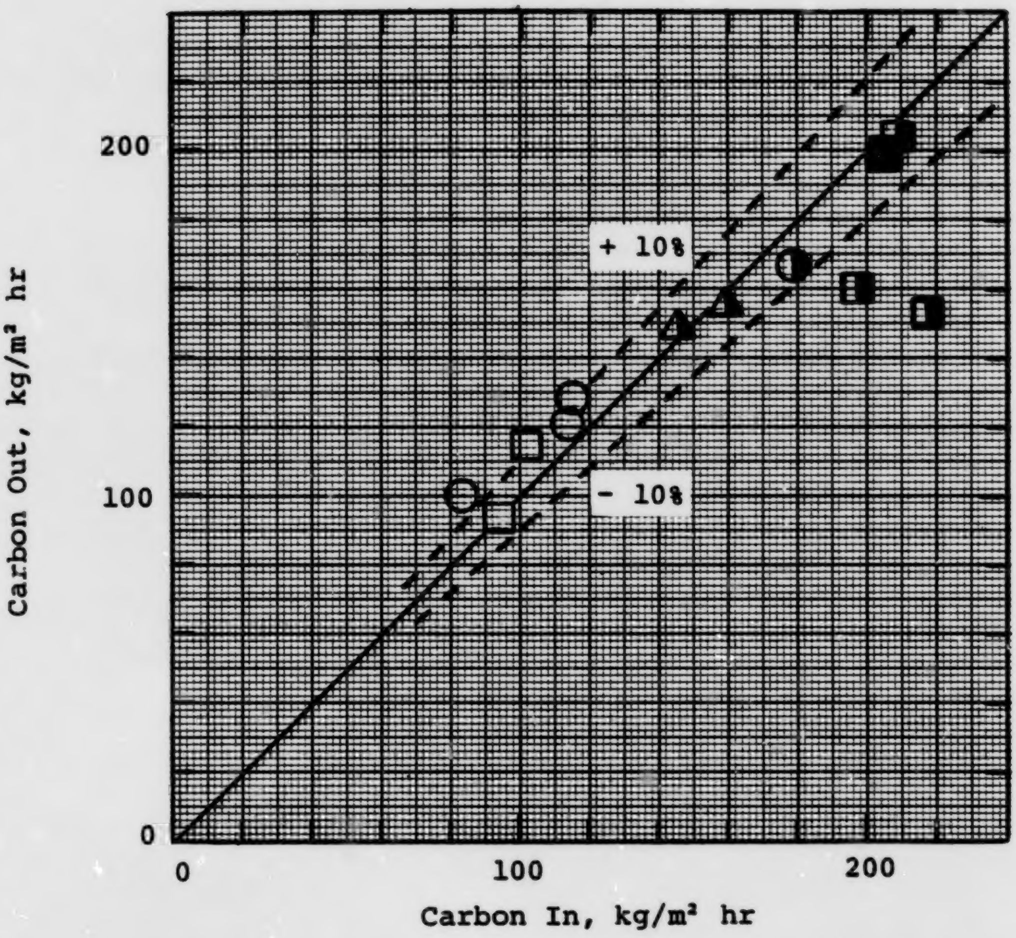

Fig. 5.16. Carbon balance check: total carbon flux per unit bed area in the product streams vs. total carbon flux per unit bed area in the feed streams.

Key to symbols:				v, m/s				coal, $\hat{D}_p$, mm
	○	△	□	1.5-1.6	○	◑	●	3.3
	◑	◮	◨	2.0-2.3	△	◮	▲	8.8
	●	▲	■	2.5-2.6	□	◨	■	16.7

within the ± 10 % boundary. Carbon balance checks for three of the runs (840105, 840215 and 840313) are missing from Fig. 5.16 because of the unavailability of CO_2 analyses of the stack gas due to instrument malfunction.

5.3 The sulphur balance

5.3.1 The sulphur content of the product solids

The sulphur concentration (wt %) in the three product streams of solids is plotted vs. the carbon concentration (wt %) in Fig. 5.17. The values in the plots are the mean values used in the material balances. The ranges of sulphur content are 7.7--12.6 % for the bed overflow solids, 3.8--7.5 % for the cyclone solids, and 4.0--5.5 % for the baghouse solids. The sulphur in the solids is reported as total sulphur. With our instrumentation for the analysis of sulphur in solids it is not possible to distinguish organic and inorganic sulphur, or sulphide and sulphate sulphur. Since the carbon content of the bed overflow solids is in the range 0.3--1.8 %, the sulphur content of the bed product is predominantly in the sulphate form ($CaSO_4$). In the case of the cyclone and baghouse products the range of carbon content is ten times that of the bed material and the residual sulphur content in the char may not be an insignificant fraction of the total suphur content of the solids.

5.3.2 Distribution of sulphur among the product solids

The distribution of sulphur among the streams of solids

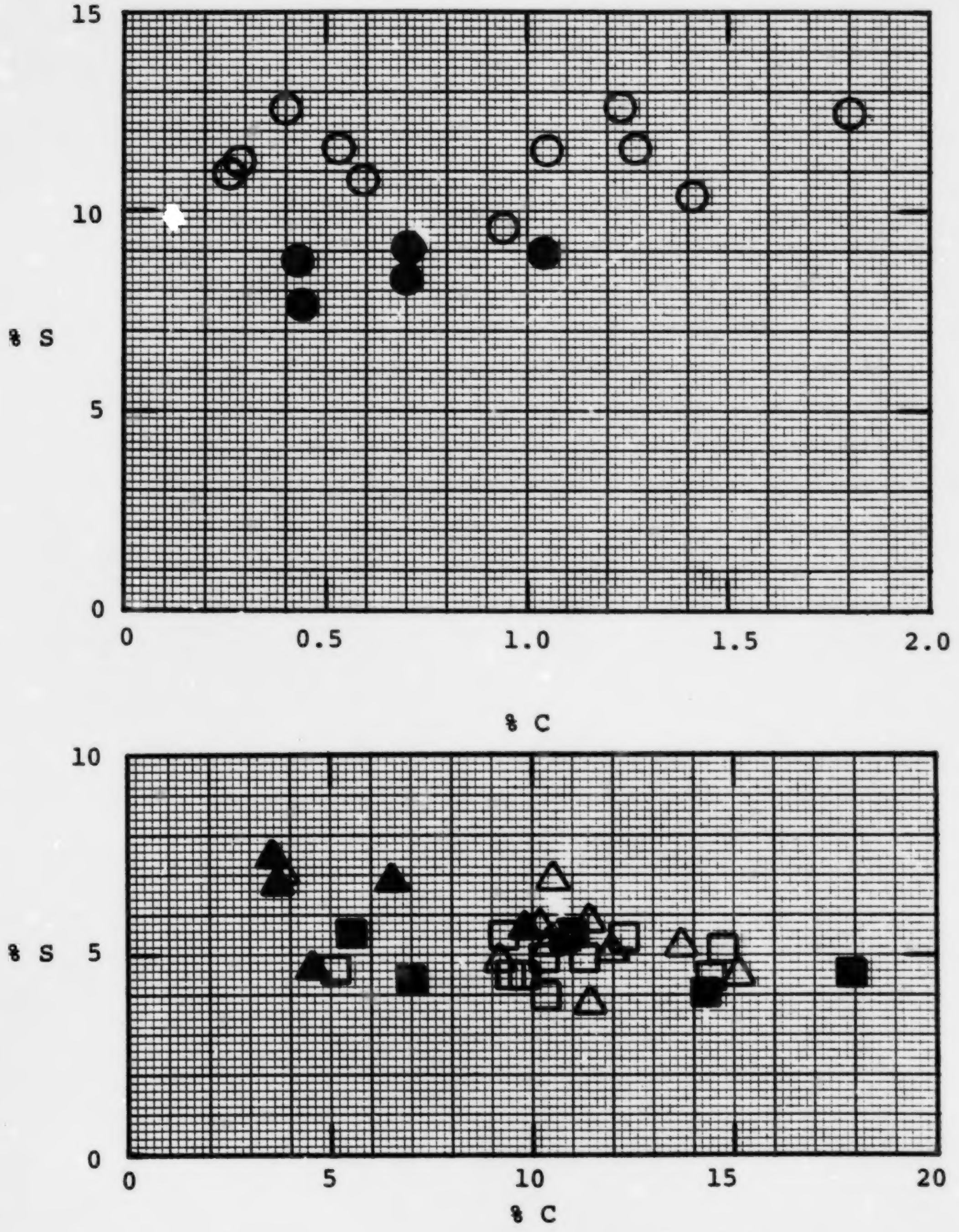

Fig. 5.17. Sulphur content of the product solids.

Product: ○ ● bed overflow; △ ▲ cyclone; □ ■ baghouse.

Sorbent $\hat{D}_p$: ○ △ □ 0.49 mm; ● ▲ ■ 1.72 mm.

from the bed, cyclone and baghouse is shown in Fig. 5.18. The distribution is expressed as a ratio of the sulphur flux in an individual stream to the total sulphur flux in the three streams of solids. As in the case of the carbon balance, the recycle fraction, r, was selected as the abscissa variable in Fig. 5.18 in order to examine the effect of r on the flux ratios. At zero recycle, 60--70 % of the sulphur in the solids is carried by the bed overflow solids while the corresponding ranges for the cyclone solids and baghouse solids are 25--36 % and 1--3 %, respectively. The effect of r is not significant in the range $0 < r < 0.5$. At a recycle fraction of 0.5, the flux ratios for the bed overflow, cyclone and baghouse are approximately 66 %, 31 % and 3 %, respectively. At total recycle of cyclone solids, about 92 % of the sulphur is carried by the bed overflow stream and 8 % by the baghouse stream.

5.3.3 Sulphur capture efficiency

The SO_2 capture efficiency, η_{SO_2}, may be estimated from the flowrate and sulphur analysis of the fuel and either the flowrate and sulphur oxide analysis of the stack gas or the flowrates and sulphur analyses of the three streams of product solids.

$$\eta_{SO_2} = 100(1 - \dot{n}_{SO_2,g}/\dot{n}_{S,f}) = 100\ \dot{n}_{S,p}/\dot{n}_{S,f} \qquad (5.3.1)$$

where $\dot{n}_{SO_2,g}$ is the molar flux of SO_2 leaving in the stack gas, $\dot{n}_{S,p}$ is the molar flux of sulphur leaving in the product solids, and $\dot{n}_{S,f}$ is the molar flux of sulphur entering in the fuel. This

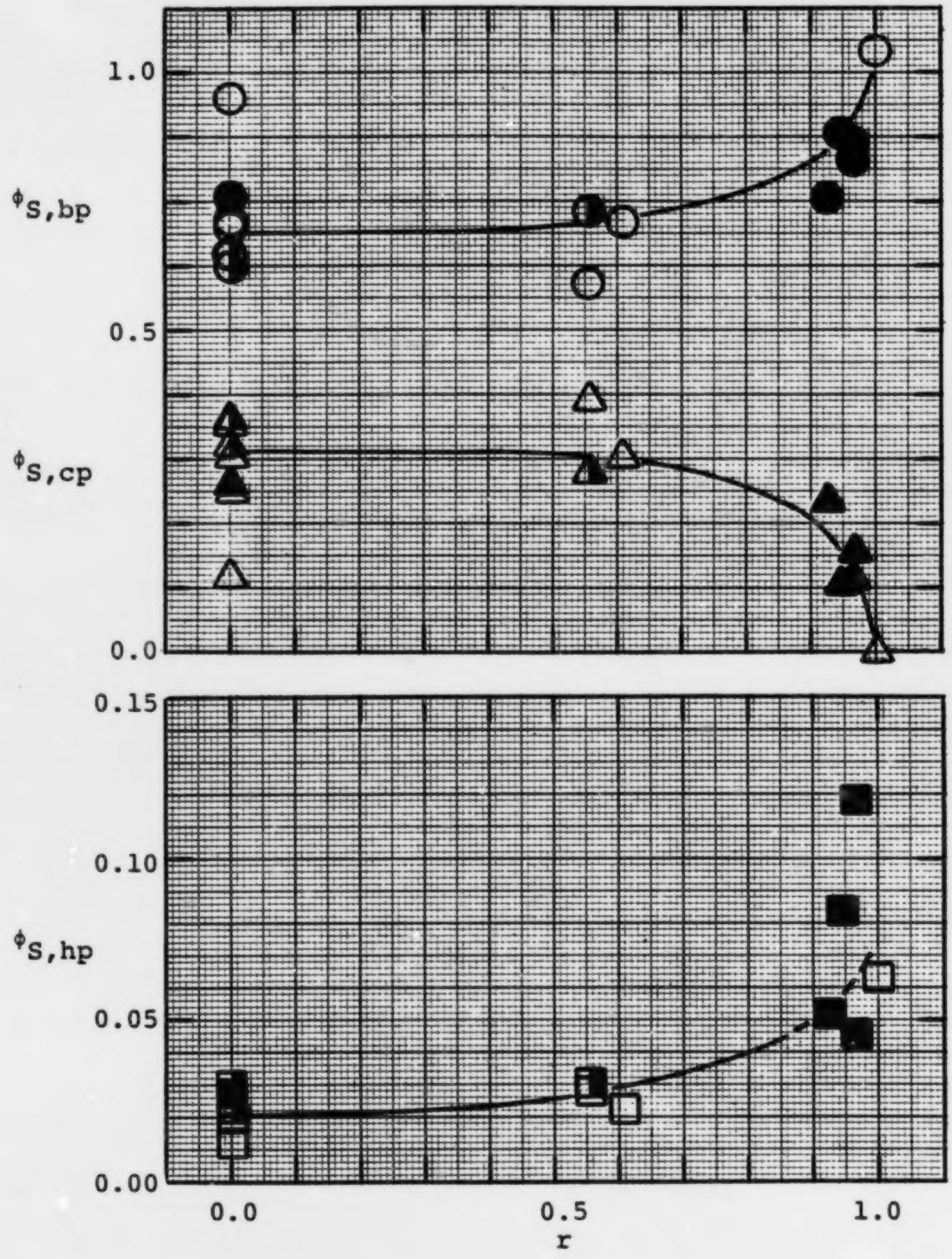

Fig. 5.18. Distribution of sulphur among solids from bed, cyclone and baghouse.

Product: ○ ◑ ● bed; △ ◮ ▲ cyclone; □ ◨ ■ baghouse.
Coal $\hat{D}_p$: ○ △ □ 16.7 mm, ◑ ◮ ◨ 8.8 mm; ● ▲ ■ 3.3 mm.

capture efficiency should be treated as a nominal value because of the small amount of unoxidized residual sulphur which may be present in the char, i.e., a small fraction of the sulphur in the solids may not be captured by the sorbent as chemically fixed sulphate sulphur. Provided the air level is sufficient for good combustion efficiency, η_{SO_2}, as defined by Eq. 5.3.1, is a valid measure of the effectiveness of the sorbent for the removal of sulphur oxides from the product gases.

SO_2 capture efficiencies based on the flowrates and analyses of the stack gas and SO_2 capture efficiencies based on the flowrates and analyses of the three streams of product solids are presented in Fig. 5.19 and Fig. 5.20, respectively. The abscissa variable in the figures, the atomic calcium-to-sulphur ratio, is based on the equivalent Ca content of the limestone sorbent, i.e., the small amount of magnesium in the limestone is included in the 'Ca' in the Ca/S ratio. The alkaline earth content of the coal is not included in the Ca/S ratio. The results for the final run in the series, in which the limestone sorbent was replaced by a local Kingston sand, are included in the figures. There is little in the way of valid quantitative conclusions which may be drawn from the results because of the wide disparity in the capture efficiencies evaluated by the two methods. It was not possible to obtain satisfactory closures of the sulphur balances. This area is examined as the next topic. Fig. 5.20 does show, at least qualitatively, the superior effectiveness for sulphur capture, at a fixed Ca/S, of the smaller sorbent

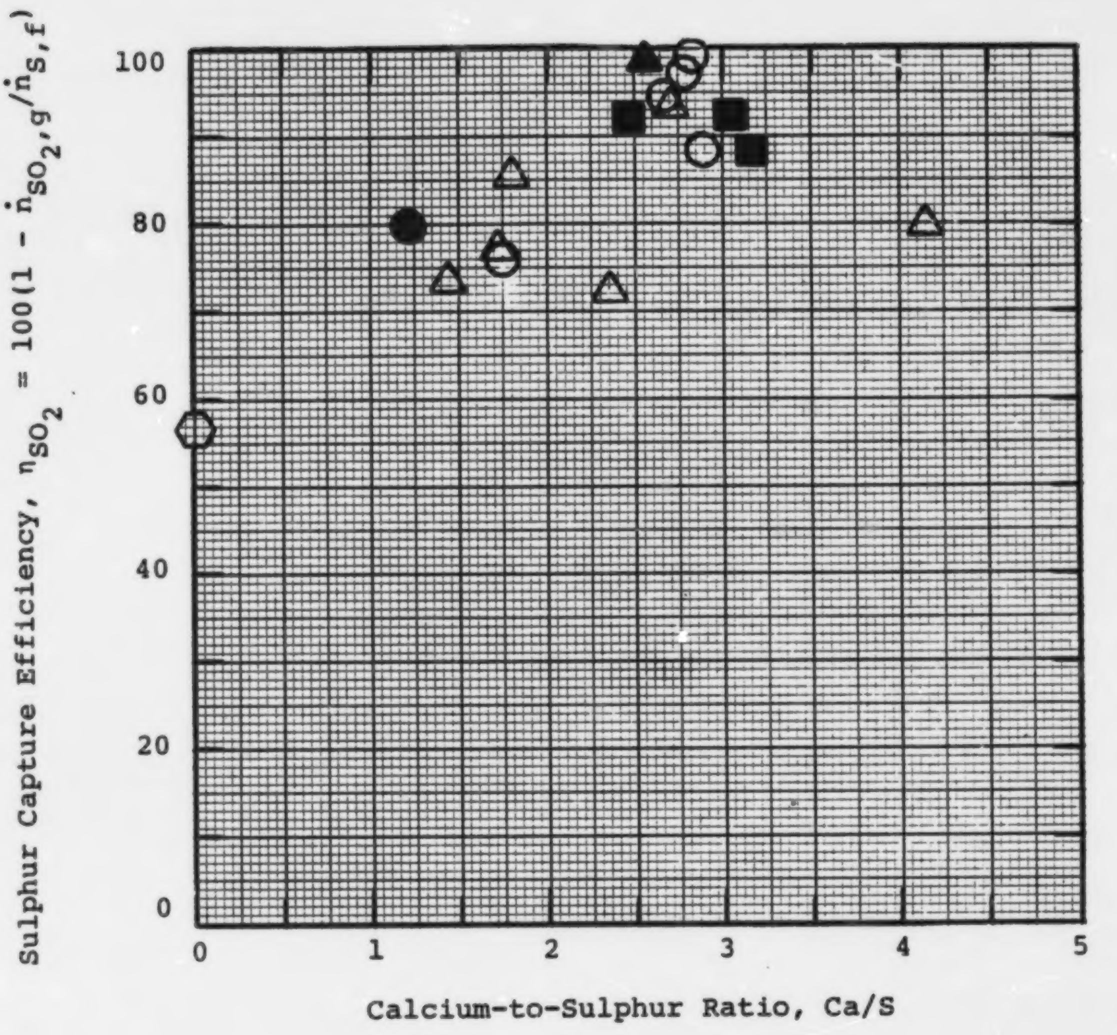

Fig. 5.19. Sulphur capture efficiencies based on product gas analyses.

Key to symbols:

	v, m/s		stone $\hat{D}_p$, mm
○ ●	1.5-1.6	○ △ □	0.49
△ ▲	2.0-2.3	● ▲ ■	1.72
□ ■	2.5-2.6	⬡ sand, $\hat{D}_p$ = 0.95 mm v = 1.5 m/s	

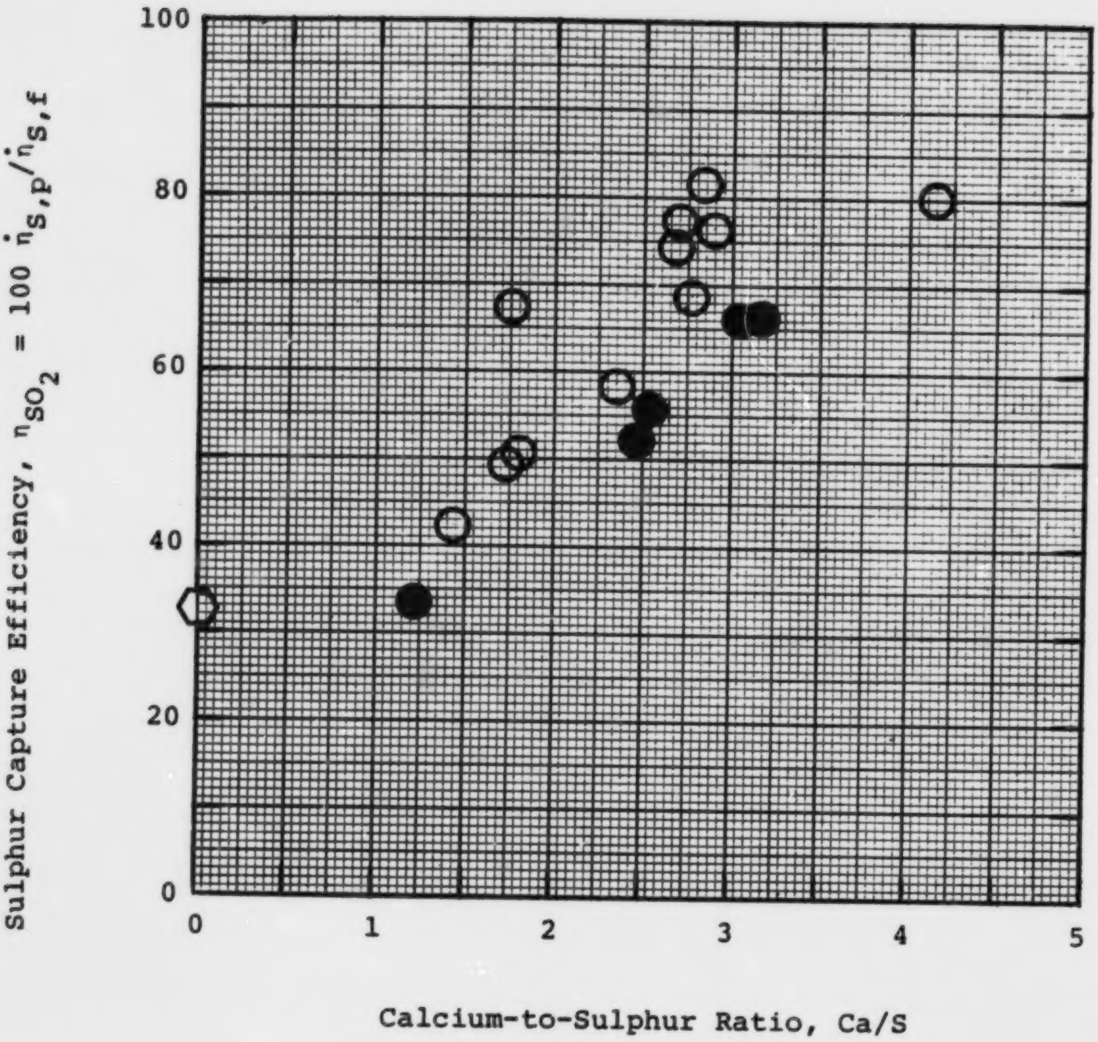

Fig. 5.20. Sulphur capture efficiencies based on analyses of product solids.

Key to symbols:

sorbent $\hat{D}_p$, mm

○ 0.49

● 1.72

⬡ sand, $\hat{D}_p$ = 0.95 mm

size fraction $\hat{D}_p = 0.49$ mm vs. $\hat{D}_p = 1.72$ mm. The SO_2 capture efficiencies, based on the analyses of the stack gas, are restructured and presented in Fig. 5.21 as the percent of the sulphur in the fuel escaping as sulphur oxide emissions vs. the calcium-to-sulphur ratio. As expected, there is a reduction in the sulphur oxide emissions with an increase in the Ca/S ratio but the wide scatter in the results and the unsatisfactory closure of the sulphur balances preclude any attempt at a quantitative regression on the data.

5.3.4 Sulphur balance check

In this final topic in the subsection on the sulphur balance, the lack of satisfactory closures on the sulphur balance is examined. The adequacy of the sulphur balance may be examined in terms of the mole ratio of the sulphur in the product streams to the sulphur in the fuel. Under steady-state conditions this mole ratio should equal unity, i.e.,

$$\phi_{S,pf} = (\dot{n}_{SO_2,g} + \dot{n}_{S,p})/\dot{n}_{S,f} = 1 \qquad (5.3.2)$$

The stack gas was sampled at two locations: downstream of the cyclone separator (port 150) and downstream of the baghouse (port 160). Analyses of samples from both locations are used in the examination which follows.

Sulphur capture efficiencies based on the analyses of the product solids are compared in Fig. 5.22 with the sulphur capture

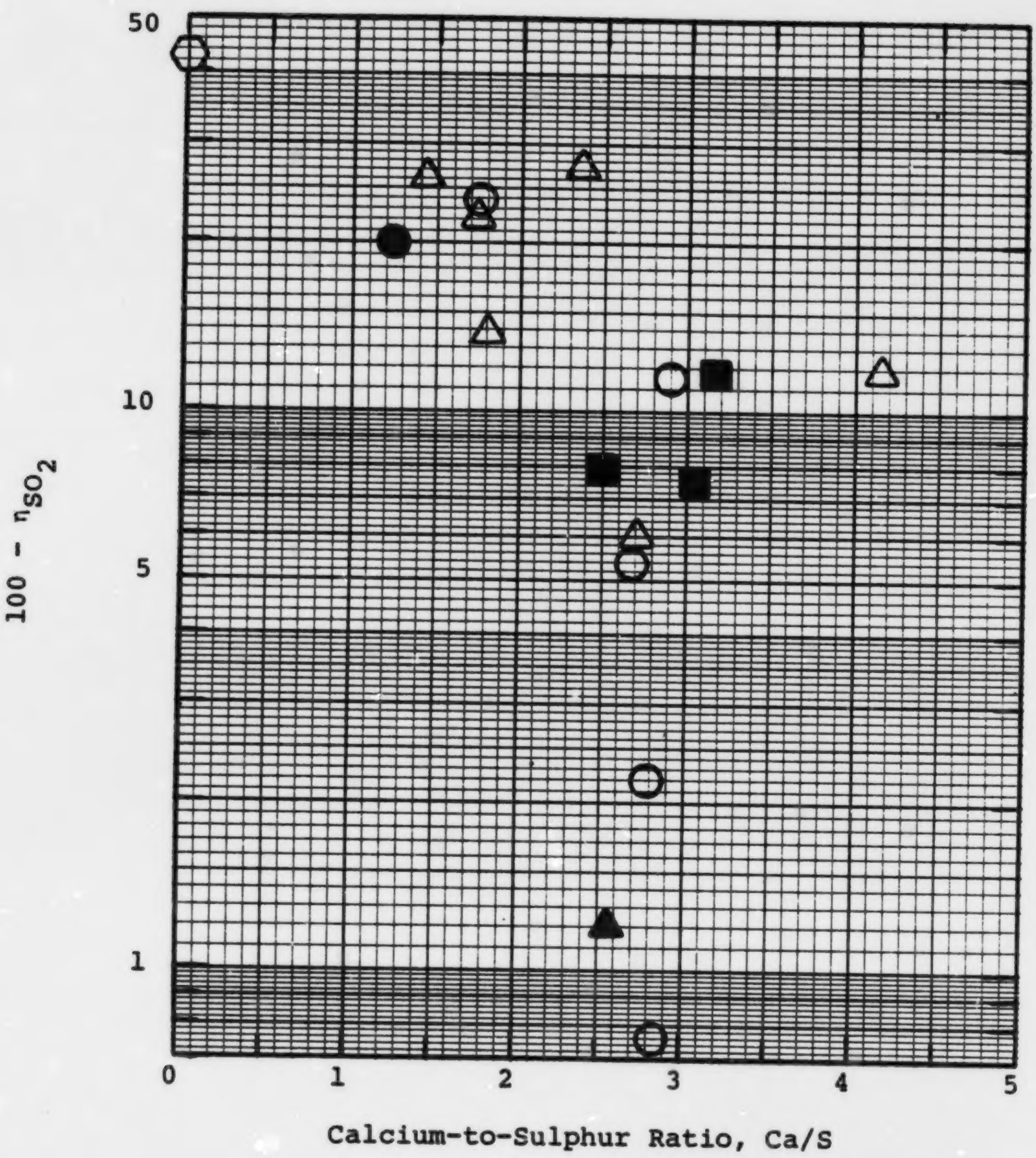

Fig. 5.21. Percent of sulphur in fuel escaping as sulphur oxide emissions.

Key to symbols:

	v, m/s		stone $\hat{D}_p$, mm
○ ●	1.5-1.6	○ △ □	0.49
△ ▲	2.0-2.3	● ▲ ■	1.72
□ ■	2.5-2.6	⬡ sand, $\hat{D}_p$ = 0.95 v = 1.5 m/s	

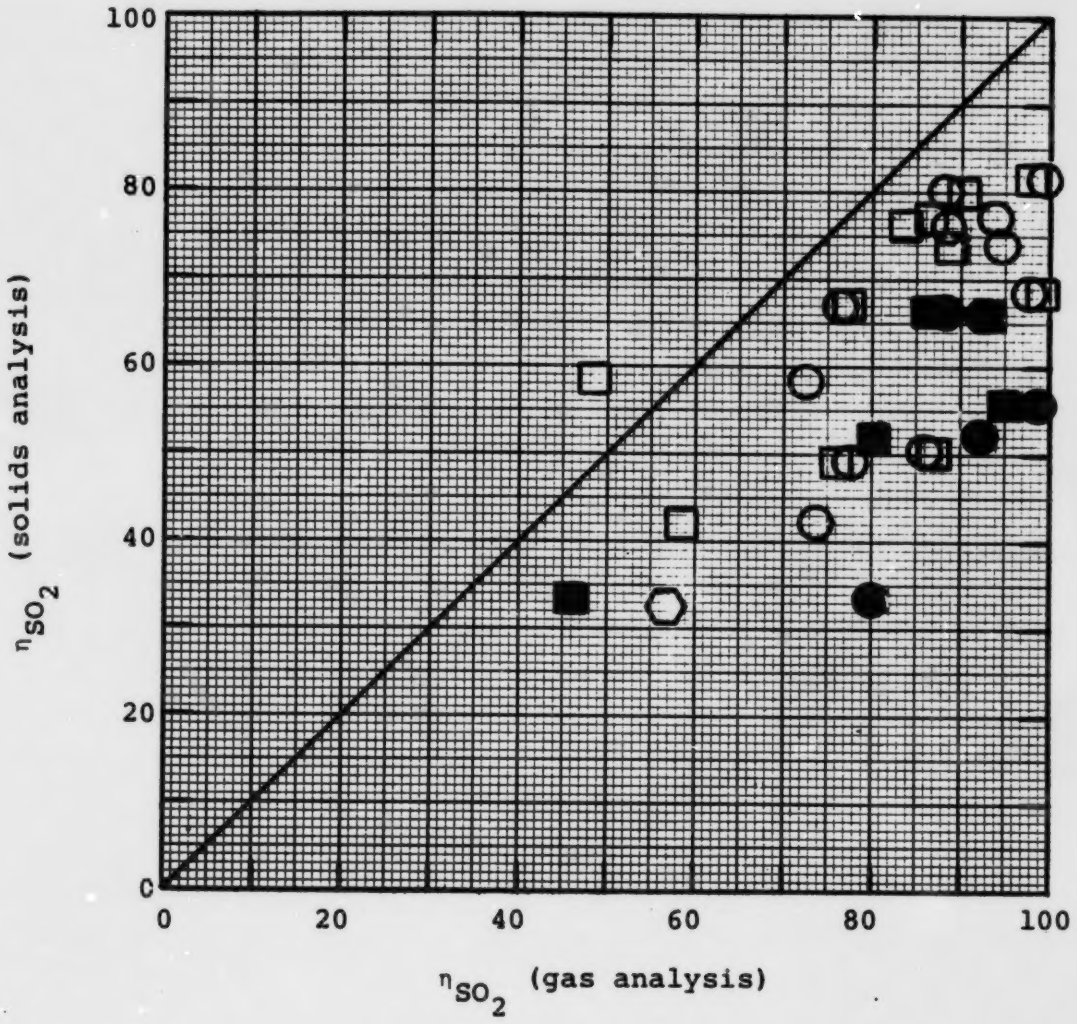

Fig. 5.22. Comparison of sulphur capture efficiencies based on solids analysis with sulphur capture efficiencies based on gas analysis.

Key to symbols:

○ ● gas analysis at port 150

□ ■ gas analysis at port 160

□ ○ sorbent $\hat{D}_p$ 0.49 mm

■ ● sorbent $\hat{D}_p$ 1.72 mm

⬡ sand, $\hat{D}_p$ = 0.95 mm

efficiencies based on the analyses of the stack gas at both port 150 and port 160. Although there are a few unsatisfactory disparities, the majority of SO_2 analyses from port 150 and port 160 show acceptable reproducibility. There is no directional bias in the analyses, i.e., the SO_2 concentrations at port 160 are not consistently higher or consistently lower than the SO_2 concentrations at port 150.

The flux ratio $\phi_{S,pf}$ is plotted vs. the bed temperature, T_b, the recycle fraction, r, and the sum of the mass fluxes of carbon in the cyclone and baghouse streams, $\dot{m}_{C,c} + \dot{m}_{C,h}$, in Fig. 5.23 through Fig. 5.25. What is clearly evident from an examination of Fig. 5.24 and Fig. 5.25 is the poorer sulphur balance checks at high recycle rates of cyclone solids, and correspondingly, at low carbon fluxes in the cyclone and baghouse solids. As an explanation for the unsatisfactory closures of the sulphur balances, one could speculate on the possible sorption of SO_2 on activated char with subsequent desorption prior to analysis of the samples. If this speculation is correct, then the better sulphur balance checks should occur at low carbon fluxes. However, since just the opposite effect is observed in Fig. 5.25, this explanation is not valid. Since the streams of product solids are the major contributors of sulphur, accurate flowrates and analyses are critical to satisfactory closure of the material balances. The $\phi_{S,pf}$ values for corresponding analyses at port 150 and at port 160 are in reasonable agreement for the majority of the runs. Based on this fact and the acceptable closures of the carbon

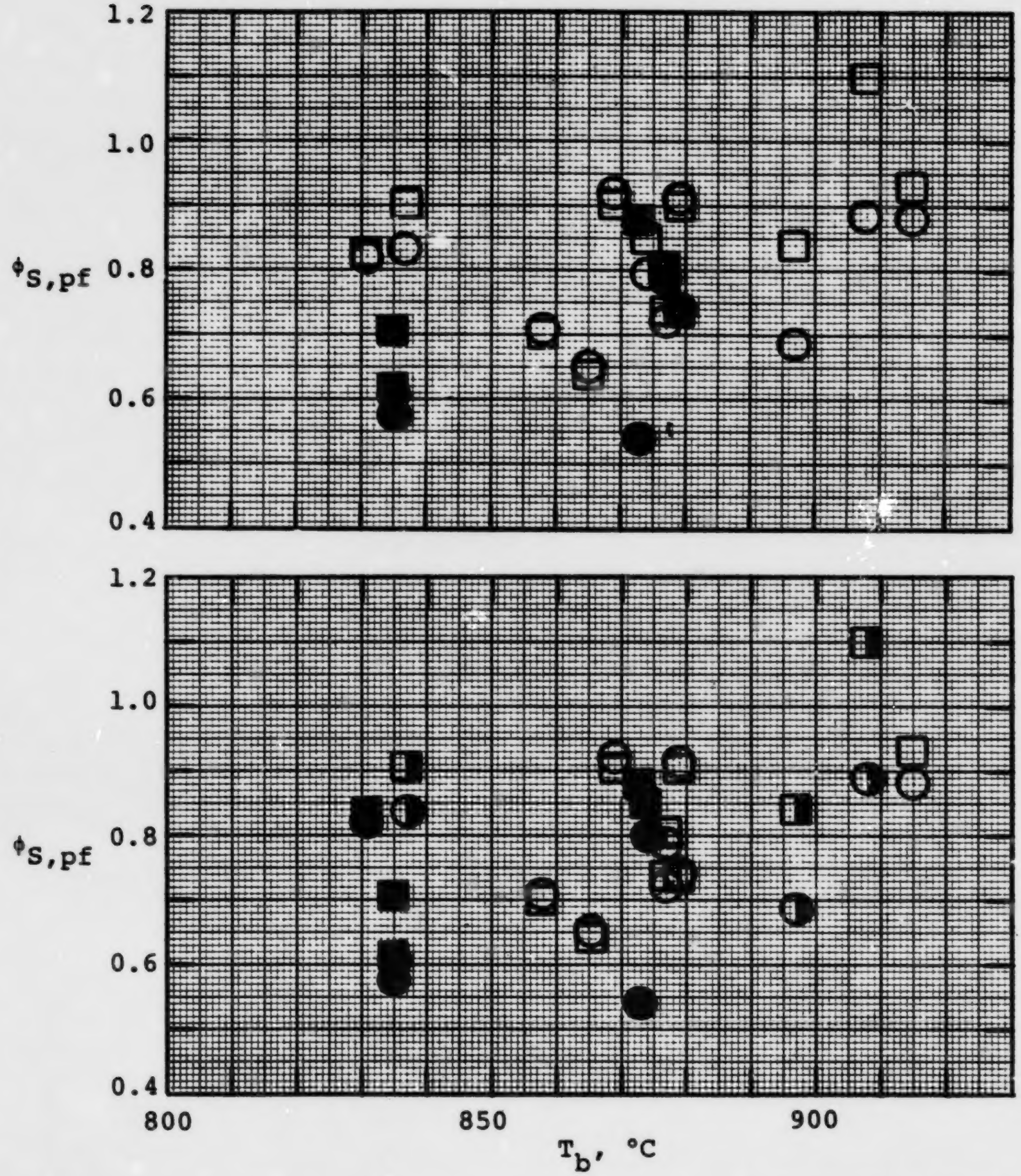

Fig. 5.23. Flux ratio of sulphur in the product streams to sulphur in the fuel vs. bed temperature, T_b.

Top Plot		Bottom Plot	
○ ●	gas analysis at port 150	○ ◐ ●	gas analysis at port 150
□ ■	gas analysis at port 160	□ ◧ ■	gas analysis at port 160
○ □	sorbent $\hat{D}_p$ 0.49 mm	○ □	coal $\hat{D}_p$ 16.7 mm
● ■	sorbent $\hat{D}_p$ 1.72 mm	◐ ◧	coal $\hat{D}_p$ 8.8 mm
		● ■	coal $\hat{D}_p$ 3.3 mm

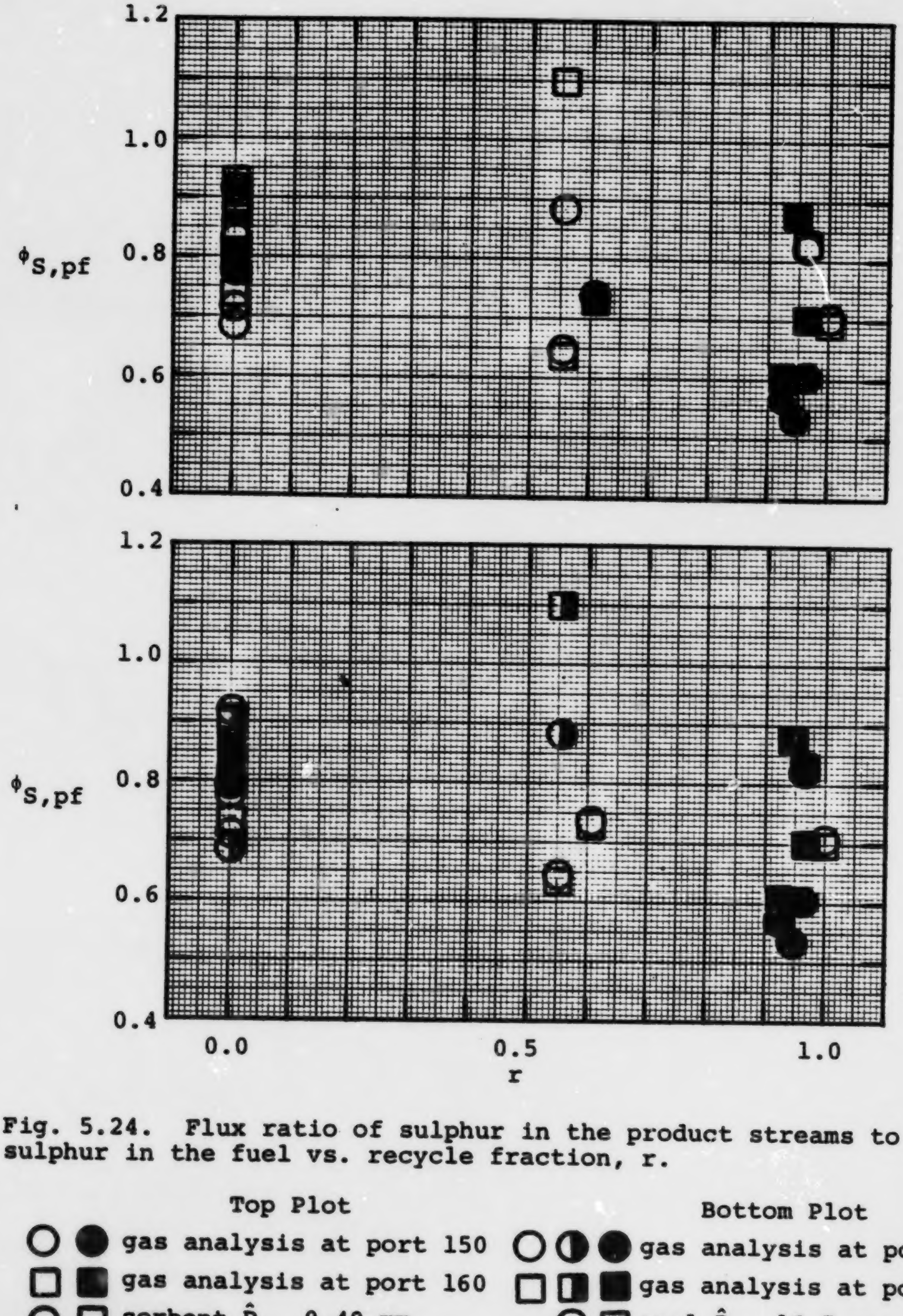

Fig. 5.24. Flux ratio of sulphur in the product streams to sulphur in the fuel vs. recycle fraction, r.

Top Plot

○ ● gas analysis at port 150
□ ■ gas analysis at port 160
○ □ sorbent $\hat{D}_p$ 0.49 mm
● ■ sorbent $\hat{D}_p$ 1.72 mm

Bottom Plot

○ ◐ ● gas analysis at port 150
□ ◧ ■ gas analysis at port 160
○ □ coal $\hat{D}_p$ 16.7 mm
◐ ◧ coal $\hat{D}_p$ 8.8 mm
● ■ coal $\hat{D}_p$ 3.3 mm

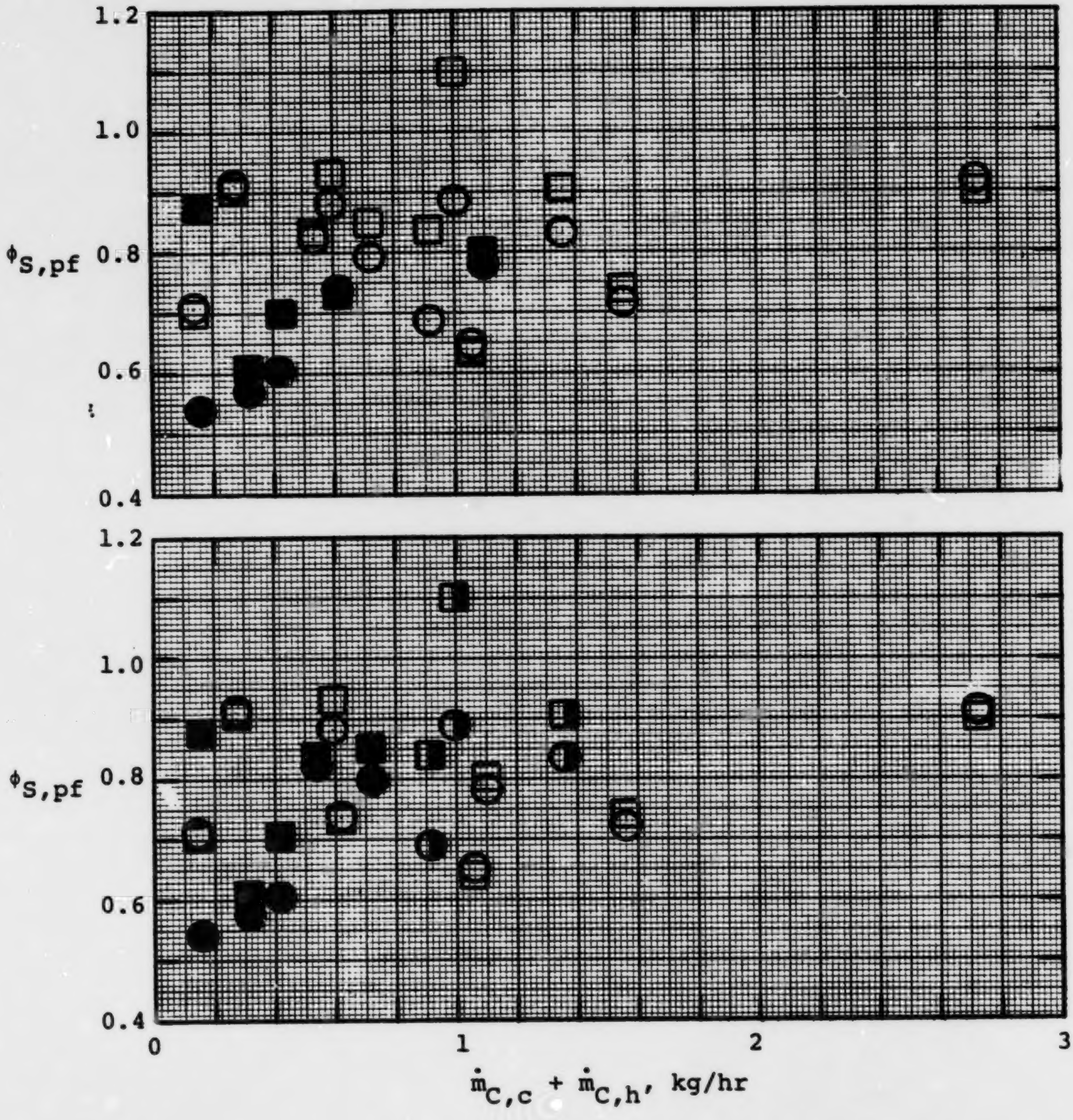

Fig. 5.25. Flux ratio of sulphur in the product streams to sulphur in the fuel vs. the mass flux of carbon in cyclone and baghouse solids.

Top Plot

○ ● gas analysis at port 150
□ ■ gas analysis at port 160
○ □ sorbent $\hat{D}_p$ 0.49 mm
● ■ sorbent $\hat{D}_p$ 1.72 mm

Bottom Plot

○ ◐ ● gas analysis at port 150
□ ◧ ■ gas analysis at port 160
○ □ coal $\hat{D}_p$ 16.7 mm
◐ ◧ coal $\hat{D}_p$ 8.8 mm
● ■ coal $\hat{D}_p$ 3.3 mm

balances where the stack gas is a major contributor, it seems reasonable to assume that the sulphur capture efficiencies based on the stack gas are the more realistic estimates.

5.4 The fuel nitrogen balance

5.4.1 Emission levels of nitrogen oxides

The NO_x levels in the stack gas on a dry basis are shown in Fig. 5.26. The use of bed temperature as the abscissa variable in Fig. 5.26 has no particular significance; it is simply a convenient device for displaying the NO_x levels. Ignoring the two abnormally low values, the emission levels are in the range 213--275 ppm NO_x. Although this range falls within the range observed in our earlier work on Minto and Devco coals (Becker and Code, 1983), it is considerably narrower. In the earlier work, approximately one-half of the runs gave NO_x levels in the range 300--415 ppm. The source of these emissions must be the fuel nitrogen. Only an insignificant amount of NO_x can be attributed to the oxidation of atmospheric nitrogen at normal operating bed temperatures.

5.4.2 The N/C ratio in the product solids

The nitrogen content of the three streams of solids from the cyclone, baghouse and bed overflow is shown in Fig. 5.27 and Fig. 5.28. The atomic N/C ratio for the three size fractions of Evans coal was in the range 0.0140--0.0146. Lines of constant N/C ratio, including the average of the N/C ratios of the fuel,

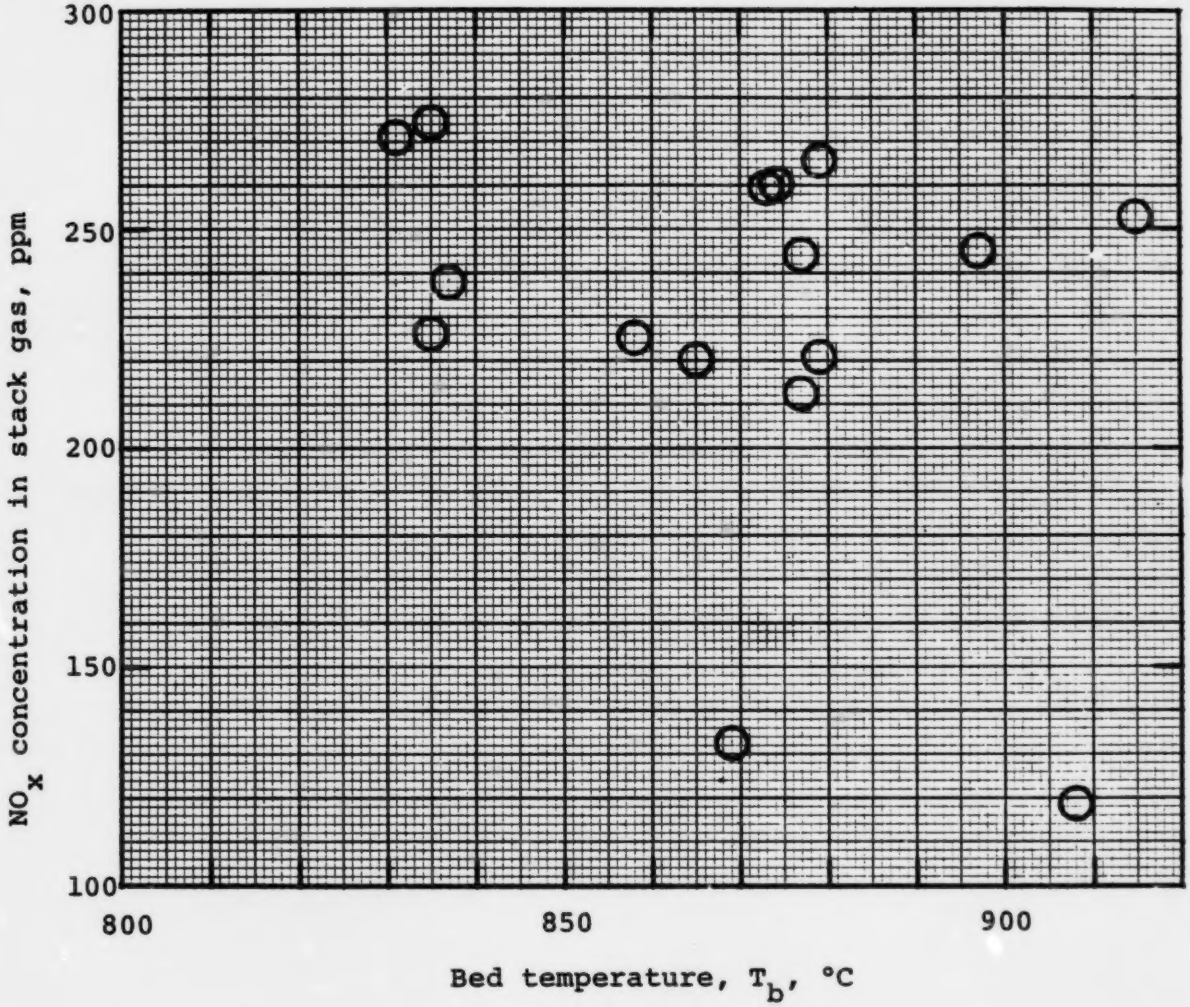

Fig. 5.26. NO_x levels in the stack gas from the fluidized-bed combustion of Evans coal.

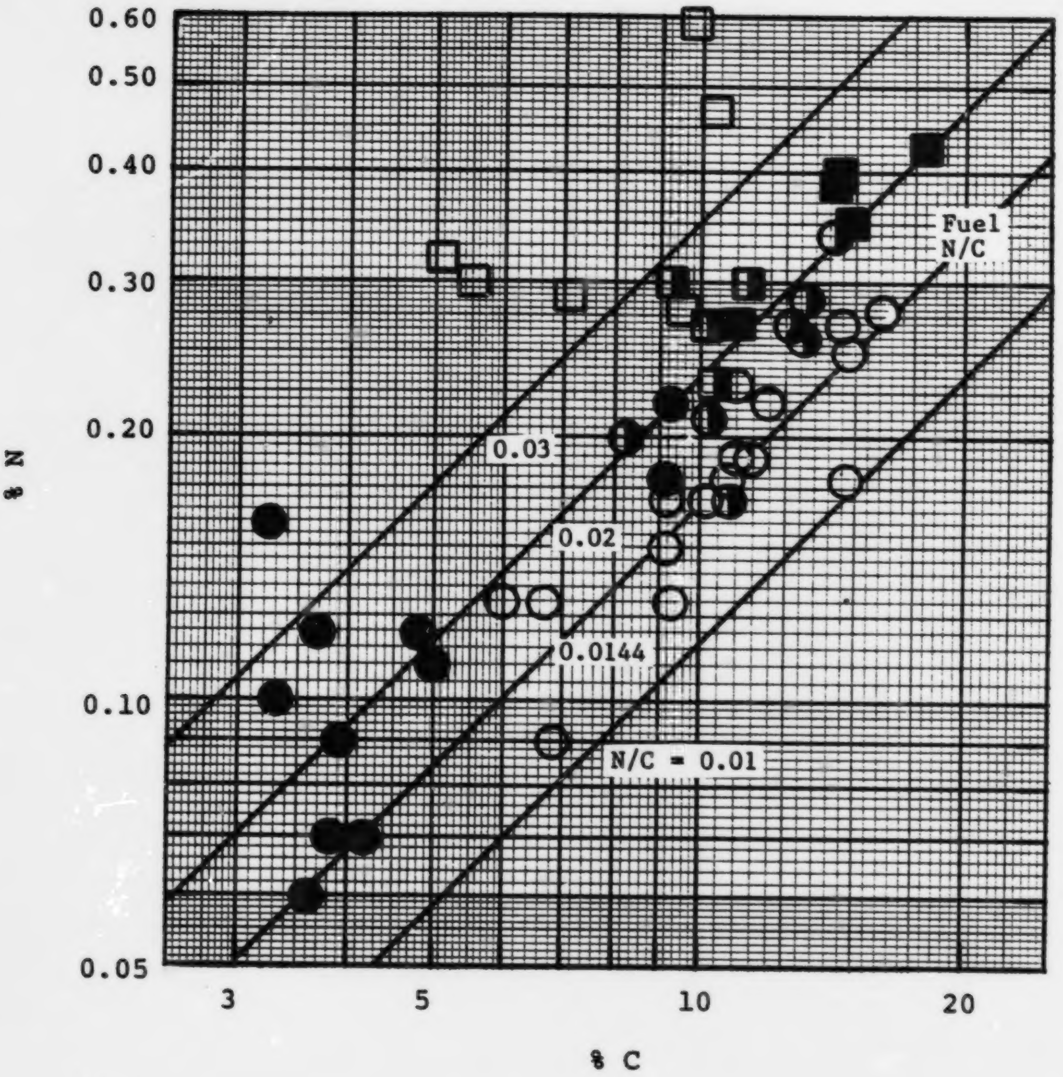

Fig. 5.27. Nitrogen content of the cyclone and baghouse solids.

Key to symbols:

○ ◐ ● cyclone solids
□ ◧ ■ baghouse solids
○ □ coal $\hat{D}_p$ 16.7 mm
◐ ◧ coal $\hat{D}_p$ 8.8 mm
● ■ coal $\hat{D}_p$ 3.3 mm

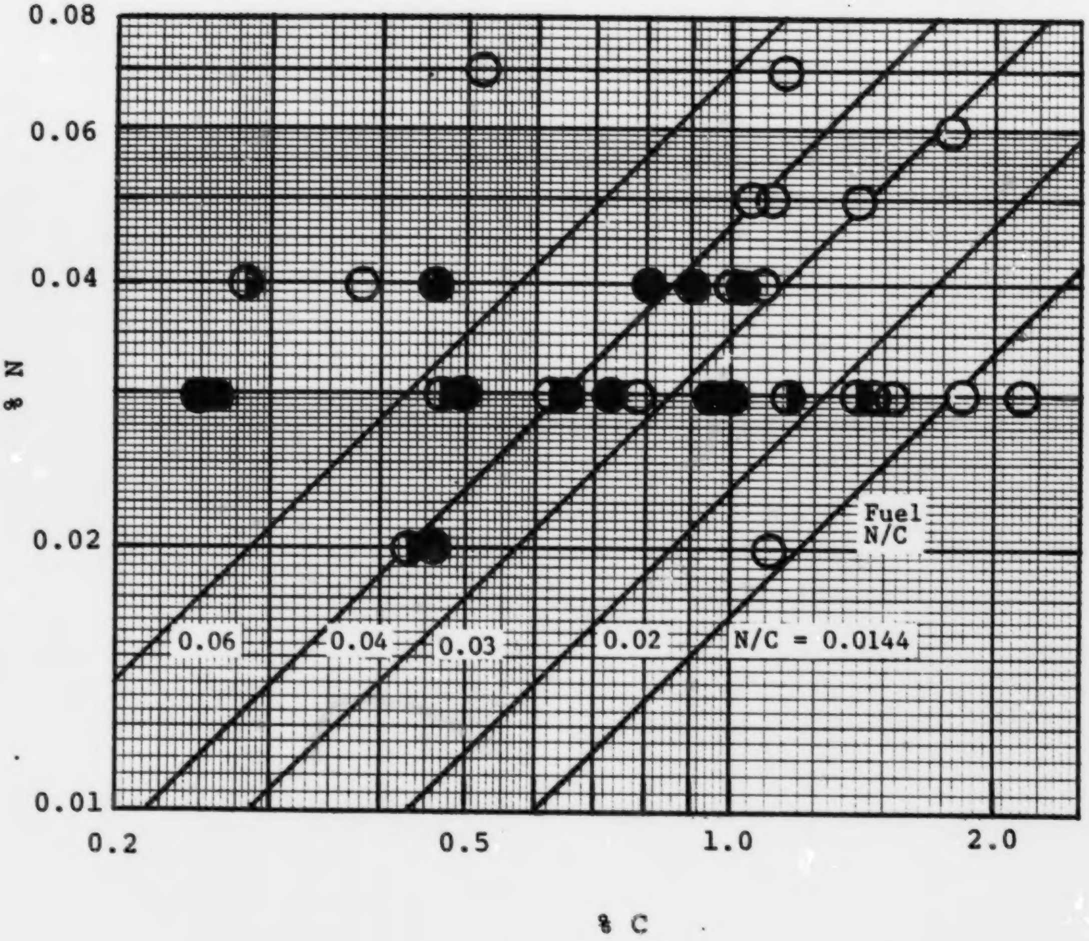

Fig. 5.28. Nitrogen content of the bed overflow solids.

Key to symbols: coal $\hat{D}_p$

○ 16.7 mm
◐ 8.8 mm
● 3.3 mm

have been superimposed on the plots in Fig. 5.27 and Fig. 5.28. In plotting the analyses, the points have been distinguished according to the mean particle diameter, $\hat{D}_p$, of the coal feed.

For the runs with the largest mean coal particle diameter (16.7 mm) there is little difference between the residual N/C ratios in the cyclone solids and the N/C ratio of the fuel. The points scatter about the constant N/C line for the fuel (Fig. 5.27). An increase in the recycle fraction lowers both the nitrogen content and the carbon content of the solids but there is no significant effect on the N/C ratio. However, for the two smaller size fractions a decrease in the fuel $\hat{D}_p$ increases the residual N/C ratio in the cyclone solids. The pronounced effect of an increase in recycle fraction ($0.92 < r < 0.97$) on the nitrogen content and the carbon content of the solids is evident for the group of points in the lower left region of Fig. 5.27 (filled circles; $\hat{D}_p = 3.3$ mm) but again, within the scatter of the analyses for individual runs, there is no apparent effect of recycle fraction on the residual N/C ratio.

The residual N/C ratios for the baghouse solids are much higher than the fuel N/C ratio, by a factor of 2 to 4. There is an effect of fuel particle diameter but it is opposite to the effect observed for the cyclone solids, i.e., the smaller size fractions give a lower residual N/C ratio. For the smallest size fraction ($\hat{D}_p = 3.3$ mm) there is no significant difference between the residual N/C ratio for the run with $r = 0$ and the

N/C ratios for the runs with $r > 0.92$.

The analyses for the bed overflow solids scatter widely and do not exhibit the linearity shown on the log-log plot by the results for the cyclone and baghouse solids. With the exception of two points, the residual N/C ratios are higher than the fuel N/C ratio, by a factor of up to 6. This increase in the N/C ratio in the product solids indicates a preferential conversion of the non-N-containing constituents in the fuel.

5.4.3 Effect of operating conditions on the conversion of fuel N to NO_x

The effect of operating conditions on the molar flux ratio $\dot{n}_{NO_x}/\dot{n}_{N,f}$ or the fractional conversion of fuel N to NO_x is examined in Fig. 5.29 through Fig. 5.31. Only 4--15 % of the fuel N is converted to NO_x in the stack gas. There is no apparent effect of bed temperature or recycle fraction on the conversion of fuel N to NO_x but both excess air level and solids residence time have positive effects. The effects of these two operating variables enhance each other and individual points need to be examined to ensure that each variable has a significant effect on the conversion of fuel N to NO_x. For example, take the two points in Fig. 5.29 for a fuel $\hat{D}_p$ of 3.3 mm: $\varepsilon_A = -7.3$ %, $\dot{n}_{NO_x}/\dot{n}_{N,f} = 0.101$; $\varepsilon_A = 2.0$ %; $\dot{n}_{NO_x}/\dot{n}_{N,f} = 0.092$. The unexpected decrease in the fractional conversion of fuel N to NO_x with the increase in the excess air level may be explained by the decrease in solids residence time as given by the inverse measures $\dot{m}_p/A_b$ or $\dot{m}_b/A_b$ (Fig. 5.31). There is also an indication of an effect of fuel particle

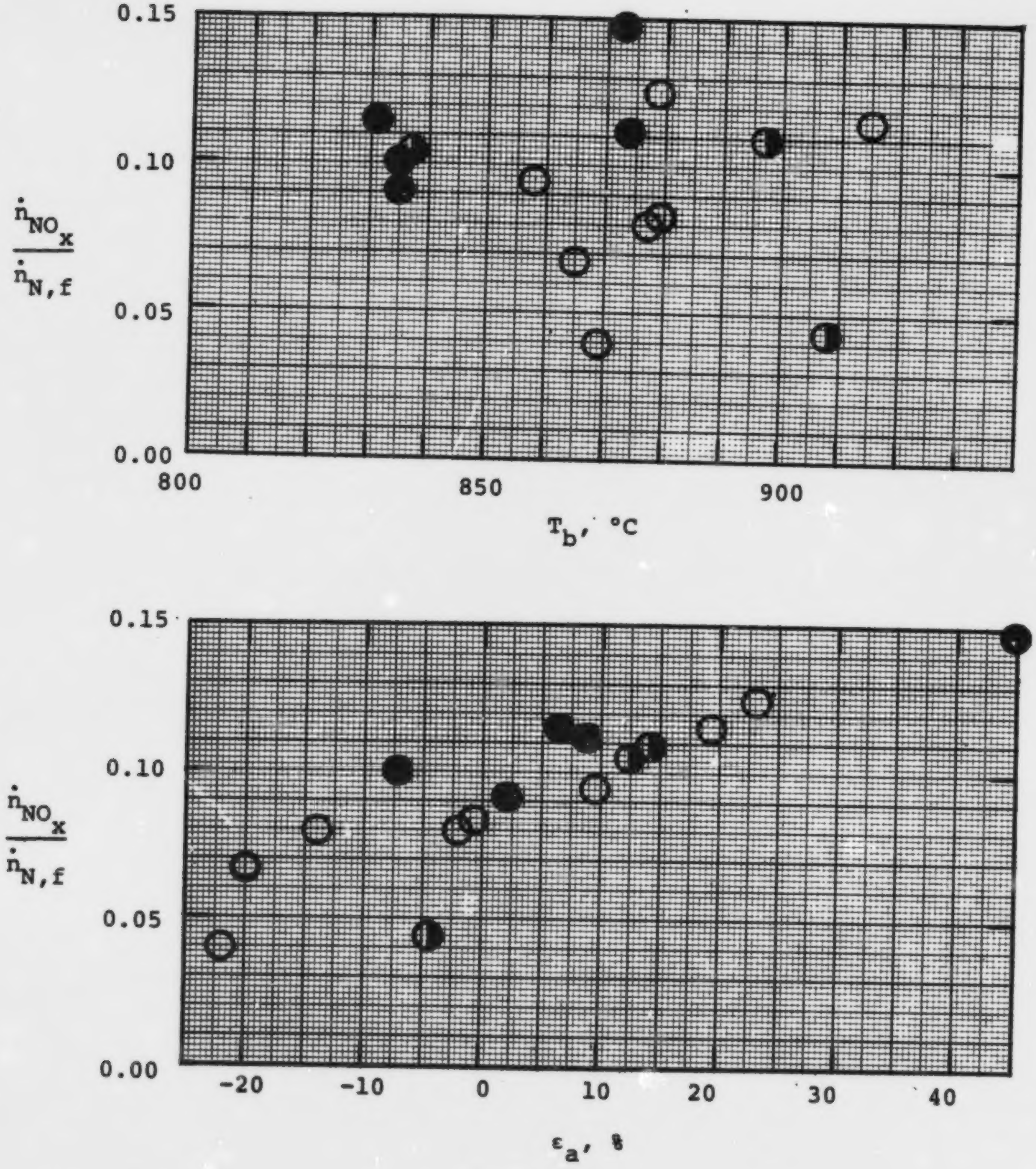

Fig. 5.29. The molar flux ratio $\dot{n}_{NO_x}/\dot{n}_{N,f}$ (fractional conversion of fuel N to NO_x) vs. bed temperature, T_b, and excess air level, ε_a.

Key to symbols: coal $\hat{D}_p$

○ 16.7 mm
◐ 8.8 mm
● 3.3 mm

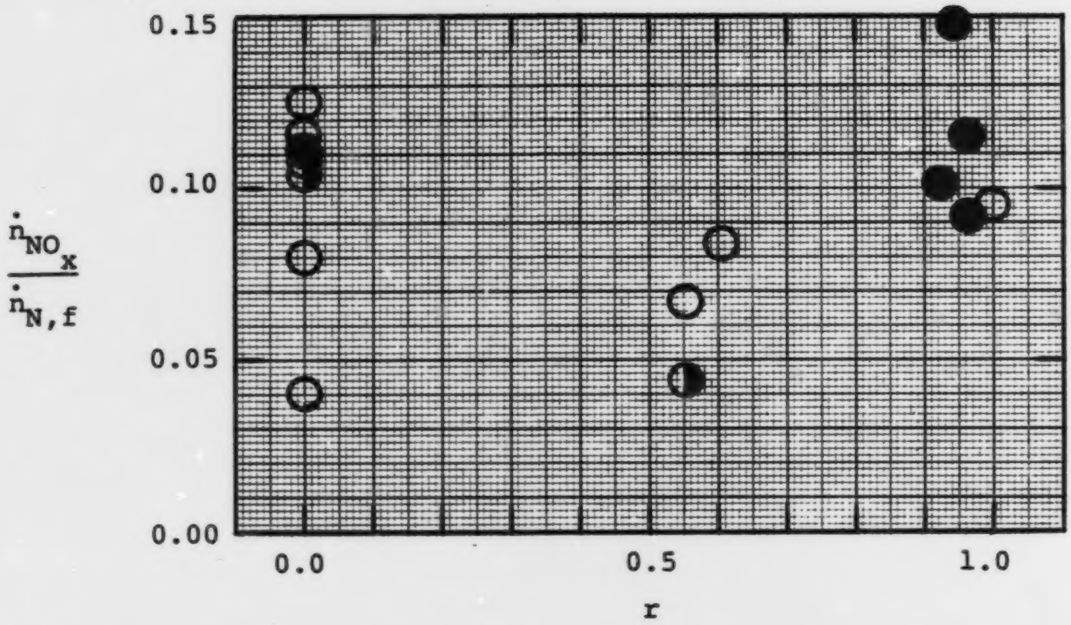

Fig. 5.30. The molar flux ratio $\dot{n}_{NO_x}/\dot{n}_{N,f}$ (fractional conversion of fuel N to NO_x) vs. recycle fraction of cyclone solids.

Key to symbols: coal $\hat{D}_p$

○ 16.7 mm
◑ 8.8 mm
● 3.3 mm

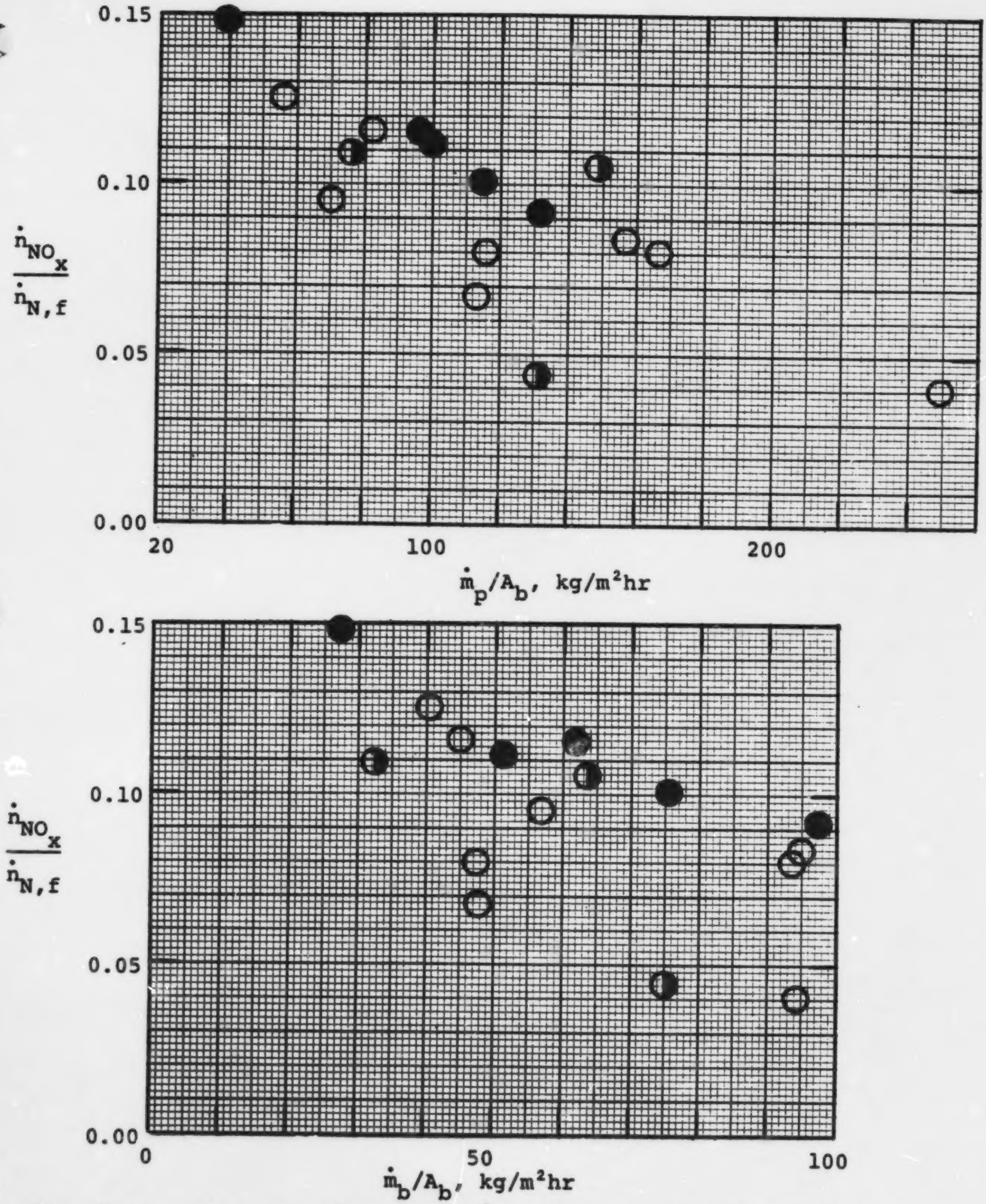

Fig. 5.31. The molar flux ratio $\dot{n}_{NO_x}/\dot{n}_{N,f}$ vs. the efflux of product solids per unit bed area, $\dot{m}_p/A_b$, and the efflux of bed overflow solids per unit bed area $\dot{m}_b/A_b$. See Fig. 5.30 for key to symbols.

size with the smaller size fraction giving higher fuel N to NO_x conversions. The NO_x in the stack gas and the residual N in the solids char account for only a portion of the fuel nitrogen. Presumably, the remaining fuel N, in excess of 70 %, is converted to N_2.

5.5 The hydrogen balance

5.5.1 The H/C ratio in the product solids

Analyses for H and C in the three streams of solids from the cyclone, baghouse and bed overflow are plotted in Fig. 5.32. Lines of constant atomic H/C ratio have been superimposed on the plots in Fig. 5.32 for comparison with the H/C ratio of the fuel. The H and C analyses of the bed overflow solids gave H/C ratios in the range 2--8. These are unrealistic values for residual H/C ratios when compared with the H/C ratio for Evans coal which for the three size fractions used as feed was in the range 0.76--0.77. These inflated values are probably due to the absorption of atmospheric moisture by the samples prior to analysis. The analyses for the cyclone solids and baghouse solids are more realistic with the bulk of the results giving H/C ratios in the range 0.2--0.8. Although these values are of the same order or less than the H/C ratio of the fuel, the possible effect of moisture absorption by the samples needs to be considered in any interpretation of the results. The relative effect of moisture absorption is much smaller for the cyclone and baghouse solids because of the higher carbon content, of the order of

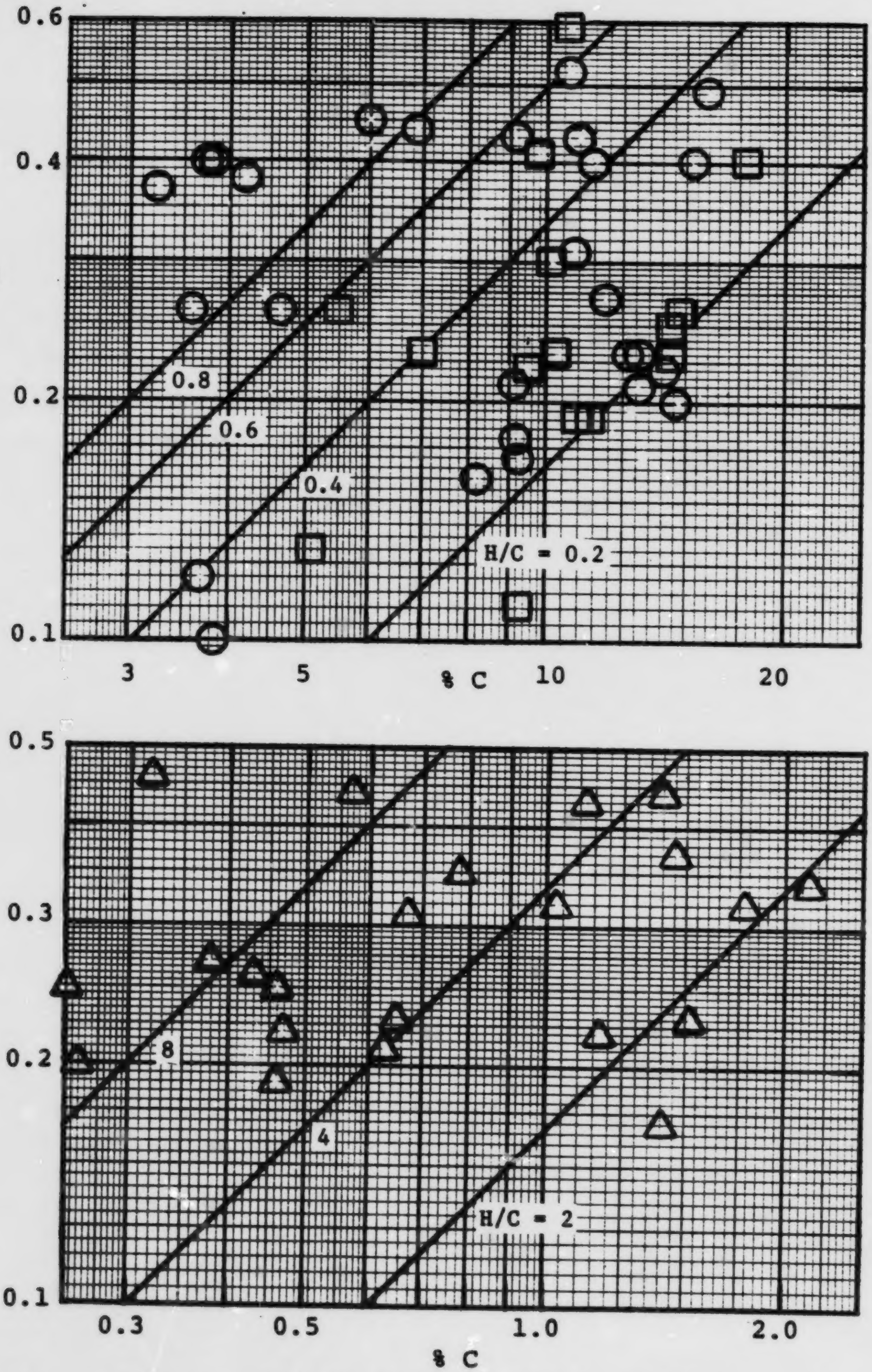

Fig. 5.32. Hydrogen content of the cyclone, baghouse, and bed overflow solids. Key to symbols: ○ cyclone solids, □ baghouse solids, △ bed overflow solids.

ten times the carbon content of the solids from the bed overflow.

5.5.2 Effect of operating conditions on the H/C ratio in the solids

The effect of operating conditions on the residual H/C ratio in the solids from the cyclone and baghouse is examined in Fig. 5.33 and Fig. 5.34. Only those analyses which gave realistic H/C ratios have been included in the plots. Thus, a number of conditions examined in earlier subsections are precluded from this analysis. Also, the potential effect of moisture absorption on the analysis for hydrogen places some reservation on any interpretation.

Two effects are apparent from an examination of Fig. 5.33 and Fig. 5.34: a decrease in the residual H/C ratio in both the cyclone solids and baghouse solids with an increase in the excess air level and a reduction in the H/C level in the baghouse solids for the runs with the smaller coal particle sizes. There is no evidence to support the increase in the H/C ratio in the cyclone solids with an increase in the bed temperature observed in our earlier work on Minto and Devco coals (Becker and Code, 1983). However, the effect of fuel particle size on the residual H/C ratio in the baghouse solids is in agreement with our earlier work.

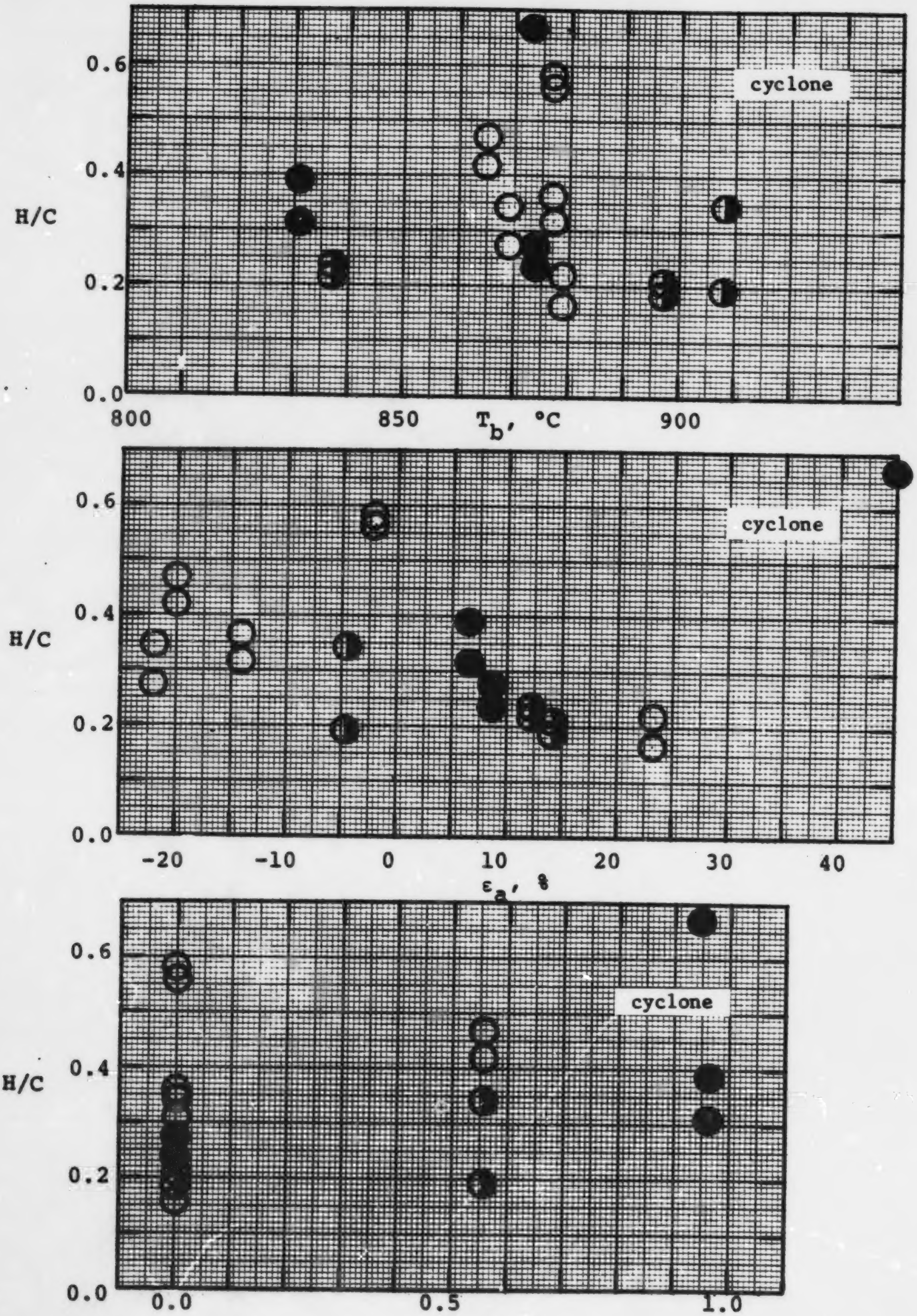

Fig. 5.33. H/C ratios in the cyclone solids vs. bed temperature, T_b excess air level, ε_a, and recycle fraction, r. Coal $\hat{D}_p$: ○ 16.7 mm; ◐ 8 mm; ● 3.3 mm.

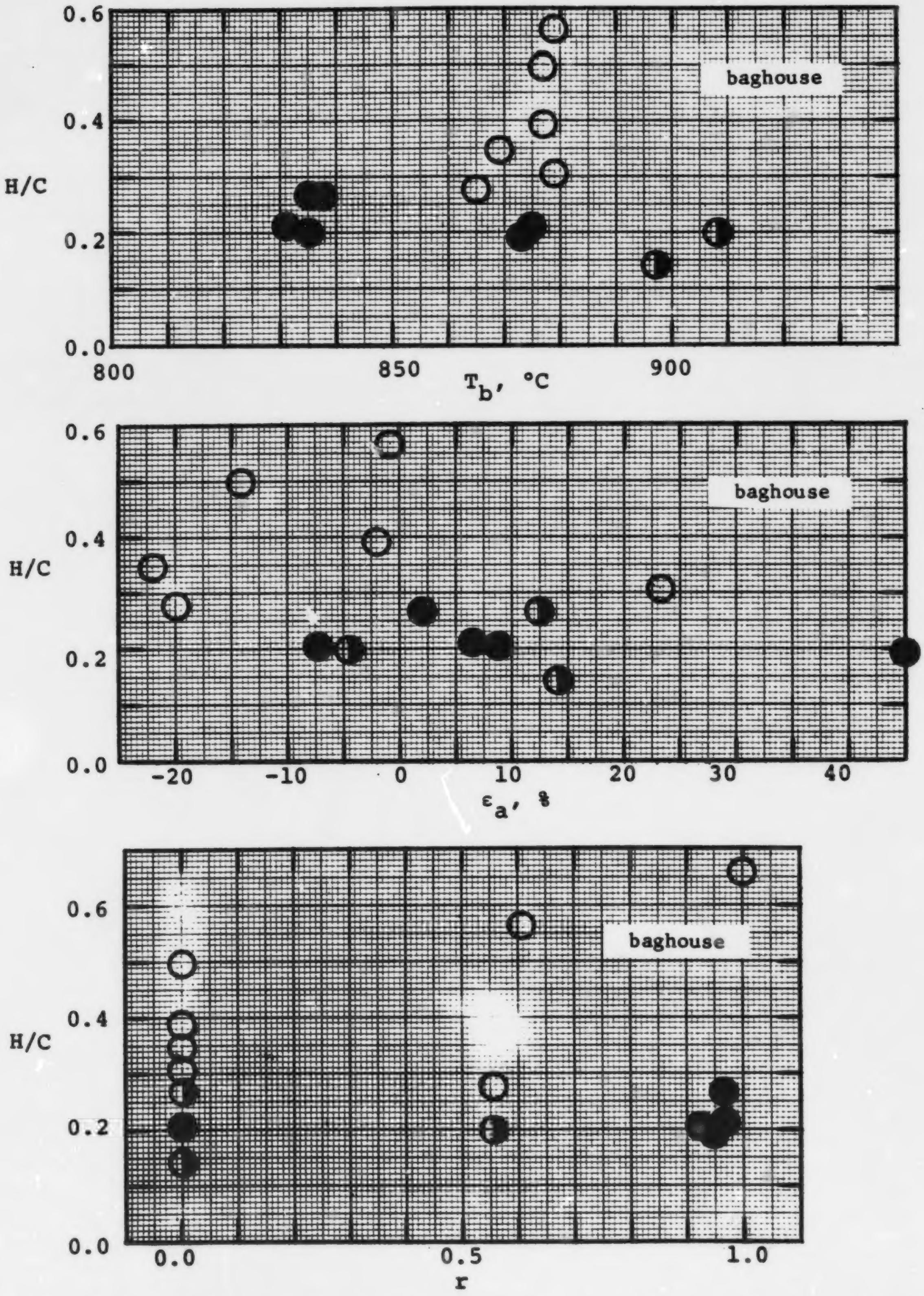

Fig. 5.34. H/C ratios in the baghouse solids vs. bed temperature, T_b, excess air level, ε_a, and recycle fraction, r. Coal $\hat{D}_p$: ○ 16.7 mm; ◐ 8.8 mm; ● 3.3 mm.

6. SYNCRUDE COKE TRIALS

6.1 Introduction

The trials on Syncrude coke involved very high bed temperatures, up to 1100 °C, and in 500 h operating time produced substantial deterioration in the refractory walls of the combustor around the bed. Some runs were aborted because of problems encountered in operating at such extreme conditions. Eight successful runs of about 50 h COT each were completed in which the Fort McMurray (Athabasca) limestone was used as sulphur sorbent. In addition, one run was performed in which the Havelock limestone was used to obtain a comparison of the Fort McMurray stone with one that we have well characterized in other work. The operating conditions of these nine runs are summarized in Table 6.1.

It was found that fluidizing velocities above 1.3 m/s could not be usefully employed; because of the small particle size of the fuel, elutriation became excessive, combustion efficiency became very poor, and it was difficult to maintain the required high bed temperature.

A further vexatious problem, limiting our control over operating conditions, arose from the fact that our combustor, because of its design, had too much bed-cooling capacity. Bed cooling in this combustor occurs by two means:

Table 6.1. Operating conditions of successful runs on Syncrude coke

Run	n_t	Fuel		Stone		Ca/S	Air		r	T_b °C	v m/s	τ_p, h	τ_b, h	COT h
		$\hat{D}_p$, mm	$\dot{m}_f$ kg/h	$\hat{D}_p$, mm	$\dot{m}_s$ kg/h		$\dot{m}_a$, kg/h	ε_a %						
		Syncrude		Havelock										
840605	0	0.34	12.1	0.3	7.4	3.38	134	4.5	0.0	1047	0.9	7.1	22.5	26.2
		Syncrude		McMurray										
840612	1	0.26	16.7	0.34	9.1	2.07	188	7.1	0	1064	1.3	5.5	22.4	40.3
840618	1	0.26	18.2	0.34	8.3	1.73	158	-17.7	0	967	1.0	4.1	12.6	55.5
840703	1	0.26	15.7	0.34	8.5	2.06	142	-13.5	0.69	1061	1.0	4.9	17.1	50.7
840731	0	0.26	17.2	0.94	11.2	2.45	155	-14.4	0.83	1039	1.1	4.5	8.8	43.7
840814	0	0.26	15.1	0.94	11.6	2.90	133	-16.5	0.69	966	0.8	5.0	9.8	47.3
840820	0	0.26	14.7	0.94	7.2	1.85	111	-28.2	0.81	1036	0.8	7.3	17.2	65.0
840827	0	0.26	15.3	0.94	7.9	1.94	130	-19.6	0.83	1105	0.9	7.4	11.3	44.0
840911	0	0.26	17.4	0.94	13.0	2.83	159	-13.3	0.75	1087	1.1	4.4	9.5	48.0

- in-bed tubes, fed with cooling water. The number of these is variable between zero and 48 and in the Syncrude trials was either zero or one.

- water-cooled, refractory-lined wall containing an array of ports for the insertion and mounting of the aforesaid tubes. The heat loss to this wall cannot be significantly controlled and is virtually fixed. This represents a substantial base cooling load which becomes a limiting factor when low fluidizing velocities are employed. At a given level of excess air, the burning rate is (but for variation in completeness of combustion) virtually proportional to the fluidizing velocity. Reduction in fluidizing velocity then leads to a point at which no in-bed tubes are employed and beyond which bed temperature cannot be maintained.

The Syncrude trials were perforce conducted around the feasible limit of operation in the reduction of fluidizing velocity. In order to attain the required high bed temperatures, compromises had to be made. The major sacrifice here was in the control over the excess air level which could not be maintained constant and in most runs, Table 6.1, was actually negative. It should be noted, though, that because of incomplete combustion, a significant oxygen level in the exhaust gases was nevertheless observed in all runs, Fig. 6.1. A further ameliorating factor

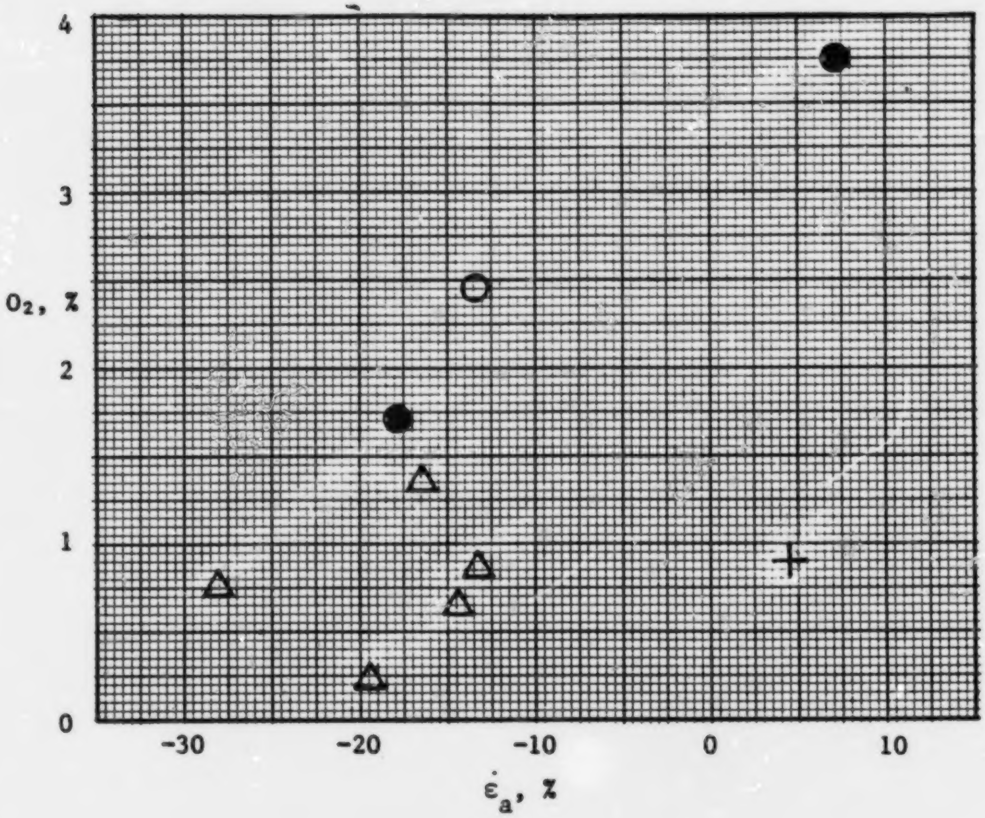

Fig. 6.1. Oxygen content (dry basis) in the exhaust gases (sampling port 150) as a function of excess air level. Symbols:

Limestones:

○ ● Δ Fort McMurray; + Havelock

Mass-median limestone dia. $\hat{D}_p$, mm: ○ ● +, 0.34; Δ, 0.94

Number of in-bed cooling tubes: Δ +, zero; ○ ●, one

Recycle fraction r: ● +, zero; ○ Δ, 0.69--0.83

is that the effect of excess air as established in previous trials on coal combustion (Becker & Code 1983) is mild, and there is no reason to suspect that it should be otherwise in the burning of the Syncrude coke. The most important variable here by far is the bed temperature, and this we were able to adequately vary.

6.2 The carbon balance

6.2.1 Carbon content of solids

Figure 6.2 shows the carbon content of the solid products from bed, cyclone and baghouse. As in coal combustion, unburnt char is concentrated in the fines, is strongly elutriated, and is thus found at high level in cyclone and baghouse products. Also, the level in the cyclone product is usually significantly higher than in the baghouse product.

6.2.2 Flux distribution

Figure 6.3 shows as a function of bed temperature the flux ratio of carbon carried by a given solids stream to the total carbon loss. The cyclone product was the major carrier, by far.

The same results are shown as a function of the recycle fraction in Fig. 6.4. A high level of correlation is apparent. At high recycle, the proportion of carbon carried by the bed product is increased and that carried by the cyclone product is

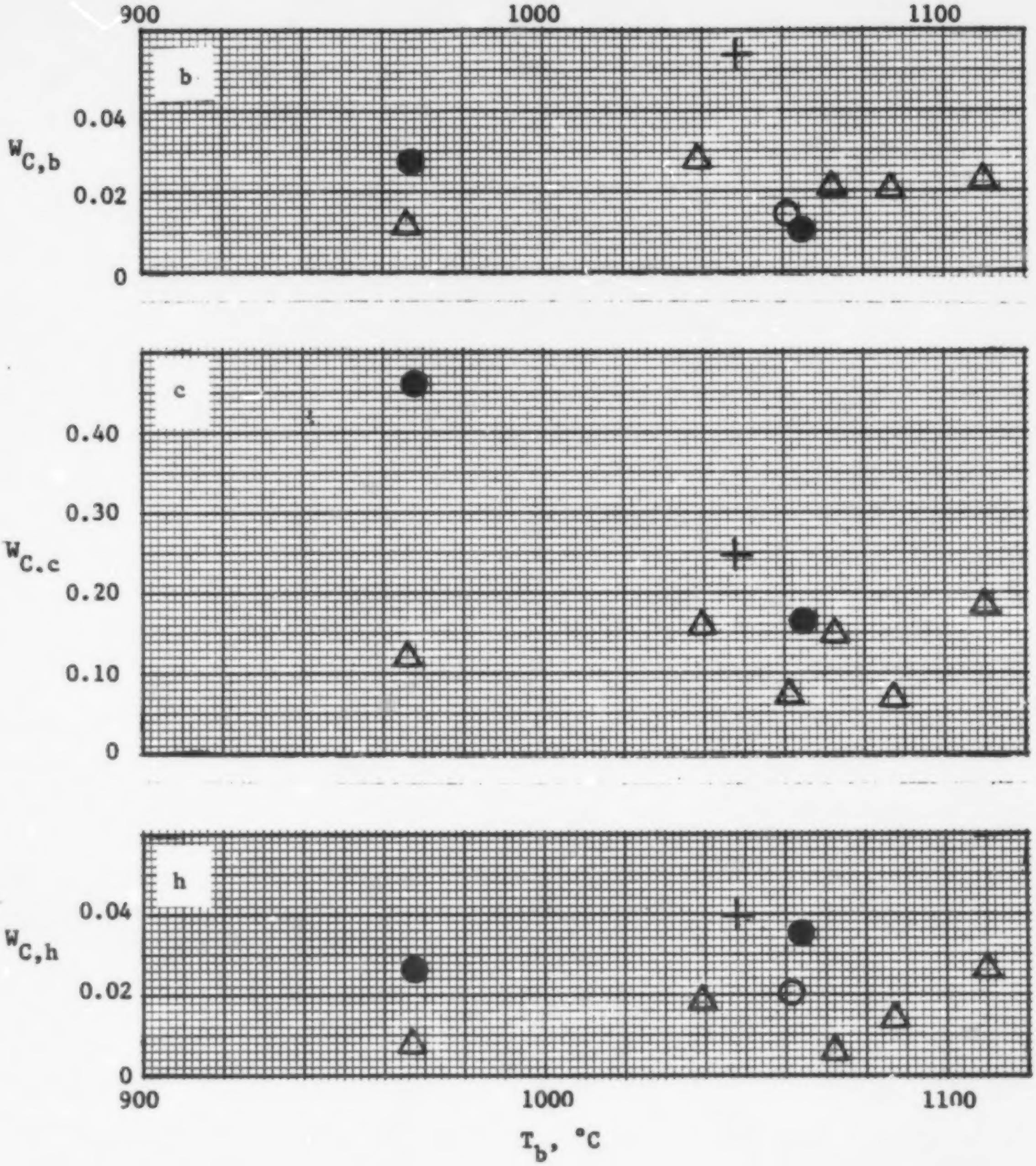

Fig. 6.2. Carbon content of solid products as a function of bed temperature. Top: i = b, the bed product; middle, i = c, the cyclone product; bottom, i = h, the baghouse product. Symbols: key in Fig. 6.1.

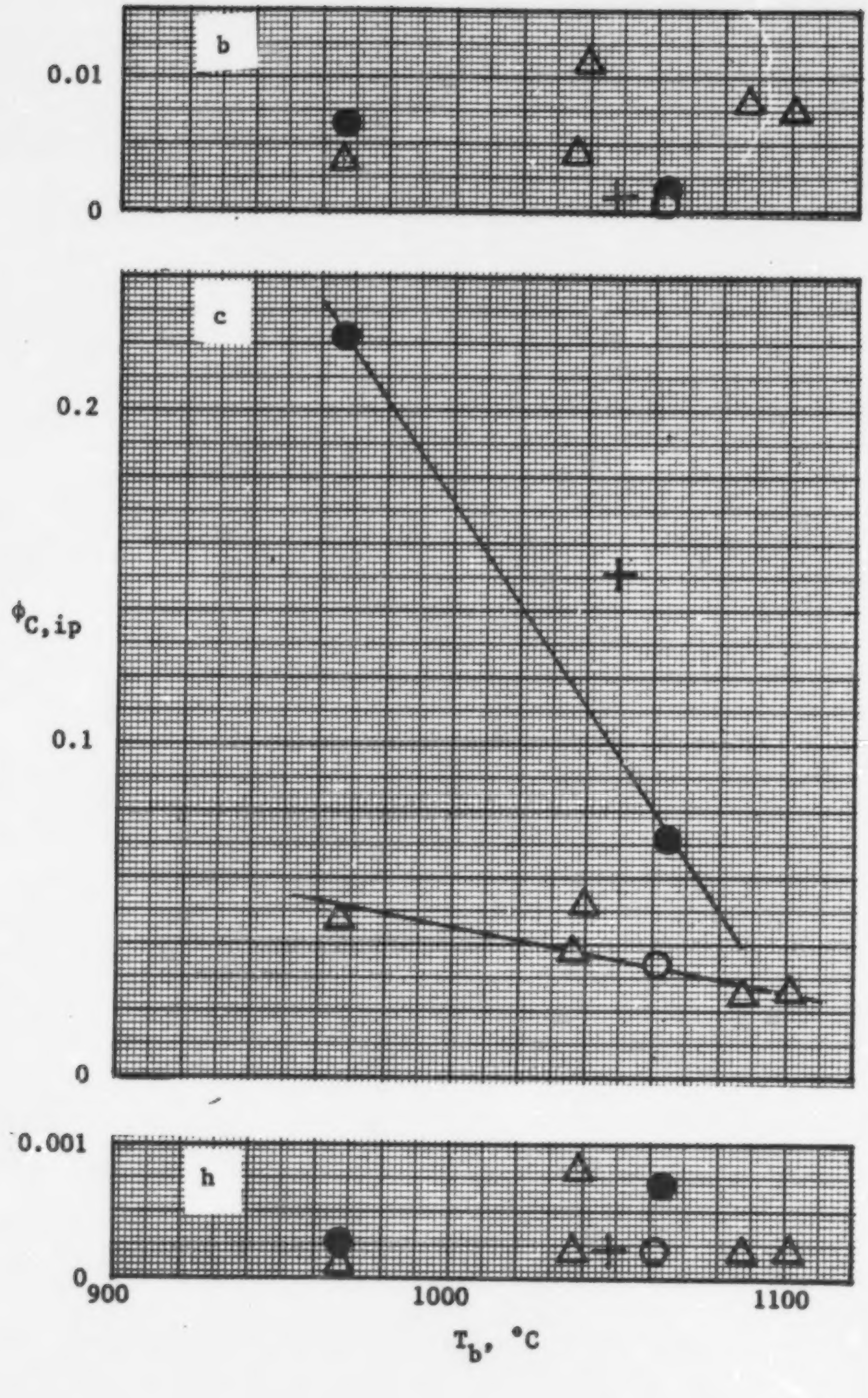

Fig. 6.3. Flux distribution of carbon in the solid products as a function of bed temperature. Symbols: key in Fig. 6.1.

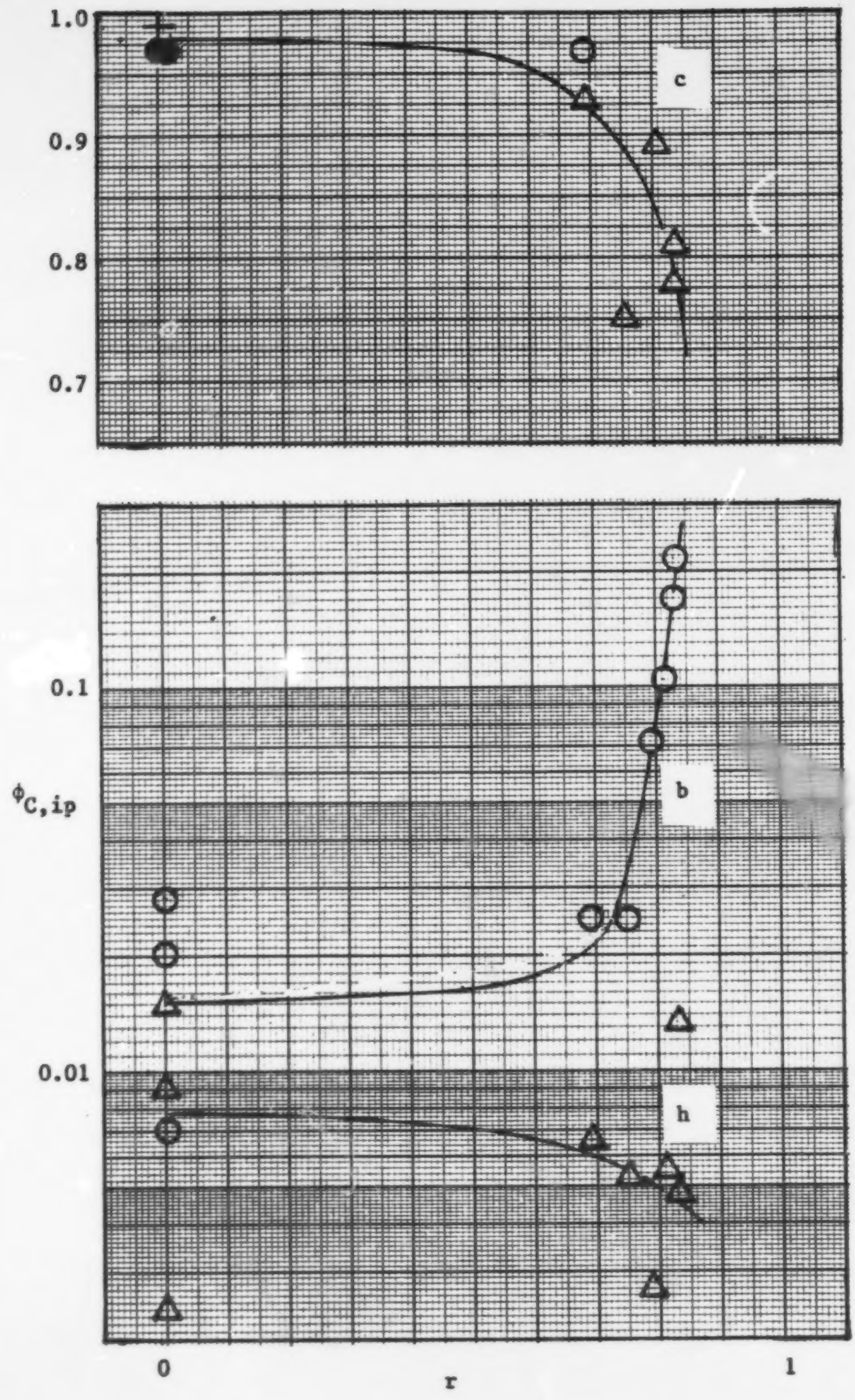

Fig. 6.4. Flux distribution of carbon in the solid products as a function of the recycle fraction. Symbols in top graph: key in Fig. 6.1. Bottom: o, bed product; Δ, baghouse product.

decreased. Recycle brings char back into the bed and, by effectively increasing char residence time in the bed, provides a greater chance for convective removal with the bed product.

6.2.3 Total carbon balance

Figure 6.5 shows as a function of bed temperature the ratio of carbon leaving the system in all streams (gaseous and solid) to carbon fed. In previous work on coal (Becker and Code 1983) the carbon balances were good within 7% maximum deviation (about 4% standard error). The balances here are considerably poorer. The only apparent reason is the refractoriness and possibly greater variability of the fuel.

6.2.4 Combustion inefficiency

Combustion inefficiency is effectively measured by incompleteness of combustion of carbon. Most of the carbon loss is in the cyclone and baghouse products. In our earlier work (Becker & Code 1983) on Minto and Devco coals an empirical correlation of the total overhead carbon loss with the operating variables was developed:

$$\dot{m}_{C,o}/\dot{m}_{C,f} = C_o \, v^{0.86} \, \hat{D}_p^{\,-0.74} \, \phi_a^{\,-0.5} \; \cdot$$

$$\cdot \; \exp(-0.36\, r) \, \exp(5200/T_b), \qquad (6.2.1)$$

C_o = 0.000335 (fluidizing velocity v in m/s, limestone particle D_p dia. in mm). It is interesting to see whether this correlation,

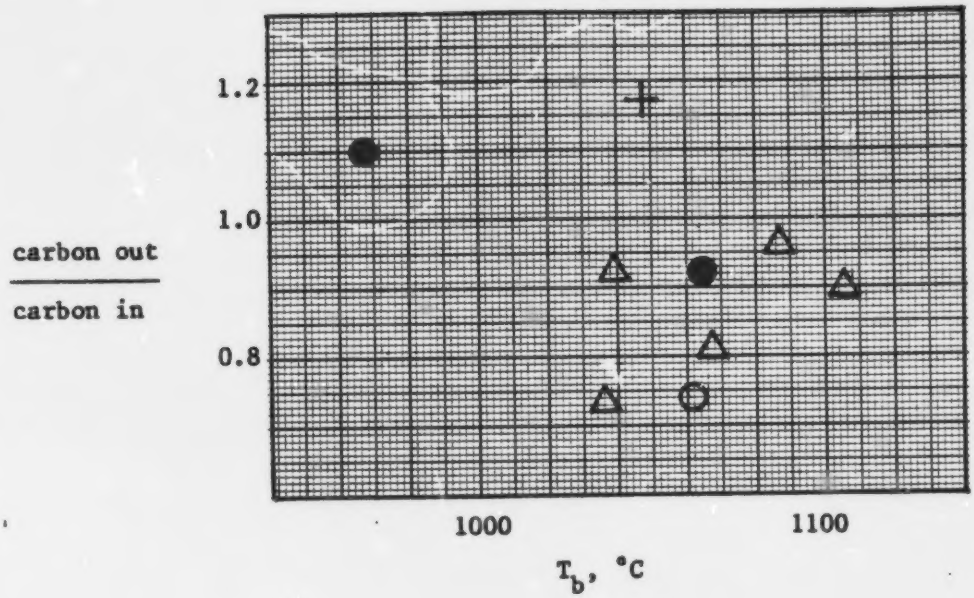

Fig. 6.5. The total carbon balance: the ratio of total carbon leaving the combustor to the carbon fed, as a function of bed temperature, as determined by analysis of the various streams. Symbols: key in Fig. 6.1.

or one like it, holds for the Syncrude coke as well.

Values of C_o in (6.2.1) are shown as a function of bed temperature in Fig. 6.6. With the exception of two runs, the results show no more deviation from $C_o = 0.000335$ than our original data (Becker & Code 1983) on the Minto and Devco coals. This close similarity is surprising, and in work currently in progress we are attempting to discover the reasons for it.

Figure 6.6 also shows values of C_o calculated from (6.2.1) from the present results on Evans, Devco and TVA coals. The new Devco results agree with the previous work, as expected. The data on the TVA coal also show insignificant deviation from $C_o = 0.000335\ (\mathrm{m/s})^{-0.86}\ \mathrm{mm}^{0.74}$. The data on the Evans coal, however, are consistently low. Elsewhere in this report (Sect. 5.2.5) it is shown that these data are best fitted by somewhat different exponents in the form (6.2.1).

Our results on the Syncrude coke are not statistically sufficient to test a complete refitting of (6.2.1). However, we have examined the behaviour of the single most important variable in the Syncrude coke trials, namely the bed temperature. We put (6.2.1) in the form

$$\dot{m}_{C,o}/\dot{m}_{C,f}\ \phi_a^{-0.5} v^{0.86} \hat{D}_p^{-0.74} e^{-0.36r} = C_o \exp(B/T_b) \qquad (6.2.2)$$

and statistically calculated C_o and B. The results are

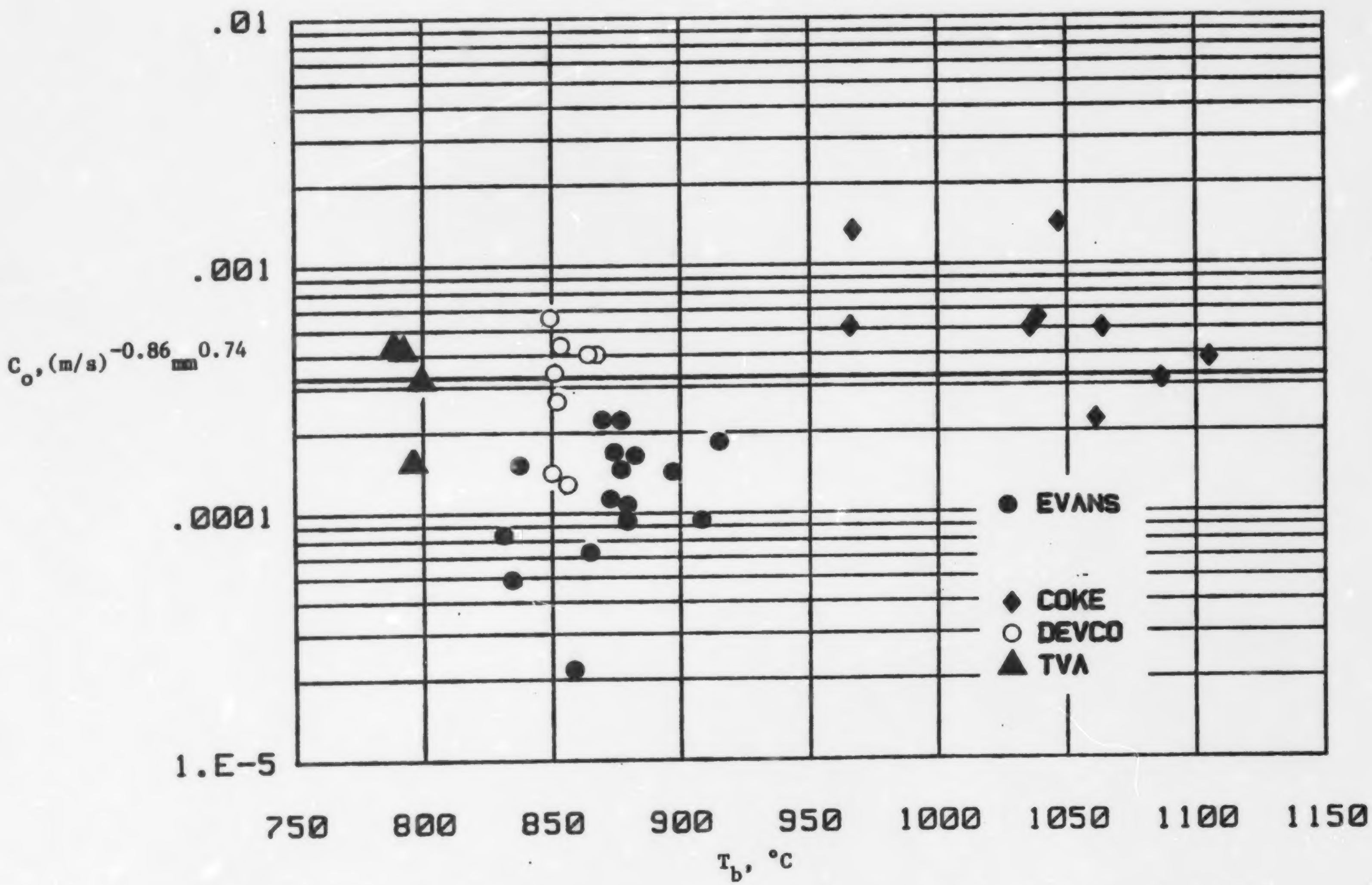

Fig. 6.6. Correlation of overhead carbon loss: the coefficient C_o in (6.2.1) as a function of bed temperature. Symbols for present trials: o, Devco coal; o, Evans coal; Δ, TVA coal; ◆, Syncrude coke. The mean value for the earlier Minto and Devco coal trials was 0.000335 $(m/s)^{-0.86}$ $mm^{0.74}$

$C_o = 4.7 \times 10^{-7} (m/s)^{-0.86} mm^{0.74}$ and B = 14830 K. Taking this value of B as given, we have then calculated C_o to demonstrate the variability in the data, Fig. 6.7. Whether or not B = 14830 K is more realistic for the Syncrude coke than the original value of 5200 K (based on Minto and Devco coal trials) is unclear because the design of the coke trials was, one might argue, distorted by inability to control the excess air level.

6.3 The sulphur balance

6.3.1 Sulphur content of solids

Figure 6.8 presents the data on sulphur content of the solids in an interesting and apparently meaningful way: the content in the cyclone and baghouse solids is shown as a function of that in the bed product, all on a carbon-free basis (CFB). High correlation is indicated for given limestone of given particle size. Decreasing limestone particle size seems to enrich the cyclone product in sulphur. Both overhead products are richer in sulphur for the Havelock limestone than for the Fort McMurray stone. In all runs except one, the CFB sulphur content of the overhead products is less than that of the bed product. The exceptional run is the one at the highest bed temperature, 1105 °C; there the sulphur content of the bed product was only 0.7% while for the overhead products it was around 2%. It appears that this capture in the overhead product may have largely occurred in the exhaust gas train, in the first heat exchanger as the gases passed through the favourable temperature range for SO_2/CaO reaction.

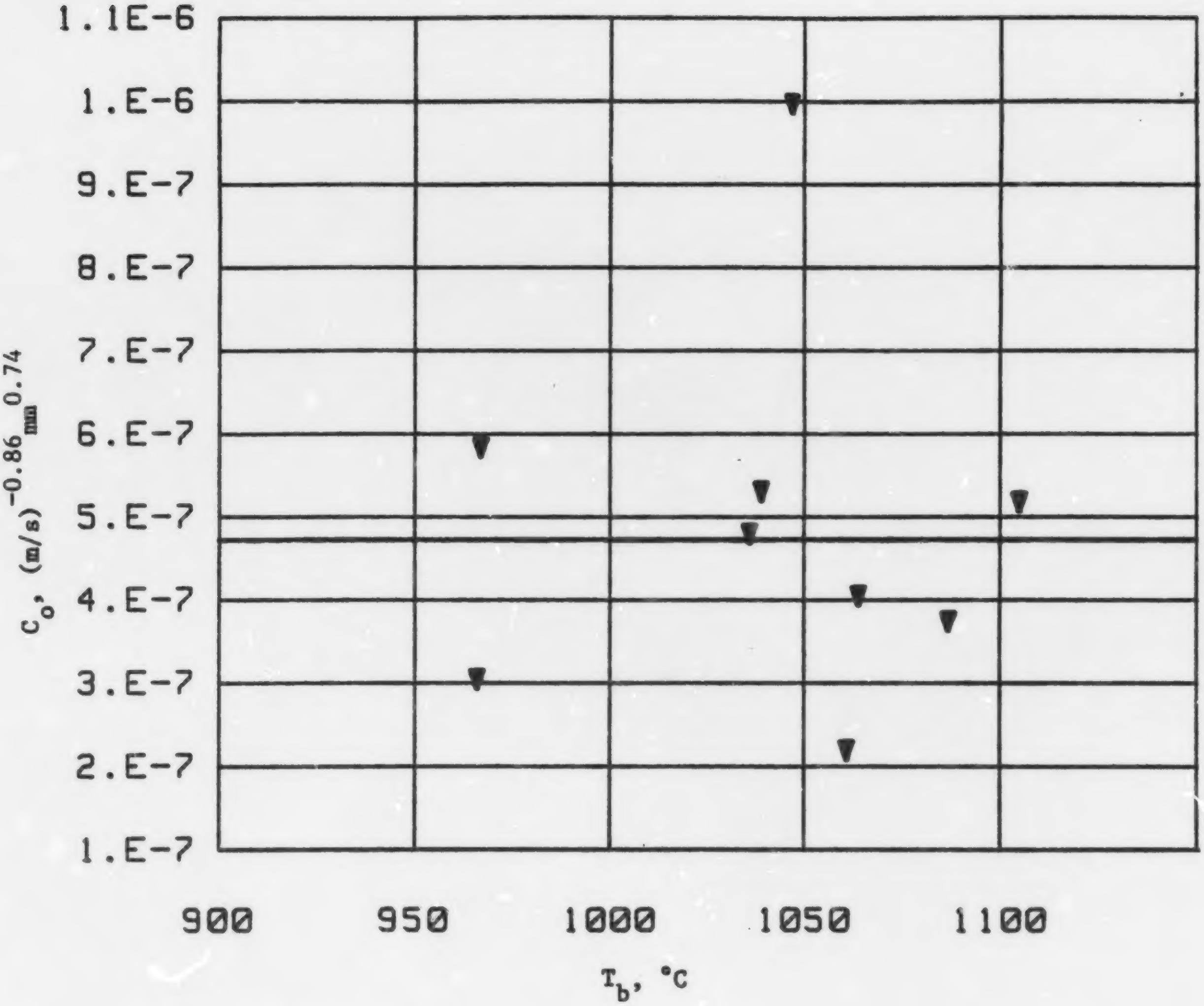

Fig. 6.7. Modified correlation of overhead carbon loss for the Syncrude coke trials: the coefficient C_o in (6.2.2) with $B = 14830$ K as a function of absolute temperature. The mean value is 4.7×10^{-7} $(m/s)^{-0.86}mm^{0.74}$.

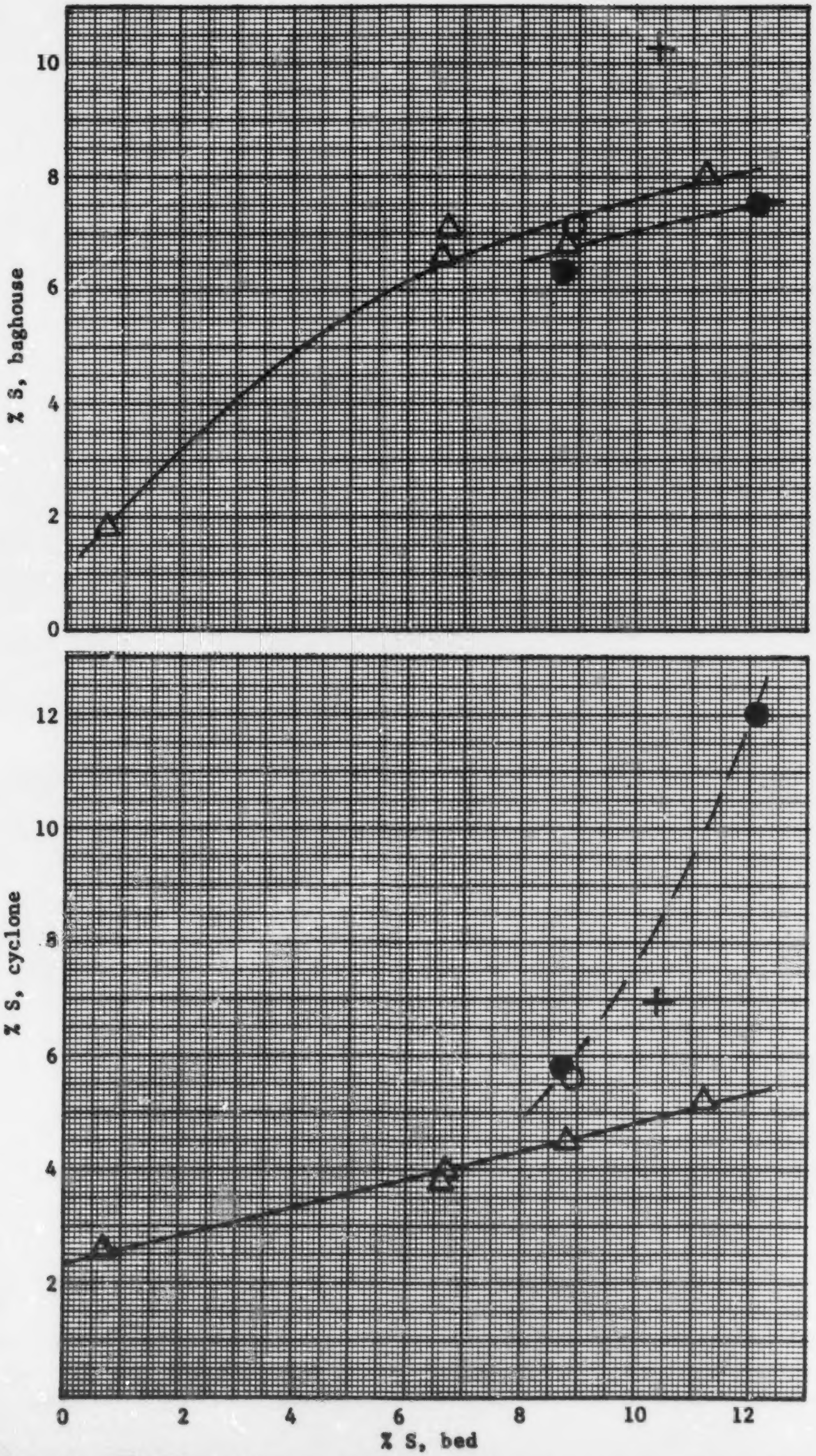

Fig. 6.8. Sulphur content of the baghouse and cyclone products as a function of that of the bed product, all on carbon-free basis. Symbols: key in Fig. 6.1.

The possible influence of bed temperature is further demonstrated in Fig. 6.9 which shows the ratio of CFB sulphur content in the overhead products to that in the bed product vs. the bed temperature.

6.3.2 Flux distribution

Like that of the carbon, Fig. 6.4, the sulphur flux distribution is highly correlated with the recycle fraction, Fig. 6.10. The trends are also similar; increasing recycle seems to increase the proportion of sulphur carried by the bed product and decreases that carried by the cyclone product. The explanation again lies in the increased residence time of particles in the bed, providing greater opportunity for removal in the bed product.

6.3.3 Sulphur capture

In coal combustion in the usual temperature range, 800--900 °C, the effect of temperature on sulphur capture is relatively flat and the Ca/S ratio is the most influential parameter for a given limestone of given particle size. We here designed our experiments so as to be sure to clearly determine the effect of the much higher temperatures. The Ca/S ratio, on the other hand, was only moderately varied, Table 6.1, just enough so we would be sure to get results in the practical range. This produced the best design that we could execute within our limitations of time and materials.

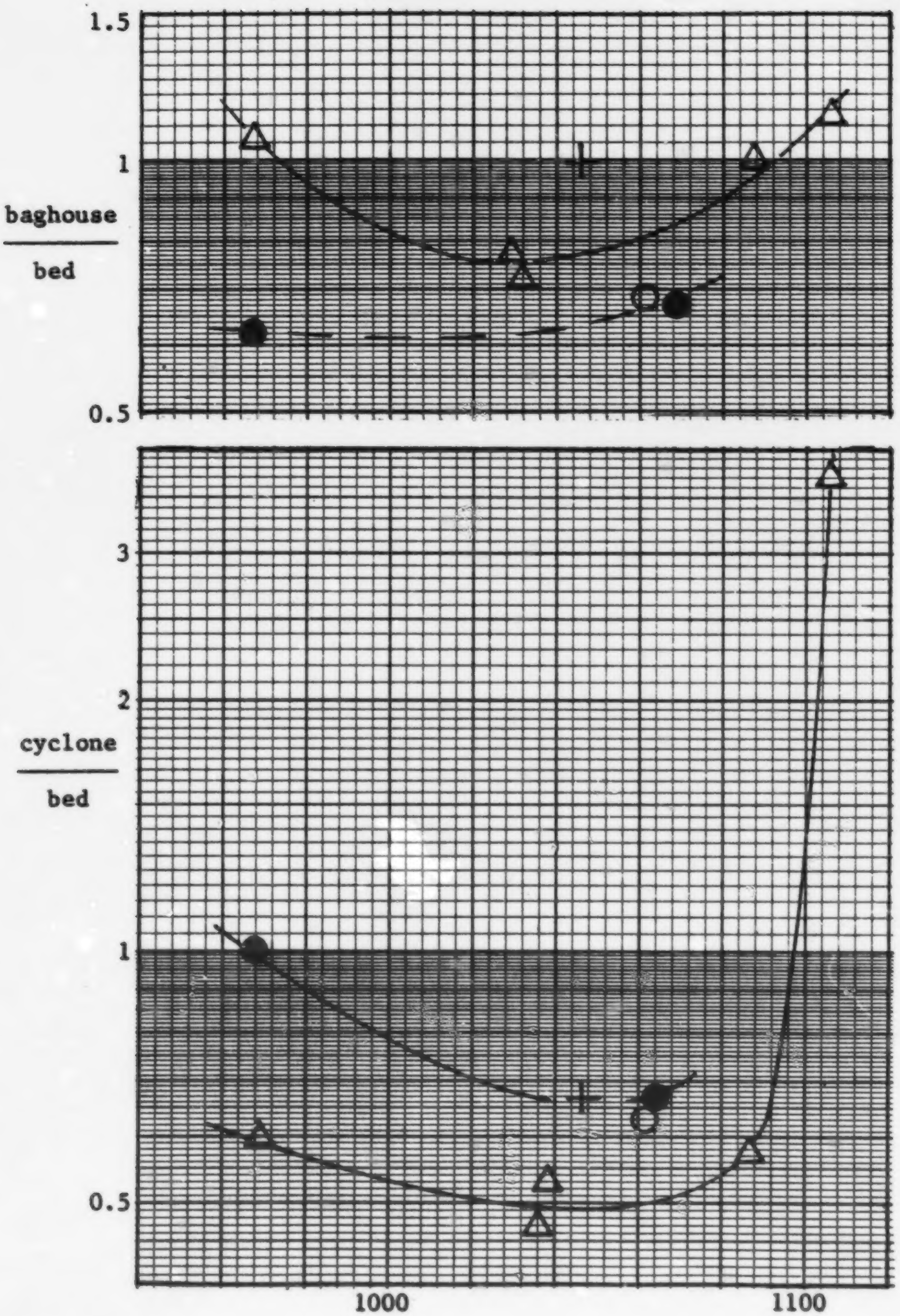

Fig. 6.9. Ratio of sulphur contents of the overhead product streams to that of the bed product (all on carbon-free basis) as a function of bed temperature. Top: baghouse product. Bottom: cyclone product. Symbols: key in Fig. 6.1.

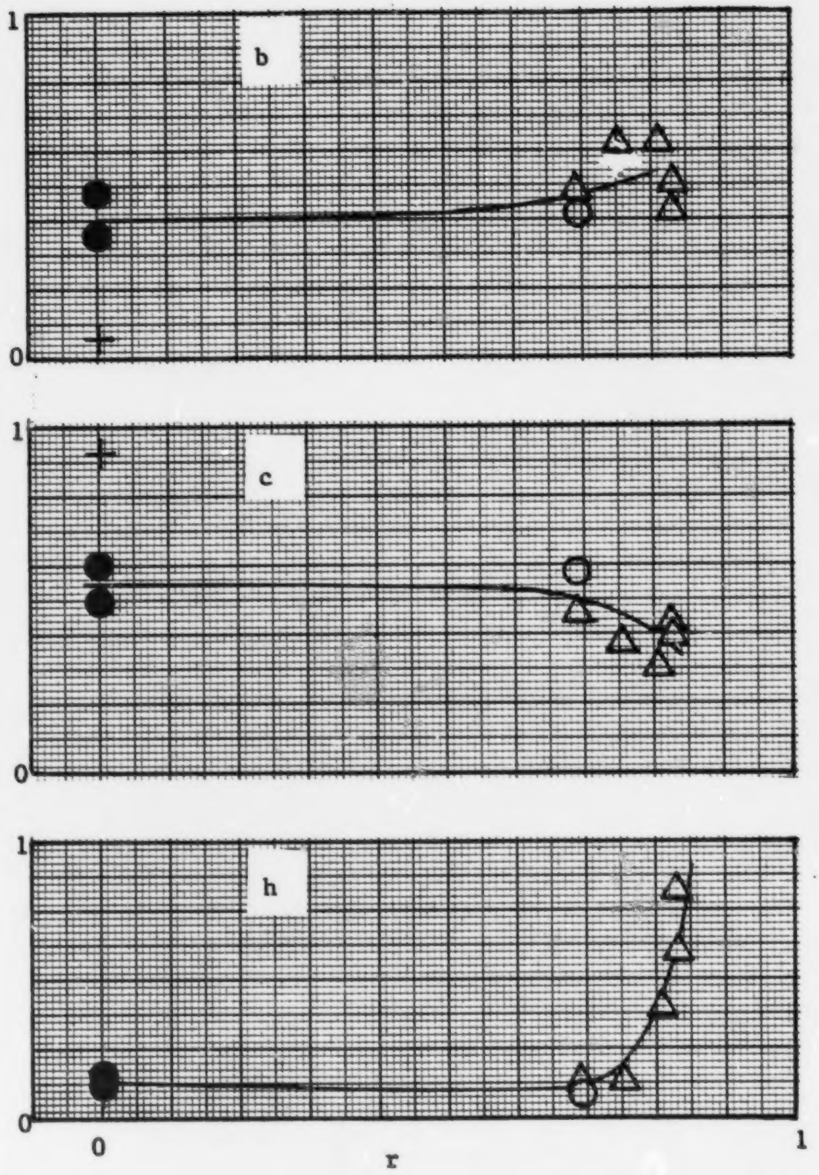

Fig. 6.10. Distribution of sulphur flux between the bed, cyclone and baghouse solid product streams, as a function of the recycle fraction. Symbols: key in Fig. 6.1.

Figure 6.11 shows the results in a graph of percentage of sulphur captured vs. bed temperature. In the direction of decreasing temperature, the results are consistent with optimum capture in the usual range, around 850 °C. With increasing temperature, the capture decreases but remains good up to about 1050 °C. It then drops very rapidly, to practically nothing beyond 1100 °C. An effect of limestone particle size is apparent, particles of 0.34 mm mass-median dia. giving somewhat better performance than those of 0.94 mm dia.

6.3.4 Total sulphur balance

Figure 6.12 shows the sulphur capture as determined by solids analysis as a function of the capture as determined by gas analysis. As usual, the values from the solids analysis are low, and most of them are very low. The difficulty of determining the full sulphur content seems to have been aggravated here, the materials being significantly more refractory than in the case of coal. Insofar as the total sulphur capture is concerned, we are contrained to believe the results based on gas analysis since the gas analyzers were carefully calibrated with standard gas mixtures and could not be so wrong.

6.4 The nitrogen balance and NO_x

Figure 6.13 shows the exhaust gas NO_x concentration as a function of the exhaust O_2 concentration. Considerable correlation is evident and the results agree with the general observation that NO_x emission is minimized by keeping the

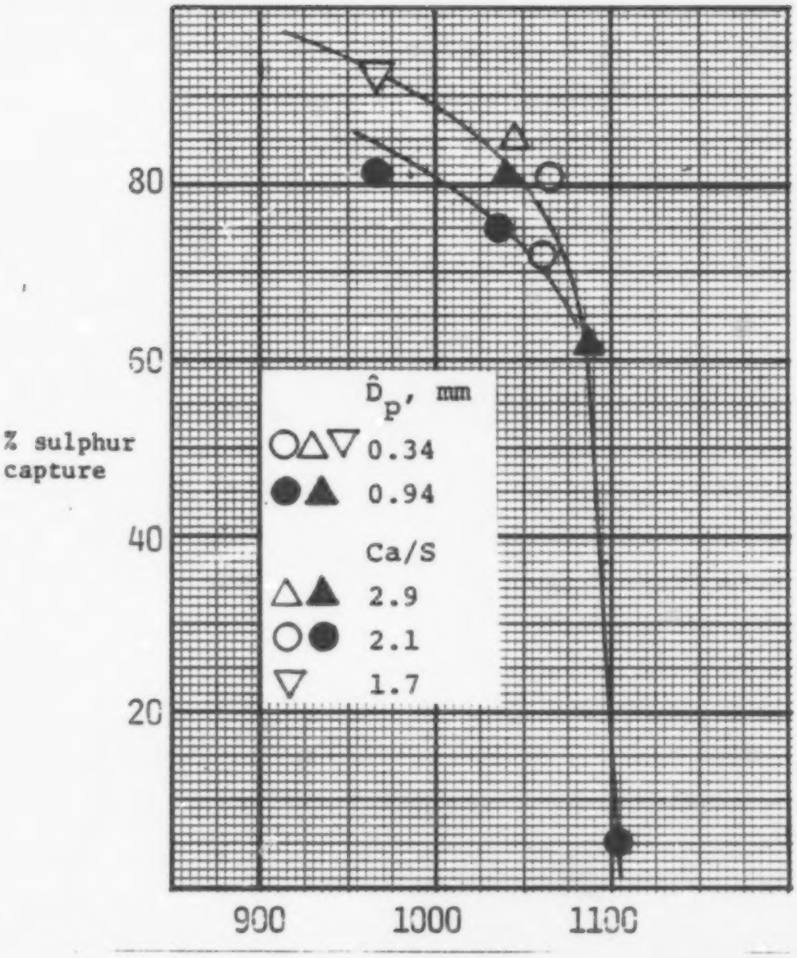

T_b, °C

Fig. 6.11. Percent sulphur capture as a function of bed temperature.

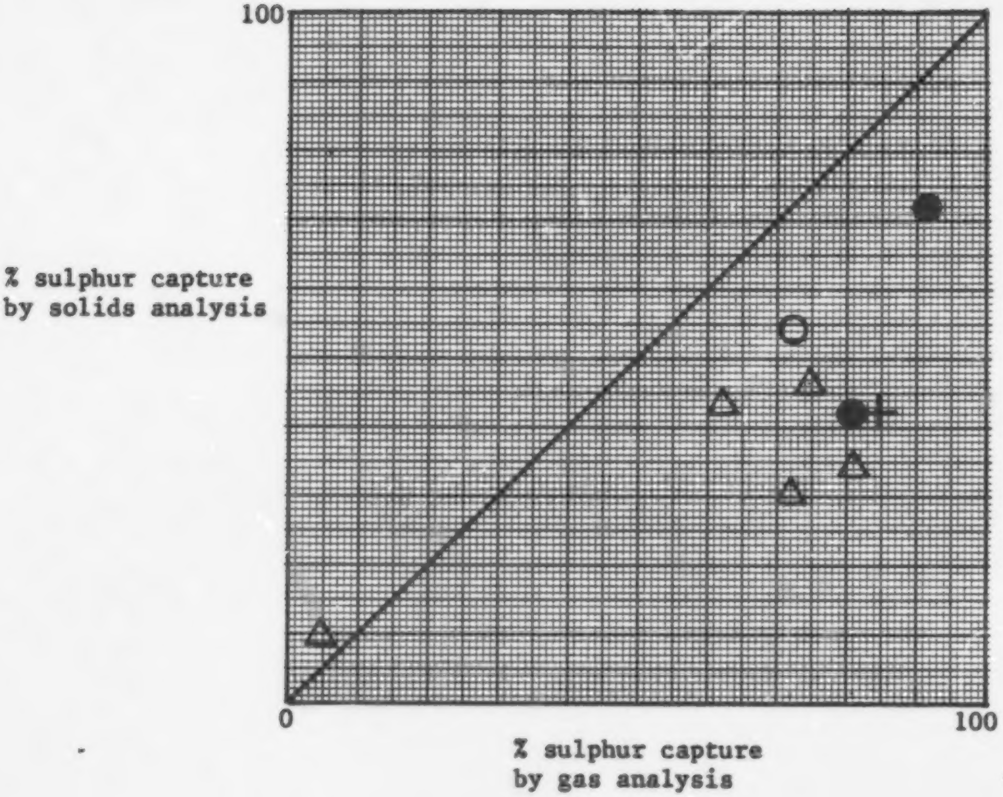

Fig. 6.12. The total sulphur balance: sulphur capture according to the solids analysis vs. the capture according to the gas analysis. Symbols: key in Fig. 6.1

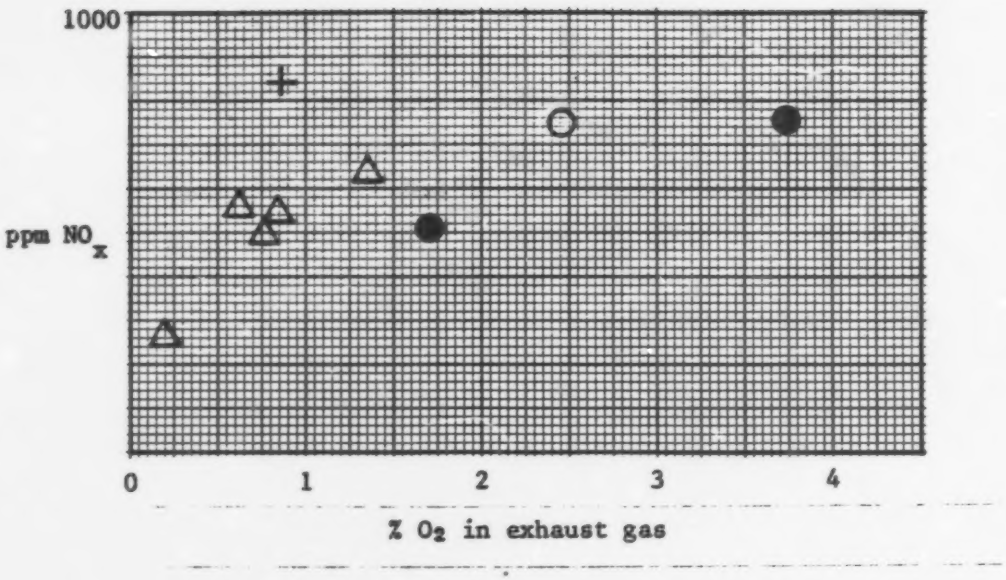

Fig. 6.13. The NO_x content in the exhaust gases as a function of the oxygen concentration, dry basis. Symbols: key in Fig. 6.1.

exhaust oxygen level low. Limestone characteristics seem to have some effect in that the result from the run with Havelock limestone is significantly higher than the results from runs with the Fort McMurray stone.

The conversion of fuel nitrogen to NO_x, Fig. 6.14, was very similar to that observed with coal, generally under 25%. No particular correlation of conversion with temperature is evident. There is some indication, though, that free-board char concentration may be influential; the conversion seems to decrease with increasing flux of elutriated carbon.

6.5 Carbon monoxide

Carbon monoxide levels in the exhaust gas, Fig. 6.15, were in the range 0.018-0.028 mole % in all runs except one. The exceptional run was that at the highest temperature, 1105 °C, and the lowest exit O_2 level, 0.2 mole %. The O_2 level in the other runs was as low as 0.6 mole % with no apparent effect on the CO concentration.

6.6 Vanadium

Syncrude coke is high in vanadium. The ignited ash, according to the analysis given in Table 4.4, contained 3.8 % V_2O_5. The sample analyzed was taken from the same shipment that provided our lot. This sample, Table 4.4, also contained 1.5 % NiO. The resulting mass ratio of V/Ni is 1.81.

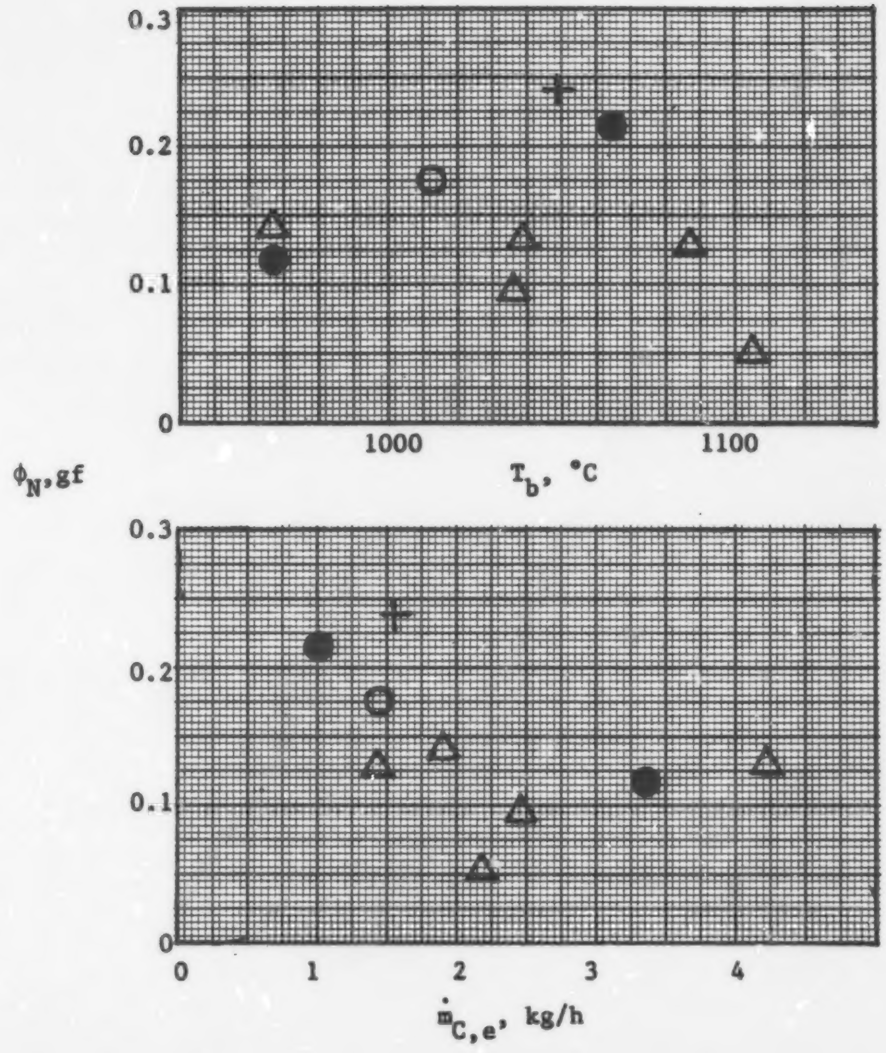

Fig. 6.14. Fraction of fuel nitrogen converted to NO_x vs bed temperature (top) and elutriated carbon flux (bottom). Symbols: key in Fig. 6.1.

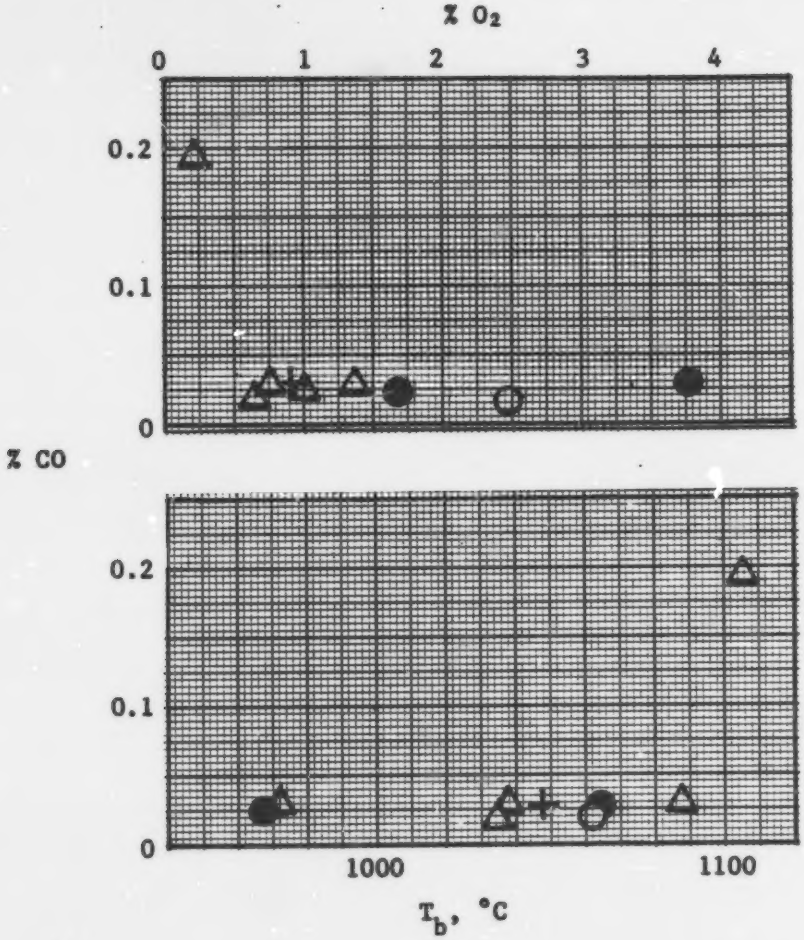

Fig. 6.15. Carbon monoxide content of the exhaust gases (dry basis) vs the oxygen content (top) and the bed temperature (bottom). Symbols: key in Fig. 6.1.

At the last moment in preparing this report an analysis was received from the Energy Research Laboratories, CANMET, of samples submitted by us of coke and limestone from the lots used in our work. The results for the ash of the coke are somewhat different from those quoted above from Table 4.4: 4.7 % V_2O_5 and 1.23 % NiO, giving V/Ni = 2.76 by mass. Table 4.4 shows our value of the ash content of our lot of coke, 6.9 %. The vanadium content of the coke given by these data is 0.182 %, and the nickel content is 0.066 %. The results for the ash of the limestone are 0.03 % V_2O_5 and 0.00 % NiO. The ash content we found for our lot of stone, Table 4.4, is 63.5 %. The vanadium content of the stone is accordingly 0.011 %.

In order to determine the fate of the vanadium from the coke, the solid products from some of the Syncrude coke trials were therefore analyzed for both vanadium and nickel. If it is assumed that the nickel is fixed in the ash of the coke ("inert"), then it can be taken as a tracer for that ash, and changes in the V/Ni ratio will indicate migration of the vanadium (if we discount the small vanadium burden contributed by the limestone). This test was carried out not only on the solids as a whole, but the solids were also divided into sieve fractions and thus analyzed. The analyses were all performed at the analytical laboratories of CANMET, Energy Mines and Resources Canada, Ottawa.

Figure 6.16 shows the V/Ni ratios of the bed and baghouse products as functions of that in the cyclone product. There appears to be a trend for V/Ni to be slightly lower in the baghouse product than in the cyclone product. It may be noted that the V/Ni ratios are generally within, or very nearly within, the range bracketted by the coke analysis by ERL in Table 4.4, 1.81, and their recent analysis of a coke sample from our lot as quoted above, 2.76. In respect to the latter analysis, allowance for the small vanadium content of the Athabasca limestone brings the overall V/Ni ratio from 2.76 to 2.84--2.89, which is exactly the upper end of the range of the data in Fig. 6.16. It would appear that, without considering analytical uncertainty, the range of variation of V/Ni in Fig. 6.16 is not inconsistent with the variability between samples of the coke.

Table 6.2 shows results for the four runs in which samples were resolved into sieve fractions. There appears to be a definite trend towards vanadium enrichment in the smaller particles. The effect, however, is not large, and it could be accounted for by shifts in the limestone/coke ratio in the origins of the particles making up the various product streams.

6.7 Fuel-ash flux distribution

Assuming, as in the preceding section, that nickel is a marker for the fuel-ash, the flux distribution of the nickel is taken as the measure of the flux distribution of fuel-ash. Figure 6.17 shows the flux fraction of the ash (measured by the Ni) carried by each product stream as a function of the flux

Table 6.2. Vanadium/nickel ratios in feed and in sieved solid products, Syncrude coke trials

Trial	Stream	Sieve interval, µm	mass fraction sample	V/Ni
840911	Feed	+0	1.	2.88
	Bed product	+0	1.	2.11
		+177	0.676	1.83
		-177	0.324	2.62
	Cyclone product	+0	1.	2.89
		+177	0.016	2.00
		-177+74	0.237	2.54
		-74	0.747	3.00
840827	Feed	+0	1.	2.84
	Bed product	+0	1.	2.64
		+177	0.882	2.63
		-177	0.118	2.71
	Cyclone product	+0	1.	2.70
		+177	0.082	2.50
		-177+74	0.685	2.62
		-74	0.233	3.05
850814	Feed product	+0	1.	2.89
	Bed	+0	1.	2.76
		+177	0.872	2.92
		-177	0.128	2.15
	Cyclone product	+0	1.	2.88
		+177	0.068	2.64
		-177+74	0.407	2.71
		-74	0.525	3.08
840612	Feed	+0	1.	2.85
	Bed product	+0	1.	2.3
		+177	0.860	2.31
		-177	0.140	error
	Cyclone product	+0	1.	2.5
		+177	0.135	error
		-177+74	0.592	2.58
		-74	0.273	2.57

*Feed is coke and limestone combined, and the recent analysis indicating 0.182% V in the coke and 0.011% V in the stone is used in the calculations.

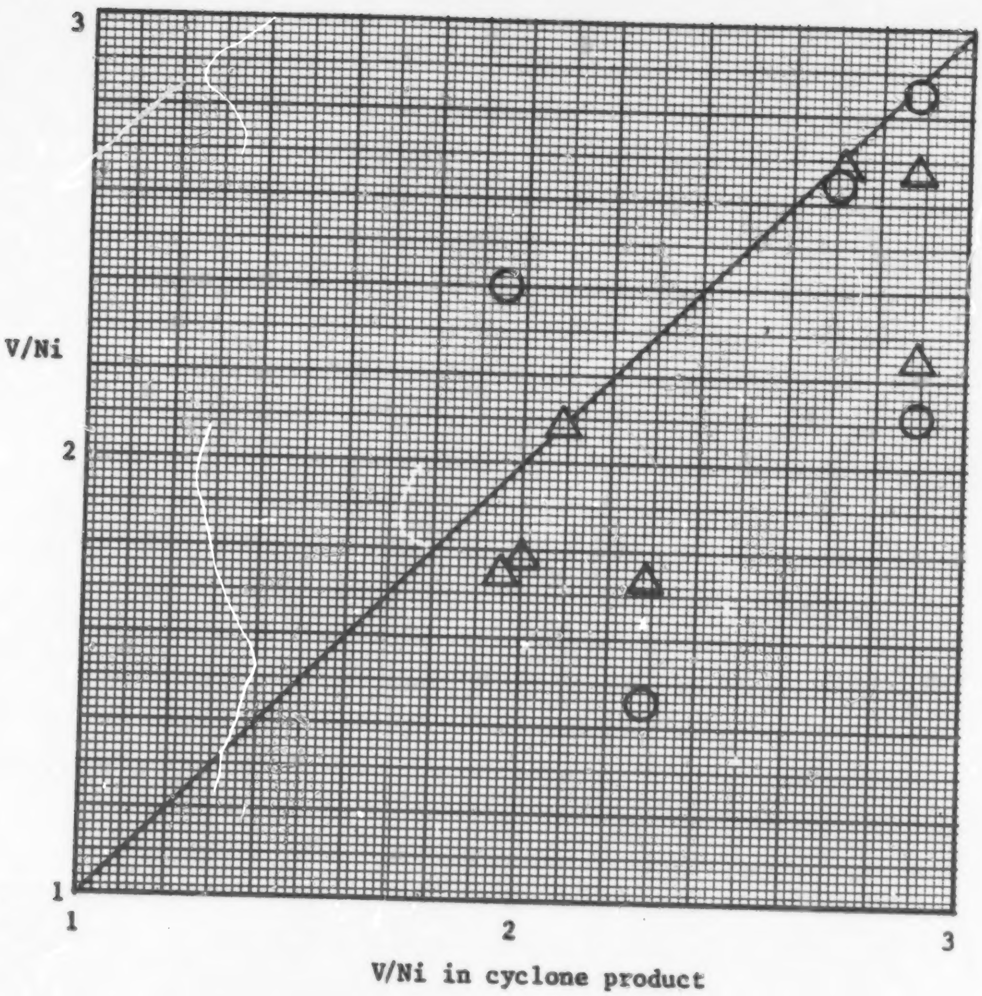

Fig. 6.16. Ratio of vanadium to nickel in the bed and baghouse products vs the ratio in the cyclone product. Symbols: o, bed; Δ, baghouse

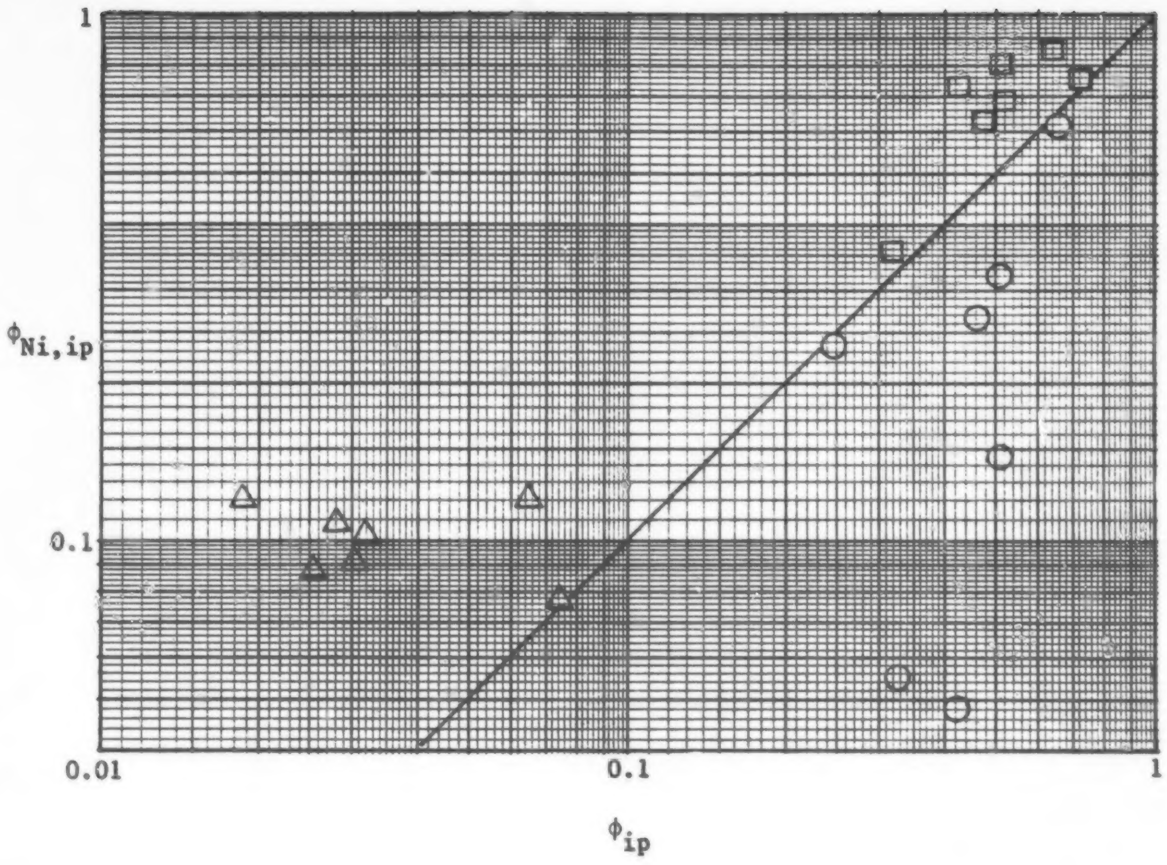

Fig. 6.17. Fraction of the flux of nickel carried by a given solid product stream vs the fraction of the product mass flux carried by that stream. Symbols: o, bed product; ☐ , cyclone product; Δ, baghouse product.

fraction of total solid products carried by that stream. As expected, the overhead streams (cyclone and baghouse) tend to be enriched in ash whereas the bed product is lean.

7. DEVCO AND KENTUCKY NO. 9 TRIALS

7.1 Introduction

The results of the work on Western Kentucky No. 9 coal have been included with the Devco results in this section since only four runs were carried out on the Kentucky No. 9 coal. The mean particle diameter of the fuel for these four runs was 2.3 mm. Reed limestone with a $\hat{D}_p$ of 1.1 mm was used as a SO_2 sorbent. In the work on Devco coal, two fuel particle size distributions with mean particle diameters of 2.1 mm and 11.2 mm were used as feed. Two limestones were used as SO_2 sorbents: Sysco with a $\hat{D}_p$ of 1.4 mm and Calpo with a $\hat{D}_p$ of 1.1 mm. The operating conditions are summarized for convenient reference in Table 7.1.

7.2 The carbon balance

7.2.1 Carbon content of the product solids

The carbon content of the solids from the bed overflow, cyclone and baghouse as functions of bed temperature, excess air level, and recycle fraction is illustrated in Fig. 7.1 to Fig. 7.3. The ranges of carbon content for the runs with Kentucky No. 9 coal are: 0.9--1.5% for the bed overflow solids, 12--18% for the cyclone solids, and 8--12% for the baghouse solids. Corresponding values for the work on Devco coal are: 0.3--1% for the bed overflow solids, 6--21% for the cyclone solids, and 7--13% for the baghouse solids.

Table 7.1. Operating conditions for the runs with Devco coal and Kentucky No. 9 coal.

Run	n_t	Coal		Stone		Ca/S	Air		r	T_b, °C	v, m/s	τ_p, hr	τ_b, hr	COT, hr
		$\hat{D}_p$, mm	$\dot{m}_f$, kg/hr	$\hat{D}_p$, mm	$\dot{m}_s$, kg/hr		$\dot{m}_a$, kg/hr	ε_a, %						
		KY No. 9		Reed										
841108	14	2.3	49.3	1.1	23.7	3.32	476	15.5	0.000	790	2.6	3.1	14.1	9.5
841112	14	2.3	54.1	1.1	36.1	4.60	494	9.2	0.000	789	2.7	2.0	8.8	8.5
841115	14	2.3	51.2	1.1	15.2	2.05	486	13.3	0.000	799	2.6	3.6	13.6	6.9
841119	14	2.3	57.4	1.1	16.1	1.94	534	11.2	0.636	796	2.9	4.0	23.2	6.7
		Devco		Sysco										
841127	12	2.1	41.8	1.4	20.6	3.43	432	19.1	0.000	851	2.5	3.5	8.5	19.1
841204	12	2.1	45.2	1.4	20.3	3.14	427	9.2	0.691	851	2.5	3.4	8.8	29.9
		Devco		Calpo										
841218	12	2.1	45.5	1.1	19.7	2.98	431	9.4	0.000	853	2.5	3.5	8.1	20.8
841219	12	2.1	43.8	1.1	20.3	3.20	433	14.4	0.775	857	2.5	3.9	8.4	8.5
850107	8	2.1	26.3	1.1	12.9	3.39	260	14.1	0.000	854	1.5	4.9	9.4	28.6
850115	8	11.2	22.4	1.1	7.0	1.91	255	27.4	0.000	864	1.5	9.4	17.4	39.0
		Devco		Sysco										
850121	8	11.2	21.9	1.4	5.9	1.68	245	25.1	0.000	849	1.4	11.7	31.5	30.0
850129	12	11.2	34.7	1.4	11.9	2.14	411	32.8	0.000	868	2.4	6.1	13.4	19.7
850304	8	11.2	23.4	1.4	10.7	2.86	257	23.2	0.000	866	1.5	7.6	14.6	38.5

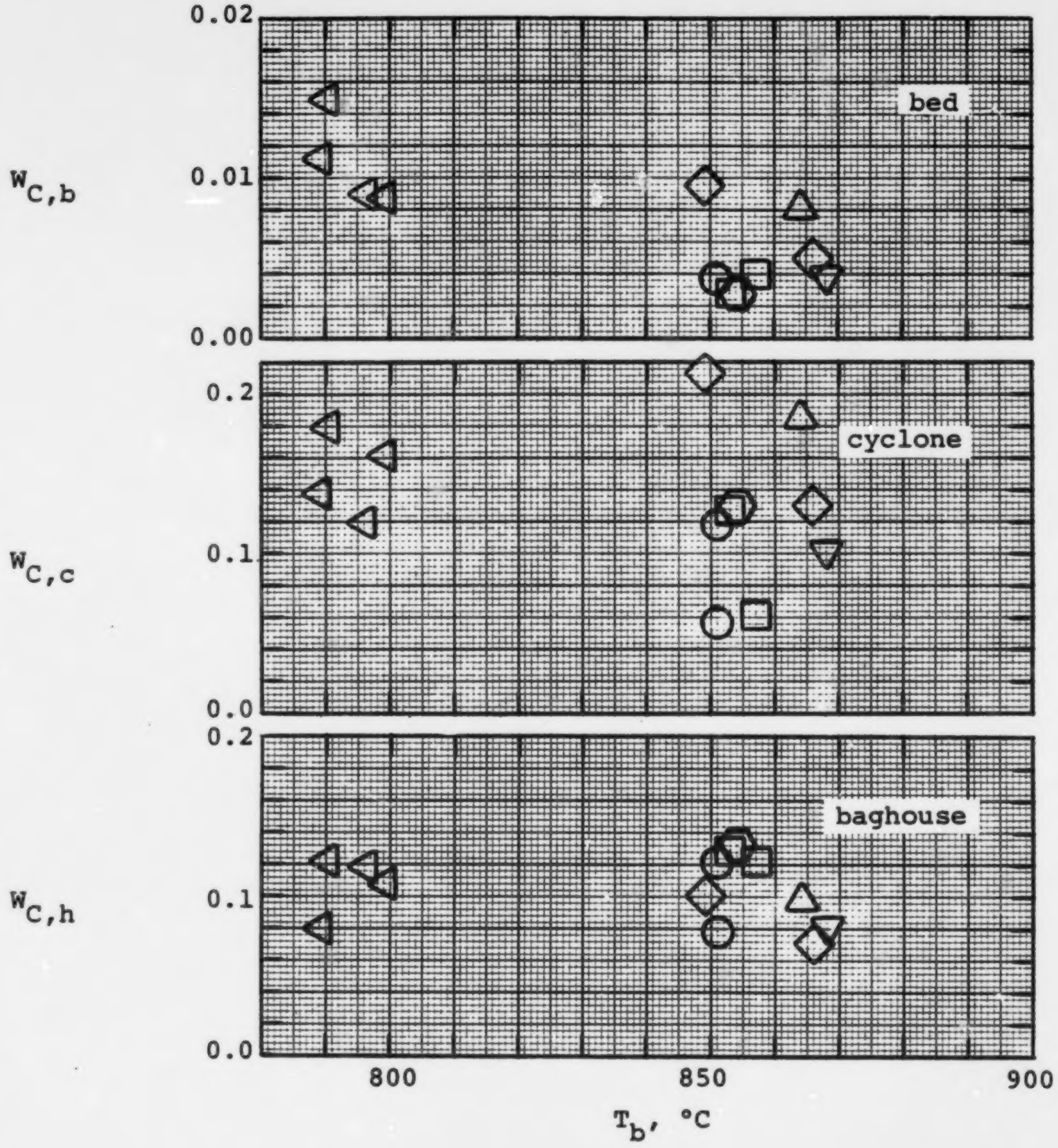

Fig. 7.1. Mass fraction carbon in solids vs. bed temperature, T_b.

Key to symbols:

	v, m/s	Coal	$\hat{D}_p$, mm	Sorbent
○	2.5	Devco	2.1	Sysco
□	2.5	Devco	2.1	Calpo
⬡	1.5	Devco	2.1	Calpo
△	1.5	Devco	11.2	Calpo
◇	1.4-1.5	Devco	11.2	Sysco
▽	2.4	Devco	11.2	Sysco
◁	2.6-2.9	KY No. 9	2.3	Reed

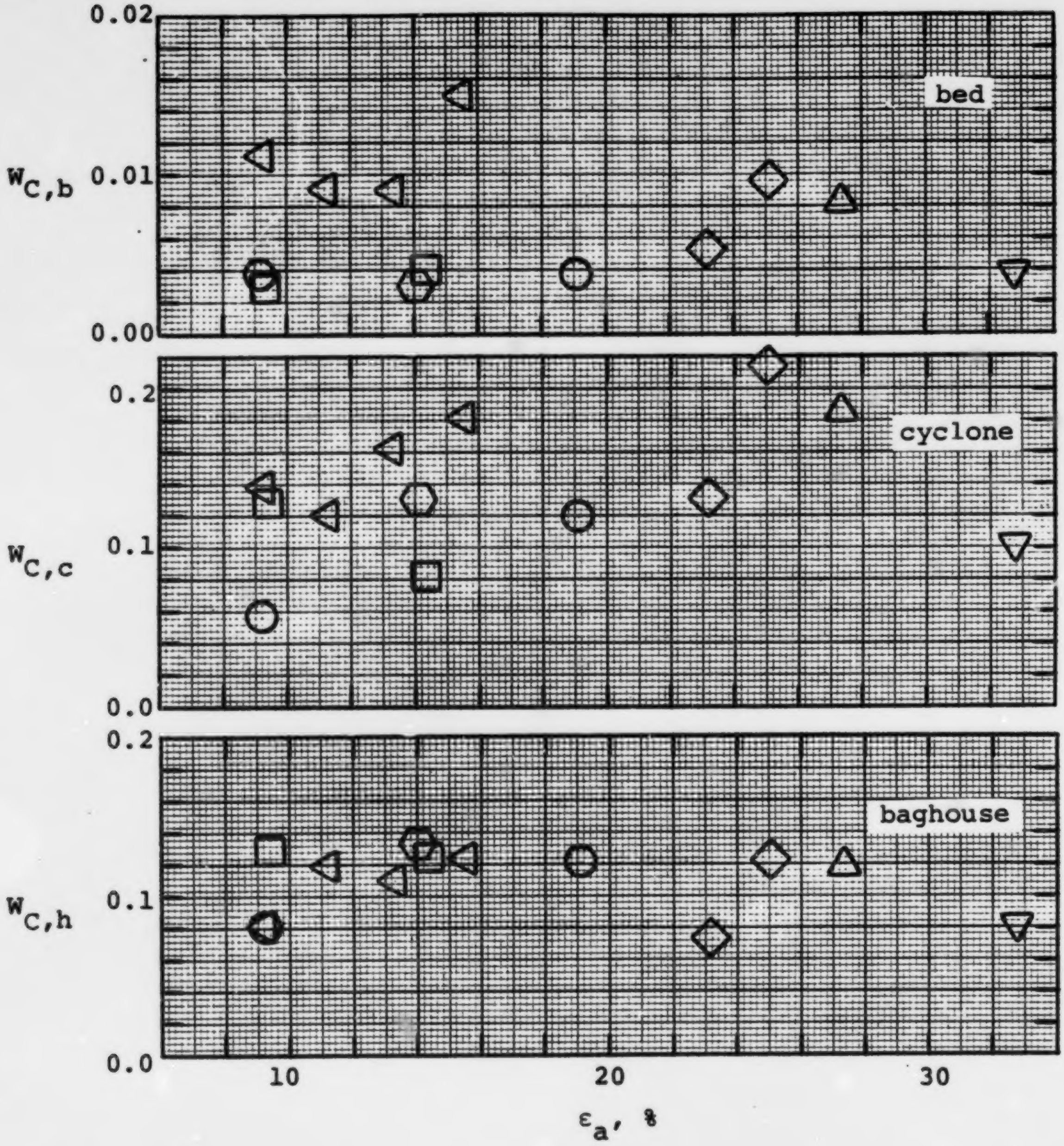

Fig. 7.2. Mass fraction carbon in solids vs. excess air level, ε_a.

Key to symbols:

	v, m/s	Coal	$\hat{D}_p$, mm	Sorbent
○	2.5	Devco	2.1	Sysco
□	2.5	Devco	2.1	Calpo
⬡	1.5	Devco	2.1	Calpo
△	1.5	Devco	11.2	Calpo
◇	1.4-1.5	Devco	11.2	Sysco
▽	2.4	Devco	11.2	Sysco
◁	2.6-2.9	KY No. 9	2.3	Reed

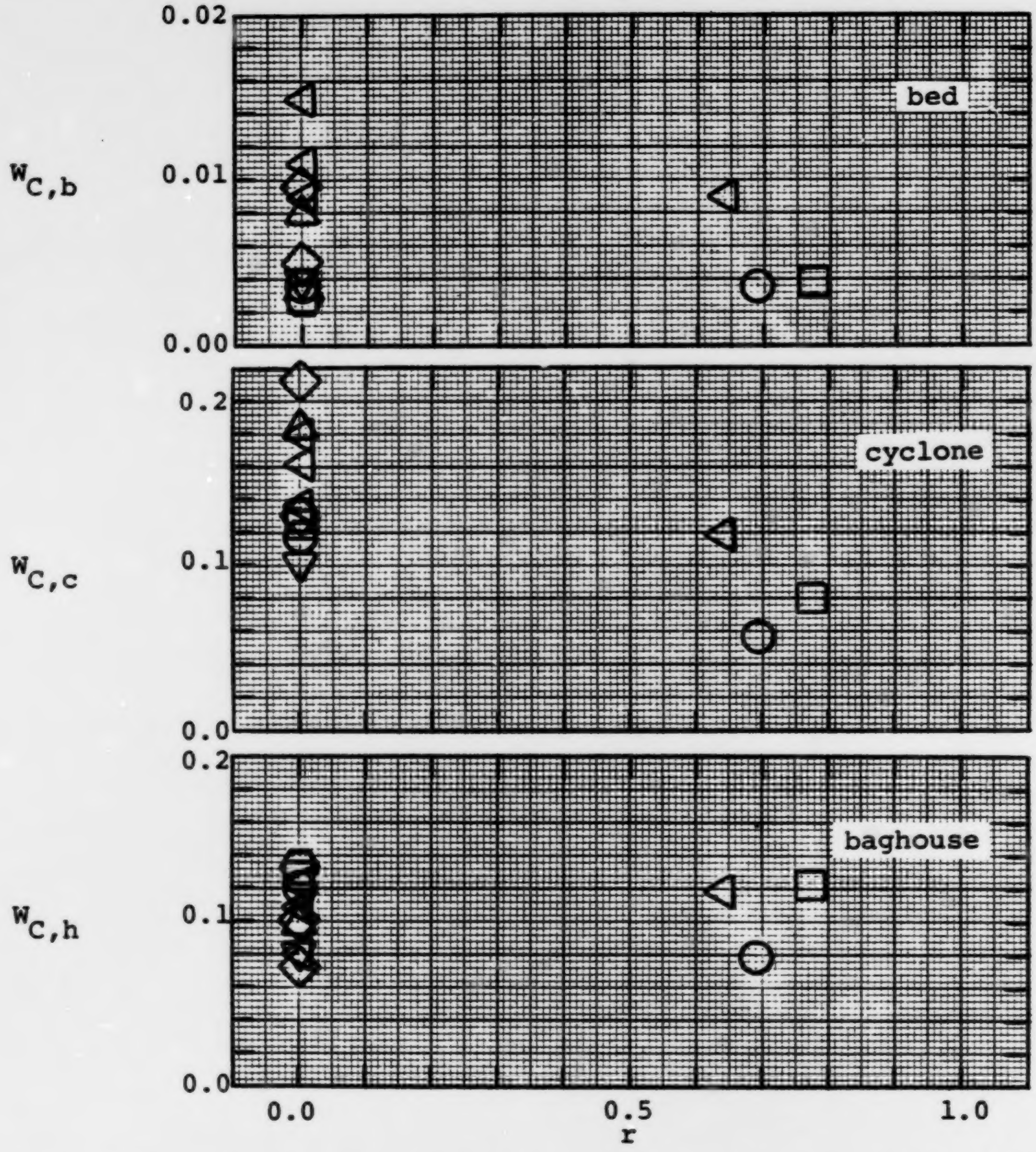

Fig. 7.3. Mass fraction carbon in solids vs. recycle fraction, r.

Key to symbols:	v, m/s	Coal	$\hat{D}_p$, mm	Sorbent
○	2.5	Devco	2.1	Sysco
□	2.5	Devco	2.1	Calpo
⬡	1.5	Devco	2.1	Calpo
△	1.5	Devco	11.2	Calpo
◇	1.4-1.5	Devco	11.2	Sysco
▽	2.4	Devco	11.2	Sysco
◁	2.6-2.9	KY No. 9	2.3	Reed

Some qualitative interpretations of the effect of operating conditions may be obtained from an examination of the figures in consultation with Table 7.1 for the specification of operating conditions. The effect of bed temperature is similar to that observed for the work on Evans coal, i.e., under the constraint of other factors being constant, the carbon content of the bed solids decreases with increasing bed temperature. The reduction in carbon content with excess air level is not as evident as in the earlier work because of the more limited range and positive values for ε_a, 9 to 33% vs. -22 to +23% for the Evans trials. The reduction in the carbon content of the cyclone solids with increase in the recycle fraction also agrees with the result on Evans coal.

7.2.2 Distribution of carbon loss

The distribution of carbon loss among the three streams of product solids is presented in Fig. 7.4 as a flux ratio of carbon loss in an individual stream to the total carbon loss in the solids vs. the recycle fraction r. At zero recycle the major portion, 89 to 95%, of the carbon loss is carried by the cyclone solids. The corresponding ranges for the bed overflow and baghouse streams are 1.8 to 5.1% and 1.5 to 8.8%, respectively. The reduction in the portion of the carbon loss carried by the cyclone solids with an increase in r is evident from an examination of the plot for the cyclone solids in Fig. 7.4. This is due to the decrease in the carbon content of the

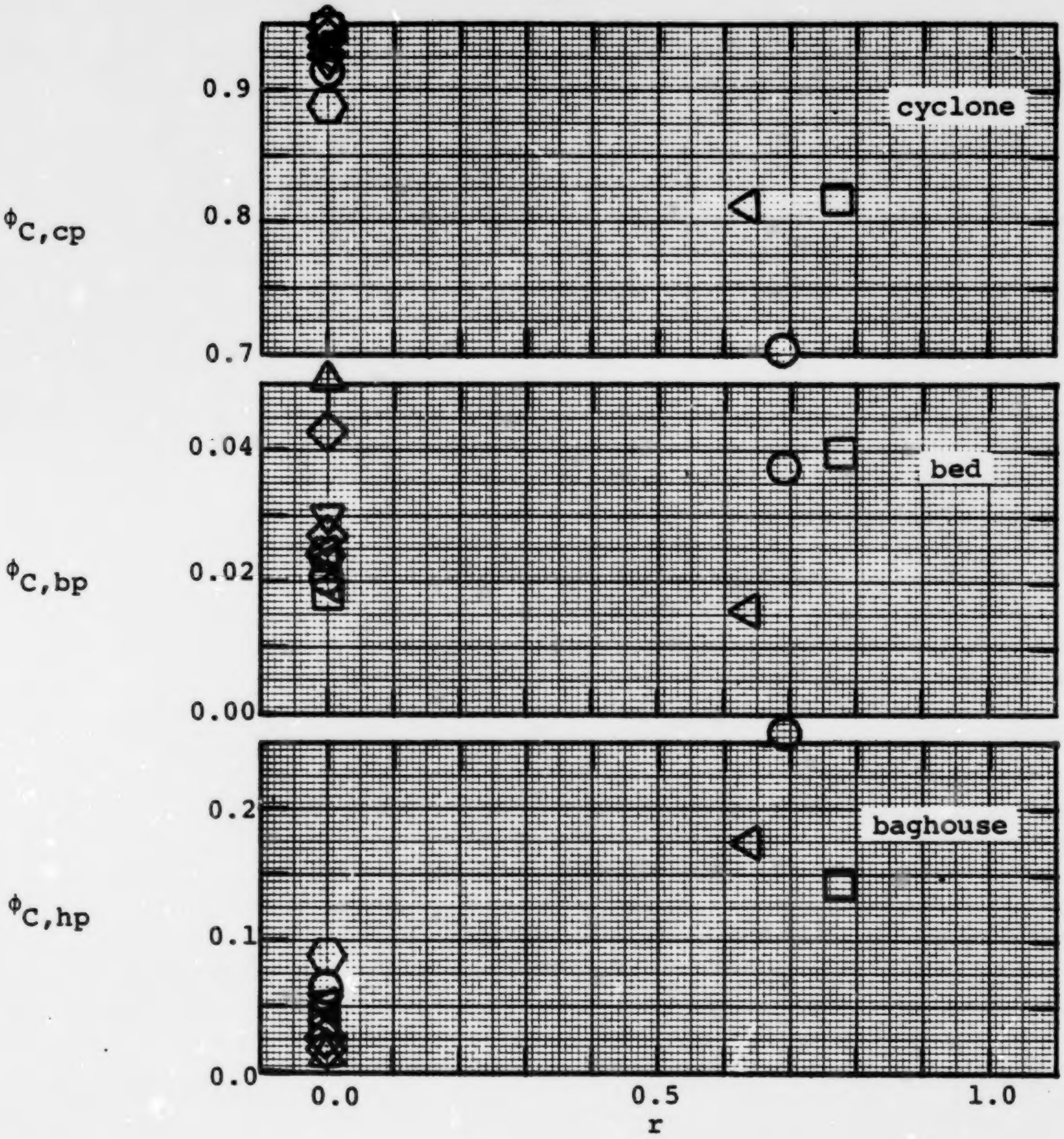

Fig. 7.4. Distribution of carbon loss among solids from bed, cyclone and baghouse - flux ratio of carbon loss in an individual stream to total carbon loss in the solids.

Key to symbols:

	v, m/s	Coal	$\hat{D}_p$, mm	Sorbent
○	2.5	Devco	2.1	Sysco
□	2.5	Devco	2.1	Calpo
⬡	1.5	Devco	2.1	Calpo
△	1.5	Devco	11.2	Calpo
◇	1.4-1.5	Devco	11.2	Sysco
▽	2.4	Devco	11.2	Sysco
◁	2.6-2.9	KY No. 9	2.3	Reed

cyclone solids and the decrease in the solids efflux from the cyclone. The corresponding increase in the solids loading on the baghouse and bed overflow results in a greater portion of the carbon loss being carried by these two streams of solids.

7.2.3 Distribution of fuel carbon among products

The fate of the carbon in the fuel is examined in Fig. 7.5 through Fig. 7.9 in terms of the ratio of the carbon flux in an individual product stream to the carbon flux in the fuel as a function of bed temperature, excess air level, recycle fraction, total solids efflux per unit bed area, and bed solids efflux per unit bed area. Only the flux ratios for the three streams of product solids are included in the figures since it is obvious that the difference between the sum of the flux ratios and unity is the fraction of the fuel carbon which is converted to gaseous products. As was pointed out in the presentation of the results on Evans coal (Section 5), the total solids efflux per unit bed area, $\dot{m}_p/A_b$, and the bed solids efflux per unit bed area, $\dot{m}_b/A_b$, may be interpreted as inverse measures of the characteristic solids residence times τ_p and τ_b.

In plotting the results, various symbols were used in an attempt to distinguish operating conditions. For additional operating conditions for specific points in the plots Table 7.1 should be consulted. In general, the results for the two fuels parallel the results for Evans coal. Under the constraint of

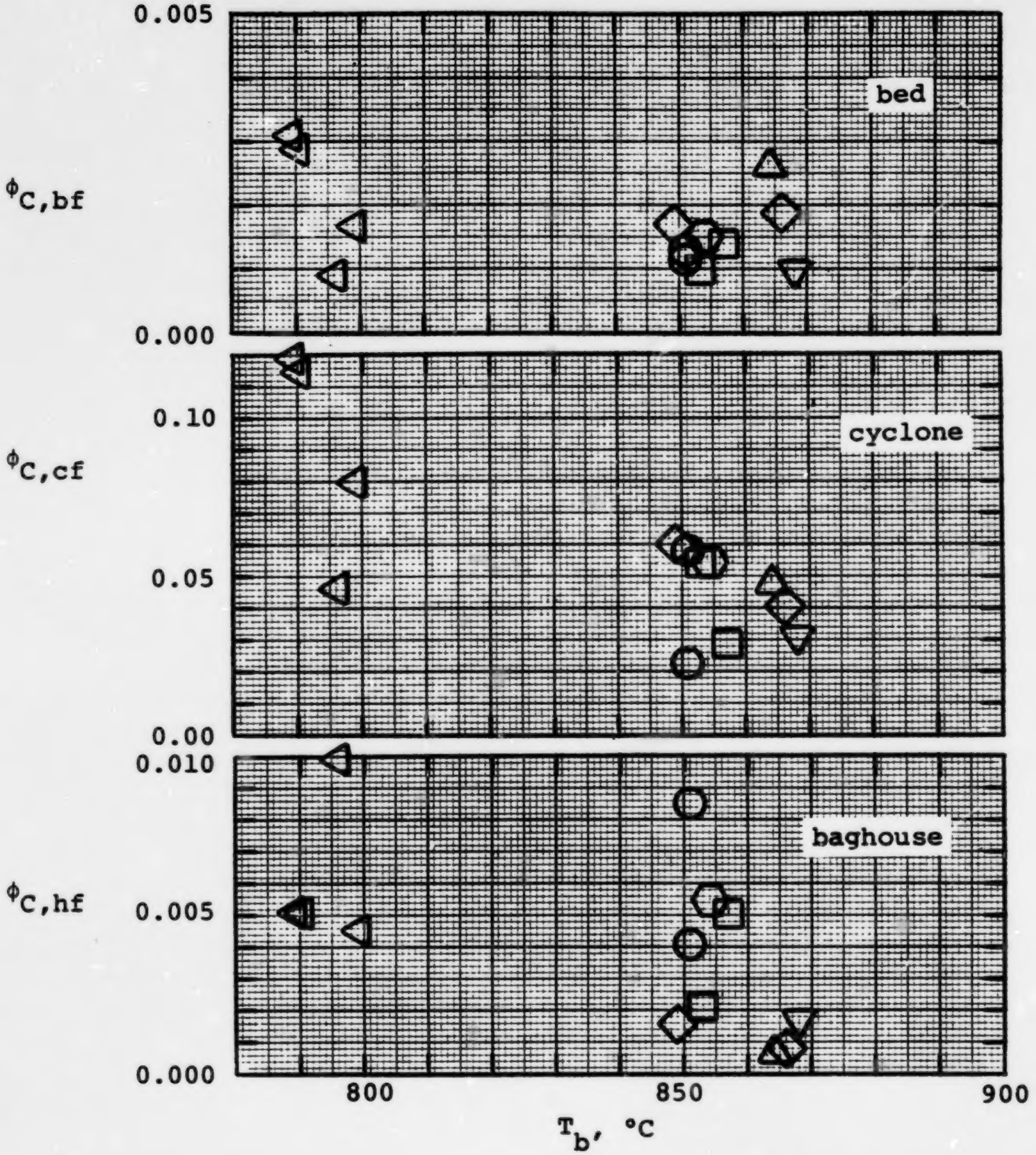

Fig. 7.5. Flux ratios of carbon loss in individual streams of solids from bed, cyclone and baghouse to carbon fed in fuel vs. bed temperature, T_b.

Key to symbols:

	v, m/s	Coal	$\hat{D}_p$, mm	Sorbent
○	2.5	Devco	2.1	Sysco
□	2.5	Devco	2.1	Calpo
⬡	1.5	Devco	2.1	Calpo
△	1.5	Devco	11.2	Calpo
◇	1.4-1.5	Devco	11.2	Sysco
▽	2.4	Devco	11.2	Sysco
◁	2.6-2.9	KY No. 9	2.3	Reed

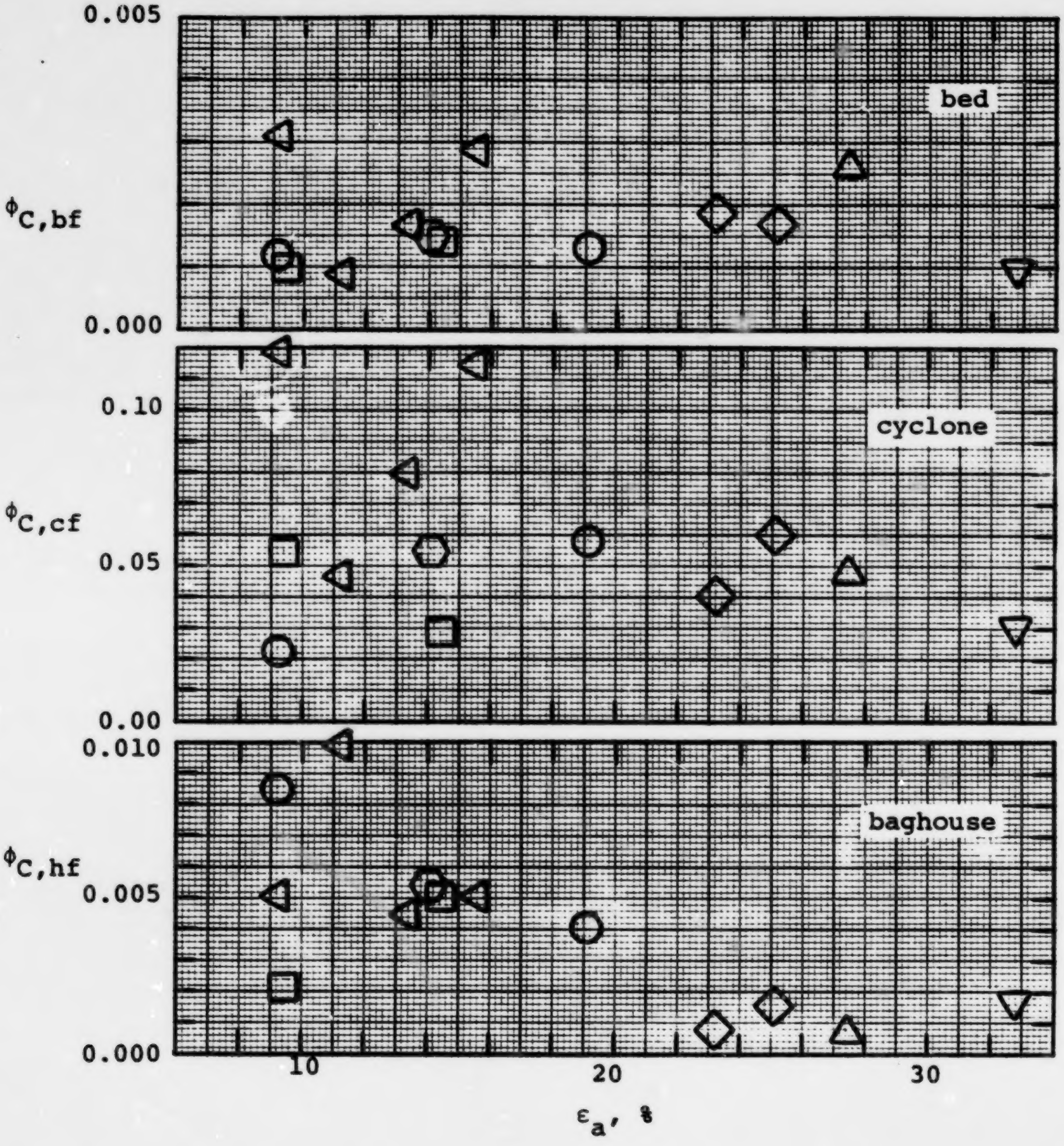

Fig. 7.6. Flux ratios of carbon loss in individual streams of solids from bed, cyclone and baghouse to carbon fed in fuel vs. excess air level, ε_a.

Key to symbols:	v, m/s	Coal	$\hat{D}_p$, mm	Sorbent
○	2.5	Devco	2.1	Sysco
□	2.5	Devco	2.1	Calpo
⬡	1.5	Devco	2.1	Calpo
△	1.5	Devco	11.2	Calpo
◇	1.4-1.5	Devco	11.2	Sysco
▽	2.4	Devco	11.2	Sysco
◁	2.6-2.9	KY No. 9	2.3	Reed

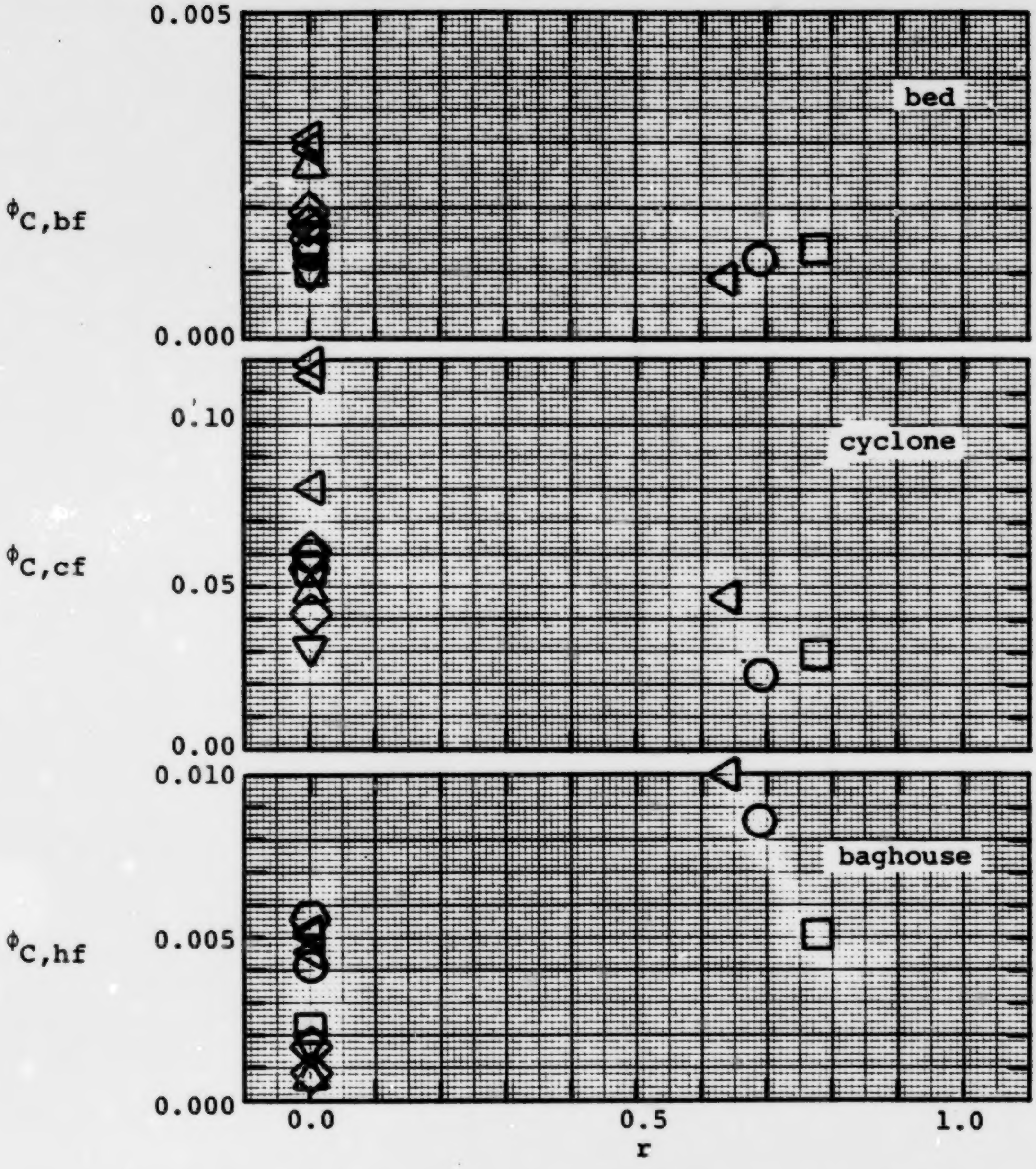

Fig. 7.7. Flux ratios of carbon loss in individual streams of solids from bed, cyclone and baghouse to carbon fed in fuel vs. recycle fraction, r.

Key to symbols:

	v, m/s	Coal	$\hat{D}_p$, mm	Sorbent
○	2.5	Devco	2.1	Sysco
□	2.5	Devco	2.1	Calpo
⬡	1.5	Devco	2.1	Calpo
△	1.5	Devco	11.2	Calpo
◇	1.4-1.5	Devco	11.2	Sysco
▽	2.4	Devco	11.2	Sysco
◁	2.6-2.9	KY No. 9	2.3	Reed

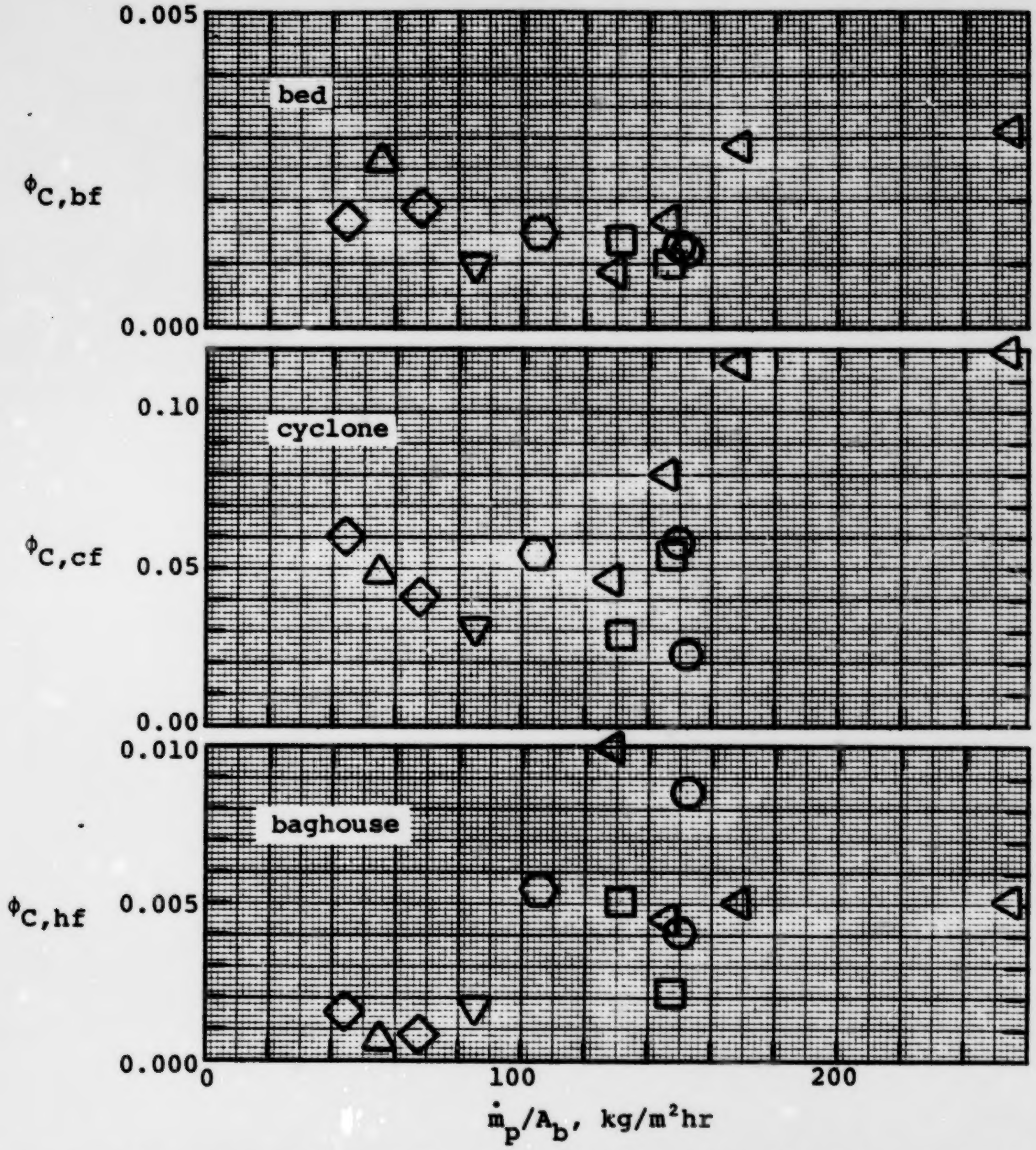

Fig. 7.8. Flux ratios of carbon loss in individual streams of solids from bed, cyclone and baghouse to carbon fed in fuel vs. total solids efflux per unit bed area, $\dot{m}_p/A_b$.

Key to symbols:

	v, m/s	Coal	$\hat{D}_p$, mm	Sorbent
○	2.5	Devco	2.1	Sysco
□	2.5	Devco	2.1	Calpo
⬡	1.5	Devco	2.1	Calpo
△	1.5	Devco	11.2	Calpo
◇	1.4-1.5	Devco	11.2	Sysco
▽	2.4	Devco	11.2	Sysco
◁	2.6-2.9	KY No. 9	2.3	Reed

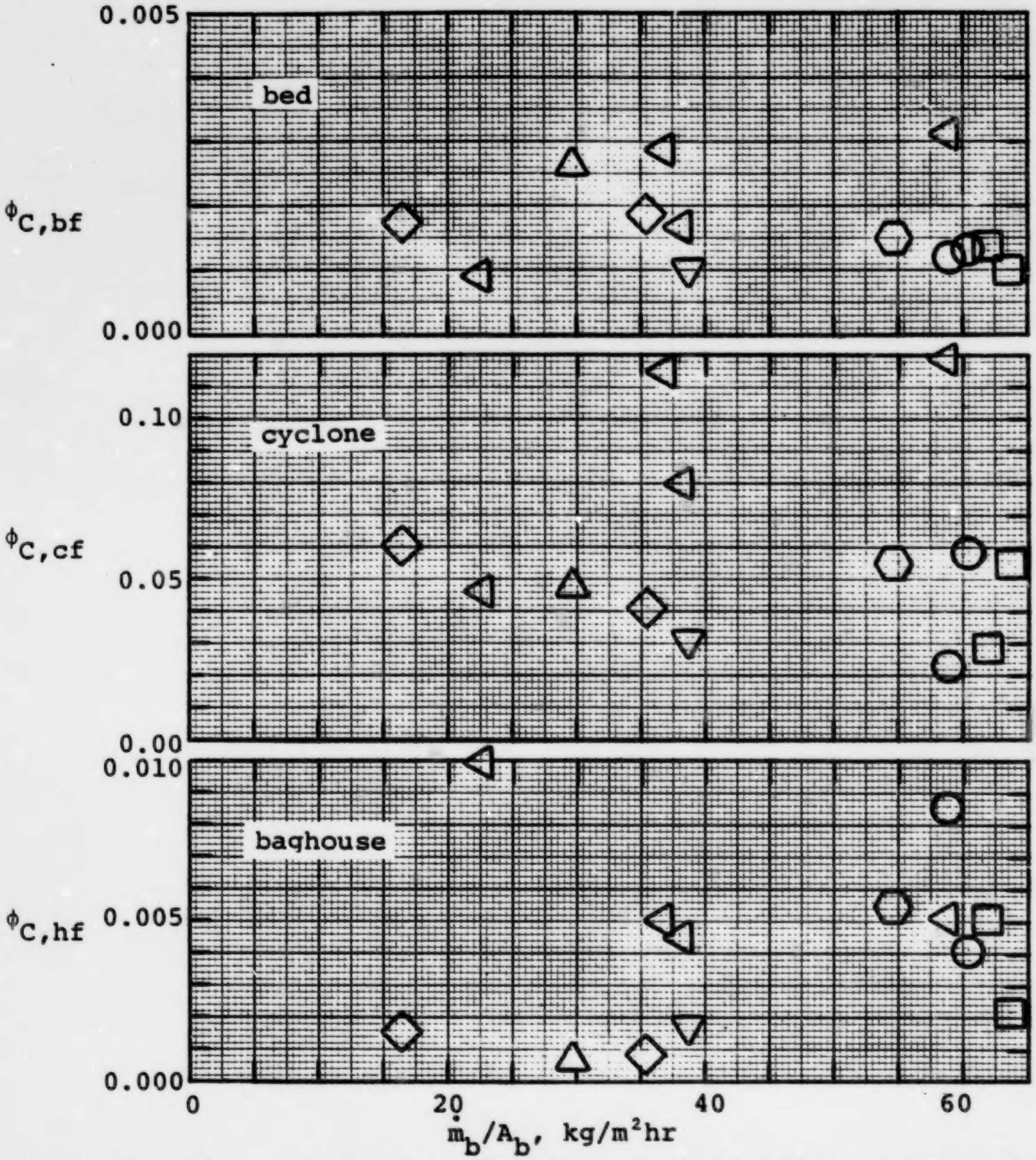

Fig. 7.9. Flux ratios of carbon loss in individual streams of solids from bed, cyclone and baghouse to carbon fed in fuel vs. bed solids efflux per unit bed area, $\dot{m}_b/A_b$.

Key to symbols:

	v, m/s	Coal	$\hat{D}_p$, mm	Sorbent
○	2.5	Devco	2.1	Sysco
□	2.5	Devco	2.1	Calpo
⬡	1.5	Devco	2.1	Calpo
△	1.5	Devco	11.2	Calpo
◇	1.4-1.5	Devco	11.2	Sysco
▽	2.4	Devco	11.2	Sysco
◁	2.6-2.9	KY No. 9	2.3	Reed

other factors being constant, there is a reduction in carbon loss in the three streams of solids with increasing bed temperature. Apparent contradictions to this statement in Fig. 7.5 may be explained by an increase in the recycle fraction and/or a decrease in the excess air level. This apparent contradiction is particularly evident for the baghouse solids where an increase in recycle fraction results in a pronounced increase in the fuel carbon loss to this stream. The effect of excess air level (Fig. 7.6) is similar to the effect of bed temperature. An increase in the recycle fraction increases the fraction of the fuel carbon which is lost in the baghouse solids and decreases the fraction of the fuel carbon which is lost to the cyclone and bed overflow solids. The net effect of an increase in the recycle fraction is a reduction in the overall loss of fuel carbon.

The flux ratios for the three streams of solids are plotted vs. the total solids efflux per unit bed area, $\dot{m}_p/A_b$, in Fig. 7.8 and vs. the bed solids efflux per unit bed area, $\dot{m}_b/A_b$, in Fig. 7.9. Although not as distinct as the results for Evans coal, there is a downward trend in the flux ratios with an increase in solids residence time (decrease in solids efflux). The trend is more pronounced at short residence times because of the limited range and positive values for the excess air level. A similar argument was given to explain the lack of a significant reduction in the carbon content of the solids with an increase in the excess air level. Again, the increase in the fuel carbon loss to the baghouse stream with an increase in the recycle fraction is evident in the plots for the baghouse solids.

The flux ratio of the total carbon loss in the product solids to the carbon fed in the fuel is shown in Fig. 7.10 and Fig. 7.11 as a function of bed temperature, excess air level, recycle fraction, total solids efflux per unit bed area, and bed solids efflux per unit bed area. The trends with respect to T_b, ε_a, $\dot{m}_p/A_b$, and $\dot{m}_b/A_b$ are similar to those observed for the carbon loss to the individual streams of solids. At zero recycle fraction, the carbon loss in the solids was in the range 8.7--12.8% of the fuel carbon for the KY No. 9 coal and 3.3--6.4% of the fuel carbon for the Devco coal. The net effect of an increase in recycle fraction is a reduction in the total loss of fuel carbon. Typically, the fuel carbon loss decreased from 12.4--12.8% at $r = 0$ to 5.8% at $r = 0.64$ for the KY No. 9 coal and from 5.8--6.4% at $r = 0$ to 3.3% at $r = 0.7$ for the Devco coal.

7.2.4 Division of carbon between cyclone and baghouse solids

The dependency of the flux ratio of the carbon loss in the cyclone solids to the carbon loss in the baghouse solids on the non-recycle fraction is examined in Fig. 7.12. Although only three runs were carried out at recycle fractions other than zero, the characteristic downward trend in the flux ratio is observed on the log-log plot as r increases. At zero recycle, the narrow range of $\phi_{C,ch}$ for the KY No. 9 coal ($\hat{D}_p = 2.3$ mm), 17.6 to 23.1, falls within the spread of the points, 10.2 to 25.0, for the smaller

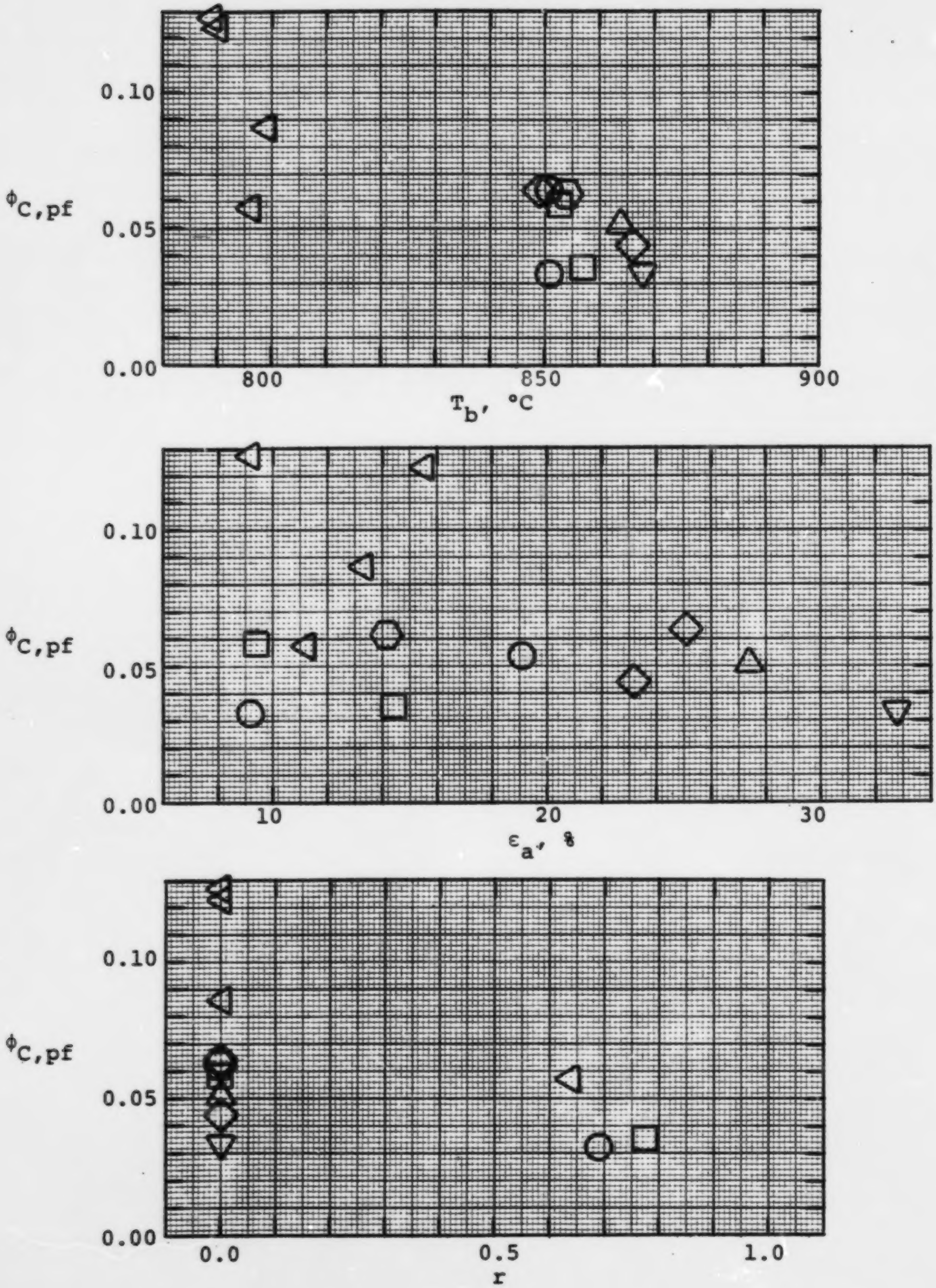

Fig. 7.10. Flux ratio of carbon loss in solids to carbon fed in fuel vs. bed temperature, T_b, excess air level, ε_a, and recycle fraction, r. A key to the symbols accompanies Fig. 7.11.

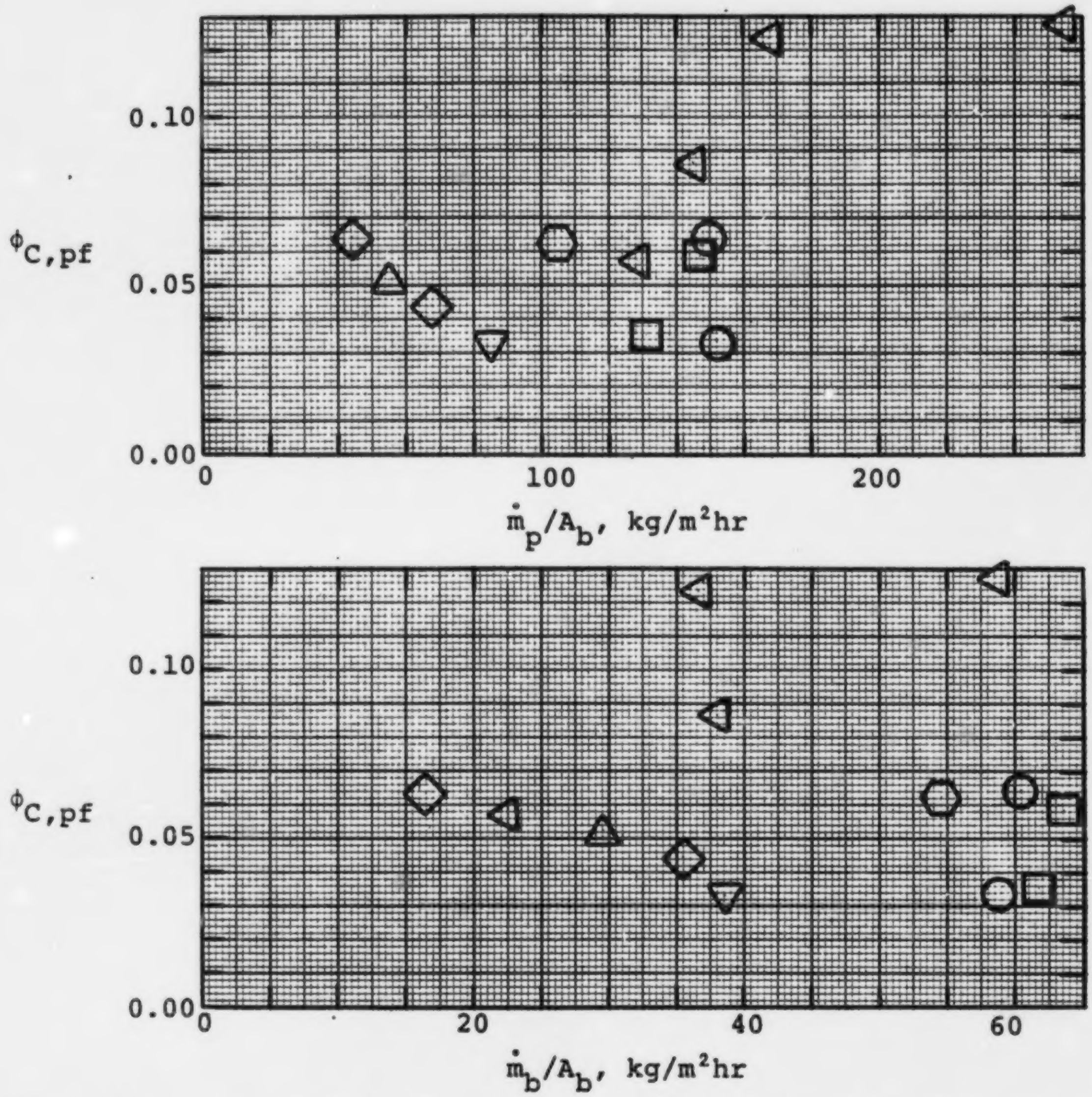

Fig. 7.11. Flux ratio of carbon loss in solids to carbon fed in fuel vs. total solids efflux per unit bed area, $\dot{m}_p/A_b$, and bed solids efflux per unit bed area, $\dot{m}_b/A_b$.

Key to symbols:	v, m/s	Coal	$\hat{D}_p$, mm	Sorbent
○	2.5	Devco	2.1	Sysco
□	2.5	Devco	2.1	Calpo
⬡	1.5	Devco	2.1	Calpo
△	1.5	Devco	11.2	Calpo
◇	1.4-1.5	Devco	11.2	Sysco
▽	2.4	Devco	11.2	Sysco
◁	2.6-2.9	KY No. 9	2.3	Reed

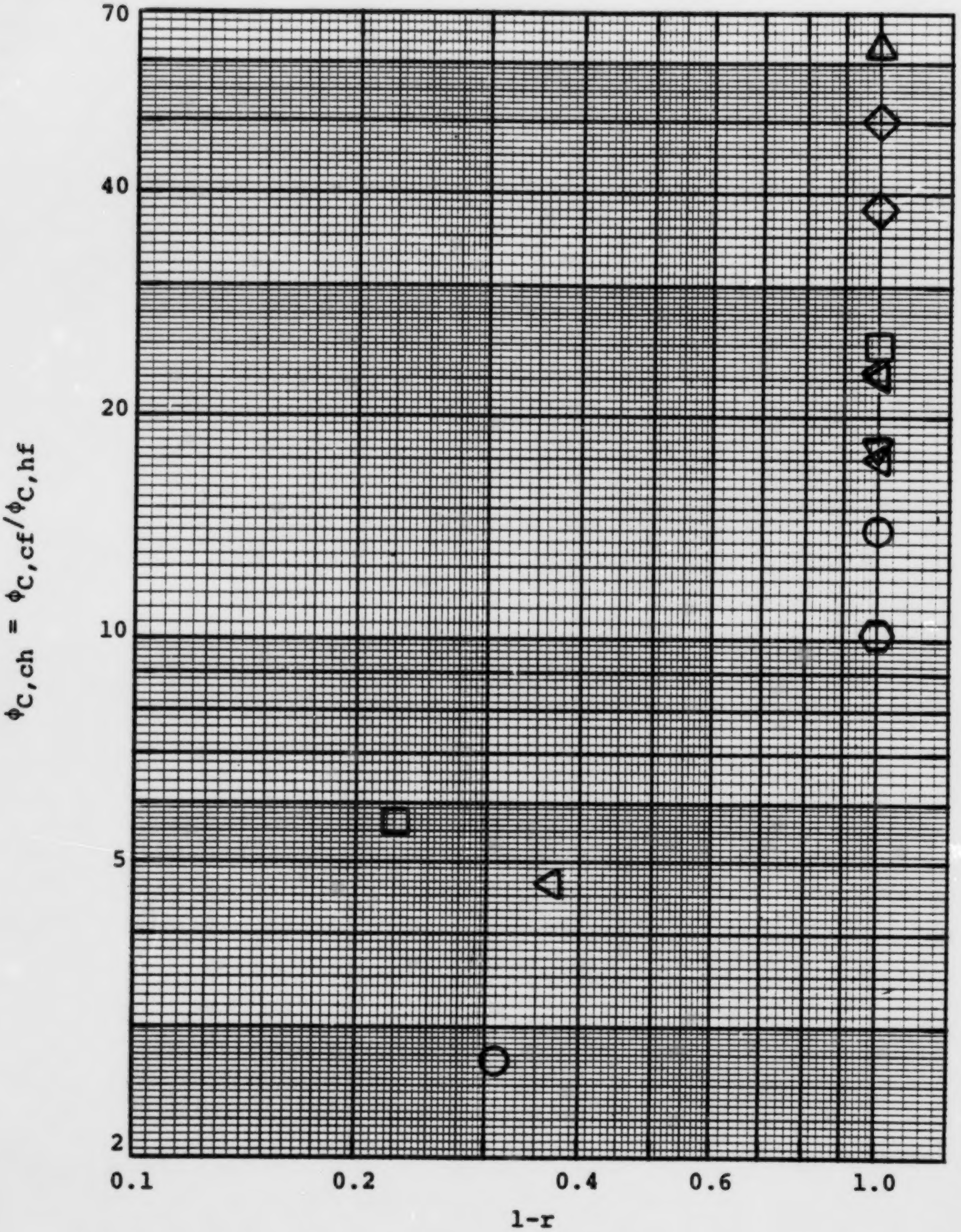

Fig. 7.12. Flux ratio of carbon loss in cyclone solids to carbon loss in baghouse solids vs. the non-recycle fraction, 1-r. A key to the symbols accompanies Fig. 7.11.

size fraction of Devco coal ($\hat{D}_p$ = 2.1 mm). The three high values of $\phi_{C,ch}$ for the larger size fraction of Devco coal ($\hat{D}_p$ = 11.2 mm) may be attributed to a reduction in the elutriation of carbon fines, i.e., a decrease in $\phi_{C,hf}$ (see ordinate variable in Fig. 7.12).

7.2.5 Correlation of overhead carbon loss

Details on the correlation of overhead carbon loss is given in subsection 5.2. Multiple linear regression on the combined data for KY No. 9 and Devco coals gave the following result:

$$(\dot{m}_{C,o}/\dot{m}_{C,f}) = 9.456 \times 10^{-7}\ v^{-0.2622}\ \hat{D}_p^{-0.2421}\ \phi_a^{-1.532}$$

$$\exp(-0.7822r)\ \exp(12897/T_b) \qquad (7.2.1)$$

The observed overhead carbon loss is compared with the carbon loss predicted by Eq. 7.2.1 in Fig. 7.13. The correlation underestimates all four of the carbon losses for KY No. 9 coal and a second regression was carried out on only the data for Devco coal with the following result:

$$(\dot{m}_{C,o}/\dot{m}_{C,f}) = 9.521 \times 10^{-16}\ v^{-0.1467}\ \hat{D}_p^{-0.6644}\ \phi_a^{0.1689}$$

$$\exp(-0.6991r)\ \exp(35974/T_b) \qquad (7.2.2)$$

The observed overhead carbon loss is compared with the carbon loss predicted by this second result in Fig. 7.14. The correlation gives an adequate prediction of overhead carbon loss with only one point

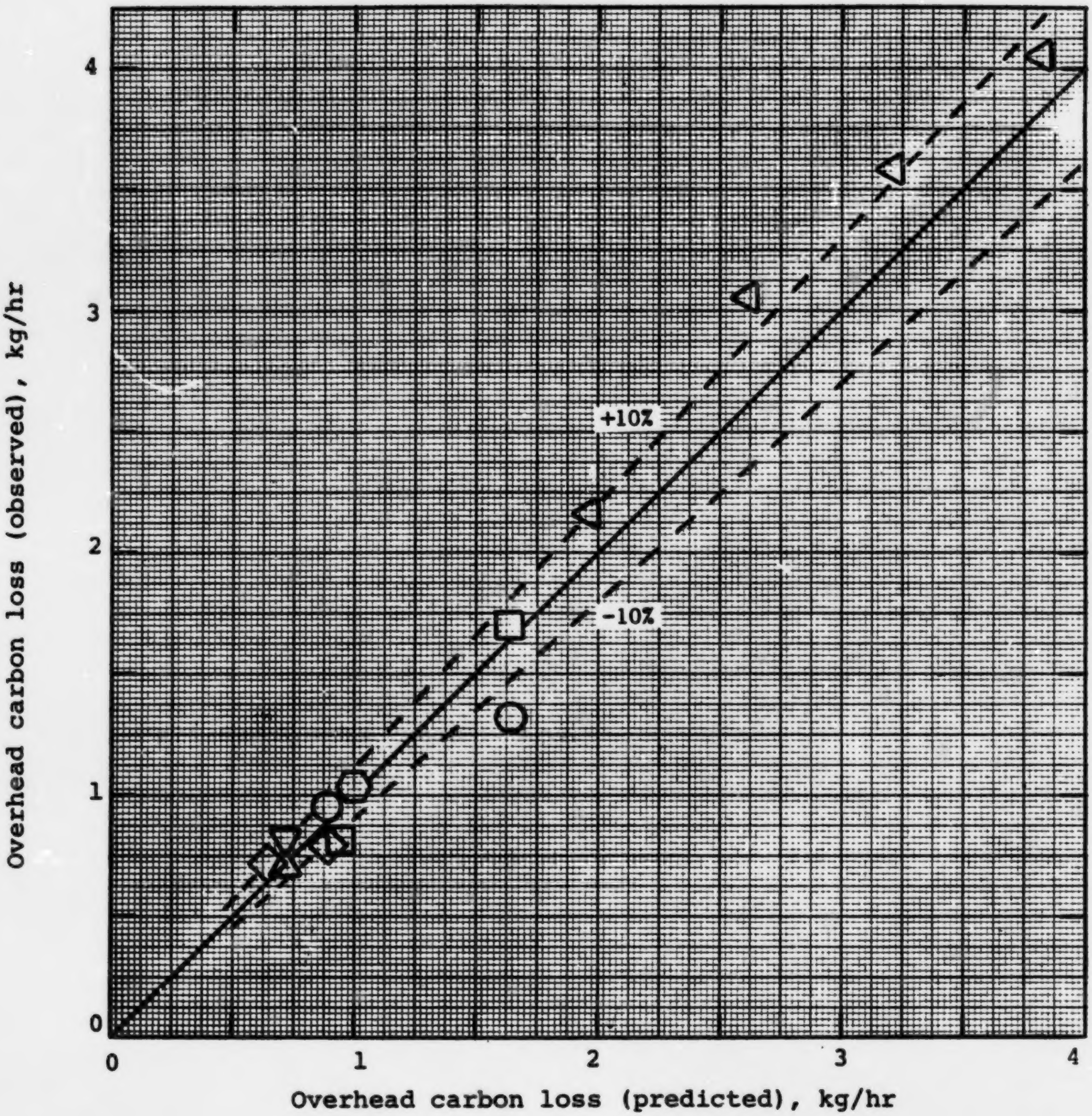

Fig. 7.13. A comparison of overhead carbon losses with values predicted by Eq. 7.2.1.

Key to symbols:	v, m/s	Coal	$\hat{D}_p$, mm	Sorbent
○	2.5	Devco	2.1	Sysco
□	2.5	Devco	2.1	Calpo
⬡	1.5	Devco	2.1	Calpo
△	1.5	Devco	11.2	Calpo
◇	1.4-1.5	Devco	11.2	Sysco
▽	2.4	Devco	11.2	Sysco
◁	2.6-2.9	KY No. 9	2.3	Reed

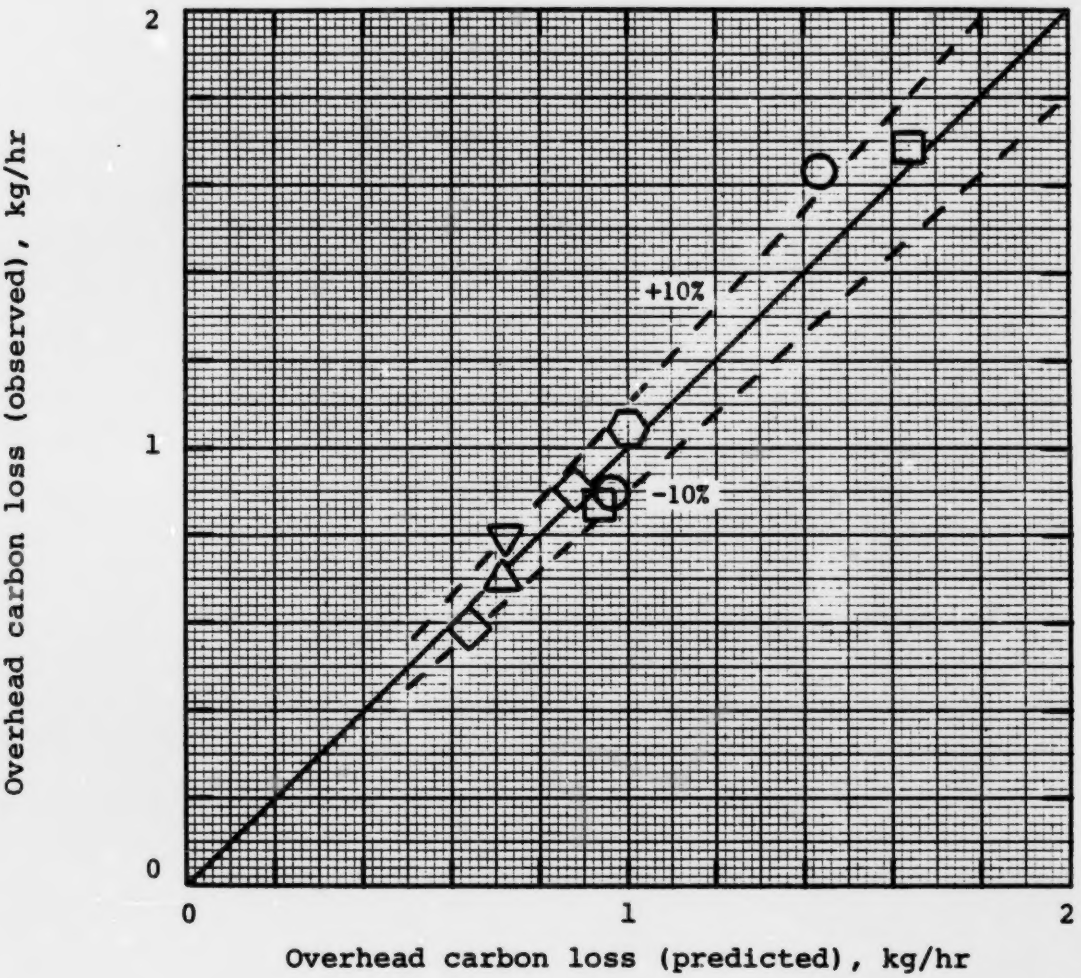

Fig. 7.14. A comparison of overhead carbon losses with values predicted by Eq. 7.2.2.

Key to symbols:	v, m/s	Coal	$\hat{D}_p$, mm	Sorbent
○	2.5	Devco	2.1	Sysco
□	2.5	Devco	2.1	Calpo
⬡	1.5	Devco	2.1	Calpo
△	1.5	Devco	11.2	Calpo
◇	1.4-1.5	Devco	11.2	Sysco
▽	2.4	Devco	11.2	Sysco

lying outside but close to the ± 10% boundary. Little can be said about the magnitudes of the empirical results for C_o and the a's since various combinations of widely differing values can result in essentially the same fit of the data. The above results for the two regressions illustrate this. Of more significance is agreement with respect to sign which indicates the same qualitative effect of a particular operating condition. The results for the two regressions are in agreement with respect to the signs accompanying the a's with the exception of a_3 the power on ϕ_a. Of more importance, however, is the disagreement of the sign on a_1, the power on the fluidizing velocity, with the results for Evans coal and our earlier work on Minto and Devco coals (Becker and Code, 1983). In this case, one would expect a positive sign on a_1, i.e., an increase in fluidizing velocity results in an increase in overhead carbon loss. Values of the coefficient C_o calculated using values of the carbon loss for individual runs are compared with the statistically fitted values for the two regressions in Fig. 7.15 and Fig. 7.16.

7.2.6 Carbon burnup efficiency

The effect of bed temperature, excess air level, and recycle fraction on the carbon burnup efficiency, defined as

$$\eta_C = 100\,(1-\dot{m}_{C,p}/\dot{m}_{C,f}) \qquad (7.2.3)$$

is examined in Fig. 7.17. For the runs with KY No. 9 coal the carbon burnup efficiency ranged from 87.2 to 91.4% at zero

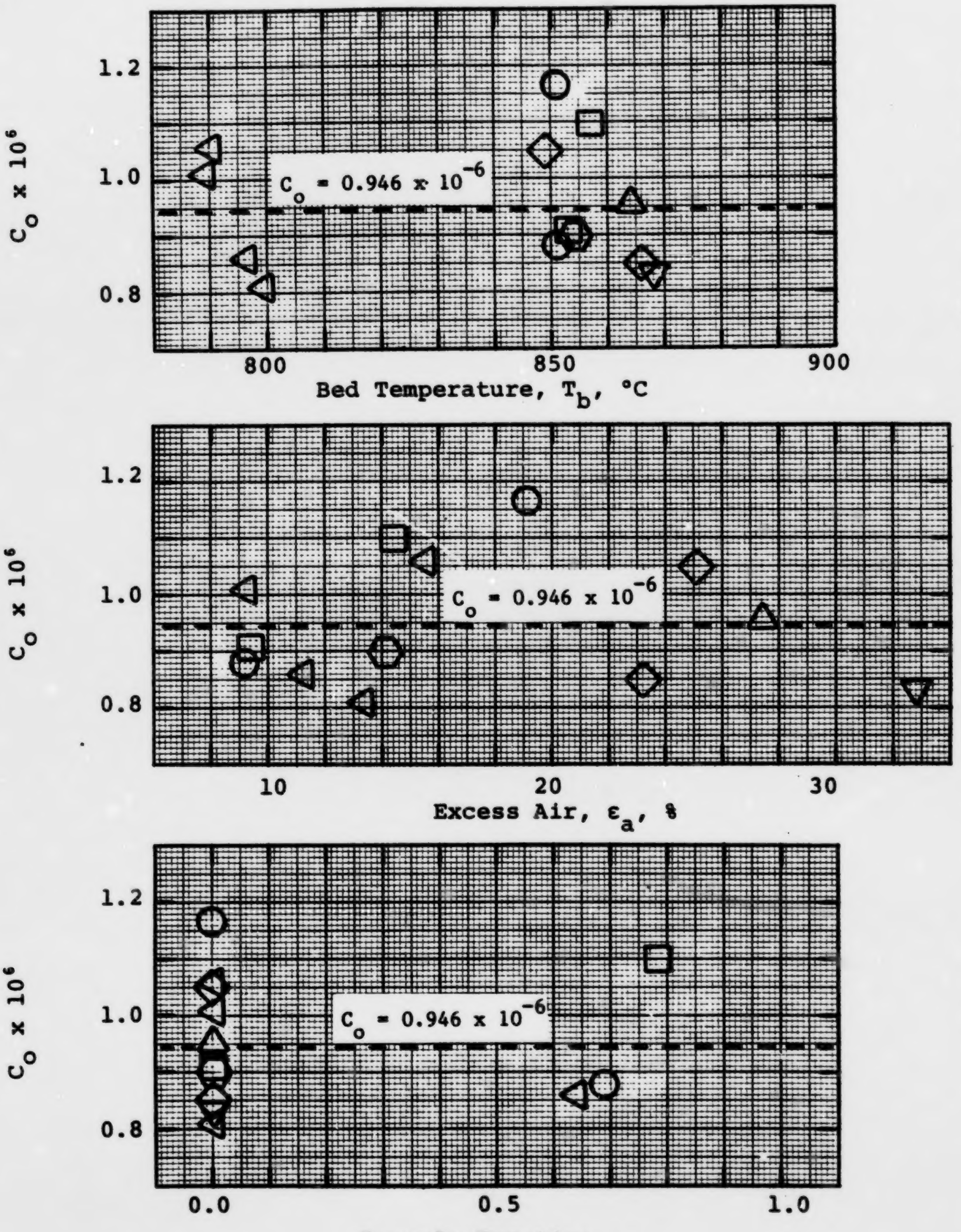

Fig. 7.15. The coefficient, C_o, in the correlation for overhead carbon loss, calculated using values of carbon loss for individual runs. $C_o = 0.946 \times 10^{-6}$ is the statistically fitted value. A key to the symbols accompanies Fig. 7.13.

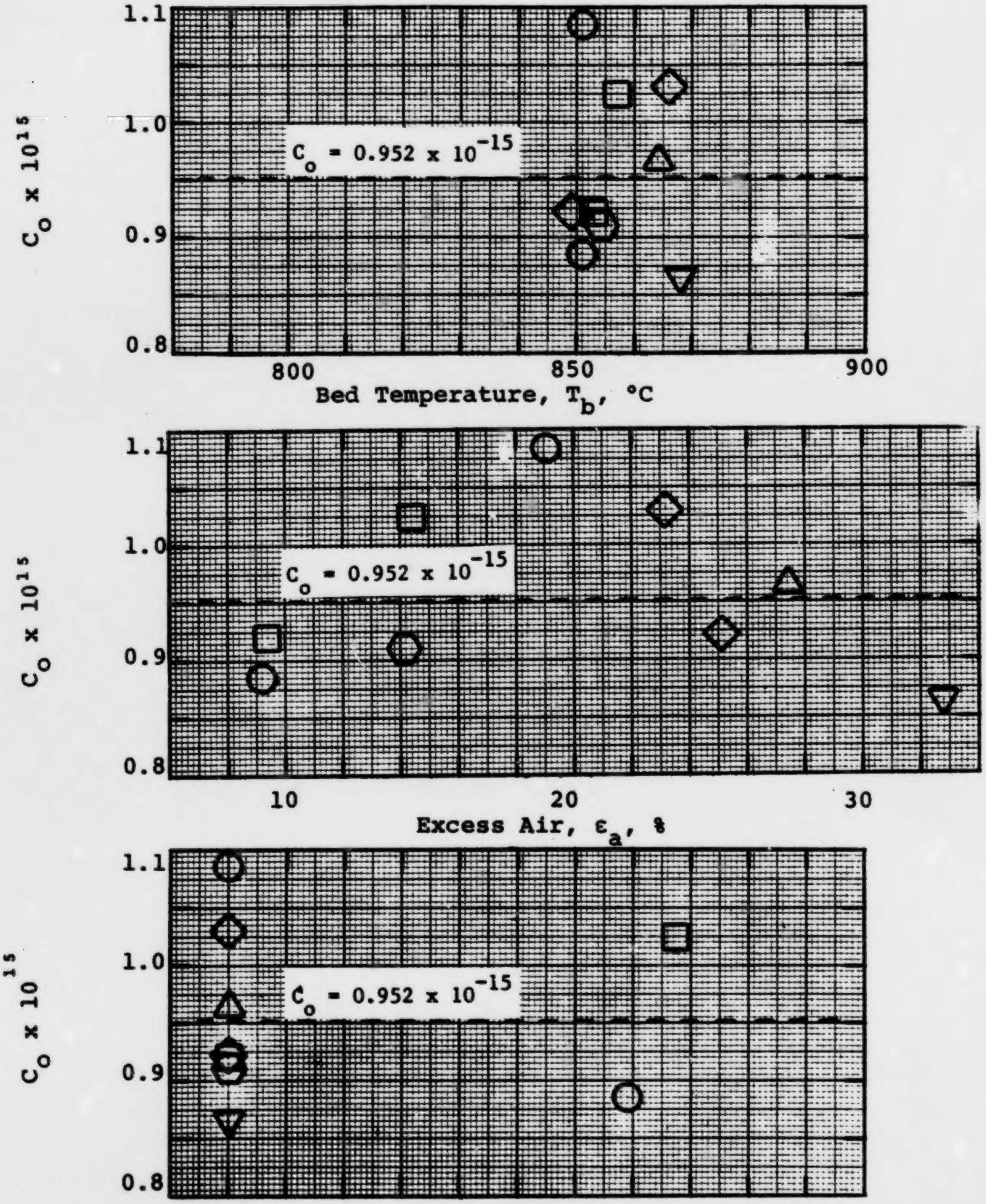

Fig. 7.16. The coefficient, C_o, in the correlation for overhead carbon loss, calculated using values of carbon loss for individual runs. $C_o = 0.952 \times 10^{-15}$ is the statistically fitted value. A key to the symbols accompanies Fig. 7.14.

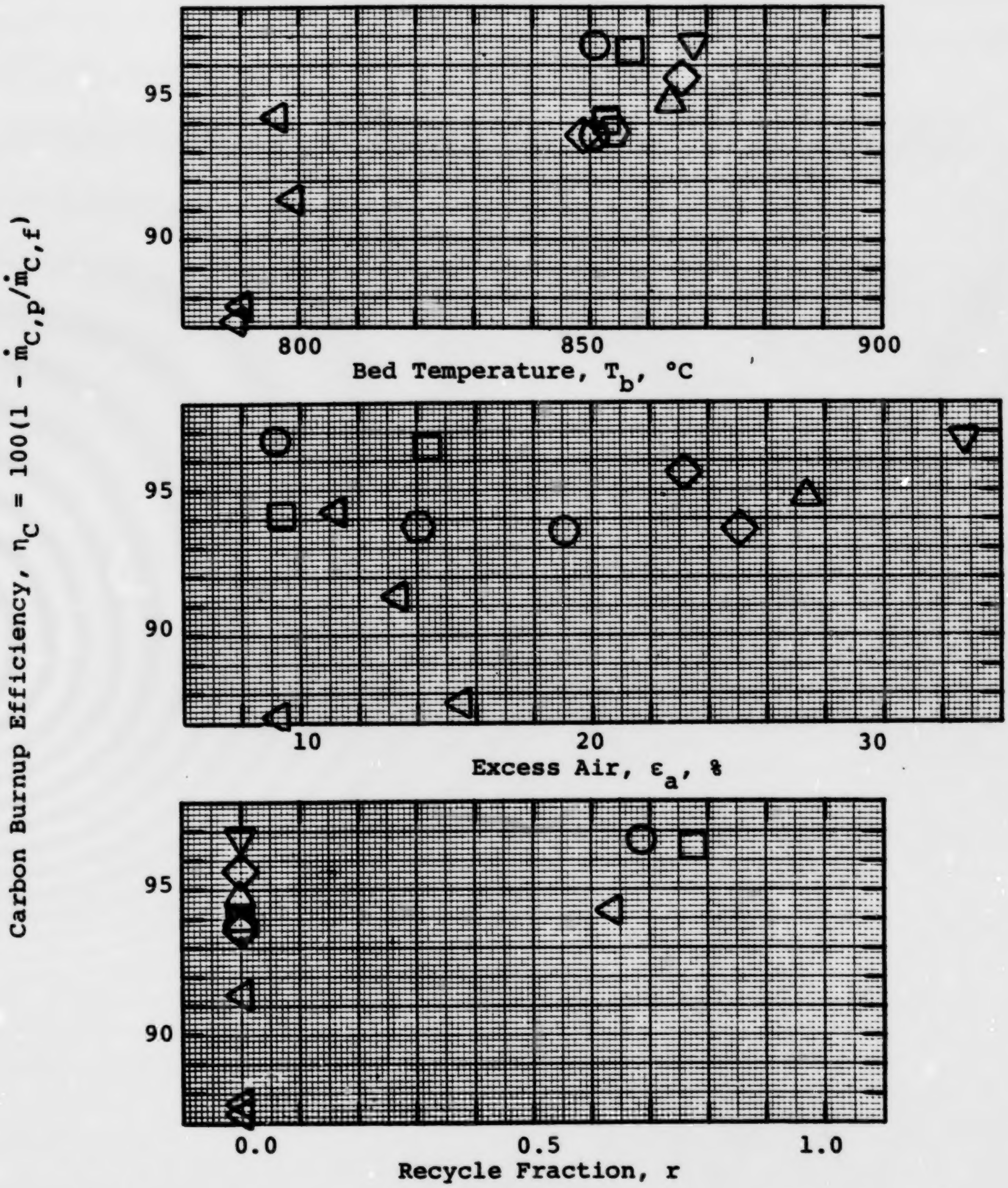

Fig. 7.17. Carbon burnup efficiencies for the fluidized-bed combustion of Devco coal and Kentucky No. 9 coal.

Key to symbols:	v, m/s	Coal	$\hat{D}_p$, mm	Sorbent
○	2.5	Devco	2.1	Sysco
□	2.5	Devco	2.1	Calpo
⬡	1.5	Devco	2.1	Calpo
△	1.5	Devco	11.2	Calpo
◇	1.4-1.5	Devco	11.2	Sysco
▽	2.4	Devco	11.2	Sysco
◁	2.6-2.9	KY No.9	2.3	Reed

recycle of cyclone solids and increased to 94.2% at a recycle fraction of 0.64. Burnup efficiencies for Devco coal were in the range 93.6 to 96.7%. The positive effects of bed temperature and recycle fraction on the carbon burnup efficiency are evident from an examination of Fig. 7.17. The smaller effect of excess air level is due to the limited range and positive values of ϵ_a.

7.2.7 Carbon balance check

The total carbon flux per unit bed area accounted for in the product streams is compared in Fig. 7.18 with the total carbon flux per unit bed area in the feed streams. Three of the nine runs (850107, 850121, 850304) with Devco coal gave carbon balance checks which fall above the + 10% line in Fig. 7.18. The carbon balance checks for the other six runs fall within the ± 10% boundary. Although two results are close to the boundary, all of the four runs with KY No. 9 coal gave carbon balance checks which fall below the - 10% line.

7.3 The sulphur balance

7.3.1 The sulphur content of the product solids

The concentration of sulphur in the three product streams of solids is plotted vs. the carbon concentration in Fig. 7.19. The sulphur is reported as total sulphur, i.e., no distinction is made in the analyses between organic and inorganic sulphur or sulphide and sulphate sulphur. However, since the carbon content of the bed overflow solids is in the range 0.9--1.5 % for the KY

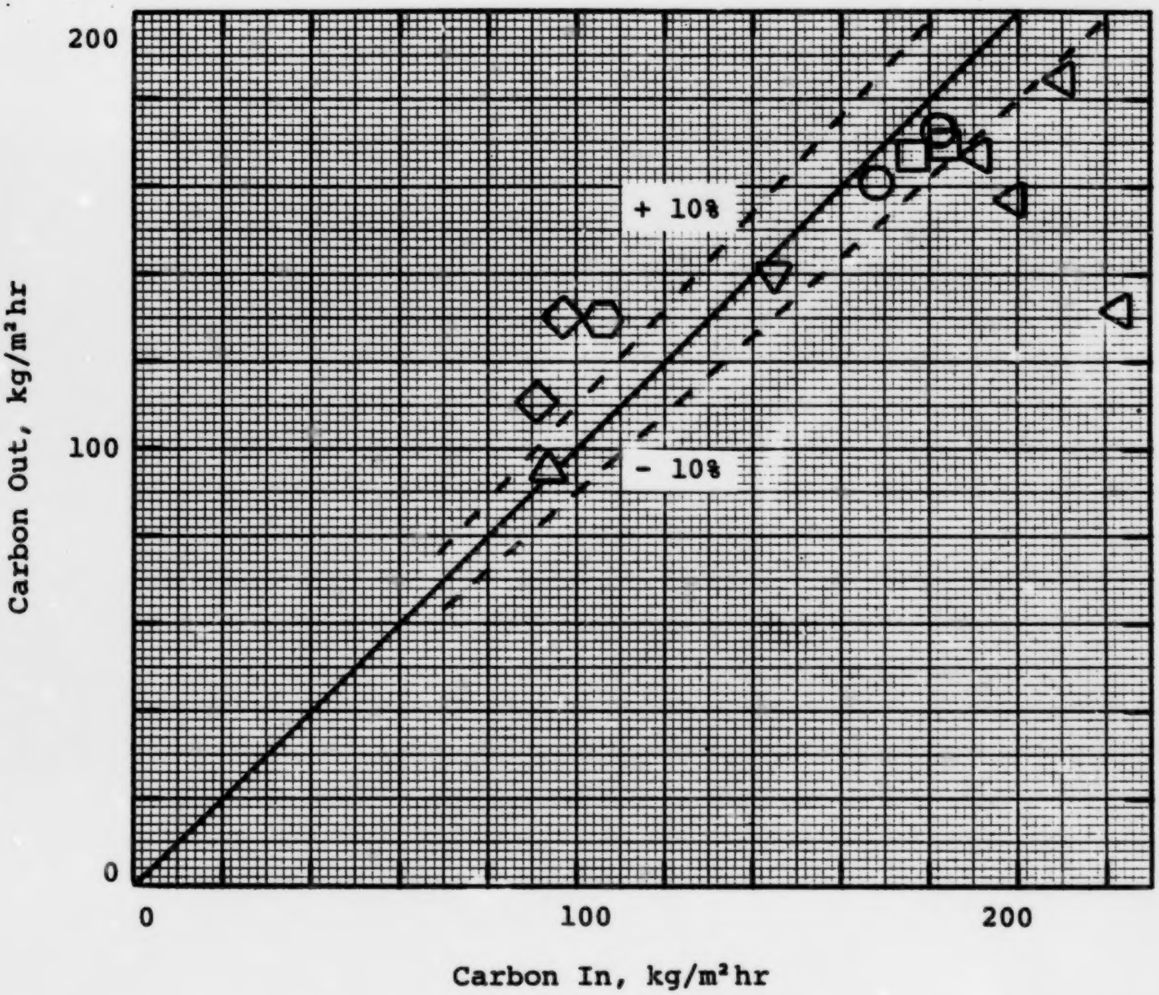

Fig. 7.18. Carbon balance check: total carbon flux per unit bed area in the product streams vs. total carbon flux per unit bed area in the feed streams.

Key to symbols:	v, m/s	Coal	$\hat{D}_p$, mm	Sorbent
○	2.5	Devco	2.1	Sysco
□	2.5	Devco	2.1	Calpo
⬡	1.5	Devco	2.1	Calpo
△	1.5	Devco	11.2	Calpo
◇	1.4-1.5	Devco	11.2	Sysco
▽	2.4	Devco	11.2	Sysco
◁	2.6-2.9	KY No. 9	2.3	Reed

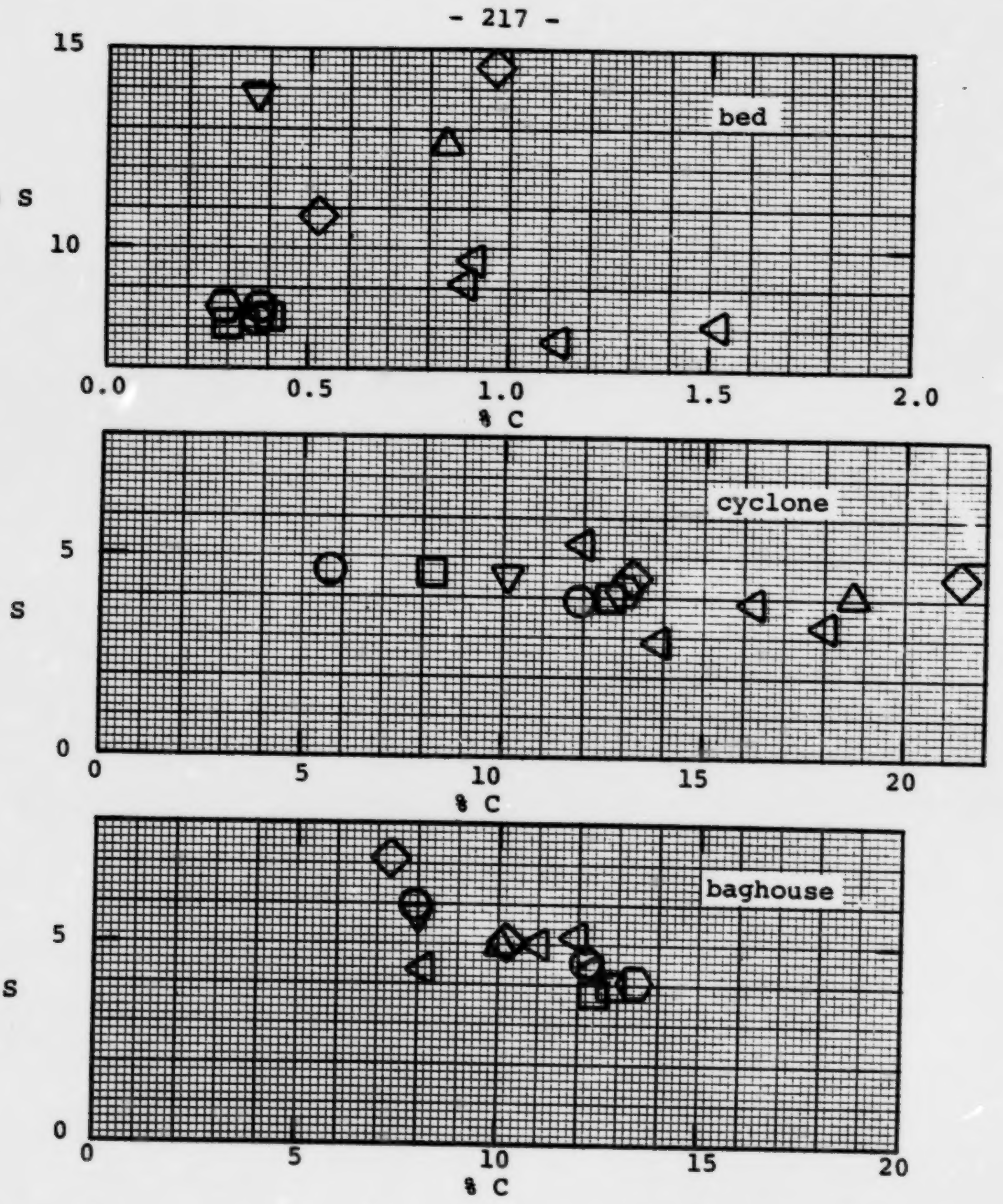

Fig. 7.19. Sulphur content of the product solids.

Key to symbols:

	v, m/s	Coal	$\hat{D}_p$, mm	Sorbent
○	2.5	Devco	2.1	Sysco
□	2.5	Devco	2.1	Calpo
⬡	1.5	Devco	2.1	Calpo
△	1.5	Devco	11.2	Calpo
◇	1.4-1.5	Devco	11.2	Sysco
▽	2.4	Devco	11.2	Sysco
◁	2.6-2.9	KY No. 9	2.3	Reed

No. 9 runs and 0.3--1 % for the Devco runs, the sulphur content of the bed product is predominantly in the sulphate form ($CaSO_4$). For the runs with Kentucky No. 9 coal the ranges of sulphur content are 7.7--9.7 % for the bed overflow solids, 2.9--5.4 % for the cyclone solids, and 4.4--8.4 % for the baghouse solids. The corresponding ranges for the Devco runs are 8.1--14.6 % for the bed overflow solids, 4.0--4.7 % for the cyclone solids, and 3.8--7.2 % for the baghouse solids. The values plotted in Fig. 7.19 are the mean values which were used in the materials balances.

7.3.2 Distribution of sulphur among the product solids

The distribution of sulphur among the three streams of product solids, expressed as a ratio of the sulphur flux in an individual stream to the total sulphur flux in the three streams of solids, is shown in Fig. 7.20. The recycle fraction was selected as the abscissa variable in Fig. 7.20 in order to examine the effect of r on the sulphur distribution. At zero recycle of cyclone solids, the distribution of sulphur for the runs with KY No. 9 coal was as follows: 40--45 % to the bed overflow solids, 48--55 % to the cyclone solids, and 5--10 % to the baghouse solids. These results were for a fluidizing velocity of 2.6--2.7 m/s and a mean fuel particle diameter of 2.3 mm. For comparison, the corresponding ranges for the Devco runs with essentially the same fluidizing velocity and fuel particle size (v = 2.5 m/s, $\hat{D}_p$ = 2.1 mm) were: 58--61 % to the bed overflow solids, 37--39% to cyclone solids, and 1.5--3.1 % to the baghouse solids. The distribution of sulphur for the run

---

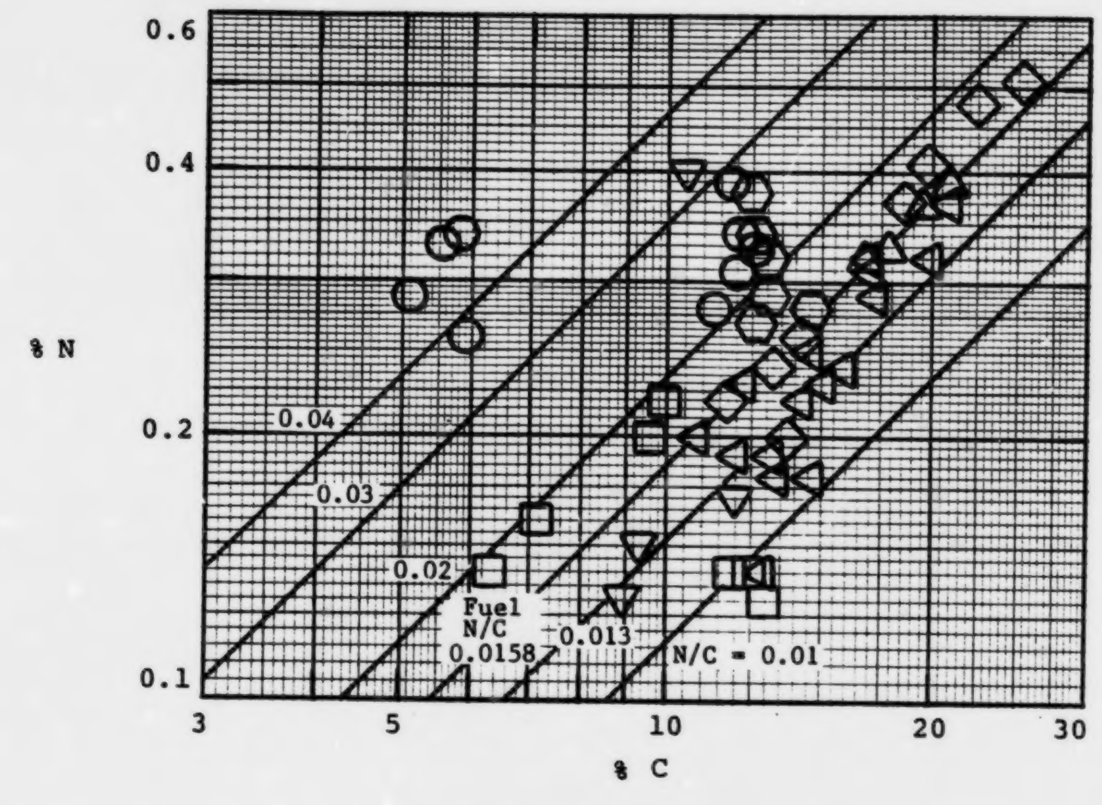

Fig. 7.28. Nitrogen content of the cyclone solids.

Key to symbols:

	v, m/s	Coal	$\hat{D}_p$, mm	Sorbent
○	2.5	Devco	2.1	Sysco
□	2.5	Devco	2.1	Calpo
⬡	1.5	Devco	2.1	Calpo
△	1.5	Devco	11.2	Calpo
◇	1.4-1.5	Devco	11.2	Sysco
▽	2.4	Devco	11.2	Sysco
◁	2.6-2.9	KY No. 9	2.3	Reed

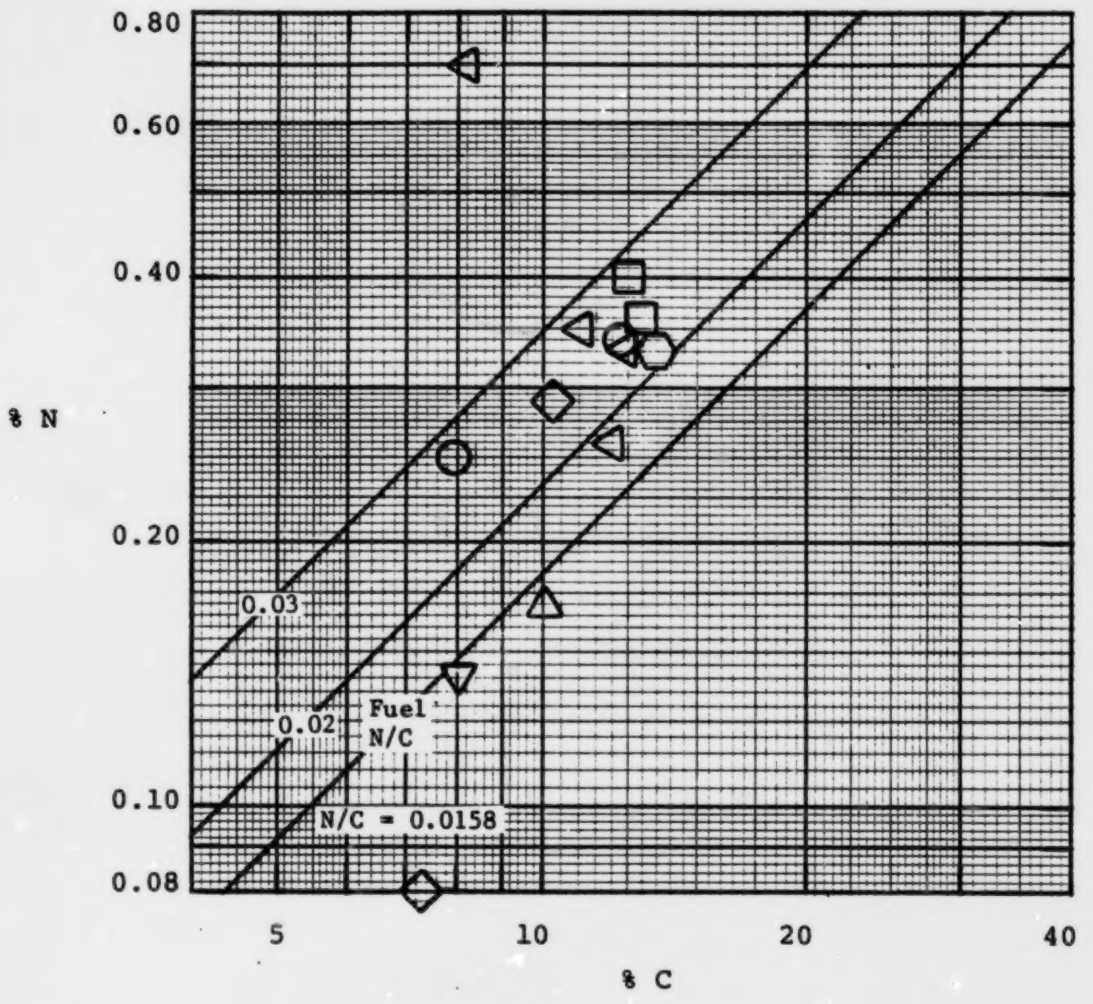

Fig. 7.29. Nitrogen content of the baghouse solids.

Key to symbols:

	v, m/s	Coal	$\hat{D}_p$, mm	Sorbent
○	2.5	Devco	2.1	Sysco
□	2.5	Devco	2.1	Calpo
⬡	1.5	Devco	2.1	Calpo
△	1.5	Devco	11.2	Calpo
◇	1.4-1.5	Devco	11.2	Sysco
▽	2.4	Devco	11.2	Sysco
◁	2.6-2.9	KY No. 9	2.3	Reed

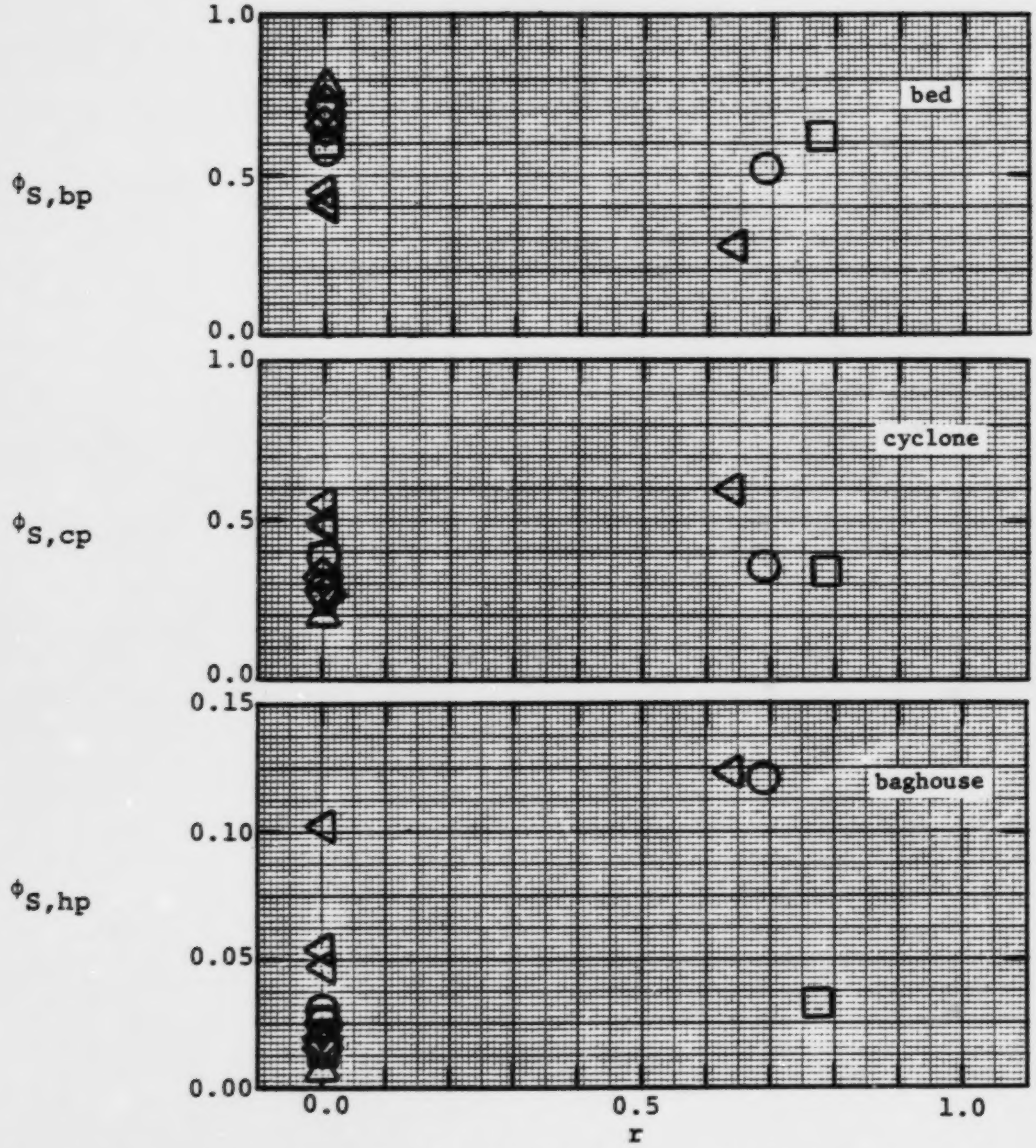

Fig. 7.20. Distribution of sulphur among solids from bed, cyclone and baghouse.

Key to symbols:

	v,m/s	Coal	$\hat{D}_p$, mm	Sorbent
○	2.5	Devco	2.1	Sysco
□	2.5	Devco	2.1	Calpo
⬡	1.5	Devco	2.1	Calpo
△	1.5	Devco	11.2	Calpo
◇	1.4-1.5	Devco	11.2	Sysco
▽	2.4	Devco	11.2	Sysco
◁	2.6-2.9	KY No. 9	2.3	Reed

with KY No. 9 coal at a recycle fraction of 0.64 was: 28 % to the bed solids, 60 % to the cyclone solids and 12 % to the baghouse solids. Corresponding values for the Devco run at r = 0.69 were: 52 % to the bed solids, 36 % to the cyclone solids and 12 % to the baghouse solids. Additional work was carried out on a larger size fraction of Devco coal ($\hat{D}_p$ = 11.2 mm) at a fluidizing velocity of 1.4--1.5 m/s with the following results: 66--78 % to the bed solids, 21--32 % to the cyclone solids, and 0.8--1.5 % to the baghouse solids.

7.3.3 Sulphur capture efficiency

Two estimates were made of the sulphur capture efficiency, η_{SO_2}, from the flowrate and sulphur analysis of the fuel and either the flowrate and sulphur oxide analysis of the stack gas or the flowrates and sulphur analyses of the three streams of product solids.

$$\eta_{SO_2} = 100\ (1-\dot{n}_{SO_2,g}/\dot{n}_{S,f}) = 100\ \dot{n}_{S,p}/\dot{n}_{S,f} \qquad (7.3.1)$$

where $\dot{n}_{SO_2,g}$ is the molar flux of SO_2 leaving in the stack gas, $\dot{n}_{S,p}$ is the molar flux of sulphur leaving in the product solids, and $\dot{n}_{S,f}$ is the molar flux of sulphur entering in the fuel. Sulphur capture efficiencies based on the flowrates and analyses of the stack gas are presented in Fig. 7.21. The second estimates of η_{SO_2} based on the analyses of the product solids are shown in Fig. 7.22. The atomic calcium-to-sulphur ratio, the abscissa variable in the figures, is based on the equivalent calcium content of the limestone

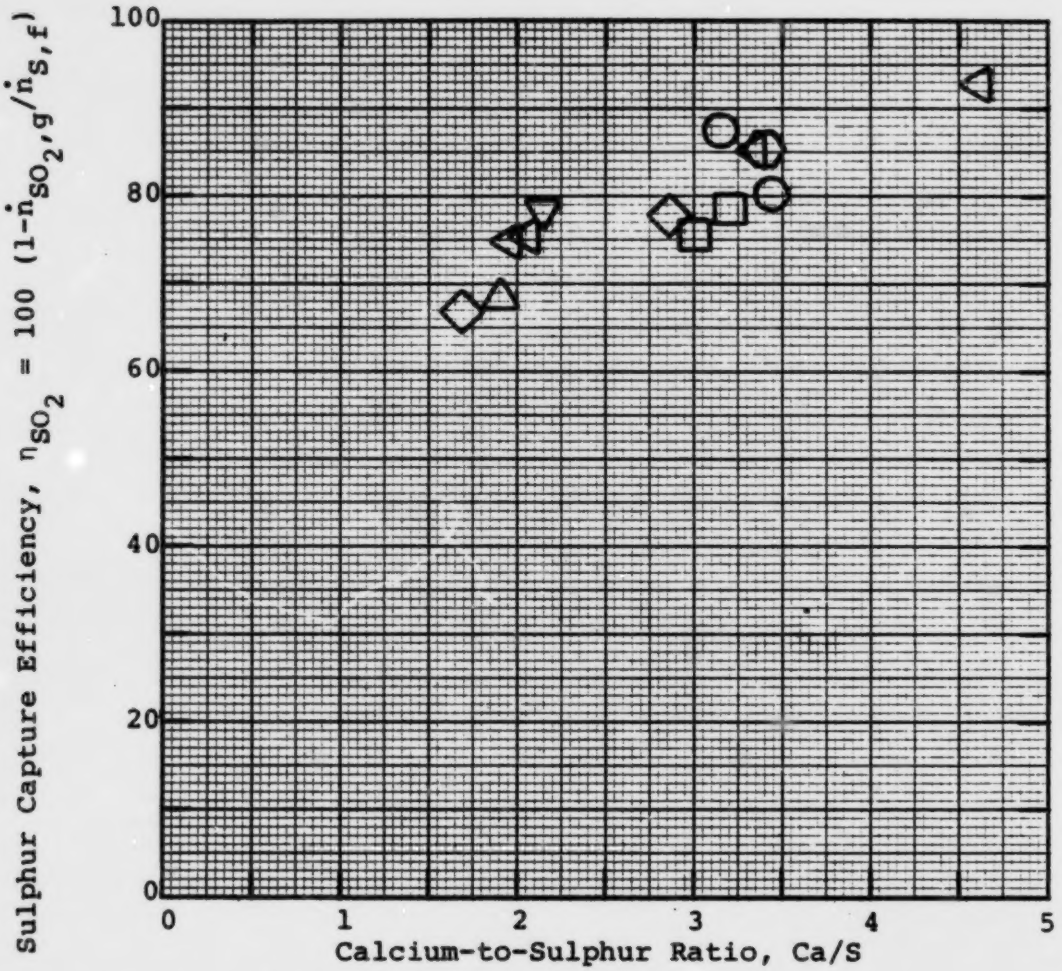

Fig. 7.21. Sulphur capture efficiencies based on product gas analyses.

Key to symbols:	v, m/s	Coal	$\hat{D}_p$, mm	Sorbent
○	2.5	Devco	2.1	Sysco
□	2.5	Devco	2.1	Calpo
⬡	1.5	Devco	2.1	Calpo
△	1.5	Devco	11.2	Calpo
◇	1.4-1.5	Devco	11.2	Sysco
▽	2.4	Devco	11.2	Sysco
◁	2.6-2.9	KY No. 9	2.3	Reed

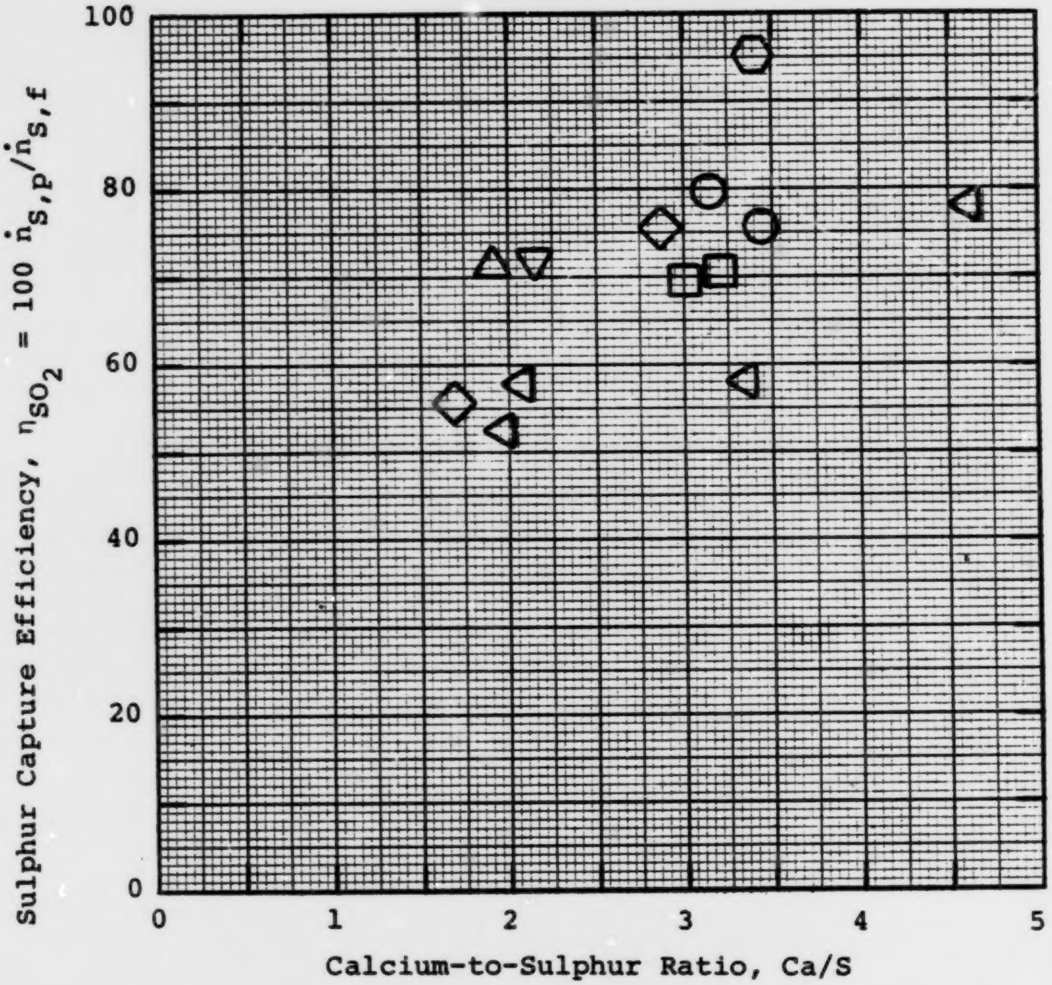

Fig. 7.22. Sulphur capture efficiencies based on the analyses of product solids.

Key to symbols:

	v, m/s	Coal	$\hat{D}_p$, mm	Sorbent
○	2.5	Devco	2.1	Sysco
□	2.5	Devco	2.1	Calpo
⬡	1.5	Devco	2.1	Calpo
△	1.5	Devco	11.2	Calpo
◇	1.4-1.5	Devco	11.2	Sysco
▽	2.4	Devco	11.2	Sysco
◁	2.6-2.9	KY No. 9	2.3	Reed

sorbent, i.e., any Mg in the limestone is included in the 'Ca' in the Ca/S ratio. Although there is still room for improvement, the agreement between the two estimates of η_{SO_2} is better than the results obtained in the work on Evans coal. This topic is examined in the sulphur balance check which follows. The particle size distributions of the three different limestones which were used as SO_2 sorbents had essentially the same $\hat{D}_p$, 1.1--1.4 mm. There is no significant difference in the sulphur capture efficiencies for the three sorbents. At a fixed Ca/S ratio, recycle of cyclone solids improves the sulphur capture efficiency.

The sulphur capture efficiencies based on the analyses of the stack gas are represented in Fig. 7.23 as the percent of the sulphur in the fuel escaping as sulphur oxide emissions vs. the calcium-to-sulphur ratio. Linear regression on the data resulted in the following correlation:

$$100-\eta_{SO_2} = 66.5\ e^{-0.434\ Ca/S} \qquad (7.3.2)$$

The results from the work on both coals were included in the regression analysis.

7.3.4 Sulphur balance check

Sulphur capture efficiencies based on the analyses of the product solids are compared in Fig. 7.24 with the sulphur capture efficiencies based on the analyses of the stack gas. With the exception of two runs, the sulphur capture efficiencies

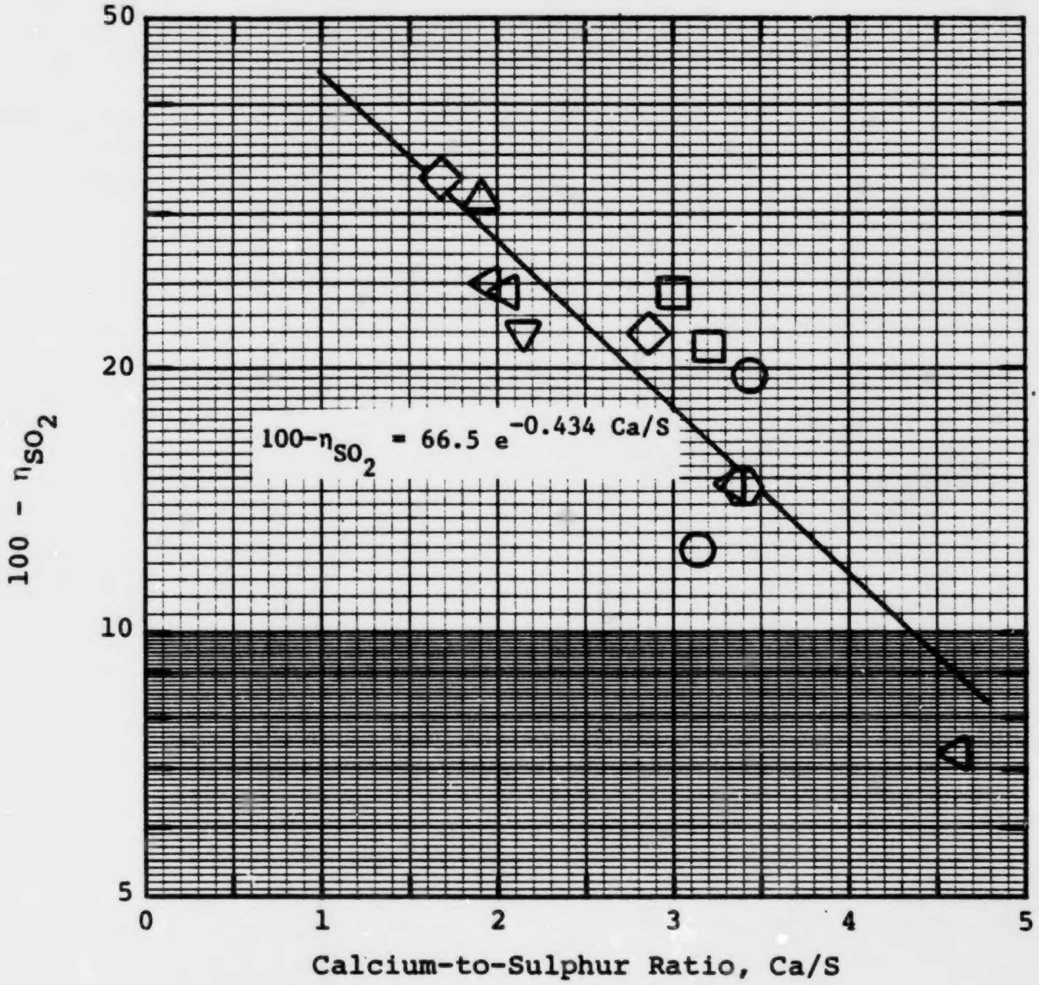

Fig. 7.23. Percent of sulphur in fuel escaping as sulphur oxide emissions.

Key to symbols:

	v, m/s	Coal	$\hat{D}_p$, mm	Sorbent
○	2.5	Devco	2.1	Sysco
□	2.5	Devco	2.1	Calpo
⬡	1.5	Devco	2.1	Calpo
△	1.5	Devco	11.2	Calpo
◇	1.4-1.5	Devco	11.2	Sysco
▽	2.4	Devco	11.2	Sysco
◁	2.6-2.9	KY No. 9	2.3	Reed

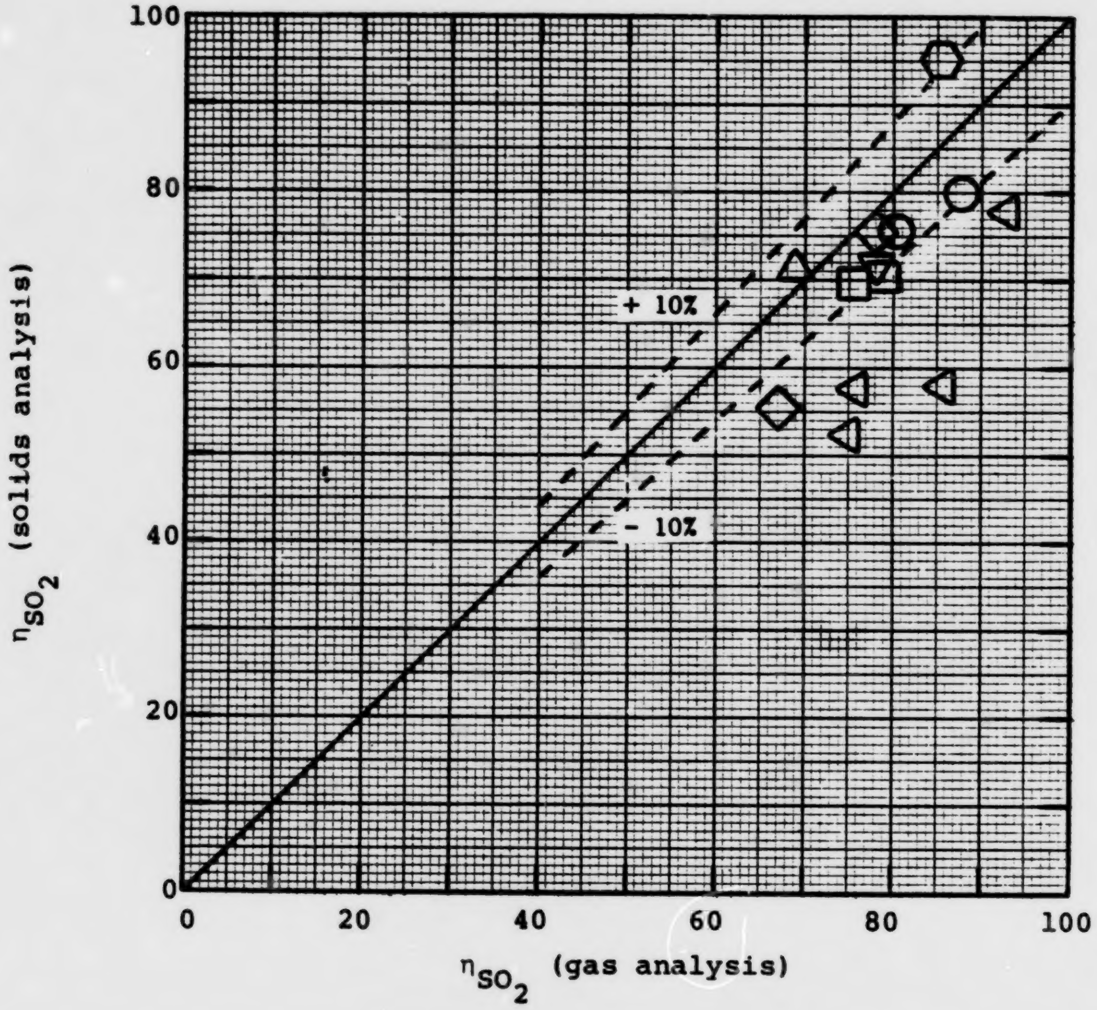

Fig. 7.24. Comparison of sulphur capture efficiencies based on solids analysis with sulphur capture efficiencies based on gas analysis.

Key to symbols:	v, m/s	Coal	$\hat{D}_p$, mm	sorbent
○	2.5	Devco	2.1	Sysco
□	2.5	Devco	2.1	Calpo
⬡	1.5	Devco	2.1	Calpo
△	1.5	Devco	11.2	Calpo
◇	1.4-1.5	Devco	11.2	Sysco
▽	2.4	Devco	11.2	Sysco
◁	2.6-2.9	KY No. 9	2.3	Reed

based on the analyses of the product solids are lower than the estimates based on the analyses of the stack gas but there is a marked improvement. particularly for the Devco runs, in the agreement between the two estimates compared to the results for Evans coal (Fig. 7.24 vs. Fig. 5.22).

The adequacy of the sulphur balance may be examined in terms of the mole ratio of sulphur in the product streams to the sulphur in the fuel. Under steady-state conditions this mole ratio should equal unity, i.e.,

$$\phi_{S,pf} = (\dot{n}_{SO_2,g} + \dot{n}_{S,p})/\dot{n}_{S,f} = 1 \qquad (7.3.3)$$

Estimates of the flux ratio $\phi_{S,pf}$ vs. the bed temperature, T_b, and vs. the excess air level, ε_a, are presented in Fig. 7.25 and Fig. 7.26, respectively. Two estimates of $\phi_{S,pf}$ were evaluated for each run. One estimate was based on the SO_2 composition of the product gas at port 150 (downstream of the cyclone separator) and the other estimate was based on the SO_2 composition of the product gas at port 160 (downstream of the baghouse). The estimates of the flux ratio based on the gas analysis at port 150 are consistently higher than the estimates based on the gas analysis at port 160 which indicates some air dilution of the product gas stream between the cyclone separator and the exhaust stack. The gas analyses at port 150 were used in all material balance calculations. The much poorer closures of the sulphur balances for the KY No. 9 runs are evident from the plots in

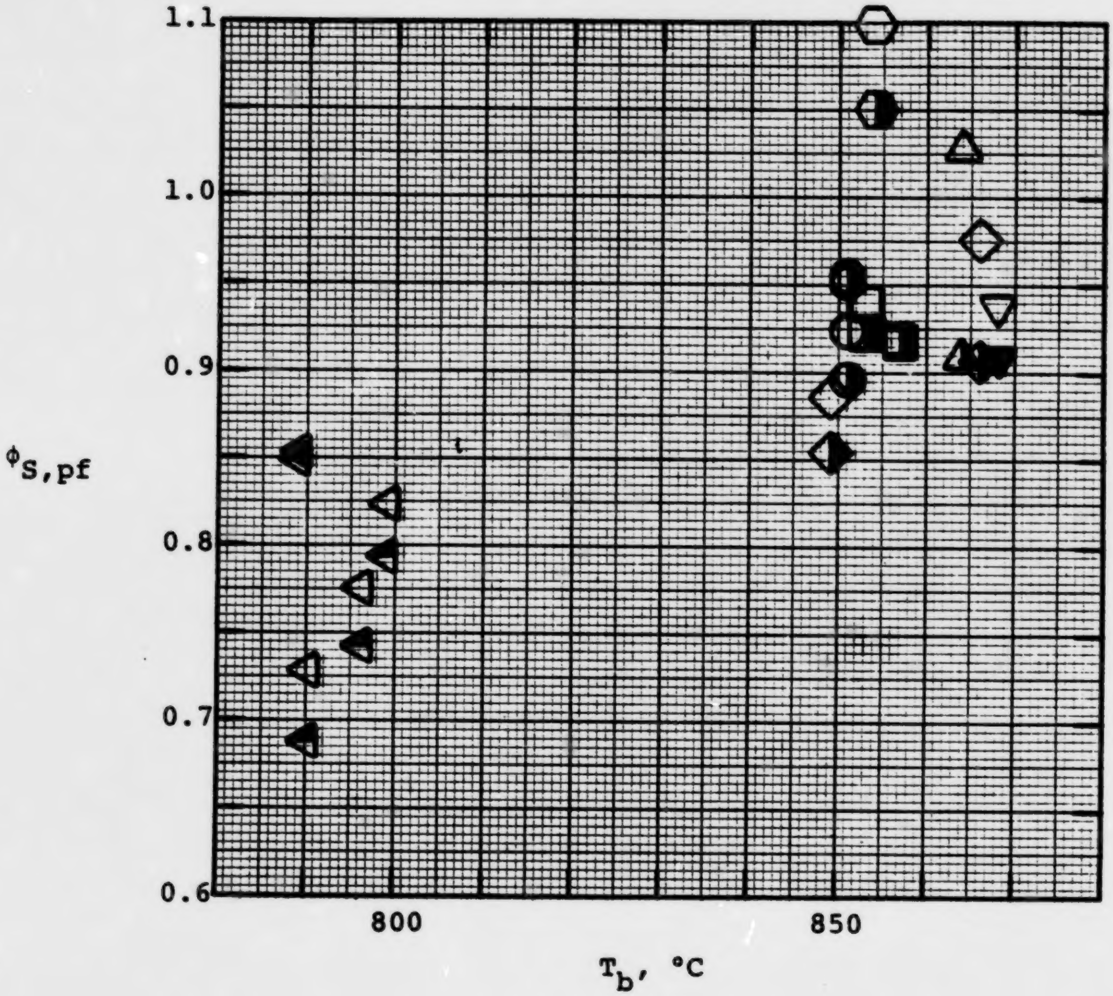

Fig. 7.25. Flux ratio of sulphur in the product streams to sulphur in the fuel, $\phi_{S,pf}$, vs. bed temperature, T_b. Unfilled symbols designate values based on gas analyses at port 150; half-filled symbols designate values based on gas analyses at port 160.

Key to symbols:	v, m/s	Coal	$\hat{D}_p$, mm	Sorbent
○ ◐	2.5	Devco	2.1	Sysco
□ ◧	2.5	Devco	2.1	Calpo
⬡ ⬢	1.5	Devco	2.1	Calpo
△ ◭	1.5	Devco	11.2	Calpo
◇ ⬖	1.4-1.5	Devco	11.2	Sysco
▽ ▼	2.4	Devco	11.2	Sysco
◁ ◀	2.6-2.9	KY No. 9	2.3	Reed

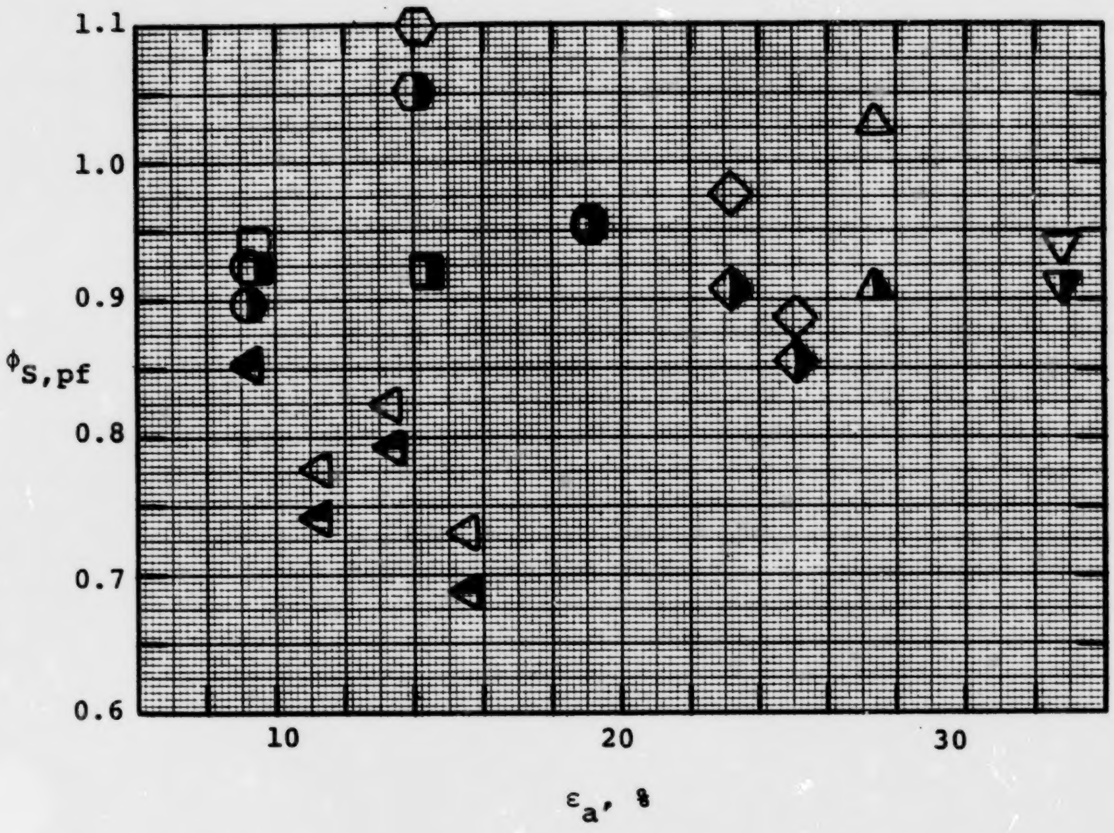

Fig. 7.26. Flux ratio of sulphur in the product streams to sulphur in the fuel, $\phi_{S,pf}$, vs. excess air level, ε_a. Unfilled symbols designate values based on gas analyses at port 150; half-filled symbols designate values based on gas analyses at port 160.

Key to symbols:		v, m/s	Coal	$\hat{D}_p$, mm	Sorbent
○	◑	2.5	Devco	2.1	Sysco
□	◨	2.5	Devco	2.1	Calpo
⬡	⬢	1.5	Devco	2.1	Calpo
△	◮	1.5	Devco	11.2	Calpo
◇	⬗	1.4-1.5	Devco	11.2	Sysco
▽	⧩	2.4	Devco	11.2	Sysco
◁	◀	2.6-2.9	KY No. 9	2.3	Reed

Fig. 7.25 and Fig. 7.26.

7.4 The fuel nitrogen balance

7.4.1 Emission levels of nitrogen oxides

The NO_x levels in the stack gas on a dry basis are shown in Fig. 7.27. Emission levels based on the analyses of gas samples from both port 150 and port 160 are included in Fig. 7.27. Ignoring the one abnormally high level (run 850129; 575 ppm NO_x), the emission levels for both fuels fall in the range 275--400 ppm NO_x with the bulk of the emissions in the range 300--360 ppm NO_x. These levels fall above the range observed with Evans coal (213--275 ppm NO_x). For comparison, the range in our earlier work on Minto and Devco coals (Becker and Code, 1983) was 200--400 ppm NO_x.

7.4.2 The N/C ratio in the product solids

The nitrogen content of the three streams of solids from the cyclone, baghouse and bed overflow is shown in Fig. 7.28 to Fig. 7.30. Lines of constant N/C ratio, including the average of the N/C ratios of the fuels, have been superimposed on the plots. The analysis of the KY No. 9 fuel gave a N/C ratio of 0.0172. For the Devco fuels the N/C ratios were: 0.0144 for the size fraction with a $\hat{D}_p$ of 11.2 mm and 0.0159 for the size fraction with a $\hat{D}_p$ of 2.1 mm.

For the runs on Devco coal with the larger mean particle diameter, there is no significant difference between the residual

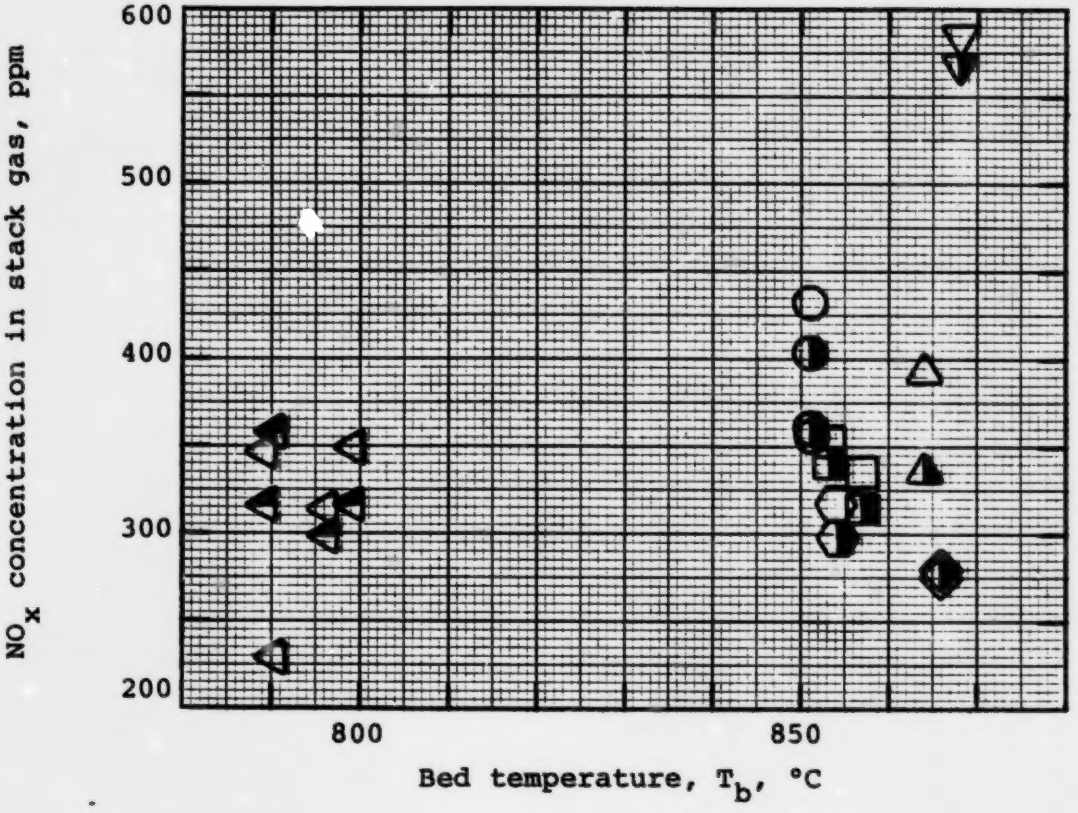

Fig. 7.27. NO_x levels in the stack gas. Unfilled symbols designate NO_x concentrations at port 150; half-filled symbols designate NO_x concentrations at port 160.

Key to symbols:	v, m/s	Coal	$\hat{D}_p$, mm	Sorbent
○ ◑	2.5	Devco	2.1	Sysco
□ ◧	2.5	Devco	2.1	Calpo
⬡ ⬢	1.5	Devco	2.1	Calpo
△ ▲	1.5	Devco	11.2	Calpo
◇ ◆	1.4-1.5	Devco	11.2	Sysco
▽ ▼	2.4	Devco	11.2	Sysco
◁ ◀	2.6-2.9	KY No. 9	2.3	Reed

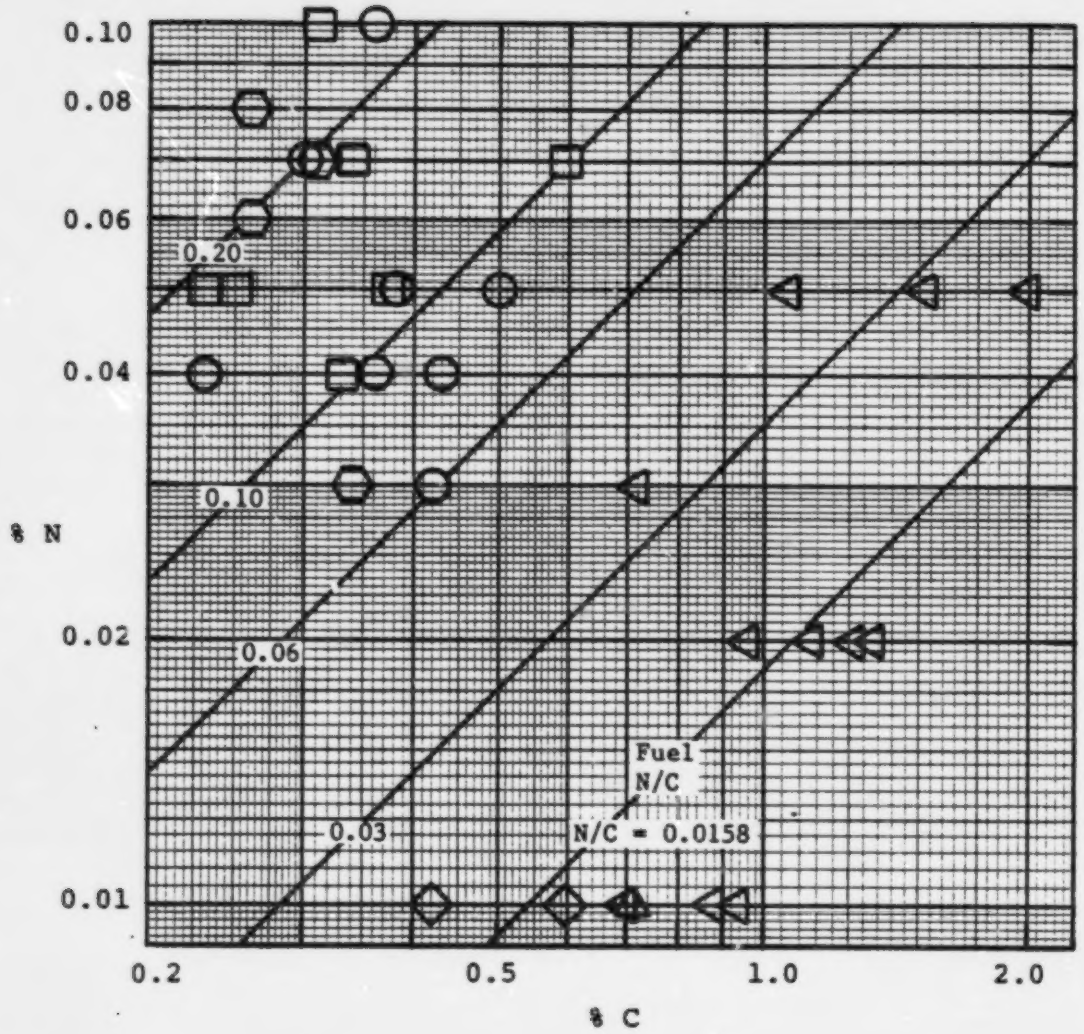

Fig. 7.30. Nitrogen content of the bed overflow solids.

Key to symbols:	v, m/s	Coal	$\hat{D}_p$, mm	Sorbent
○	2.5	Devco	2.1	Sysco
□	2.5	Devco	2.1	Calpo
⬡	1.5	Devco	2.1	Calpo
△	1.5	Devco	11.2	Calpo
◇	1.4-1.5	Devco	11.2	Sysco
◁	2.6-2.9	KY No. 9	2.3	Reed

N/C ratios of the cyclone solids and the N/C ratio of the fuel. However, there is an increase in the residual N/C ratio for the smaller size fraction of Devco coal. This observation is in agreement with the results on Evans coal. All four runs with KY No. 9 coal gave a lower N/C ratio in the cyclone solids than the N/C ratio of the fuel (0.017). In the work on Evans coal it was observed that recycle of cyclone solids reduced both the carbon content and the nitrogen content of the cyclone solids but did not change the residual N/C ratio significantly. Only two runs were carried out on Devco coal at a recycle fraction other than zero and the results are inconclusive. For run 841204 (group of circles on the left; r = 0.69) the increase in the N/C ratio is due to a reduction in the carbon content. There is no significant change in the nitrogen content of the solids. The results for the other run (841219; squares; r = 0.78) is in agreement with the results on Evans coal.

The residual N/C ratios for the baghouse solids are higher than the fuel N/C ratio with nine of the thirteen results falling in the range 0.02--0.03. This range covers the results for all five runs with the smaller diameter Devco coal and three of the four results with KY No. 9 coal. Three of the four results with the larger diameter Devco coal fall below this range with two results essentially on the fuel N/C line (N/C = 0.014). The apparent positive effect of recycle fraction is small.

The analyses for the bed overflow solids scatter widely and do not exhibit the linearity shown on the log-log plot by the results for the cyclone and baghouse solids. This problem is due to the low carbon content of the bed solids which is of the order of one-tenth of the carbon content of the cyclone solids. The N/C ratios for the smaller size fraction of Devco coal are much higher than the N/C ratios for the larger size fraction of Devco coal and the KY No. 9 coal which are in the region of the N/C ratio of the fuel.

7.4.3 Effect of operating conditions on the conversion of fuel N to NO_x

The effect of operating conditions on the molar flux ratio $\dot{n}_{NO_x}/\dot{n}_{N,f}$ or the fractional conversion of fuel N to NO_x is examined in Fig. 7.31 and Fig. 7.32. The conversion of fuel N to NO_x in the stack gas is in the range 9--13 % for the runs with KY No. 9 coal. With the exception of one abnormally high value (run 850129; 31 %) the conversions for the runs with Devco coal fall in the range 13--20 %. The remaining fuel N is converted to N_2. There is no significant effect of bed temperature on the conversion of fuel N to NO_x. The positive effects of excess air level and solids residence time observed in the work on Evans coal are not as apparent because of the more limited range of operating conditions.

7.5 The hydrogen balance

7.5.1 The H/C ratio in the product solids

The analyses for H and C in the three streams of solids

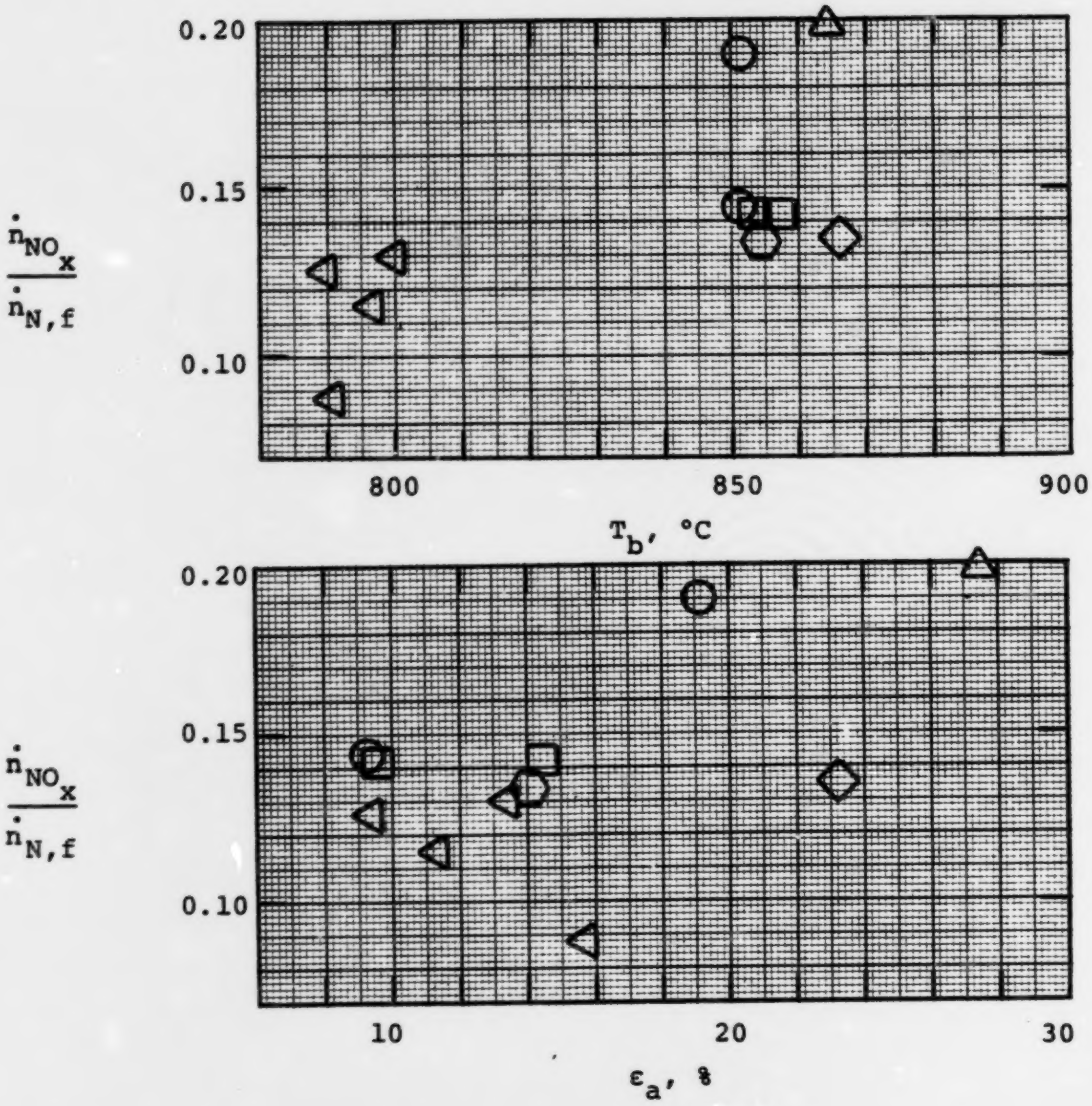

Fig. 7.31. The molar flux ratio $\dot{n}_{NO_x}/\dot{n}_{N,f}$ (fractional conversion of fuel N to NO_x) vs. bed temperature, T_b, and excess air level, ε_a.

Key to symbols:	v, m/s	Coal	$\hat{D}_p$, mm	Sorbent
○	2.5	Devco	2.1	Sysco
□	2.5	Devco	2.1	Calpo
⬡	1.5	Devco	2.1	Calpo
△	1.5	Devco	11.2	Calpo
◇	1.4-1.5	Devco	11.2	Sysco
◁	2.6-2.9	KY No. 9	2.3	Reed

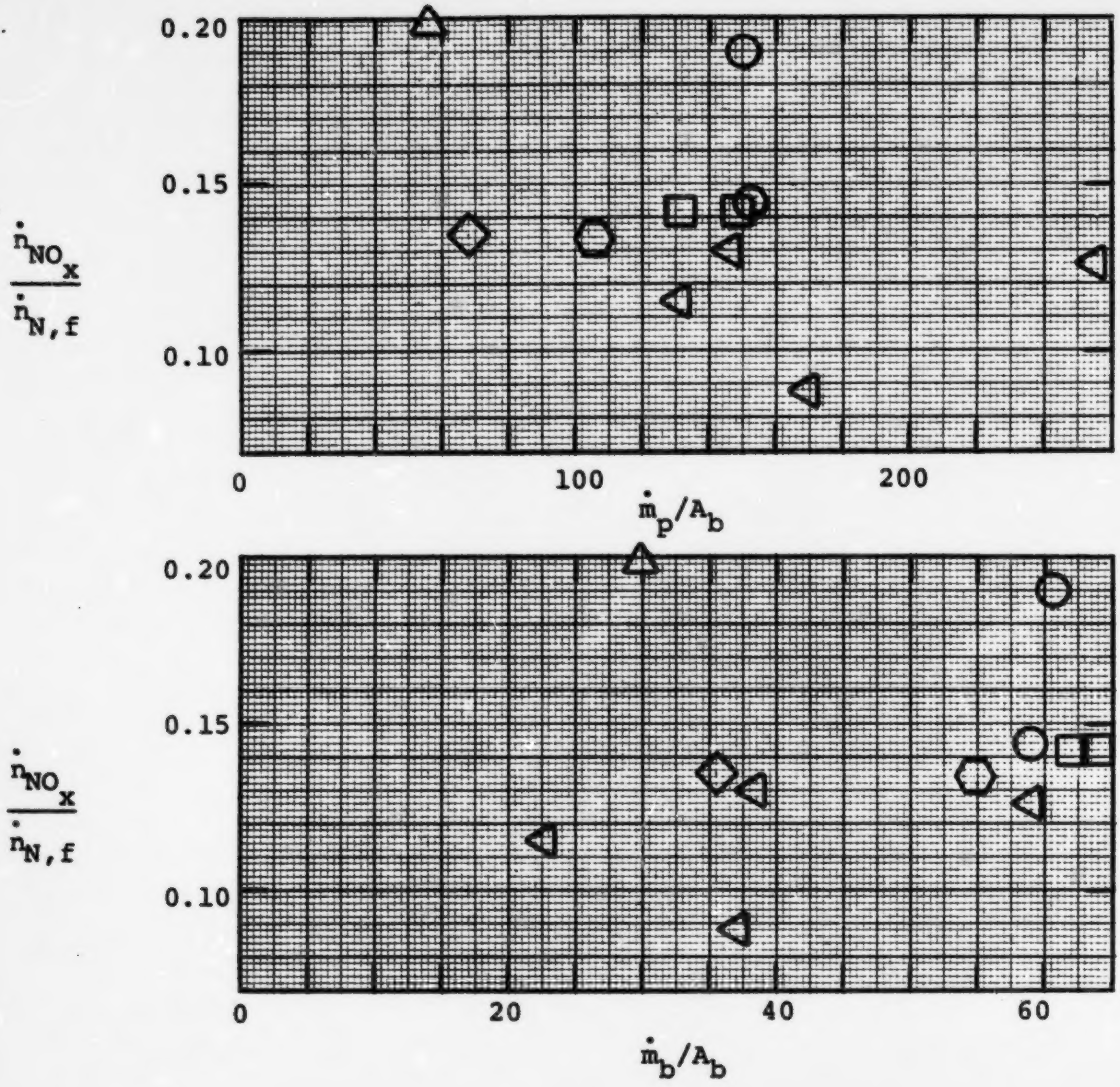

Fig. 7.32. The molar flux ratio $\dot{n}_{NO_x}/\dot{n}_{N,f}$ vs. the efflux of product solids per unit bed area, $\dot{m}_p/A_b$, and the efflux of bed overflow solids per unit bed area $\dot{m}_b/A_b$.

Key to symbols:	v, m/s	Coal	$\hat{D}_p$, mm	Sorbent
○	2.5	Devco	2.1	Sysco
□	2.5	Devco	2.1	Calpo
⬡	1.5	Devco	2.1	Calpo
△	1.5	Devco	11.2	Calpo
◇	1.4-1.5	Devco	11.2	Sysco
◁	2.6-2.9	KY No. 9	2.3	Reed

from the cyclone, baghouse, and bed overflow are plotted in Fig. 7.33 through Fig. 7.35. Lines of constant H/C ratio have been superimposed on the plots for comparison with the H/C ratios of the fuels. The analyses of the two fractions of Devco coal gave a H/C ratio of 0.77 for the fraction with a $\hat{D}_p$ of 11.2 mm and a H/C ratio for 0.82 for the fraction with a $\hat{D}_p$ of 2.1 mm. The H/C ratio for KY No. 9 coal is 0.85.

The absorption of moisture by the samples of solids prior to analysis was given as an explanation for the unrealistically high H/C ratios in the bed solids from the combustion of Evans coal. Although the range of H/C ratios (0.2--1.0, Fig. 7.35) for the bed solids from the combustion of Devco and KY No. 9 coals is realistic, the potential problem of moisture contamination of the samples places reservations on the results. The analyses of a number of samples indicated undetectable levels of hydrogen and one questions whether the low H concentrations, 0.01--0.06 %, are not primarily due to the absorption of atmospheric moisture. The relative effect of moisture absorption is more critical for the bed solids because of the much lower carbon content, of the order of one-tenth of the carbon content of the cyclone and baghouse solids. The ranges of the H/C ratios for the cyclone solids and the baghouse solids are, respectively, 0.02--0.17 and 0.15--0.4.

7.5.2 Effect of operating conditions on the H/C ratio in the solids

The effects of bed temperature and excess air level on the residual H/C ratio in the solids from the cyclone and baghouse are

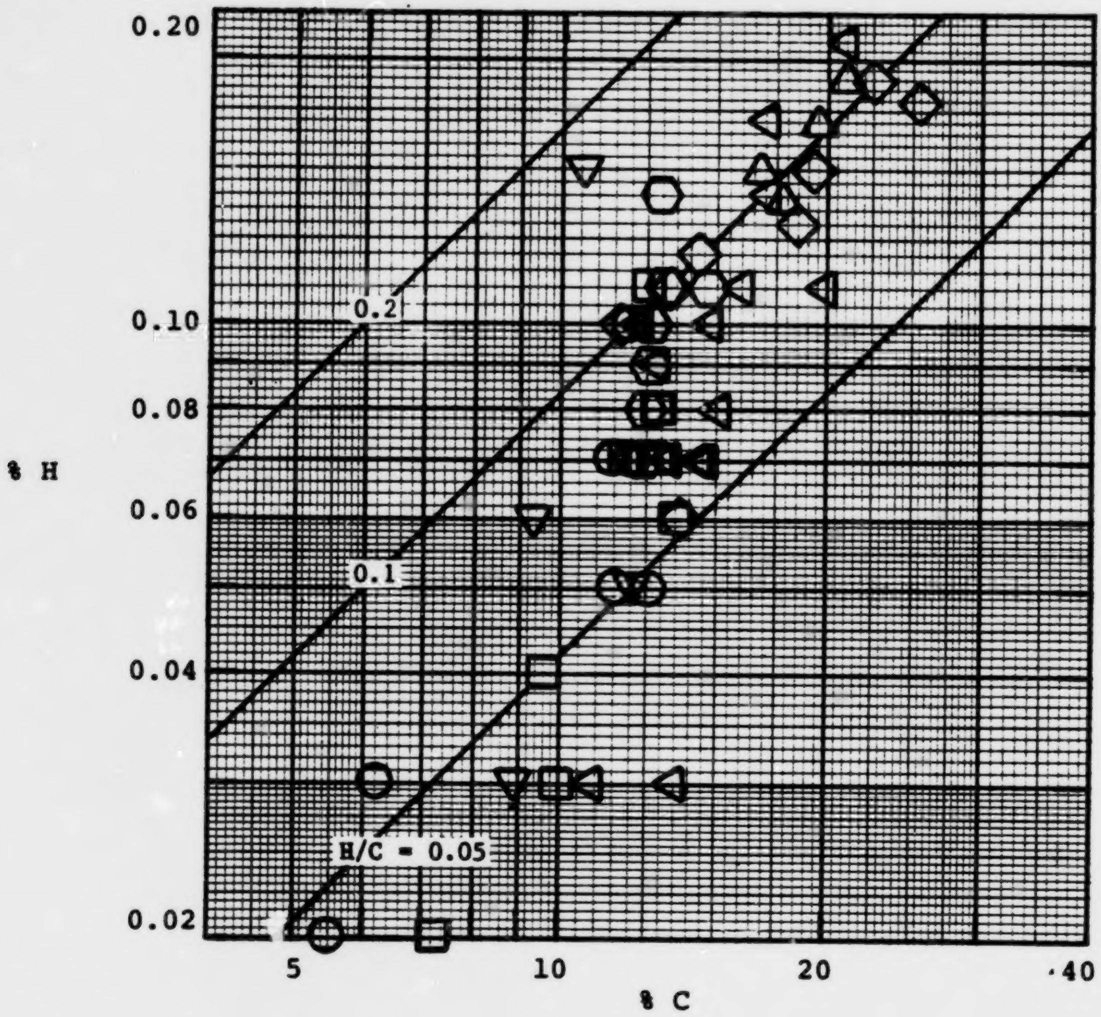

Fig. 7.33. Hydrogen content of the cyclone solids.

Key to symbols:	v, m/s	Coal	$\hat{D}_p$, mm	Sorbent
○	2.5	Devco	2.1	Sysco
□	2.5	Devco	2.1	Calpo
⬡	1.5	Devco	2.1	Calpo
△	1.5	Devco	11.2	Calpo
◇	1.4-1.5	Devco	11.2	Sysco
▽	2.4	Devco	11.2	Sysco
◁	2.6-2.9	KY No. 9	2.3	Reed

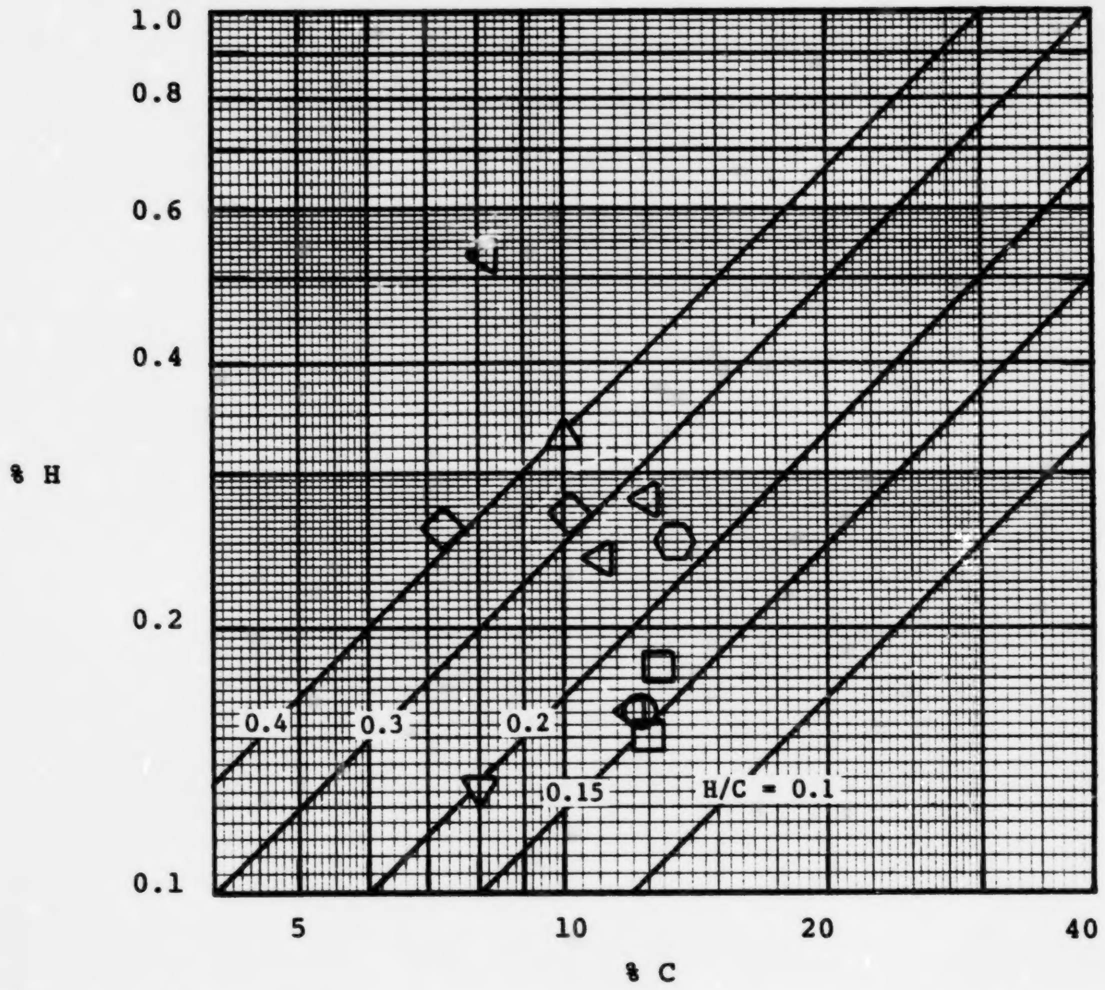

Fig. 7.34. Hydrogen content of the baghouse solids.

Key to symbols:	v, m/s	Coal	$\hat{D}_p$, mm	Sorbent
○	2.5	Devco	2.1	Sysco
□	2.5	Devco	2.1	Calpo
⬡	1.5	Devco	2.1	Calpo
△	1.5	Devco	11.2	Calpo
◇	1.4-1.5	Devco	11.2	Sysco
▽	2.4	Devco	11.2	Sysco
◁	2.6-2.9	KY No. 9	2.3	Reed

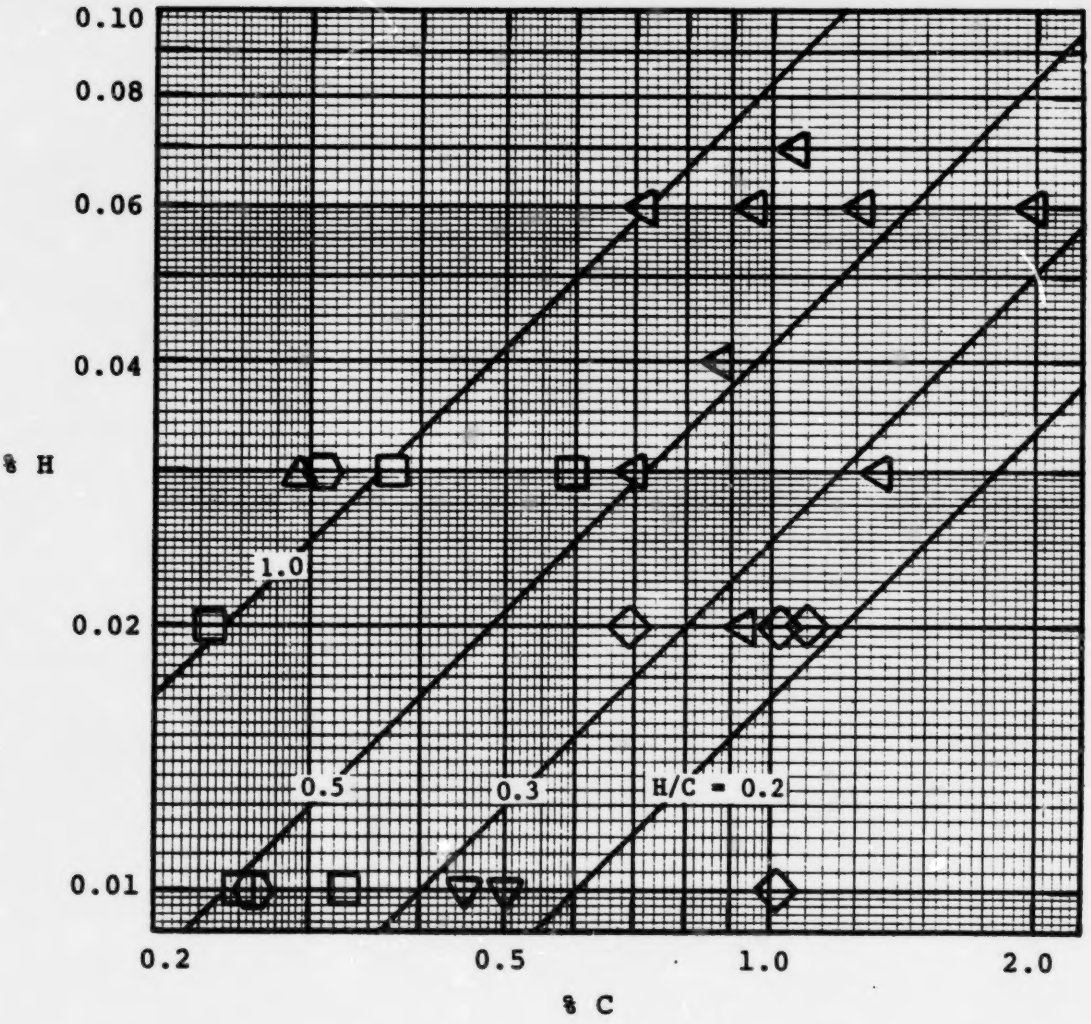

Fig. 7.35. Hydrogen content of bed overflow solids.

Key to symbols:

	v, m/s	Coal	$\hat{D}_p$, mm	Sorbent
□	2.5	Devco	2.1	Calpo
⬡	1.5	Devco	2.1	Calpo
△	1.5	Devco	11.2	Calpo
◇	1.4-1.5	Devco	11.2	Sysco
▽	2.4	Devco	11.2	Sysco
◁	2.6-2.9	KY No. 9	2.3	Reed

examined in Fig. 7.36 and Fig. 7.37. Within the narrow temperature ranges investigated, 789--799 °C for the runs with KY No. 9 coal and 849--868 °C for the runs with Devco coal, bed temperature has no effect on the residual H/C ratio. A similar result was obtained in the work on Evans coal where a broader temperature range was examined, 831--908 °C. An increase in the H/C ratio in the cyclone solids with an increase in the bed temperature was observed in our earlier work on Minto and Devco coals (Becker and Code, 1983). Although a narrower range of excess air levels was examined, there is no evidence to support the decrease in the H/C ratio with an increase in excess air level observed in the work on Evans coal. The recycle of cyclone solids decreased the residual H/C ratio in the baghouse solids. In the runs with KY No. 9 coal, the H/C ratio decreased from 0.26--0.27 at $r = 0$ to 0.16 at $r = 0.64$. A similar result was obtained with Devco coal where the H/C ratio decreased from 0.16 (run 841127; $r = 0$) to 0.076 (run 841204; $r = 0.69$) and from 0.17 (run 841218; $r = 0$) to 0.15 (run 841219; $r = 0.78$).

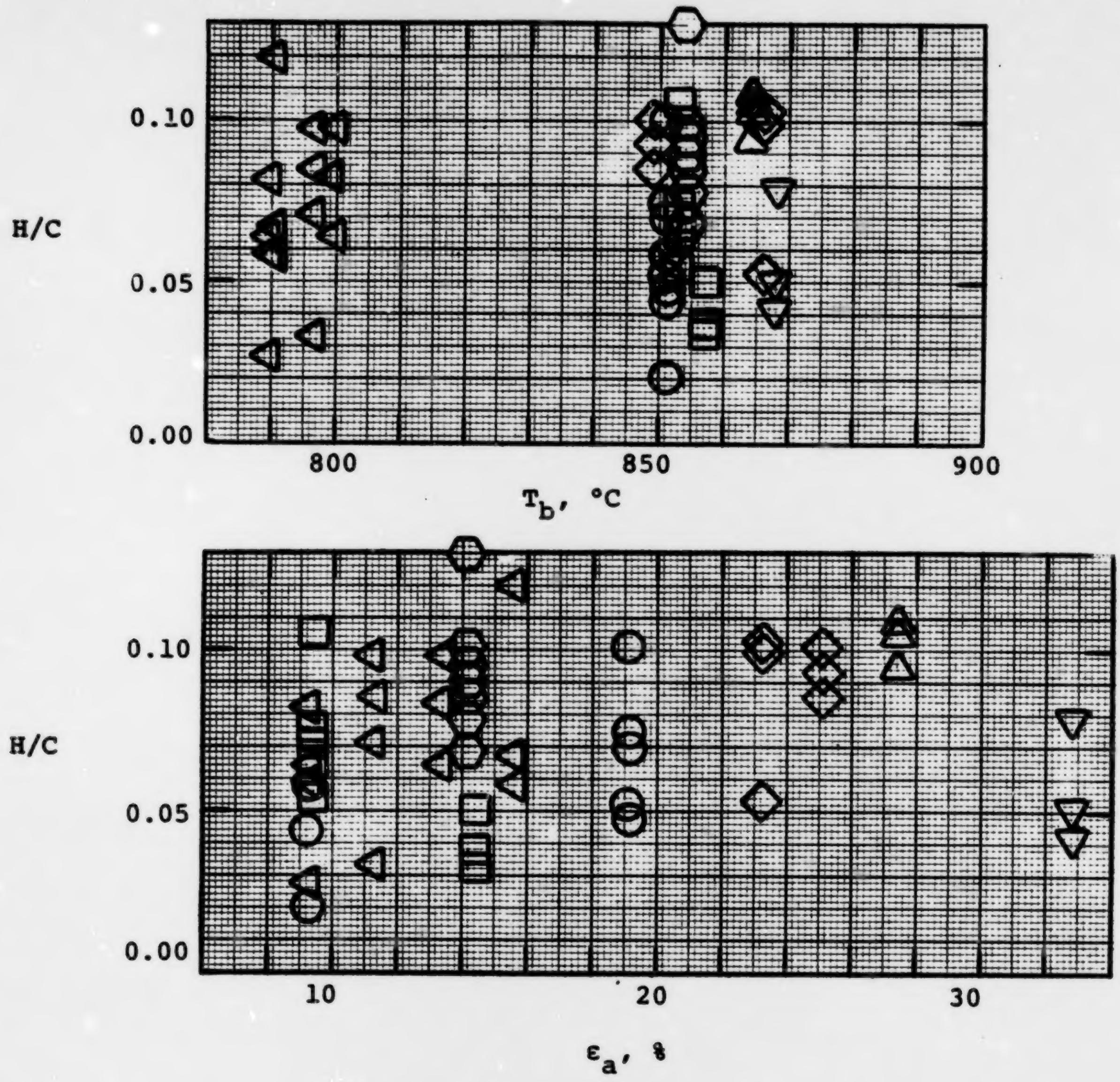

Fig. 7.36. H/C ratios in the cyclone solids vs. bed temperature, T_b, and excess air level, ε_a.

Key to symbols:		v, m/s	Coal	$\hat{D}_p$, mm	Sorbent
	○	2.5	Devco	2.1	Sysco
	□	2.5	Devco	2.1	Calpo
	⬡	1.5	Devco	2.1	Calpo
	△	1.5	Devco	11.2	Calpo
	◇	1.4-1.5	Devco	11.2	Sysco
	▽	2.4	Devco	11.2	Sysco
	◁	2.6-2.9	KY No. 9	2.3	Reed

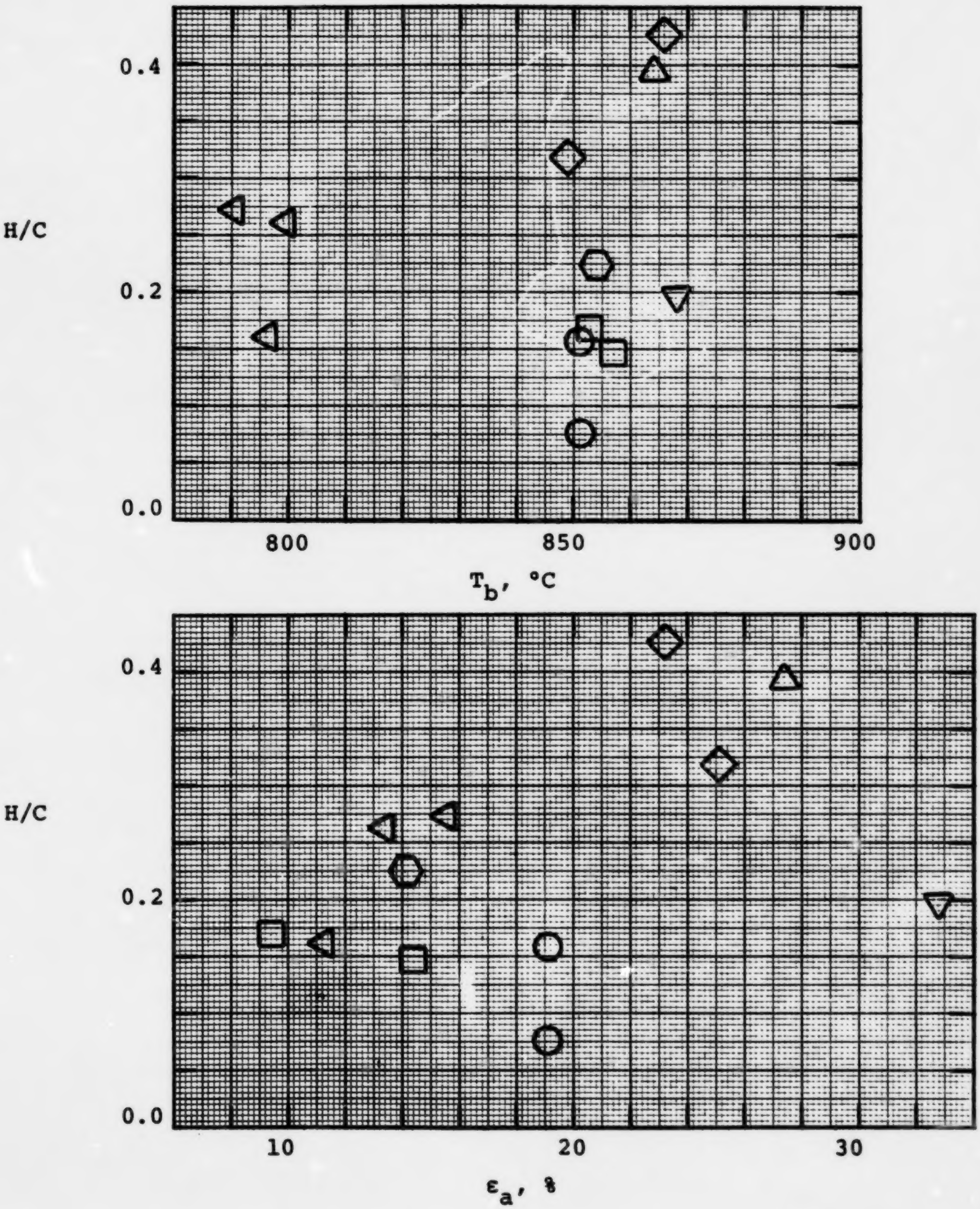

Fig. 7.37. H/C ratios in the baghouse solids vs. bed temperature, T_b, and excess air level, ε_a. A key to the symbols accompanies Fig. 7.36.

8. DISCUSSION OF RESULTS ON CARBON LOSS AND SULPHUR CAPTURE

8.1 Introduction

The preceding chapters have presented the results of each set of the trials comprising the present work. In this chapter comparisons are made between these results and literature data in the matter of the two most important output characteristics: the carbon loss (the measure of combustion inefficiency) and the sulphur capture (the measure of the effectiveness of limestone in combatting the major form of pollution). The comparisons with the literature are confined to results on the same fuels and limestones. A comparison with other fuels and sulphur sorbents (generally non-Canadian) raises questions that are best addressed within a context of mathematical modelling and will be attempted in later publications.

8.2 Overhead carbon loss

We have here presented correlations of overhead carbon loss (cyclone and baghouse combined) for three groups of trials:

[] the seventeen Evans trials, with Havelock limestone, Sect. 5.2
[] the nine Syncrude trials, Sect. 6.2.4
[] the nine Devco and four Kentucky No. 9 trials, Sect. 7.2.5

However, not all of these sets were well designed for determining such correlations. In particular, the Devco trials were in fact intended to allow good comparison of three limestones (Havelock, Sysco and Calpo) under favourable conditions of limestone particle size and bed temperature for sulphur capture. Bed temperature, for instance, was virtually constant in the Devco runs. The Kentucky No. 9 runs were designed to reproduce operating conditions at the 20 MW TVA demonstration plant and had nearly everything fixed except the Ca/S ratio. The correlation, equation (7.2.2), of the Devco and Kentucky No. 9 results is thus not expected to be very significant; the one interesting and evidently meaningful feature of it is that, despite the poor (for this purpose) experimental design, the exponents and coefficients, with the exception of that on fluidizing velocity, are of the same sign and similar magnitude to those found in the present Evans trials and the earlier (Becker and Code 1983) Minto/Devco trials.

The Syncrude trials also had limitations affecting the validity and generality of the carbon loss correlation. The fuel, the Syncrude coke, was of small and fixed mean particle size. Because of the fineness of the fuel, the variation of fluidizing velocity was severely restricted. Also, the temperature range was generally higher and outside that of the coal trials, a fact that must be remembered in any comparisons with the coal trials.

It is therefore most reasonable to focus on the correlations based on the present Evans trials and the earlier

Minto trials, to compare these with each other and to compare with them the results on the present Syncrude, Devco and Kentucky No. 9 trials.

Our hypothesized carbon loss correlation is of the general form

$$y = a_0 + a_1x_1 + a_2x_2 + a_3x_3 + a_4x_4 + a_5x_5 + a_6x_6 , \qquad (8.1.1)$$

$y = \ln(\dot{m}_{C,o}/\dot{m}_{C,f})$

$x_1 = \ln v$

$x_2 = \ln \hat{D}_{p,s}$

$x_3 = \ln \phi_a$

$x_4 = r$

$x_5 = 1/T_b$

$x_6 = \dot{m}_b$

$x_7 = \ln \hat{D}_{p,f}$

where $\hat{D}_{p,s}$ is the mass-median particle diameter of the limestone and $\hat{D}_{p,f}$ is that of the fuel. The corresponding power-law form for the overhead carbon loss is

$$\dot{m}_{C,o} = C_o \dot{m}_{C,f}\, v^{a_1}\, \hat{D}_{p,s}^{a_2}\, \phi_a^{a_3}\, e^{a_4 r} \cdot$$

$$\cdot\, e^{a_5/T_b}\, \dot{m}_b^{a_6}\, D_{p,f}^{a_7} \qquad (8.1.2)$$

where $C_o = \ln a_0$. We earlier determined (Becker and Code 1983) that a_7 was effectively zero for the Minto and Devco trials of our preceding contract, the standard error in a_7 being very much larger than the absolute value. The present work has shown this to be true for the Evans coal as well. This means that for Minto, Devco and Evans coals, coal particle diameter as fed insignificantly affects the overhead carbon loss.

The variable $\dot{m}_b$, the bed product flux, was introduced into this statistical analysis in a paper presented at the Eighth International Conference on Fluidized Bed Combustion (Anthony, Becker, Code, Liang and Stephenson 1985). It is actually meant to account for possible effects of the mean residence time of bed-product particles in the bed, $\tau_b \simeq m_b/\dot{m}_b$. Since the subject trials only involved one combustor, and that was operated with the bed-height control fixed, we effectively did not vary the bed mass m_b; thus the product flux $\dot{m}_b$, which was accurately determined, gives an adequate representation of τ_b. The statistical analysis shows that for the Minto, Devco and Evans trials, a_6 is effectively zero for overhead carbon loss. This means that the residence time of bed product particles insignificantly affects the overhead carbon loss.

In view of these findings, the multiple linear regression analysis for overhead carbon loss was repeated with $\hat{D}_{p,f}$ and $\dot{m}_b$ omitted. This gave the results reported for the Evans trials in Sect. 5.2 and for the earlier Minto and Devco trials as presented in the final report on those (Becker and Code 1983). Table 8.1 summarizes the values of the coefficients a_n and shows as well their standard errors. Several features are evident:

[] the level of correlation in the Evans trials is significantly lower than in the Minto/Devco. It appears that this difference is partly intrinsic (i.e., characteristic of the coals), but another part is due to less felicitous experimental design in the Evans trials, with narrower variation of some variables and, overall, a less revealing pattern of variation.

[] the differences in the exponents or coefficients of v, $\hat{D}_{p,s}$, ϕ_a and $1/T_b$ mostly are, or verge upon, statistical insignificance. However, it does appear that the effect of recycle on the overhead carbon loss was significantly greater in the Evans trials. Based on the exponents found, a_4 = - 0.36 ± 0.09 for Minto/Devco and - 0.94 ± 0.31 for Evans, the effect of going from zero to total recycle of the cyclone dustfall is to decrease overhead carbon loss by 30 % for Minto/Devco, but by 61 % for Evans.

Table 8.1 Correlation of overhead carbon loss: results of multiple linear regression analysis on the form $y = \Sigma_n a_n x_n$, $y = \ln(\dot{m}_{C,o}/\dot{m}_{C,f})$

n	0	1	2	3	4	5
x_n	1	$\ln v$	$\ln \hat{D}_{p,s}$	$\ln \phi_a$	r	$1/T_b$
Minto and Devco trials (Becker & Code 1983) $s_y = 0.10$, $R^2 = 0.969$						
a_n'	- 8.0	0.88	- 0.74	- 0.46	- 0.36	5200
s_a	1.5	0.28	0.08	0.48	0.09	1500
t	- 5.4	3.2	- 8.8	- 1.0	- 4.1	3.4
Evans trials $s_y = 0.40$, $R^2 = 0.752$						
a_n	- 6.2	0.58	- 0.35	- 0.71	- 0.94	2832
s_a	5.5	0.78	0.26	0.91	0.31	6248
t	- 1.1	0.75	- 1.38	- 0.78	- 3.0	0.45

Statistics:

s_y = standard error of estimate of y

s_a = standard error of estimate of a_n

t = t-statistic for estimate of a_n

R^2 = multiple regression coefficient

Because the correlation for the Minto/Devco results shows the higher levels of statistical significance, by a considerable margin, it seems to provide the best general basis for a comparison of fuels. In such a comparison, we assume that the coefficients a_1, a_2, a_3, a_4 and a_5 are generally the same as for the Minto/Devco results. Differences then observed in $C_o = \ln a_0$ are taken as measures of variation in basic reactivity of char in the overhead products. We used this approach in our preceding final report (Becker and Code 1983, Sect. 18.2.3) to compare our results on Minto/Devco with those of Stover, et al. (1981) on Minto and Highvale coals. In the following discussion, we use it to interpret overhead carbon losses from the fuels used in the present trials. The idea has already been introduced in Sect. 6.6, and Fig. 6.2 shows C_o so calculated from the present results on the Evans trials with Havelock limestone, Devco trials with Sysco and Calpo limestone, Kentucky No. 9 or "TVA" trials with Reed limestone, and the Syncrude trials with Fort McMurray limestone.

It is seen in Fig. 6.6 that the "relative reactivity factors" C_o, as above defined, for the present Devco, Kentucky No. 9 ("TVA") and Syncrude coke trials, agree as closely as could possibly be expected with the standard value of 0.000335 $(m/s)^{-0.86}$ $mm^{0.74}$. The Evans coal results, however, fall significantly low. Examination of the data shows what we have already alluded to above: the effect of recycle is greater for the Evans coal than for Minto and Devco, and the lowest values of C_o (signifying the lowest carbon loss) are for the highest recycle. The Evans results for small recycle fractions r indicate roughly $C_o \simeq 0.00015$, an overhead carbon loss only half as great as for Minto and Devco.

Apart from the behaviour of the Evans coal, the most notable feature about the results is that, if our interpretation is at all valid, the overhead carbon loss of Syncrude coke is remarkably similar to that of the main group of coals. This is quite unexpected; we rather thought beforehand that it would be very much higher than the roughly 50 % more indicated by Fig. 6.6.

On the basis of the above discussion, then, the overhead carbon losses indicate that Minto, Devco, and Kentucky No. 9 coals and Syncrude coke are similar in reactivity as indicated by the coefficient C_o, whereas Evans coal is significantly more reactive. This interpretation is upheld by the effect of recycle which improves the burning of Evans considerably more than the others.

8.3 Bed product carbon loss

As noted elsewhere in this report and in our preceding final report (Becker and Code 1983), the overhead product streams are usually the principal vehicles for carbon loss. However, the loss in the bed product, though usually much smaller, is still of significant interest. We have applied the form (8.1.1) to the bed product carbon loss as well (Anthony, et al. 1985) for the earlier Minto/Devco trials, with very interesting results. The correlation obtained is

$$\dot{m}_{C,b} = 9.5 \times 10^{-6}\, \dot{m}_{C,f}\, v^{-0.93}\, \hat{D}_{p,s}^{0.80} \cdot$$

$$\cdot\, \phi_a^{-2}\, e^{-0.3r}\, e^{7000/T_b}\, \dot{m}_b^{0.5}\ , \qquad (8.1.3)$$

with v in m/s and $\hat{D}_{p,s}$ in mm. A comparison between the exponents/coefficients of this equation and those of the overhead carbon loss, Table 8.2, is most revealing; we note that:

[] as should be expected, the effects of v and $\hat{D}_{p,s}$ are almost exactly inverted. Increasing v increases the overhead carbon loss but decreases the bed carbon loss. Increasing $\hat{D}_{p,s}$ decreases the overhead carbon loss but increases that from the bed. The effects of these parameters are clearly associated with elutriation.

[] the effect of excess air is in the same direction but possibly much stronger for the bed carbon loss (the large statistical uncertainty leaves the issue unsettled). It would appear that excess air might strongly affect the availability of oxygen in the emulsion phase of the bed, and this would account for a stronger influence.

Table 8.2 Correlations of carbon loss for the Minto and Devco trials (Becker and Code 1983): results of multiple linear regression analysis on the form $y = \Sigma_n a_n x_n$, $y = \ln(\dot{m}_{C,o}/\dot{m}_{C,f})$

n	0	1	2	3	4	5	6
x_n	1	$\ln v$	$\ln \hat{D}_{p,s}$	$\ln \phi_a$	r	$1/T_b$	$\ln \dot{m}_b$
Overhead carbon loss* $s_y = 0.10$, $R^2 = 0.969$							
a_n	- 8.0	0.88	- 0.74	- 0.46	- 0.36	5200	0
s_a	1.5	0.28	0.08	0.48	0.09	1500	--
t	- 5.4	3.2	- 8.8	- 1.0	- 4.1	3.4	--
Bed carbon loss $s_y = 0.25$, $R^2 = 0.81$							
a_n	- 11.56	0.93	- 0.80	- 2.0	- 0.3	7000	0.5
s_a	3.9	1.0	0.27	2.1	0.2	4300	0.5
t	2.6	- 1.6	3.1	0.5	- 1.3	1.4	0.9

* Inclusion of $x_6 = \ln \dot{m}_b$ gives $a_6 = 0.0$; parameters shown are for fit with a_6 taken as zero and x_6 omitted.

Statistics:

s_y = standard error of estimate of y
s_a = standard error of estimate of a_n
t = t-statistic for estimate of a_n
R^2 = multiple regression coefficient

[] the differences in the effects of recycle and bed temperature appear to be statistically insignificant.

[] the bed product carbon loss appears to be affected by the residence time of bed particles, as represented by $\dot{m}_b$. The greater the bed product flux, the shorter the residence time and the greater the carbon loss. The indicated functionality is actually a square-root dependancy, $\dot{m}_{C,b} \propto \tau_b^{-0.5}$.

We have again employed the result on the earlier Minto/Devco trials, here (8.1.3), as a reference correlation, defining reactivity through the coefficient C_o in (8.1.3), $C_o = 9.5 \times 10^{-6}$ $(m/s)^{-0.93}$ $mm^{0.80}$. Values of C_o calculated from the data of the present trials are shown in Fig. 8.1. Somewhat different trends are seen than in the overhead carbon loss:

[] the Kentucky No. 9 and Devco coals show about 50 % the carbon loss found in the earlier Minto/Devco trials. [It should be remembered that the present Devco trials were different from the earlier ones in that Sysco and Calpo limestones were used rather than Havelock.]

[] the Evans results for low recycle are close to the Minto/Devco data, but recycle (as in the case of the overhead loss) affects the bed carbon loss more strongly for the Evans coal, and the values for high recycle are around 1/3 those at no recycle. This again supports the conclusion that Evans is a

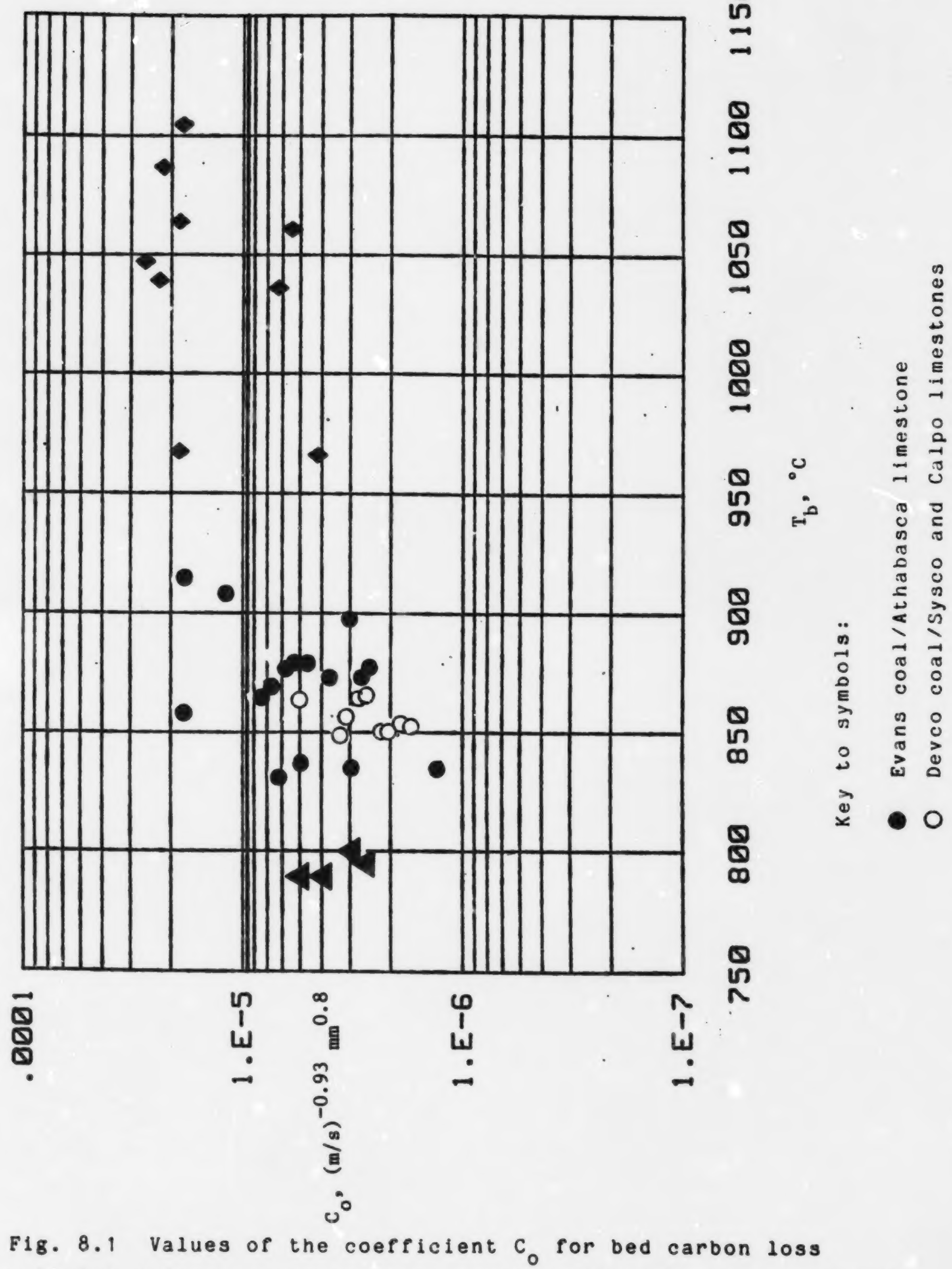

Fig. 8.1 Values of the coefficient C_o for bed carbon loss calculated from the correlating equation (8.1.3) for the Minto/

more reactive coal than the others tested.

[] the Syncrude coke data again show surprizing similarity to the coals.

It should be noted that "reactivity" of fuels as spoken of here encompasses a complex of effects involving fragmentation and attrition as well as chemical reactiveness with oxygen.

8.4 Comparison of carbon loss with the Ahlstrom trials on Syncrude coke

Friedrich, Lee, Desai, and Kuivalainen (1982) describe trials on Syncrude coke using the Ahlstrom atmospheric recirculating fluidized bed combustion (ARFBC) system. This system features high fluidizing velocities and correspondingly high elutriation which is dealt with by recycling all of the cyclone dustfall (hence the adjective "recirculating"). The solid product streams consist of the bed product and the material escaping the cyclone (principally baghouse product when a baghouse is used). The refractory-lined cyclone is run hot, and the resulting opportunity for additional combustion could lead to significantly higher combustion efficiency than in our "conventional" AFBC system.

The mass-median diameter of the Swedish limestone used in the Ahlstrom trials was 0.08 mm. The range of fluidizing velocities was 2.4--5.5 m/s, and that of the bed temperature was 818--948 °C. Eight runs were made in total, with 7--10 h of "stable operation" in each. The bed "inventory" (bed mass m_b) was not determined, so it is not possible to judge how closely steady state was approached. Problems in accurately determining the solid product fluxes were also reported. These factors leave considerable uncertainty in the calculated carbon losses.

Figure 8.2 shows the total fractional carbon loss $\dot{m}_{C,p}/\dot{m}_{C,f}$, $\dot{m}_{C,p} = \dot{m}_{C,b} + \dot{m}_{C,c} + \dot{m}_{C,h}$, as a function of bed temperature. This graph gives an interesting view of our data as well as a comparison with the Ahlstrom results. We carried out runs with no recycle ($r = 0$) and a number with recycle of 69--83 % of the cyclone catch ($r = 0.69$--0.83). Friedrich, et al. (1982) recycled all of the cyclone catch and either none or 75 % of the baghouse catch. The simplest interpretation of the data suggested by Fig. 8.2 is that recycle and bed temperature are of dominant importance and other variables can be neglected by comparison. Our data indicate a fairly strong effect of recirculating cyclone dust, describable by a factor of $\exp(-1.3r)$. This is a little stronger than in the Evans trials and very much stronger than in the Minto/Devco trials, Table 8.1. The temperature effect is roughly given by a factor of $\exp(12000/T_b)$. Thus for our trials, roughly,

$$\dot{m}_{C,p}/\dot{m}_{C,f} \propto e^{-1.3r}\, e^{11000/T_b} \qquad (8.4.1)$$

The Ahlstrom trials, as noted above, had total recycle of the cyclone catch and, in addition, the option of recycling a

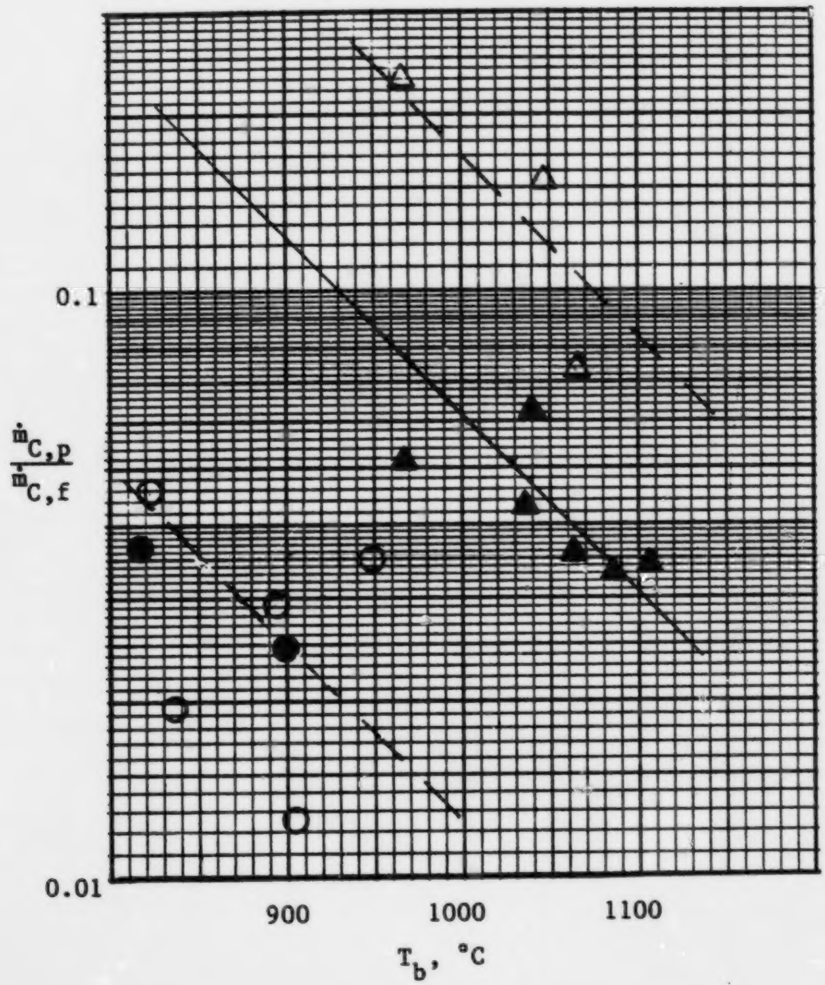

Fig. 8.2 Total fractional carbon loss vs. bed temperature, Syncrude coke trials. Key to symbols:

- △▲ present results, AFBC
- ○●+ Friedrich, et al (1982), ARFBC
  - △ r = 0 (no recycle)
  - ▲ r = 0.67--0.83 (partial recycle of cyclone catch)
  - ○+ r = 1 (full recycle of cyclone catch)
  - ● r = 1 (full recycle of cyclone catch, and 75% of baghouse catch)
  - + inert bed, no limestone feed, no bed product stream; all other trials were with limestone feed

fraction of the baghouse catch. The effect of recycling 75 % of the baghouse catch, however, seems to be weak; the total carbon loss is evidently decreased by no more than 20 %, and the decrease may actually be insignificant.

If the data are compared directly, then the total carbon loss at $r = 1$ seems to be, on average, about 60 % less in the ARFBC rig compared to our conventional AFBC rig. However, if a temperature coefficient of $\exp(11000/T_b)$ is assumed, as suggested by our results, then the carbon loss by ARFBC was only 1/5 as large at a given temperature, a very substantial difference. It is unfortunate that the temperature ranges of the Ahlstrom trials and ours did not substantially overlap in order to clarify the temperature effect. However, our system would not operate well on Syncrude coke below 950 °C. In the Ahlstrom trials it was apparently thought that temperatures above 950 °C would be of no interest because of bad sulphur capture. There may also have been materials limitations, particularly in the hot cyclone.

The overhead carbon loss in all the trials accounted for the bulk of the total carbon loss. Thus the behaviour of the overhead loss factor $\dot{m}_{C,o}/\dot{m}_{C,f}$, $\dot{m}_{C,o} = \dot{m}_{C,c} + \dot{m}_{C,h}$, Fig. 8.3, is not visibly different from that of $\dot{m}_{C,p}/\dot{m}_{C,f}$, Fig. 8.2. The bed carbon loss, Fig. 8.4, was small and behaved erratically but there is a suggestion of increased loss with increasing recycle.

We have noted in Sects. 6.2 and 8.3 that the present

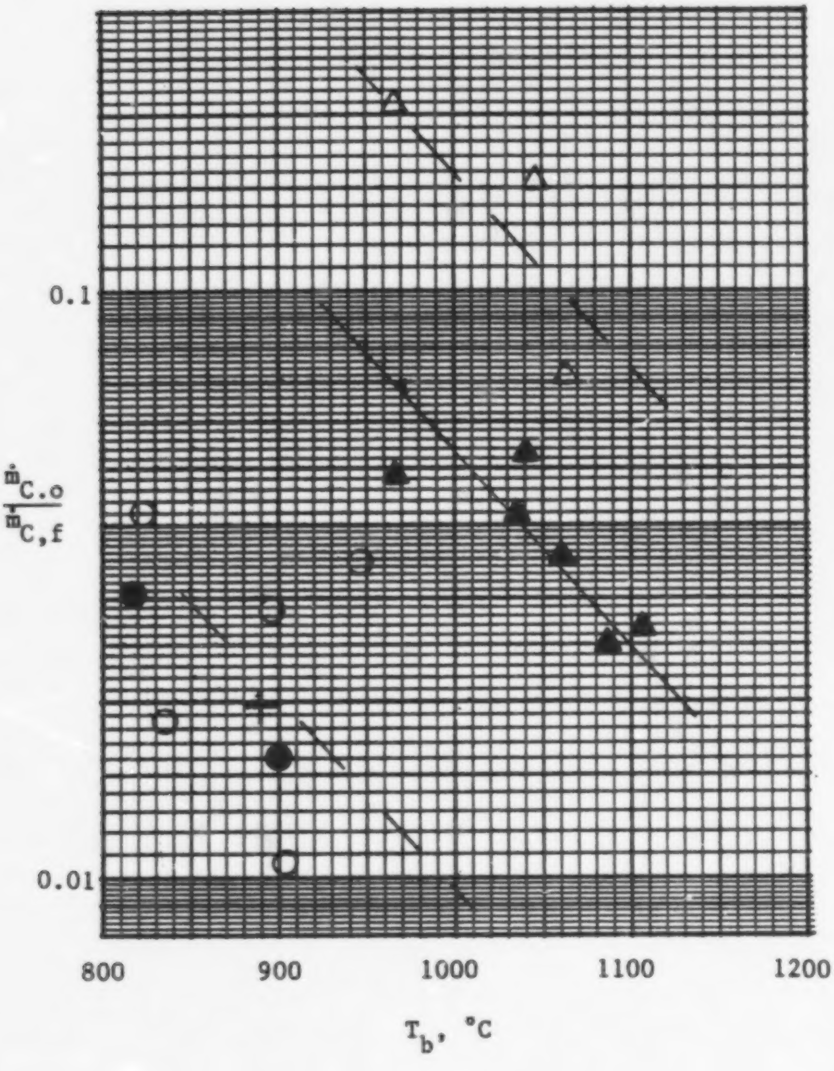

Fig. 8.3 Fractional overhead carbon loss vs. bed temperature, Syncrude coke trials. Key to data: see Fig. 8.2.

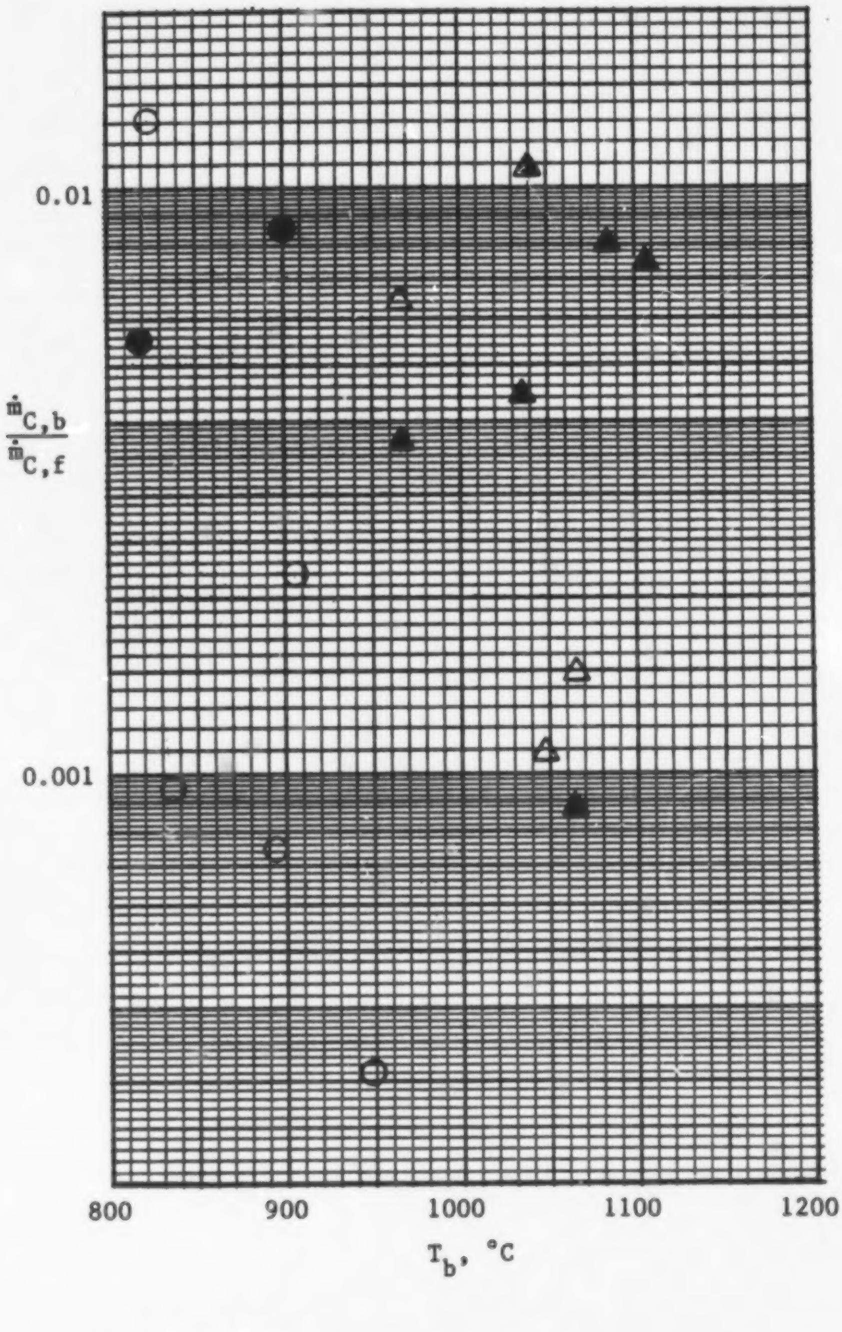

Fig. 8.4 Fractional bed carbon loss vs. bed temperature, Syncrude coke trials. Key to data: see Fig. 8.2.

results on Syncrude coke, when fitted to our Minto/Devco correlations of overhead and bed carbon loss, show remarkable similarity in magnitude to results on the various coals with the exception of the Evans. This similarity may be partly fortuitous, and in the above we have noted apparently stronger effects of temperature and recycle on the overhead carbon loss of the Syncrude coke, and an absence of visible effects of limestone particle diameter and fluidizing velocity. It is interesting to see how the Ahlstrom ARFBC results compare with the Minto/Devco correlations. Figure 8.5 shows values of C_o for the overhead carbon loss, calculated from (6.2.1), as a function of temperature. They lie in the range $(1--4) \times 10^{-5}$, compared to the mean value of 3.3×10^{-4} for the Minto/Devco trials, all in units of $(m/s)^{-0.86}\ mm^{0.74}$. This may be construed as evidence of substantially better (seemingly by a factor of almost 10) combustion efficiencies by ARFBC.

8.5 Sulphur capture

Figure 8.6 shows on one graph the mean curves of percentage sulphur capture (according to gas analysis) as a function of Ca/S ratio for the previous Minto/Devco trials with Havelock limestone, the present Evans trials with Havelock limestone, the present Devco trials with Sysco and Calpo limestones, and the Kentucky No. 9 trials with Reed limestone, all for limestone particle diameters in the optimum range (below 1.5 mm dia.). The Havelock limestone gave similar performance for all of three coals (Minto, Devco and Evans) at Ca/S > 2, and

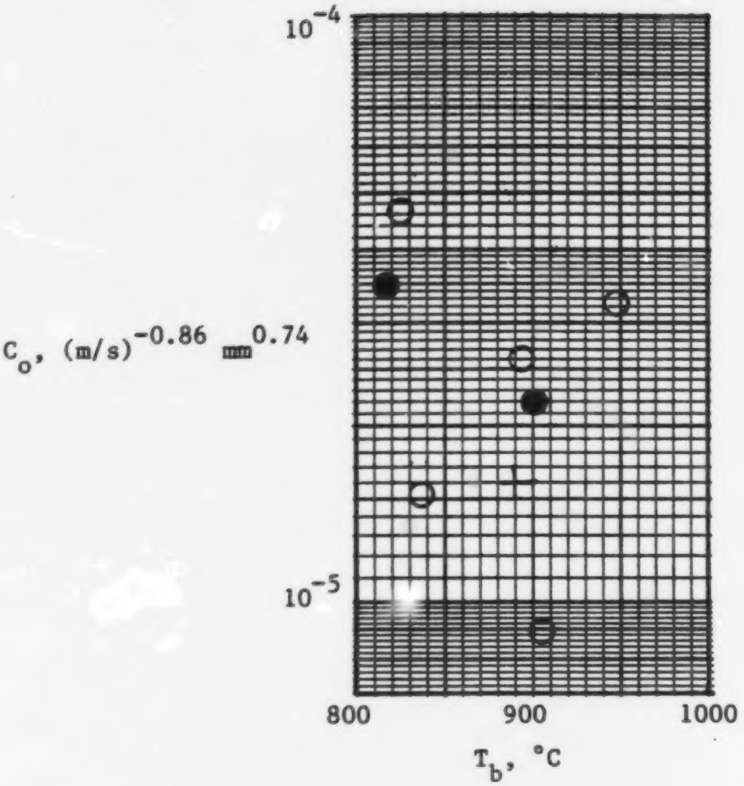

Fig. 8.5 Ahlstrom ARFBC Syncrude coke trials (Friedrich, et al 1982): values for the coefficient C_o for overhead carbon loss calculated from the correlating equation (6.2.1) for the Minto/Devco coal trials. Key to data: see Fig. 8.2.

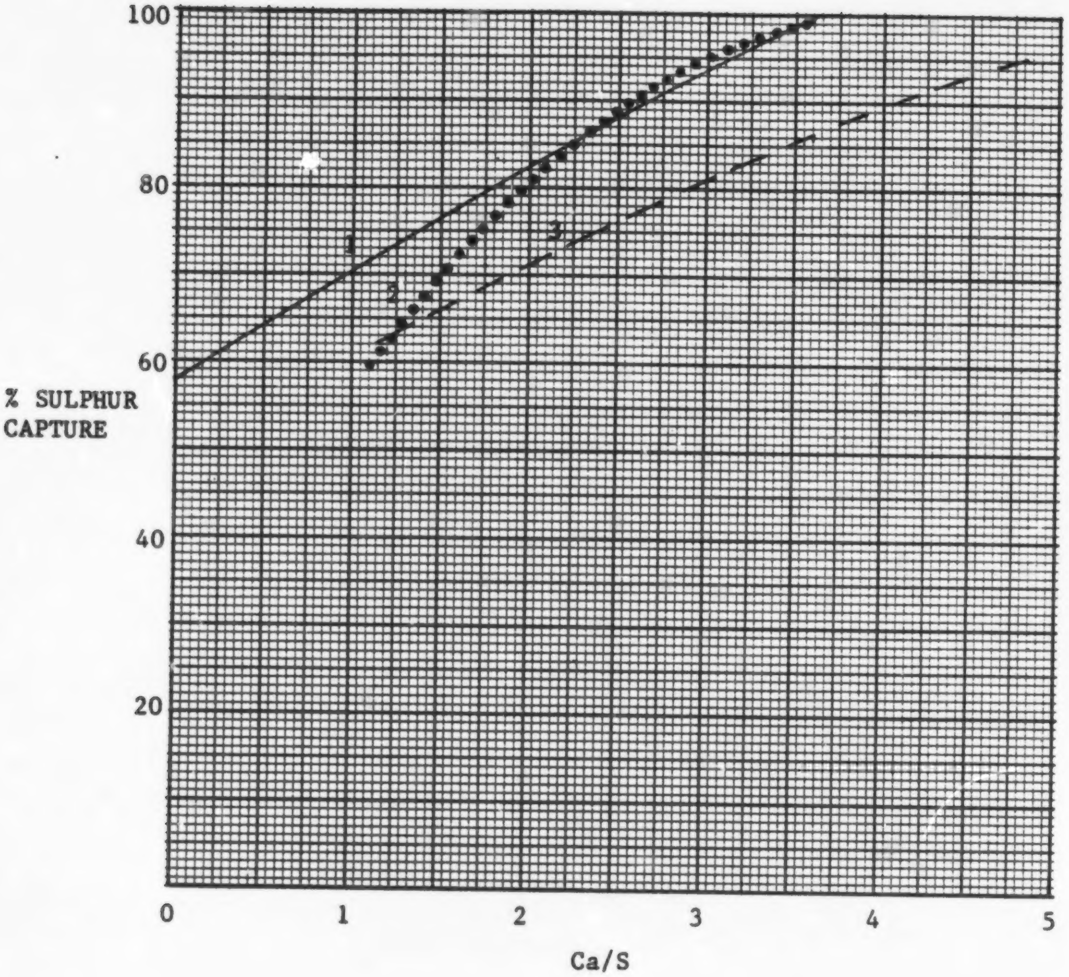

Fig. 8.6 Sulphur capture as a function of Ca/S, trials with limestone particle diameter near optimum ($\hat{D}_p$ = 0.5--1.5 mm). Curves:

1. Evans coal trials with Havelock limestone

2. Minto and Devco coal trials with Havelock limestone (Becker and Code 1983)

3. Devco coal trials with Sysco and Calpo limestones and Kentucky No. 9 coal trials with Reed limestone

evidently coal characteristics, including particle size, do not visibly affect sulphur capture at reasonably high Ca/S. At small Ca/S, however, the Evans coal showed a suprizingly high sulphur capture by its ash.

The Sysco, Calpo and Reed limestones all performed similarly and not as well as the Havelock. Roughly for these stones Ca/S must be one unit higher than for Havelock in order to get the same capture.

The really surprizing outcome in respect to sulphur capture is the good performance observed of the Athabasca limestone in the Syncrude coke trials at temperatures up to 1050 °C, Fig. 6.11. A considerably faster fall in capture with rising temperature was expected, based on observations and suggestions in the literature. The results do, though, agree with the literature in suggesting that the optimum is around 850 °C. Good capture at temperatures up to 950 °C, their highest, was also observed by Friedrich, et al. (1982) in the Ahlstrom ARFBC trials. They report no detailed numerical results in their paper but do observe that sulphur capture was above 90 % over their whole temperature range of 818--948 °C and, "contrary to accepted theory, showed little effect of bed temperature". They used a Swedish (Gotland) limestone and we an Athabasca limestone, yet the results agree on this matter. The explanation of these observations would require detailed research on the limestone properties and, perhaps, further pilot plant trials in which Syncrude coke would be burned with a limestone of known performance with coal, e.g., the Havelock limestone.

9. HEAT TRANSFER

9.1 Introduction

Background material on heat transfer in fluidized bed combustion is included in our previous report (Becker and Code, 1983). In this section of the report, the procedure used for the evaluation of bed-side coefficients is outlined and the effect of changes in operating conditions on the magnitude of the coefficients is examined.

9.2 Configuration of the arrays of in-bed tubes

The arrangement of the ports for the accommodation of the in-bed tubes is treated in the description of module 3 of the combustor (Fig. 2.5). Each tube is 1.12 m long with a length of 380 mm exposed to the bed. The tubes are connected in series of two or four by long-radius bends of 19 mm ID heavy-wall rubber hose designed for service up to 90 °C. The arrangement of the cooling water circuits used in the current study is illustrated in Fig. 9.1. The mean height of a circuit above the distributor plate, Z, is indicated on the diagram. The circuit number identifies the rotameter used to measure the flowrate of cooling water which enters and leaves the circuit on the north face. The temperatures of the cooling water at the inlet and outlet of the circuits are measured by thermocouples with backup dial thermometers. Limiting the outlet temperature of the water to 55--60 °C was sufficient to avoid boiling.

FBC IN-BED HEAT EXCHANGER (SOUTH FACE)

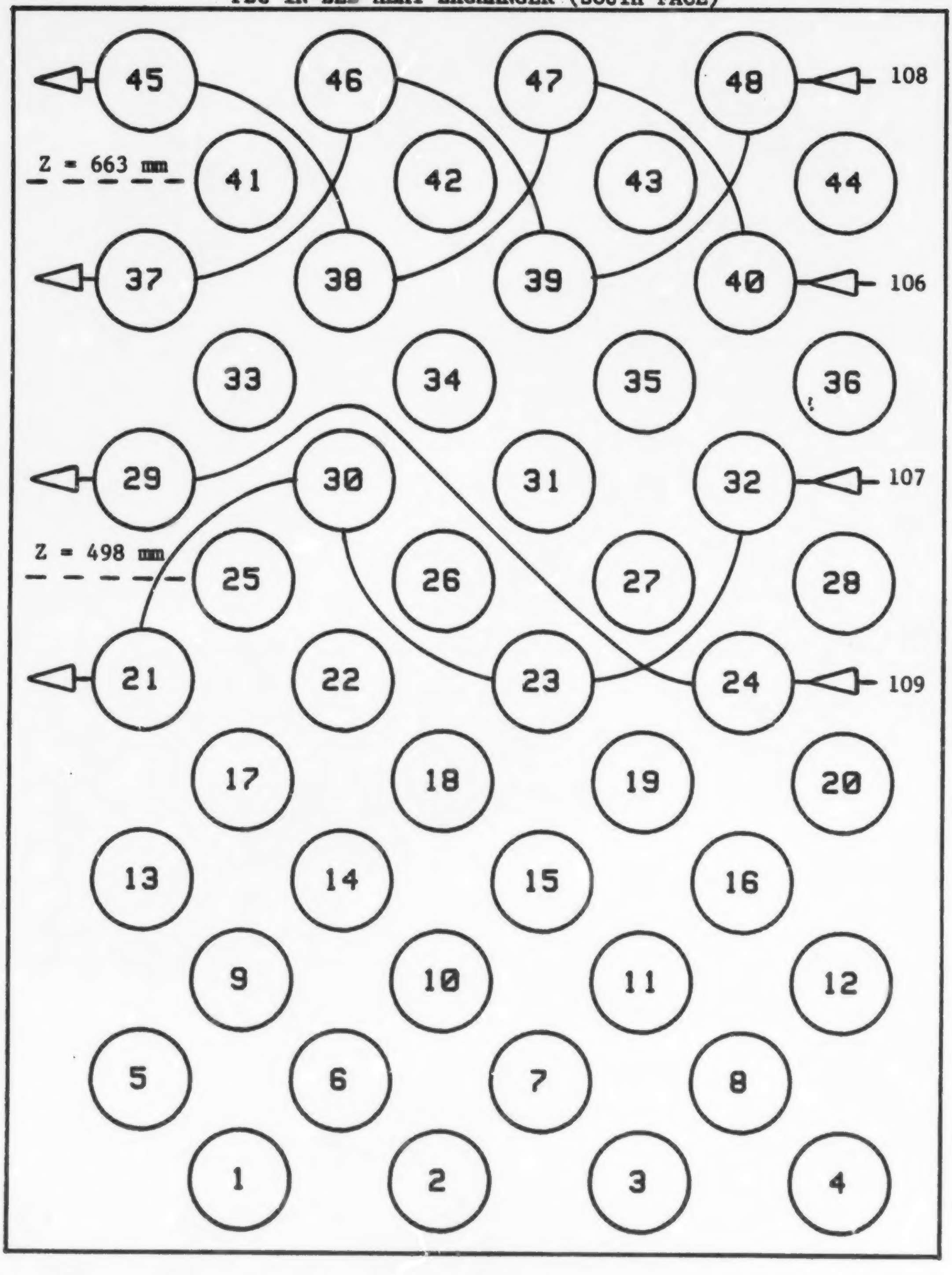
45
46
47
48
108
Z = 663 mm
41
42
43
44
37
38
39
40
106
33
34
35
36
29
30
31
32
107
Z = 498 mm
25
26
27
28
21
22
23
24
109
17
18
19
20
13
14
15
16
9
10
11
12
5
6
7
8
1
2
3
4

Fig. 9.1 Cooling water circuits used for the measurement of bed-side heat transfer coefficients. The circuit numbers refer to the rotameters used to measure the water flowrates. Cooling water enters and leaves the circuits on the north face.

9.3 Evaluation of heat transfer coefficients

Applying a differential energy balance on the cooling water over a circuit segment of length dx,

$$\dot{m}\, c_p \frac{d\tilde{T}}{dx} + \dot{Q}' = 0 \qquad (9.3.1)$$

where $\dot{Q}'$ is the heat flux out of the cooling water per unit length at distance x along the circuit, $\tilde{T}$ is the stream-average or 'bulk' temperature of the water crossing section x, $\dot{m}$ is the mass flowrate of water and c_p is the heat capacity of the water at temperature $\tilde{T}$. Over the temperature range in question the variation in the heat capacity of water is small and c_p may be treated as a constant, 4180 J/kg K. Integration of Eq. 9.3.1 over the circuit length results in the overall expression

$$\dot{m}\, c_p(T_{out} - T_{in}) + \dot{Q} = 0 \qquad (9.3.2)$$

where,

$$\dot{Q} = \int \dot{Q}'\, dx \qquad (9.3.3)$$

The sign convention followed in the above development is that fluxes are positive when directed out of a system. The heat flux $\dot{Q}$ out of a circuit may be determined from Eq. 9.3.2 and the experimentally measured inlet and outlet temperatures of the cooling water and the mass flowrate of cooling water $\dot{m}$.

In order to evaluate the heat transfer coefficients, a number of acceptable approximations were required. The first simplification was the assumption that the tube circuits operated adiabatically over the portions which were not exposed to the bed. With this assumption, the heat flux $\dot{Q}'$ for the exposed portions may be equated to the product of the overall conductance per unit length of tube, B', and the overall temperature driving force, $\bar{T} - T_b$.

$$\dot{Q}' = B'(\bar{T} - T_b) \tag{9.3.4}$$

In this system the total conductance consists of three conductances in series: the tube-side or 'inside' conductance, the conductance of the tube wall, and the bed-side or 'outside' conductance. Applying the reciprocal rule for summing conductances in series,

$$\frac{1}{B'} = \frac{1}{B_i'} + \frac{1}{B_w'} + \frac{1}{B_o'} \tag{9.3.5}$$

where for cylindrical tubes,

$$B_i' = \pi D_i h_i \tag{9.3.6}$$

$$B_w' = 2\pi\, k_w/\ln(D_o/D_i) \tag{9.3.7}$$

$$B_o' = \pi D_o h_o \tag{9.3.8}$$

The resistance of the metal wall of the tubes, $R'_w = 1/\beta'_w$, is small and may be neglected. This simplification implies that $T_o = T_w = T_i$. Substitution for Q' in Eq. 9.3.1 in terms of the inside and outside conductances and the overall temperature driving force and integration over the length of the circuit exposed to the bed, L, gives

$$- \int_{T_{in}}^{T_{out}} \left[\frac{1}{\pi D_o h_o} + \frac{1}{\pi D_i h_i} \right] \frac{d\tilde{T}}{\tilde{T} - T_b} = \frac{L}{\dot{m} c_p} \qquad (9.3.9)$$

The integral in Eq. 9.3.9 may be evaluated analytically if the inside and outside coefficients, h_i and h_o, are treated as constants. The result arranged explicitly in terms of h_o is

$$\frac{1}{h_o} = \frac{\pi D_o L}{\dot{m} c_p \ln \left[\dfrac{T_b - T_{in}}{T_b - T_{out}} \right]} - \frac{D_o}{D_i h_i} \qquad (9.3.10)$$

Arguments in support of the above simplification are given by Becker and Code (1983). In summary the arguments are:

- the bed temperature T_b is large and changes in the wall temperature T_w effect only a small variation in the bed-side temperature difference, $T_b - T_w$

- correspondingly, there is little variation in the unit-length heat flux, which can be written as

$$\dot{Q}' = \pi D_o h_o (T_w - T_b) \qquad (9.3.11)$$

- the tube-side coefficient is of the order of ten times the bed-side coefficient and modest accuracy in its estimation is sufficient, i.e., the bed-side resistance is the predominant resistance.

The computational procedure developed for the evaluation of the bed-side coefficients involved the following sequence of steps:

1. From the experimental measurements of the inlet and outlet temperatures and mass flowrate of the cooling water for a given circuit, estimate $\dot{Q}$ from Eq. 9.3.2 and evaluate the unit-length heat flux, $\dot{Q}' = \dot{Q}/L$.

2. Set

$$T_{w,o} = T_{in} \quad \text{and} \quad T_{w,L} = 100 \text{ °C}$$

where $T_{w,o}$ is the wall temperature at the start of the first active section of the circuit and $T_{w,L}$ is the wall temperature at the end of the last active section of the circuit.

3. Estimate the tube-side heat transfer coefficient h_i from the correlation of Sieder and Tate (1936):

$$Nu = 0.027\ Re^{0.8}\ Pr^{1/3}\ (\mu/\mu_w)^{0.14} \tag{9.3.12}$$

where $Nu \equiv h_i D_i/k$, $Re \equiv 4\dot{m}/\pi D_i \mu$, and $Pr \equiv c_p/\mu k$. In applying Eq. 9.3.12, evaluate the stream fluid properties μ, c_p and k at the median stream temperature $(T_{in} + T_{out})/2$. Evaluate μ_w at the median wall temperature $(T_{w,o} + T_{w,L})/2$.

4. Estimate the wall temperature at the exit, $T_{w,L}$, from the tube-side heat flux equation

$$\dot{Q}' = \pi D_i h_i (T - T_w) \tag{9.3.13}$$

i.e.,

$$T_{w,L} = T_{out} - \dot{Q}'/\pi D_i h_i \tag{9.3.14}$$

5. Using the value of $T_{w,L}$ from step 4, repeat steps 3 to 5. Iterate until the value of $T_{w,L}$ converges within 1 °C or less.

6. Using the value of h_i corresponding to the final converged value for $T_{w,L}$ from step 5, evaluate the bed-side heat transfer coefficient, h_o, from Eq. 9.3.10.

9.4 Results and discussion

9.4.1 Results

The bed-side heat transfer coefficients evaluated by the procedure outlined in 9.3 are summarized in Table 9.1 and Table 9.2. The mean heights of the cooling water circuits were at levels of 498 mm and 663 mm above the distributor plate and this distinction has been made in tabulating the results. Relevant conditions have been included in the tables for convenient reference. Although circuits 106 and 108 were at the same mean level in the bed, circuit 108 gave consistently higher coefficients than circuit 106. This disagreement ranged from 7.8 % for the runs with Evans coal to 5.2 % for the runs with Kentucky No. 9 coal to 2.5 % for the runs with Devco coal. These estimates were obtained by expressing the difference as a percentage of the average of the two coefficients for a given run and then taking the average of the percentages.

The coefficients for the three coals are plotted vs. the efflux of elutriated solids per unit bed cross-section in Fig. 9.2 and Fig. 9.3. The same distinction with respect to the circuit levels in the bed has been made in the plots. In parallel with the tables, operating conditions are distinguished symbolically but in order to reduce the confusion of symbols a particular geometry is used for a given fuel, e.g., triangles in various orientations and shadings denote the coefficients for Evans coal.

Table 9.1 Bed-side heat transfer coefficients, h_o, for cooling water circuits with a mean height, Z, above the distributor plate of 498 mm.

Run No.	Coolant Circuit	Fuel $\hat{D}_p$, mm	Sorbent $\hat{D}_p$, mm	v, m/s	m_e/A_b kg/m²hr	Re	Pr	Nu	h_i, W/m²K	h_o, W/m²K
		Evans	Havelock							
831115	107	16.7	0.49	2.1	155	14388	5.44	110.8	4341	302
831122	107	16.7	0.49	2.1	69	16887	5.26	124.6	4899	407
831124	107	16.7	0.49	2.2	139	17075	5.35	127.1	4989	408
831213	107	16.7	1.72	2.5	73	11551	5.10	91.6	3615	338
831213	109	16.7	1.72	2.5	73	8381	6.53	80.7	3099	375
831214	107	16.7	1.72	2.6	151	11229	5.20	90.8	3576	318
831214	109	16.7	1.72	2.6	151	8423	6.71	81.1	3105	349
840105	107	3.3	1.72	2.6	693	9183	5.58	80.1	3130	306
840111	107	3.3	1.72	2.0	406	4963	5.20	50.3	1980	378
840207	107	8.8	0.49	2.1	44	13335	5.49	106.6	4173	394
840215	107	8.8	0.49	2.3	119	12573	5.10	99.5	3927	377
840216	107	8.8	0.49	2.2	85	12316	5.52	98.8	3863	371
		Syncrude	Athabasca							
840612	107*	0.26	0.34	1.3	40	4615	4.75	47.1	1869	399
840618	107*	0.26	0.34	1.0	47	6901	5.77	67.2	2617	432
840703	107*	0.26	0.34	1.0	133	8252	5.81	75.8	2950	305

* For the runs with Syncrude coke, cooling water circuit 107 consisted of a single tube at a mean height of 530 mm.

Table 9.1 Continuation

Run No.	Coolant Circuit	Fuel $\hat{D}_p$, mm	Sorbent $\hat{D}_p$, mm	v, m/s	m_e/A_b kg/m²hr	Re	Pr	Nu	h_i, W/m²K	h_o, W/m²K
		KY No. 9	Reed							
841108	107*	2.3	1.1	2.6	131	19756	4.74	134.1	5325	327
841112	107*	2.3	1.1	2.7	196	20375	4.95	137.7	5446	325
841115	107*	2.3	1.1	2.6	107	19297	5.04	133.0	5254	312
841119	107*	2.3	1.1	2.9	259	20348	5.38	140.9	5529	312
		Devco	Sysco							
841127	107	2.1	1.4	2.5	89	12640	4.86	96.3	3817	348
841204	107	2.1	1.4	2.5	258	11891	4.99	93.1	3681	336
850129	107	11.2	1.4	2.4	47	10770	5.82	93.1	3622	435
		Devco	Calpo							
841218	107	2.1	1.1	2.5	83	12419	5.41	98.7	3870	340
841219	107	2.1	1.1	2.5	283	12478	5.44	99.4	3893	344

* For the runs with Kentucky No. 9 coal, cooling water circuit 107 consisted of six tubes connected in the sequence 32, 30, 23, 21, 22, 29 (Fig. 10.1).

Table 9.2 Bed-side heat transfer coefficients, h_o, for cooling water circuits with a mean height, Z, above the distributor plate of 663 mm.

Run No.	Coolant Circuit	Fuel $\hat{D}_p$, mm	Sorbent $\hat{D}_p$, mm	v, m/s	m_e/A_b kg/m²hr	Re	Pr	Nu	h_i, W/m²K	h_o, W/m²K
		Evans	Havelock							
831115	106	16.7	0.49	2.1	155	11066	5.81	91.8	3571	203
831115	108	16.7	0.49	2.1	155	12733	5.87	100.8	3916	228
831122	106	16.7	0.49	2.1	69	15434	5.64	119.3	4653	333
831122	108	16.7	0.49	2.1	69	15372	5.32	116.5	4578	364
831124	106	16.7	0.49	2.2	139	14863	5.61	115.3	4503	329
831124	108	16.7	0.49	2.2	139	14982	5.25	113.2	4454	367
831213	106	16.7	1.72	2.5	73	10075	5.06	82.0	3235	296
831213	108	16.7	1.72	2.5	73	10559	5.03	84.7	3345	313
831214	106	16.7	1.72	2.6	151	10006	5.09	81.8	3228	289
831214	108	16.7	1.72	2.6	151	10573	5.11	85.7	3380	304
840105	106	3.3	1.72	2.6	693	7455	5.58	66.5	2597	248
840111	106	3.3	1.72	2.0	406	8583	5.20	72.7	2863	299
840117	106	3.3	1.72	1.5	115	9350	5.26	79.9	3141	315
840124	106	3.3	0.49	1.5	406	9540	5.06	79.5	3139	333
840126	106	3.3	0.49	1.6	48	10106	4.86	82.5	3267	349
840207	106	8.8	0.49	2.1	44	10312	5.33	85.6	3360	311

Table 9.2 Continuation

Run No.	Coolant Circuit	Fuel $\hat{D}_p$, mm	Sorbent $\hat{D}_p$, mm	v, m/s	$\dot{m}_e/A_b$ kg/m²hr	Re	Pr	Nu	h_i, W/m²K	h_o, W/m²K
		Evans	Havelock							
840215	106	8.8	0.49	2.3	119	11053	5.13	88.6	3492	329
840215	108	8.8	0.49	2.3	119	11718	5.06	93.7	3700	353
840216	106	8.8	0.49	2.2	85	10599	5.50	87.6	3427	319
840216	108	8.8	0.49	2.2	85	11776	5.73	97.6	3804	338
840313	106	16.7	0.49	1.5	583	10317	5.20	85.9	3383	352
840314	106	16.7	0.49	1.6	37	10955	5.37	90.1	3535	323
840320	106	16.7	0.49	1.5	16	10210	5.61	85.6	3344	306
		Evans	Sand							
840404	106	16.7	0.95	1.5	-	12055	4.82	93.4	3702	381
		KY No. 9	Reed							
841108	106	2.3	1.1	2.6	131	10995	5.07	86.2	3402	250
841108	108	2.3	1.1	2.6	131	10520	4.67	80.6	3205	273
841112	106	2.3	1.1	2.7	196	10392	4.70	80.1	3182	274
841112	108	2.3	1.1	2.7	196	10767	4.65	83.5	3322	288
841115	106	2.3	1.1	2.6	107	10126	5.04	81.7	3228	251
841115	108	2.3	1.1	2.6	107	10211	4.99	81.8	3232	257
841119	106	2.3	1.1	2.9	259	11792	5.81	96.6	3758	237
841119	108	2.3	1.1	2.9	259	11792	5.71	95.5	3720	248

Table 9.2 Continuation

Run No.	Coolant Circuit	Fuel $\hat{D}_p$, mm	Sorbent $\hat{D}_p$, mm	v, m/s	m_e/A_b kg/m²hr	Re	Pr	Nu	h_i, W/m²K	h_o, W/m²K
		Devco	Sysco							
841127	106	2.1	1.4	2.5	89	10726	4.92	85.4	3380	290
841127	108	2.1	1.4	2.5	89	11805	5.16	92.9	3661	300
841204	106	2.1	1.4	2.5	258	10101	4.92	81.1	3210	290
841204	108	2.1	1.4	2.5	258	10307	4.84	81.5	3232	301
850121	106	11.2	1.4	1.4	28	10097	5.71	87.6	3415	413
850121	108	11.2	1.4	1.4	28	10187	5.62	87.4	3412	421
850129	106	11.2	1.4	2.4	47	9419	5.49	82.3	3222	394
850129	108	11.2	1.4	2.4	47	9552	5.46	83.0	3250	401
850304	106	11.2	1.4	1.5	32	10658	5.76	91.9	3579	423
850304	108	11.2	1.4	1.5	32	10520	5.55	90.5	3540	428
		Devco	Calpo							
841218	106	2.1	1.1	2.5	83	9835	4.95	79.4	3142	295
841218	108	2.1	1.1	2.5	83	10397	5.04	84.0	3317	306
841219	106	2.1	1.1	2.5	283	9868	4.96	79.7	3152	299
841219	108	2.1	1.1	2.5	283	10361	5.09	84.2	3323	305
850107	106	2.1	1.1	1.5	50	10356	5.44	86.9	3404	331
850107	108	2.1	1.1	1.5	50	10327	5.27	84.9	3337	341
850115	106	11.2	1.1	1.5	26	10681	5.39	90.2	3536	433
850115	108	11.2	1.1	1.5	26	10913	5.42	92.1	3608	440

9.4.2 Effect of operating conditions on h_o

The bed-side heat transfer coefficients in Fig. 9.2 and Fig. 9.3 are plotted vs. the flux density of elutriated solids in order to examine any effect of an increase in the flux of fine particles passing up through the bed as a result of an increase in the rate of recycle of cyclone solids. Within the scatter of the data for a given group of points with the same operating conditions, there is no significant effect of $\dot{m}_e/A_b$ on h_o. This result which is in agreement with our ealier work (Becker and Code, 1983) implies that the addition of fines does not improve the contact heat transfer between the solids and the tube wall.

With the exception of the coefficients for Devco coal with a $\hat{D}_p$ of 11.2 mm, the bulk of the coefficients fall in the ranges 300--400 W/m²K and 250--350 W/m²K corresponding, respectively, to mean circuit heights of 498 mm and 663 mm above the distributor plate. This effect of circuit level in the bed is of the same order of magnitude as in our previous work (Becker and Code, 1983) on Minto and Devco coals but the ranges in the current study are approximately 50 W/m²K higher. The values of h_o are of the same order of magnitude as the range predicted by the equation of Gelperin (Botterill et al., 1981) for the maximum heat transfer coefficient for a fully immersed tube bundle in a bed at 850 °C

$$h_o = 34 D_p^{-0.34} \qquad (9.4.1)$$

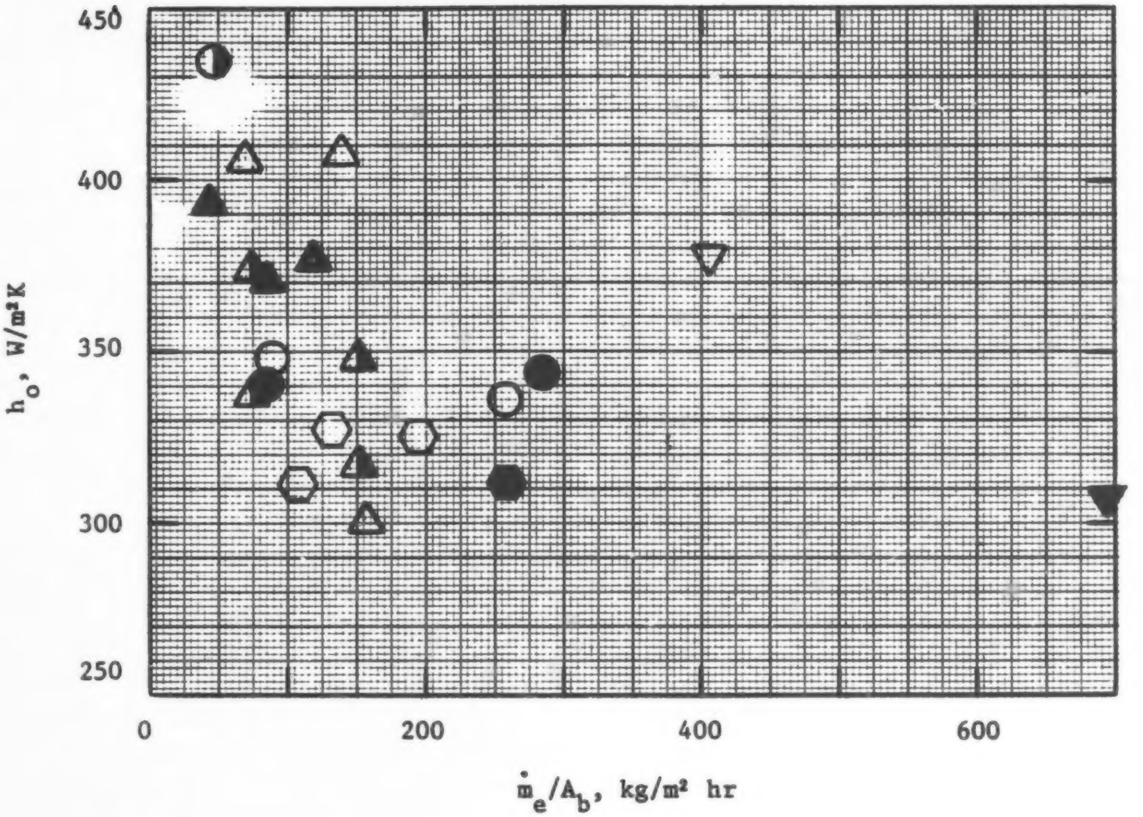

Fig. 9.2 Bed-side heat transfer coefficient for cooling water circuits with a mean height of 498 mm above the distributor plate vs. the flux density of elutriated solids.

Key to symbols:	Fuel	$\hat{D}_p$, mm	Sorbent	$\hat{D}_p$, mm	v, m/s
△	Evans	16.7	Havelock	0.49	2.1-2.2
◭	Evans	16.7	Havelock	1.72	2.5-2.6
▲	Evans	8.8	Havelock	0.49	2.1-2.3
▽	Evans	3.3	Havelock	1.72	2.0
▼	Evans	3.3	Havelock	1.72	2.6
⬡	KY No. 9	2.3	Reed	1.1	2.6-2.7
⬢	KY No. 9	2.3	Reed	1.1	2.9
○	Devco	2.1	Sysco	1.4	2.5
◑	Devco	11.2	Sysco	1.4	2.4
●	Devco	2.1	Calpo	1.1	2.5

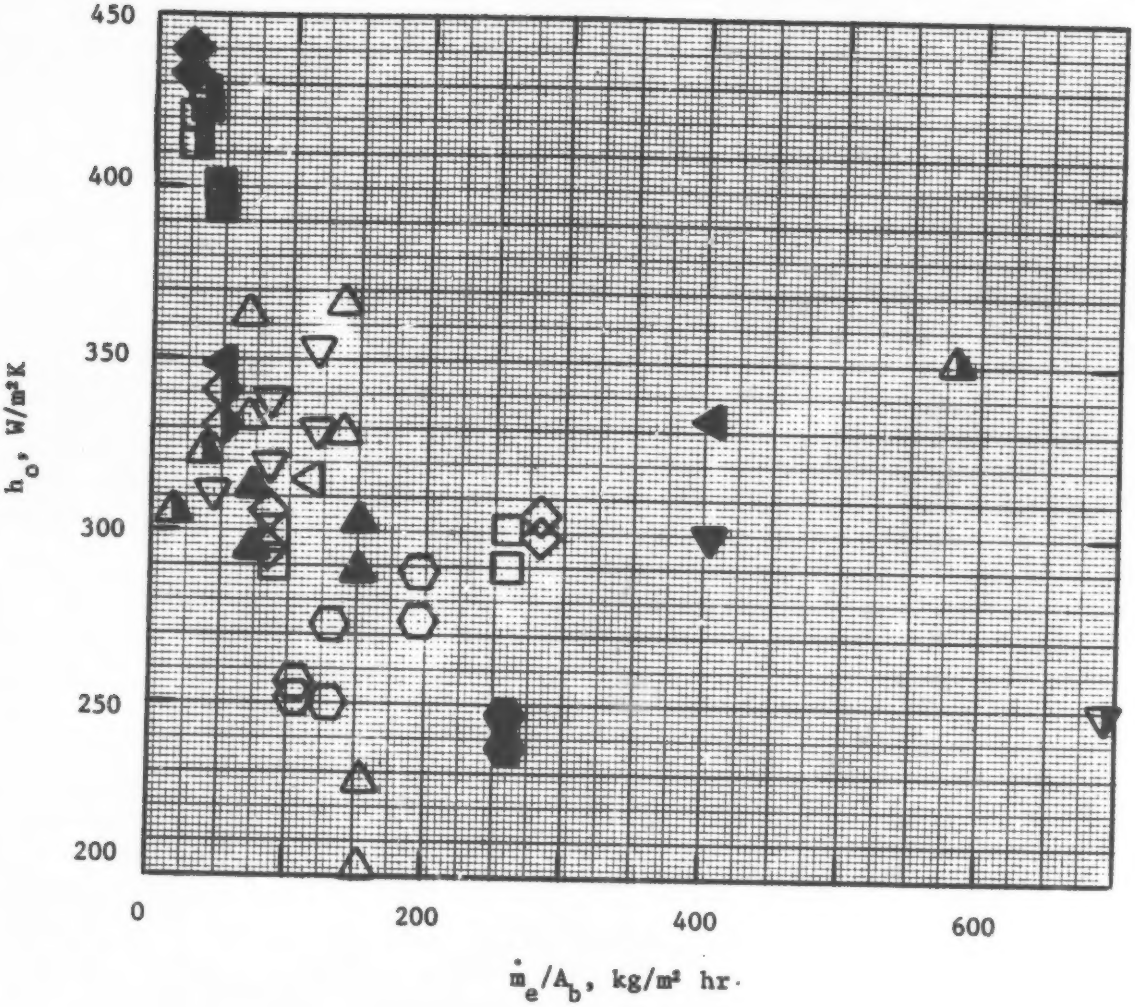

Fig. 9.3 Bed-side heat transfer coefficient for cooling water circuits with a mean height of 663 mm above the distributor plate vs. the flux density of elutriated solids. A key to the symbols accompanies Fig. 9.5.

if the maximum and minimum mean diameters of the limestone feed are substituted for D_p. Substitution of 0.00172 m and 0.00049 m for D_p in Eq. 9.4.1 results in a range for h_o of 300--450 W/m²K.

It is evident from the plots in Fig. 9.2 and Fig. 9.3 that coal type has an influence on the magnitude of h_o. This observation is in agreement with our earlier work on Minto and Devco coals but the effect of coal particle size on h_o in the current work on Devco coal was unexpected. The coefficients for a coal $\hat{D}_p$ of 11.2 mm are consistently higher by approximately 100 W/m²K than the coefficients for a coal $\hat{D}_p$ of 2.1 mm. Can a difference of this magnitude be explained by the effect of the different particle size distributions of the ash from the two feeds on the particle size distribution of the bed material? Additional work is required to resolve this controversial result.

The heat transfer coefficients were fitted by a power function of the form:

$$h_o = C\, v^a\, \hat{D}_p^b \qquad (9.4.2)$$

$\hat{D}_p$ of the solids at the bed level of the cooling water circuit is the appropriate characteristic particle diameter to use in Eq. 9.4.2 but in the absence of this information $\hat{D}_p$ of the limestone feed was used in the regression. At least for a particular fuel, the change in $\hat{D}_p$ of the limestone represents some measure of the change in the $\hat{D}_p$ of the bed solids. The results of the regression analyses on six combinations of the data are given in Table 9.3.

The most significant result to emerge from the analysis is the negative sign accompanying all of the values for the exponent a on the superficial fluidizing velocity, i.e., an increase in v results in a decrease in h_o for the velocity range covered by the data. This result is in agreement with our earlier work on Minto and Devco coals (Becker and Code, 1983). A portion of the heat transfer from the bed to the tube wall is by contact of the hot particles with the wall and a plausible explanation for the negative sign is that contact between the swarms of particles moving around the tubes is better under more quiescent conditions for the limited range of v in the current study (1.5 m/s to 2.5 m/s).

The results for the exponent b on the particle diameter $\hat{D}_p$ are not as clear since both negative and positive signs accompany the values of b. This inconsistency could be attributable to the use of the mean particle diameter of the limestone feed in the regression analysis instead of the more appropriate mean particle diameter of the bed solids. However, the values are small and the effect of $\hat{D}_p$ on h_o is therefore small for the range of particle sizes covered in the current study. Using the particle-tube contact argument given in the preceding paragraph, one would expect a negative sign on b, i.e., a decrease in $\hat{D}_p$ results in an increase in h_o. As the particle

Table 9.3 Regression results for the bed-side heat transfer coefficient, $h_o = C\ v^a \hat{D}_p^b$.

Data	Circuit Level, Z, mm	a	b	C $(W/m^2K)(m/s)^{-a}(mm)^{-b}$
Evans	498	-0.241	-0.046	437
Evans	663	-0.164	-0.033	347
Devco	663	-0.485	-0.322	456
Evans + Devco	498	-0.365	-0.021	491
Evans + Devco	663	-0.388	0.055	432
Evans + Devco + KY No. 9	663	-0.482	0.051	453

size is reduced, the coverage of the tube surface is improved. However, there is a lower limit on this effect of a reduction in $\hat{D}_p$ due to the interaction effects of v and $\hat{D}_p$ described in the preceding paragraph. This argument is supported by the lack of a significant effect of fines recycle on h_o.

The adequacy of the correlations obtained using combined data for different coals was examined by evaluating the coefficient C from individual measurements of h_o. The need to restrict this type of correlation to individual fuels is evident from an examination of the results in Fig. 9.4 and Fig. 9.5. Although the choice of $\hat{D}_p$ of the limestone as the characteristic particle diameter is more convenient to use since this information would be readily available for design calculations, it restricts the resulting correlation to single fuels. The effect of the different particle size distributions of the ash from different coals on the particle size distribution of the bed solids was given as a possible explanation for the inconsistency in the sign on the exponent b when $\hat{D}_p$ of the limestone is used as the characteristic particle diameter. This same argument may be used here to explain the restriction of correlations to individual fuels.

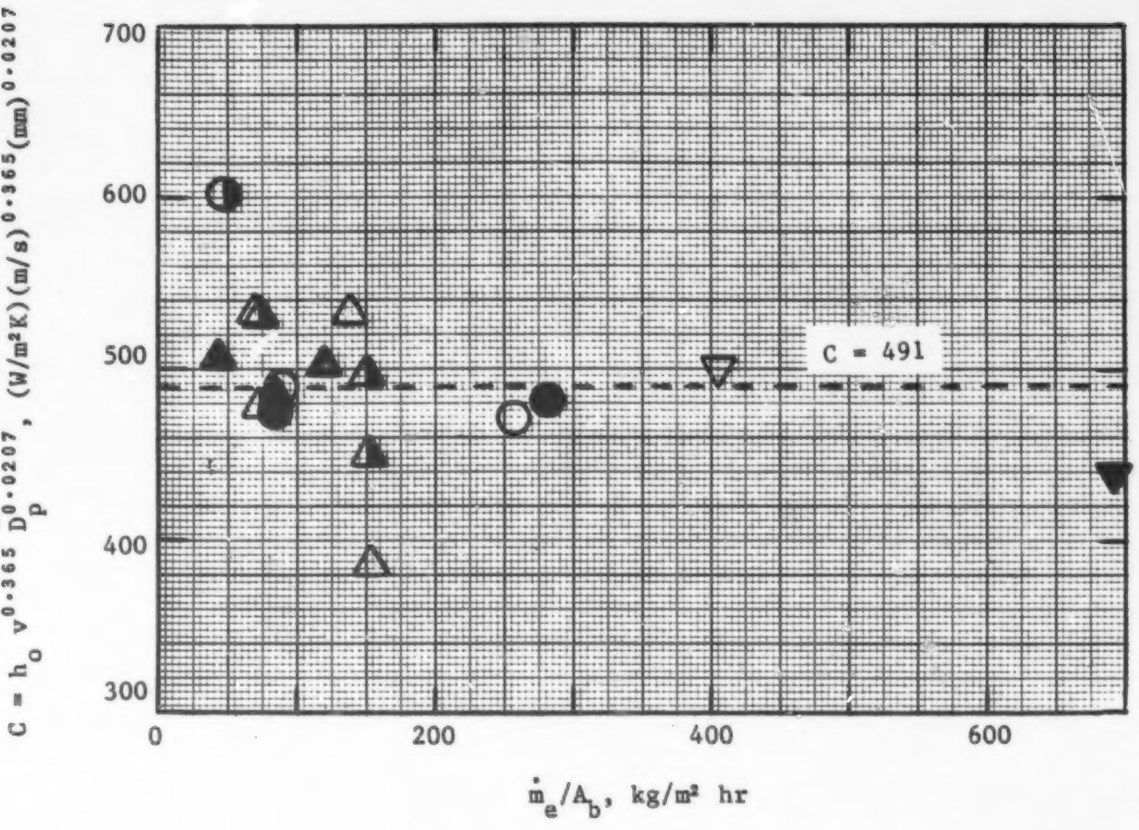

Fig. 9.4 The coefficient, C, in the correlation of bed-side heat transfer coefficients. Points evaluated from individual measurements of h_o: $C = h_o v^{0.365} \hat{D}_p^{0.0207}$. Mean height of cooling water circuits above the distributor plate 498 mm.

Key to symbols:	Fuel	$\hat{D}_p$, mm	Sorbent	$\hat{D}_p$, mm	v, m/s
△	Evans	16.7	Havelock	0.49	2.1-2.2
◭	Evans	16.7	Havelock	1.72	2.5-2.6
▲	Evans	8.8	Havelock	0.49	2.1-2.3
▽	Evans	3.3	Havelock	1.72	2.0
▼	Evans	3.3	Havelock	1.72	2.6
○	Devco	2.1	Sysco	1.4	2.5
◐	Devco	11.2	Sysco	1.4	2.4
●	Devco	2.1	Calpo	1.1	2.5

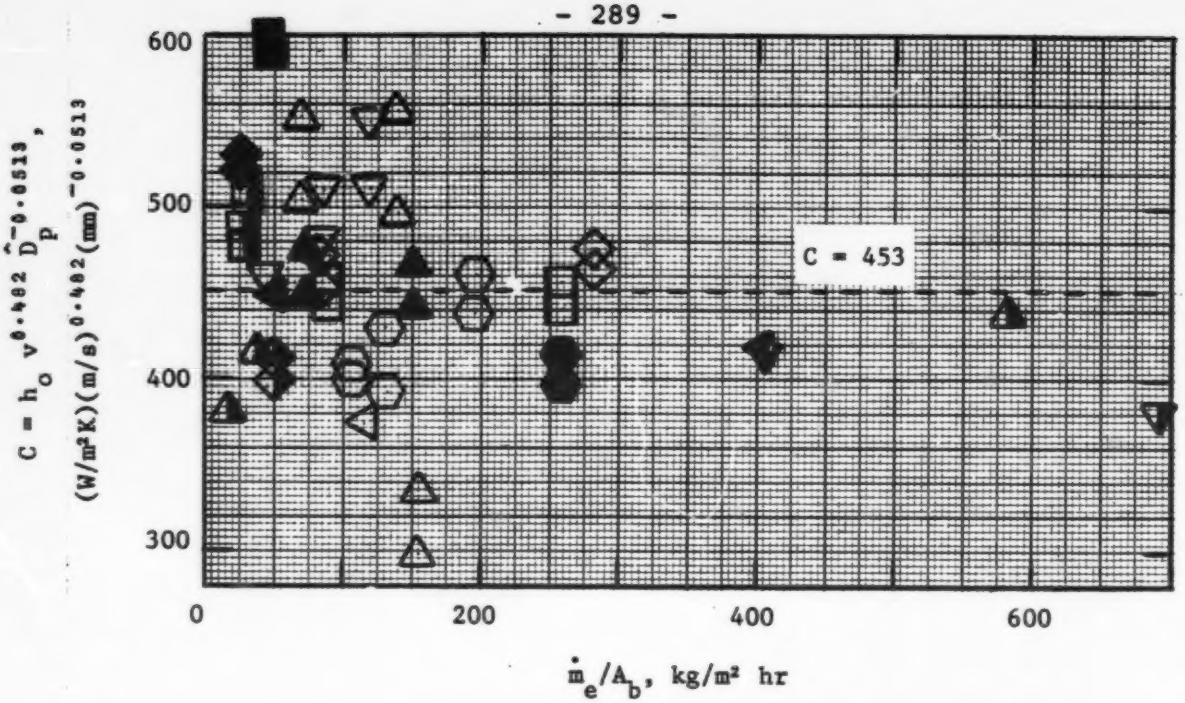

Fig. 9.5 The coefficient, C, in the correlation of bed-side heat transfer coefficients. Points evaluated from individual measurements of h_o: $C = h_o\,v^{0.482}\,\hat{D}_p^{-0.0513}$. Mean height of cooling water circuits above the distributor plate 663 mm.

Key to symbols:	Fuel	$\hat{D}_p$, mm	Sorbent	$\hat{D}_p$, mm	v, m/s
△	Evans	16.7	Havelock	0.49	2.1-2.2
◭	Evans	16.7	Havelock	0.49	1.5-1.6
▲	Evans	16.7	Havelock	1.72	2.5-2.6
▽	Evans	8.8	Havelock	0.49	2.1-2.3
⧨	Evans	3.3	Havelock	1.72	2.6
▼	Evans	3.3	Havelock	1.72	2.0
◁	Evans	3.3	Havelock	1.72	1.5
◀	Evans	3.3	Havelock	0.49	1.5-1.6
⬡	KY No. 9	2.3	Reed	1.1	2.6-2.7
⬢	KY No. 9	2.3	Reed	1.1	2.9
□	Devco	2.1	Sysco	1.4	2.5
◧	Devco	11.2	Sysco	1.4	1.4-1.5
■	Devco	11.2	Sysco	1.4	2.4
◇	Devco	2.1	Calpo	1.1	2.5
⬖	Devco	2.1	Calpo	1.1	1.5
◆	Devco	11.2	Calpo	1.1	1.5

10. CONCLUSION

10.1 Summary of findings

Following is a list of principal observations and conclusions from the present study:

1. The previous finding (Becker and Code 1983) that coal particle diameter does not appreciably affect combustion efficiency was confirmed for another Eastern Canadian coal, namely Evans. The earlier work had demonstrated it for Minto and Devco coals. The present work also indicates that this may be true of an Appalachian coal that was tested, Kentucky No. 9.

2. The previous finding that overhead carbon loss (via the cyclone and baghouse products) is unaffected by the mean residence time $\tau_b = m_b/\dot{m}_b$ of bed particles was similarly upheld.

3. The correlation of overhead carbon loss previously developed (Becker and Code 1983), describing the results of Minto/Devco coal trials, also gives a good accounting of the results of the present coal trials with the exception of those on Evans coal. Multiple linear regression analysis of the Evans data indicates a significantly stronger effect of recycle of cyclone dust and generally lower carbon losses.

4. A correlation of carbon loss in the bed product stream,

also first developed (Anthony, et al. 1985) for the earlier Minto/Devco results (Becker and Code 1983), fits the data on the present coals moderately well.

5. Carbon losses in the burning of Syncrude coke fit the aforementioned correlations unexpectedly well. However, this may be partly fortuitous and there are indications that the effects of bed temperature and recycle of cyclone dust are considerably stronger for the coke.

6. Two Nova Scotia limestones (Sysco and Calpo) and an Appalachian stone (Reed) gave similar performance for sulphur capture. Havelock stone, used in our ealier work and in the present Evans trials, is better than these. Roughly, one unit less of Ca/S ratio is required to get a given sulphur capture with the Havelock.

7. Sulphur capture in the burning of Syncrude coke is surprizingly good up to quite high temperatures. However, the performance deteriorates rapidly above 1050 °C bed temperature, and drops to nothing around 1100 °C. An Athabasca limestone was used in this work. Friedrich, et al. (1982) burned Syncrude coke in an ARFBC (atmospheric recirculating fluidized bed combustion) rig at temperatures up to 950 °C and found little drop in sulphur capture with increasing temperature; this agrees with our findings. They used a Swedish stone.

8. Syncrude coke has a high vanadium content. Measurements of the V/Ni ratio indicate that the vanadium remains fixed in the ash of the coke. The ash tends to be concentrated in the baghouse product and is low in the bed product.

9. Nitrogen oxide emissions show, as in our earlier work (Becker and Code 1983), that less than 25 % of the fuel nitrogen is converted to NO. Conversion is diminished by operation with low exit oxygen concentration.

10.2 Unfinished comparisons

The Evans coal has been burned, with Havelock limestone, for sulphur capture, in an AFBC demonstration boiler at CFB Summerside, Prince Edward Island. A comparison with results from that system is being attempted and will be included in a subsequent publication when completed. Similarly, the Kentucky No. 9 coal and Reed limestone have been used in the TVA 20 MW plant in the U.S.A. and we are making comparisons with that plant's performance.

10.3 Recommendations

The following recommendations are offered for practical operation:

1. Coal particle size, for the coals tested, has negligible effect on combustion performance. We therefore recommend that in practice these coals should not be crushed any finer than necessary. Particles should be small enough for the feeder and

air-lock system used, and small enough to freely pass between in-bed heat exchanger tubes. If provision for rock removal from the bottom of the bed is lacking, then the largest rocks accompanying the coal must be fluidizable and crushing to - 10 mm or less may be necessary.

2. As before (Becker and Code 1983), the evidence indicates that increasing limestone particle size decreases carbon loss. However, large limestone particle size tends to encourage clinkering. Decreasing limestone particle size increases efficiency of sulphur capture, up to a point. The overall optimum mean limestone particle size is around 1 mm, and values of 0.5--1.5 mm are acceptable for AFBC.

3. Fluidizing velocities of 2--3 m/s per second give reasonable performance and productivity in coal combustion by AFBC. Values not much higher tend to give heavy elutriation and are suitable for ARFBC (recirculating beds) but not for conventional AFBC.

4. The optimum bed temperature for coal combustion is around 850 °C. The range 800--950 °C can be worked if variation of bed temperature is part of a load-following strategy.

5. In burning Syncrude coke, fluidizing velocities below about 1.3 m/s seem to be necessary to avoid blowing the coke away (elutriating) too quickly. A value of 1 m/s gives good

performance.

6. It appears that a bed temperature around 1000 °C is optimum for burning of Syncrude coke by AFBC. Combustion efficiency, combustion stability, and sulphur capture (at least by Athabasca limestone) are all good.

7. As always, operating with low excess air reduces NO_x emission. The penalty in terms of combustion efficiency is very modest.

10.4 Results on supporting studies

The following studies are thesis projects of graduate students and will be reported in later theses, reports and papers:

1. Development of the general mathematical model to date: Ph.D. thesis of Fernando Preto, ready for defence at time of issuing this report.

2. Studies of heat and mass transfer and fluidization dynamics in cold models: also in Preto's thesis.

3. TGA studies of reaction of single limestone particles: Ph.D. thesis of Michel Couturier, in last stages of writing.

4. Studies of pyrolysis and combustion of single coal

particles in a bench-scale fluidized bed reactor: Ph.D. research of Jia Qu Zhang, about one year from completion.

5. Studies of elutriation using cold models: M.Sc. thesis research of Robert McCleave, about one year from completion.

6. Studies of carbon distribution with particle size in AFBC product streams: M.Sc. thesis research of David Poirier, about four months from completion.

This list does not include two new endeavours related to our new (1985-87) DSS/EMR contract:

7. Residence time distribution of particles in AFBC: Ph.D. thesis research of Gordon Kubanek, six months underway.

8. Aspects of fluidization dynamics related to AFBC: M.Sc. thesis research of Nicholas Farkas, just begun.

REFERENCES

Adibhatla, S. and Jones, T.M. 1984, Testing of Western Kentucky No. 9 Coal in an Atmospheric Fluidized Bed Combustor. Report IMMR 84/099, Kentucky Center for Energy Research Laboratory, Lexington

Anthony, E.J. 1984, private communication, Energy Research Laboratories, Energy Mines and Resources Canada, CANMET, Ottawa

Anthony, E.J., Becker, H.A., Code, R.K., Liang, D.T. and Stephenson, J.R. 1985, Combustion of High-Sulphur Eastern Canadian Coals by AFBC, Proceedings of Eighth International Conference on Fluidized Bed Combustion, Houston, Texas

Becker, H.A. and Code, R.K. 1982, The Pilot Plant Installation at Queen's University for Studies of Atmospheric Fluidized Bed Combustion. Report QFBC.TR.82.1, Queen's Fluidized Bed Combustion Laboratory, Department of Chemical Engineering, Queen's University, Kingston, Canada K7L 3N6

Becker, H.A. and Code, R.K. 1983, Pilot Plant Trials on Atmospheric Fluidized Bed Combustion of High-Sulphur Eastern Canadian Coals (Minto and Devco) with Limestone Addition for Sulphur Capture. Report to Energy Mines and Resources Canada, Energy Research Laboratories, CANMET, Ottawa. Report QFBC.TR.83.1, Queen's Fluidized Bed Combustion Laboratory, Department of Chemical Engineering, Queen's University, Kingston, Canada K7L 3N6

Becker, H.A., Code, R.K., McCleave, R.W. and Stephenson, J.R. 1985, Queen's University Atmospheric Fluidized Bed Combustion Waste Sample and Information Collection Program 1984-85. Report to Environment Protection Service, Environment Canada, Ottawa. Report QFBC.TR.85.1, Queen's Fluidized Bed Combustion Laboratory, Department of Chemical Engineering, Queen's University, Kingston, Canada K7L 3N6

Botterill, J.S.M., Teoman, Y. and Yuregir, K.R. 1981, A.I.Ch.E. Symposium Series 77 (No. 208), 330

Campbell, J.C. 1981, private communication, Cape Breton Development Corporation, Sydney

Friedrich, F.D., Lee, G.K., Desai, D.L. and Kuivalainen, R. 1982, Fluidized Bed Combustion of Petroleum Coke, ASME Paper No. 82-JPGC-Fu-3, American Soc. Mech. Engineers, 345 E. 47th St., New York, N.Y. 10017

Friedrich, F.D., Lee, G.K., Desai, D.L., Kuivalainen, R. and Osakeyhtio, A.A. 1982, Fluidized Bed Combustion of Petroleum Coke. Energy Mines and Resources Canada, CANMET, Ottawa and Hans Ahlstrom laboratory, Karhula, Finland. Presented at Joint Power General Conference, Denver, Colorado, October 1982

Hamer, C.A. 1983, SO_2 Sorbent Utilization in Fluidized Beds. Division Report ERP/MSL 83-6 (IR), Mineral Science Laboratories, Energy Mines and Resources Canada, CANMET, Ottawa

Heaton, D. 1984, private communication, Syncrude Canada Limited, Edmonton

Sieder, E.N. and Tate, G.E. 1936, Ind. Eng. Chem. 28, 1429

Stover, N.S.H., Anthony, E.J., Desai, D.L. and Friedrich, F.D. 1981, Combustion Performance and Sulphur Capture During Fluid Bed Combustion of a Western Sub-Bituminous Coal and an Eastern Bituminous Coal. Report ERP/ERL 81-36 (J), Energy Research Laboratories, Energy Mines and Resources Canada, CANMET, Ottawa. Also issued as ASME paper 81-WA/Fu-5, American Society of Mechanical Engineers, 345 E. 47th St., New York 10017

Tibbetts, T.E. and Montgomery, W.J. 1976, Evaluation of Canadian Commercial Coals: Nova Scotia and New Brunswick-1975. Report 76-40, Energy Research Laboratories, Department of Energy Mines and Resources Canada, CANMET, Ottawa

POOR
QUALITY
ORIGINAL